
The University Of Sheffield.

# Determining the role of N-cadherin in the formation of the myeloma niche

**Thesis submitted for the degree of doctor of philosophy by**

**Osama Mohammed Al-Amer**

**Supervised by**

**Prof. Peter Croucher**

**Dr. Colby Eaton**

**Dr. Allan Williams**

**Department of human metabolism**

**Medical school**

**Submitted January 2014**

## Acknowledgements

Firstly, I would like to thank Allah to give me power to end this project. After that, I would like to express my sincere thanks to my supervisors, Dr. Colby Eaton, Prof. Peter Croucher and Dr. Allan Williams, who gave me the opportunity to come to Sheffield and offered me this unforgettable experience in addition to their continuous advice and unlimited encouragement.

I would like to express many thanks and appreciation to Dr. Michelle Lawson, Dr. Clive Buckle, Julia Hough, Orla Gallagher, Anne Fowles and Jenny Lippitt-Down for their help during the PhD practical work.

I would like to express many thanks and appreciation to Dr Karin Vanderkerken (Free University Brussels, Belgium) for her kind gift 5T33MM cells and Dr Claire Edwards (University of Oxford, UK) for her kind gifts 5TGM1 cells.

Finally, I wish to dedicate this work to my parents, my wife and my daughters. I want to thanks my family for their unlimited encouragement to finish my study.

## List of abstracts presented

- A.J. Williams, M.A. Lawson, **Osama Al-Amer**, J. Hough, T. Bos, K. Vanderkerken & P.I. Croucher. Multiphoton imaging of individual myeloma cells in calvariae: association of myeloma development with sites of bone turnover. 10th International conference Cancer-Induced Bone Disease, Sheffield, UK, September, 22nd-25th 2010.

- **Osama Al-Amer**, A.J. Williams, J. Hough & P.I. Croucher. Myeloma cells retain the molecular machinery utilised by hematopoietic stem cells to localise to the hematopoietic stem cell niche. 2nd Mellanby Research Day, Sheffield, UK, June, 16th 2011.

- A.J. williams, M.A. Lawson, **Osama Al-Amer**, J. Hough, T. Bos, K. vanderkerken & P.I. Croucher. Multiphoton imaging of individual myeloma, cells in calvariae: Association of myeloma, development with sites of bone turnover. 2nd Mellanby Research Day, Sheffield, UK, June, 16th 2011.

- **Osama Al-Amer**, A.J. Wiliams, J. Hough & P.I. Croucher. Determining the role of N-cadherin during myeloma colonisation in bone. Medical school research meeting, Sheffield, UK, June, 20th-21th 2011.

- A.J. Williams, M.A. Lawson, **Osama Al-Amer**, J. Hough, T. Bosb, K. Vanderkerken & Pl Croucher. Association of myeloma development with sites of bone turnover. Medical school research meeting, Sheffield, UK, June, 20th-21th 2011.

- **Osama Al-Amer**, A.J. Williams, J. Hough & P.I. Croucher. Myeloma cells retain the molecular machinery utilised by hematopoietic stem cells to remain quiescent in bone. 5th International Saudi Conference, the University of Warwick, Warwick, UK, June, 23rd-26th 2011.

- **Osama Al-Amer**, Allan Williams, Clive Buckle, Colby Eaton & Peter Croucher. Myeloma cells utilise N-cadherin to adhere to osteoblasts. 25th UK Adhesion Society Meeting, Sheffield, UK, April, 17th 2012.

- **Osama Al-Amer**, Allan Williams, Clive Buckle, Colby Eaton & Peter Croucher. N-cadherin is an important mediator of interactions between myeloma cells and bone. Medical school research meeting, Sheffield, UK, June, 11th-12th 2012.

- J. Hough, M. Lawson, **Osama Al-Amer**, C. Eaton & P. Croucher. Identification of molecular determinants of myeloma cell engagement in the osteoblast niche in bone. Medical school research meeting, Sheffield, UK, June, 11th-12th 2012.

- **Osama Al-Amer**, Allan Williams, Clive Buckle, Colby Eaton & Peter Croucher. N-cadherin is an important mediator of interactions between myeloma cells and osteoblasts. 3rd Mellanby Research Day, Sheffield, UK, June, 21st 2012.

- J. Hough, M. Lawson, **Osama Al-Amer**, C Eaton & Pl Croucher. Identification of molecular determinants of myeloma cell engagement in the osteoblast niche in bone. 3rd Mellanby Research Day, Sheffield, UK, June, 21st 2012.

- **Osama Al-Amer**, A.J. Williams, Clive Buckle, Colby Eaton & Peter Croucher. N-cadherin is an important mediator of interactions between myeloma cells and osteoblasts. 6th International Saudi Conference, the Brunel University, London, UK, October, 11th-14th 2012.

- **Osama Al-Amer**, A.J. Williams, Clive Buckle, Colby Eaton & Peter Croucher. N-cadherin is an important mediator of interactions between myeloma cells and osteoblasts. 12th International conference Cancer-Induced Bone Disease, Lyon, France, November, 15th-17th 2012.

- Victor Njom, Mark Dickman, **Osama Al-Amer**, Ian Duce, and David Buttle. Molecular targets for plant cysteine proteinases on parasite nematode cuticles. Medical school research meeting, Sheffield, UK, June, 17th-18th 2013.

# Table of Contents

## List of abbreviations

| | |
|---|---|
| Adenomatous polyposis coli protein | APC |
| Adenosine triphosphatase | ATPase |
| Angiopoietin-1 | Ang-1 |
| β2-microglobulin | β2-M |
| Bone marrow | BM |
| Bone mineral density | BMD |
| Bone morphogenic proteins | BMPs |
| Connective tissue growth factor | CTGF |
| C-X-C chemokine ligand 12 | CXCL12 |
| C-X-C chemokine receptor type 4 | CXCR-4 |
| Deoxynucleoside triphosphates | dNTPs |
| Dickkopf | Dkk |
| Estrogen receptor α | ERα |
| Extracellular matrix | ECM |
| Extracellular signal-regulated kinases | ERK |
| Fas/Fas ligand | FasL |
| Fibroblast growth factor | FGF |
| Frizzle-related protein-2 | sFRP-2 |
| Glycogen synthase kinase 3β | GSK3β |
| Green fluorescent protein | GFP |

| | |
|---|---|
| Hematopoietic progenitor cells | HPCs |
| Hematopoietic stem cells | HSCs |
| Hydrogen chloride | HCl |
| Insulin like growth factor | IGF |
| Interleukin-1 | IL-1 |
| Interleukin-3 | IL-3 |
| Interleukin-6 | IL-6 |
| Jagged 1 | Jag 1 |
| lipoprotein receptor related protein-5/6 | LRP-5/6 |
| Long-term reconstituting | LTR |
| Low-density lipoprotein receptor | LDLr |
| Low-density lipoprotein receptor-related protein 5 | LRP5 |
| Macrophage colony-stimulating factor | M-CSF |
| Macrophage inflammatory protein-1α | MIP-1α |
| Mesenchymal stem cells | MSCs |
| Mitogen-activated protein kinases | MAPK |
| Monoclonal gammopathy of undetermined significance | MGUS |
| Multiple myeloma | MM |
| Osteoprotegerin | OPG |
| Osteopontin | OPN |
| Parathyroid hormone | PTH |

| | |
|---|---|
| phosphatidylinositide 3-kinases | PI3K |
| PTH/PTHrP receptors | PPRs |
| Platelet-derived growth factor | PDGF |
| Receptor activator nuclear factor kappa | RANK |
| Receptor activator nuclear factor kappa ligand | RANKL |
| Runt-related transcription factor 2 | Runx2 |
| Short-term reconstituting | STR |
| Soluble frizzled-related proteins | SFRPs |
| Spindle-shaped N-cadherin$^{+}$ osteoblastic | SNO |
| Stromal cell-derived factor 1 | SDF-1 |
| Transforming growth factor β | TGFβ |
| Tyrosine kinase receptor 2 | Tie2 |
| Tumour necrosis factor | TNF |
| Tumour necrosis factor-α | TNF-α |
| Vascular endothelial growth factor | VEGF |
| Wnt-inhibitory factor 1 | WIF1 |

## Summary

**Introduction:** Multiple myeloma is a plasma cell malignancy that causes extensive osteolytic bone disease. Present treatments target end stage disease but understanding how bone lesions are initiated may offer new approaches to prevent/suppress colonization. It is clear that myeloma cells form specific interactions with the bone microenvironment, where they can remain dormant and protected from current therapy to eventually proliferate and cause disease progression. N-cadherin is an adhesion molecule that has been implicated in the localization of haematopoietic stem cells (HSCs) to 'niches' containing osteoblasts on endosteal bone surfaces. In this study, we have tested the hypothesis that myeloma cells utilise N-cadherin to adhere to osteoblasts *in vitro* and *in vivo* during the colonization into the bone.

**Findings:** N-cadherin mRNA and protein were expressed by osteoblasts and myeloma cells. We showed focal expression of N-cadherin in myeloma cells, whereas expression was observed contiguously on the membranes of adjacent osteoblasts. N-cadherin expression significantly increased during osteoblastogenesis. Immunohistochemistry demonstrated staining of N-cadherin when myeloma cells were in contact with osteoblasts *in vitro* and *in vivo*. Blocking N-cadherin mediated interactions, using specific antibodies against N-cadherin, significantly reduced adherence of myeloma cells to osteoblasts *in vitro*. Attempts were made to block the adhesion of myeloma cells to bone cells in calvarial bones *in vivo*. These studies were in conclusion suggested that there may be a role of N-cadherin in these interactions.

**Conclusion:** These studies provide evidence that adherence of myeloma cells to osteoblasts is mediated by N-cadherin *in vitro* and *in vivo,* suggesting that myeloma cells may occupy a niche similar to that used by HSCs in bone.

# 1 Chapter 1: Introduction and Background

## 1.1 Bone Biology

### 1.1.1 General structure and function of bone

The mammalian skeleton is formed by two different tissues, bone and cartilage. Bone is a dynamic connective tissue composed of an organized matrix of collagen proteoglycan that supports and protects the various organs of the body, hardened by mineralization with calcium phosphate in the form of hydroxyapatite ([Ca3(PO4)2]Ca(OH)2). Bone structure is not a uniformly solid material, but composed of outside solid bone, cortical or compact, and inside spongy bones, trabecular (Figure 1.1). Cortical bone is an outside solid bone, which is dense, ordered structure and found mainly in the shaft of long bones and the surfaces of flat bones. Trabecular bone is an inside spongy bones, which is lighter, less compact and has an irregular structure (Datta et al., 2008). Bone types include long bones such as those in limbs, short bones such as wrist and ankle, flat bones such as skull and irregular bones such as spine and hips. Osteoclasts, osteoblast, bone lining cells and osteocytes are the cell types responsible for bone turnover and maintenance of bone cells (Karsenty, 1999, Watkins et al., 2001). The essential role of bone is to provide structural anchorage between muscles, movement of the body, providing mineral, chiefly calcium and phosphate, balance for the body, in addition to protection of the brain, spinal cord, heart and lungs (Cohen, 2006).

The marrow cavity within bone is the main site of hematopoiesis in the adult human and comprises of extracellular matrix (ECM), Hematopoietic stem cells (HSCs), Mesenchymal stem cells (MSCs), blood cells, osteoblasts, osteoclasts, fibroblasts, endothelial cells and adipocytes. The ECM is composed of an organic component and an inorganic component, in which organic matrix represents approximately 35% of the total weight of bone compared with inorganic matrix which represents 65% (Downey and Siegel, 2006). Bone growth, metabolism and remodeling are regulated by two interacting, coupled processes; bone resorption and bone formation. Bone remodeling regulates calcium homeostasis and repairs micro-damaged bones in addition to maintaining the shape and sculpture of the skeleton during growth. Osteoclasts resorb

bone while osteoblasts produce bone matrix and facilitate mineralization. The cooperative activities of osteoclasts and osteoblasts results in a healthy bone and maintain normal skeletal development. (Fliedner, 1998, Wang et al., 2006, Muguruma et al., 2006).

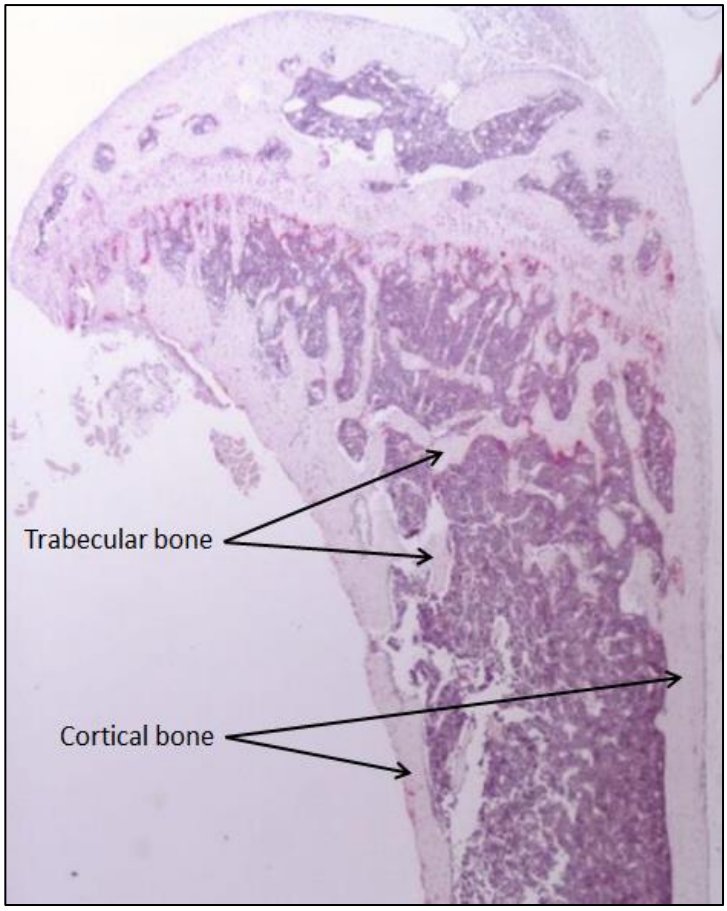


**Figure 1.1: Structure of the long bone (tibia) of C57BL/KalwRij male mice.** Bone is a dynamic connective tissue is composed of cortical and trabecular bones. Cortical bone is composed of the hard outer layer of bones. Trabecular bone is composed of spongy bones, which is lighter, less compact and has an irregular structure. Images were captured at 2.5x resolution using osteomeasure software with a Leitz DMRB microscope.

### 1.1.2 Cells of bone

Within the skeleton there are 4 basic types of bone cells; osteoclasts, osteoblast, bone lining cells and osteocytes. Osteoclasts (Figure 1.2A) are multinucleated cells derived from monocytes that are ultimately from HSCs first discovered in 1873 by Kolliker. Osteoclast maturation requires the presence of receptor activator of nuclear factor κβ ligand (RANKL) and Macrophage colony-stimulating factor (M-CSF) (Nijweide et al., 1986, Teitelbaum, 2000, Watkins et al., 2001). Overexpression of osteoprotegerin

(OPG), soluble receptor that competes with RANK for RANKL, reduces osteoclastogenesis in mice. On the other hand, lack of OPG has been shown to accelerate osteoclastogenesis and OPG Ko mice (*OPG*$^{-/-}$ mice) develop severe osteoporosis (Bucay et al., 1998).

Osteoclasts form at skeletal sites, in which stromal cells and osteoblasts express RANKL and M-CSF and it is the interaction of these ligands with their receptors on monocyte/macrophage cells that induce commitment to the osteoclast phenotype. Osteoclasts have a critical role in the regulation of bone formation and regulation of bone mass, in which mature and active osteoclasts are responsible for resorbing mineralized bone matrix and breaking up the organic bone (90% collagen). Differentiated osteoclasts express αvβ3 integrin, which binds to bone matrix via RGD-containing proteins leading to the formation of sealed pocket for the secretion of cathepsin K, the major protease involved in the degradation of type I collagen (Nakamura et al., 1996, Nakamura et al., 2007a). After attachment, osteoclasts exhibit a highly polarized cytoplasmic organization. The intracellular pH of osteoclasts is maintained by $HCO_3^-/Cl^-$ exchanger at the antiresorptive surfaces. Activated osteoclasts generate ruffled membranes in which $Cl^-$ ions pass through the membrane increasing the acidity charge-coupled to the vacuolar $H^+$– adenosine triphosphatase (ATPase) results in secretion of hydrogen chloride (HCl) into the resorptive microenvironment and increase the pH to ~4.5. These acidify an extracellular microenvironment resulting in demineralization of the organic component of bone (Karsenty, 1999, Teitelbaum, 2000).

Osteoblasts (Figure 1.2B) are mononucleate cells derived from putative MSCs that are responsible for bone formation and for a regulation of osteoclast differentiation. Bone morphogenic proteins (BMPs), Wnt/β-catenin and Notch signalling all play a major role in osteoblastogenesis (Chen et al., 2004, Milat and Ng, 2009, Engin and Lee, 2010). In addition, Runt-related transcription factor 2 (RUNX2) has been shown to be an essential transcription factor for osteoblastogenesis. It was found that Runx2-/- mice failed to

develop calvarial bones and mice died at birth. Runx2 also regulates another transcription factor necessary for osteoblastogenesis, osterix (Lian and Stein, 2003). Osteoblast differentiation from MSCs can be characterized in multiple commonly accepted stages, pre-osteoblasts, osteoblasts, bone lining cells and osteocytes (Yin and Li, 2006, Wu et al., 2009). Mature osteoblasts are identified by their cuboidal structure and their location on the endosteal surface. Type I collagen is the major product of the bone-forming osteoblast, in addition to osteocalcin and osteonectin (Di Lullo et al., 2002). In addition, osteoblasts express relatively high amounts of alkaline phosphatase (Ducy et al., 1996). Terminally differentiated osteoblasts either become bone lining cells or differentiate into osteocytes surrounded by mineral matrix or undergo apoptosis by activation of intrinsic (mitochondria) death signals. Apoptosis can mediated by cell surface death receptors of the tumour necrosis factor (TNF) receptor superfamily such as osteoprotegerin (OPG), which subsequently activates caspases inducing cell death (Manolagas, 2000, Hock et al., 2001).

Bone lining cells (Figure 1.2C) are elongated cells with slightly ovoid nuclei. The non-remodelling bone surface is covered by a thin layer of bone lining cells (Everts et al., 2002). Mineralized collagen matrix synthesis stops once bone formation is inactivated by the conversion of osteoblasts into bone lining cells in a reversible process which represents one of the fates of osteoblasts that have completed their bone forming function. It is suggested that bone lining cells have a little involvement in the bone formation mechanism (Manolagas, 2000).

Following active bone formation some osteoblasts are eventually embedded within the matrix. Matrix-producing osteoblasts express alkaline phosphase and collagen, which are necessary for the production of osteoid, unmineralized bone matrix. A subpopulation of osteoblasts becomes encased in osteoid as osteoid osteocytes, which regulate mineralization, then into mineralizing osteocytes and mature osteocytes. When osteoblasts are differentiated into osteocytes, alkaline phosphatase is reduced and casein

kinase II is increased (Mikuni-Takagaki et al., 1995, Bonewald, 2011). Osteocytes (Figure 1.2D) are the most numerous cells found in mature bone and are characterized by a stellate morphology with a dendritic network similar to that of the nervous system. These cells, embedded in mineralized matrix, directly contact with each other or with osteoblasts via long cytoplasmic extensions passing through bone in canals called canaliculi (Aarden et al., 1994, Bonewald, 2011). Although osteocytes are relatively inert cells, they have an important function. Osteocytes act as mechanosensor cells, in which they are sensitive to applied stress of bone loading to maintaining bone structure. The need for bone increase or bone reduction during functional adaptation of the skeleton in addition to repair of micro-damage can be detected by osteocytes. Osteocytes express some molecules such as, phosphate-regulating neutral endopeptidase, X-linked (PHEX), dentin matrix acidic phosphoprotein-1 (DMP-1), matrix extracellular phosphoglycoprotein (MEPE) and fibroblast growth factor 23 (FGF-23) that play an important role in phosphate homeostasis (Klein-Nulend et al., 2003, Bonewald, 2011). Osteocytes can also detect changes in the levels of hormones, such as estrogen and glucocorticoids (Manolagas, 2000). In addition, they control the bone formation via sclerostin, SOST gene, a BMP antagonist.Winkler et al (2003) demonstrated that sclerostin released from osteocytes mediates bone homeostasis (Winkler et al., 2003). Osteocytes also act as inducers of osteoclast activation. Zhao et al (2002) demonstrated that osteocyte-like cells, MLO-Y4, support osteoclast formation and activation by expressing RANKL on their surface and by expression and secretion large amounts of M-CSF (Zhao et al., 2002).

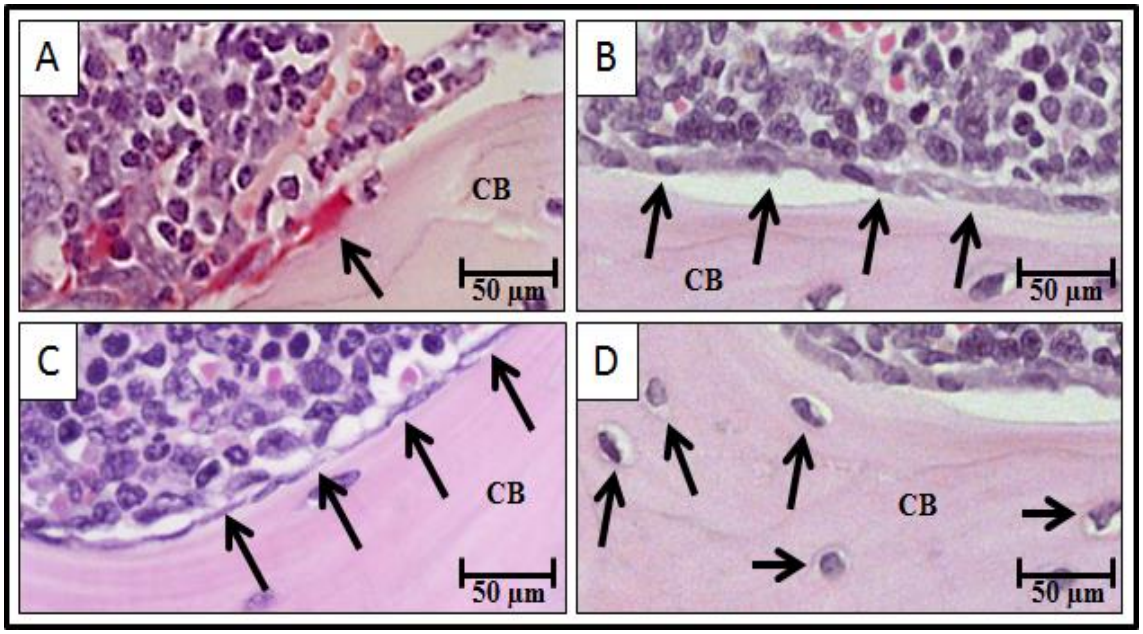


**Figure 1.2: Cells of bone on the cortical surfaces of the calvarial bones in male C57BL/KalwRij mice aged 6 weeks.** Panel A shows positive tartrate resistant acid phosphatase (TRAP) stain for osteoclast (denoted by black arrow) on the endosteal surfaces of calvarial bones. Panel B shows osteoblasts (denoted by black arrows) cover the cortical bone surface of calvarial bones. Panel C shows the bone lining cells (denoted by black arrows) cover the cortical bone surface of calvarial bones. Panel D shows the osteocytes (denoted by black arrows) embedded within the mineralized matrix. Bar size equal 50 µm. CB is cortical bone.

### 1.1.3 Bone modeling

In order to maintain its functions and maintain serum calcium levels during vertebrate life, bone is regulated by two processes; modeling and remodeling. Bone modeling is an adaptive process of generalized and continuous growth in bone shape, length and width until the adult bone structure is attained. This growth requires normal activity of bone cells; osteoblasts and osteoclasts. The modeling process differs from remodeling which is a locally coupled process of bone resorption and formation maintaining skeletal mass and morphology. During development approximately 100% of bone surfaces are active during the modeling process until proper bone size and shape is achieved. In contrast, only 20% of bone surfaces are active in remodeling processes at any given time (Watkins et al., 2001).

During foetal development, bone formation is regulated through two unique mechanisms: intramembranous ossification and endochondral ossification. In intramembranous ossification, some bones such as the prefiguring part of the skull and the clavicles are developed through differentiation of MSCs into osteoblasts directly, which subsequently form woven bone with characteristic irregular calcification and an assembly of collagen fibres. In endochondral ossification, the rest of the bones, long bones, are developed through differentiation of MSCs into chondrocytes forming the cartilage anlagen. Cells from the perichondrium of cartilage anlagen differentiate into osteoblasts, and the periphery of the cartilage anlage become hypertrophic. Finally, the matrix surrounding these hypertrophic chondrocytes calcifies and longitudinal growth is stimulated as cartilaginous matrix. Once bone becomes mature, the remodelling process starts to control the reshaping, replacement of bone following injuries and maintains calcium homeostasis (Karsenty, 1999, Ferretti et al., 2002, Robling et al., 2006).

### 1.1.4 Bone remodeling

In order to maintain stability and integrity of bone in addition to calcium homeostasis, bones are continuously undergoing remodeling (Figure 1.3). Bone remodelling is a complex process, in which mature bone tissue is removed by a process called bone resorption and new bone tissue is formed by a process called bone formation. In this process, cellular activity and molecular mechanisms are closely coordinated to ensure the bone resorption-formation sequence is carried out at a mutual location thus sustaining bone mass. Cells responsible for bone resorption are osteoclasts, and cells responsible for bone formation are osteoblasts. The remodeling cycle is divided into four consecutive phases: activation, resorption, reversal, and formation, which is regulated both systemically and locally by cytokines, hormones and growth factors, affecting tissue quality and mass. Disruptions in the interaction of osteoclasts or osteoblasts and imbalance in the regulation of bone remodeling can result in irregular bone turnover cycles and subsequently results in many metabolic bone diseases such as Multiple Myeloma (MM) bone disease (Hadjidakis and Androulakis, 2006, Proff and Romer, 2009, Raggatt and Partridge, 2010).

During the bone remodeling process, old bone is resorbed and replaced with new bone by osteoclasts and osteoblasts, respectively. The cellular mechanism of bone remodeling process starts with an activation phase, in which osteoclasts precursors are recruited and differentiated into pre-osteoclasts then into mature osteoclasts. After osteoclast activation, the resorption phase takes place in which mature osteoclasts resorb bone surfaces. Following resorption, the reversal phase, in which mature osteoclasts go into apoptosis and osteoblast precursors are recruited and differentiated into pre-osteoblasts then into mature osteoblasts at resorbed bone surfaces. Ultimately, the formation phase takes place in which mature osteoblasts secrete new bone matrix which mineralized to generate new bone (Raggatt and Partridge, 2010).

#### *1.1.4.1 Regulation of osteoclast activity*

Osteoclastic bone resorption is controlled by receptor activator of nuclear factor kappa-B ligand (RANKL), growth factors, cytokines and hormones. RANKL is a tumour necrosis factor (TNF)-related cytokine expressed by osteoblasts and stromal cells. RANKL has an important role in osteoclast differentiation, in which it binds to its receptor, receptor activator of nuclear factor kappa-B (RANK) on the surface of osteoclast precursors. Binding of RANKL to RANK starts the osteoclastogenesis process and stimulates osteoclast activity and bone resorption (Boyle et al., 2003). Simonet et al (1997) demonstrated that using recombinant osteoprotegerin (OPG), an osteoclastogenesis inhibitory factor blocked the differentiation of osteoclasts from precursor cells *in vitro*. *In vivo*, overexpression of OPG in transgenic mice induced a reduction in the later stages of osteoclast differentiation resulting in non-lethal osteopetrosis (Simonet et al., 1997).

Transforming growth factor β (TGF-β), Bone morphogenetic proteins (BMPs) and fibroblast growth factor (FGF) all have important roles in the regulation of osteoclast activity. TGF-β is a factor released during bone resorption. Quinn et al (2001) demonstrated that TGF-β regulated osteoclast differentiation. In culture TGF-β inhibited osteoclast formation, osteoclastogenesis in addition to decreased RANKL (Quinn et al., 2001). BMPs are a group of growth factors that induce formation of bone and cartilage. It was found that BMPs stimulate the differentiation of osteoclasts and osteoblasts during bone development. Okamoto et al (2006) demonstrated that mice overexpressing BMP-4 in bone developed severe osteopenia in addition to increased osteoclast numbers. In contrast, mice overexpressing noggin (a BMP antagonist) had increased bone volume and decreased osteoclast numbers (Okamoto et al., 2006). The FGF has been shown to family of growth factors also has been shown to be involved in the regulation of bone formation: FGF stimulate osteoclast recruitment, osteoclast differentiation and bone resorption (Hurley et al., 1998, Collin-Osdoby et al., 2002).

In addition to RANKL and growth factors discussed upon, cytokines have been shown to play an important role during bone remodeling. Interleukin-1 (IL-1), interleukin-6 (IL-6) and Tumour Necrosis Factor-α (TNF-α) all play a major role in induction of osteoclast differentiation and mediation of bone resorption. Thomson et al (1986) demonstrated that osteoblasts mediate IL-1 stimulated osteoclast activity and increase osteoclastic bone resorption (Thomson et al., 1986). Kurihara et al (1990) demonstrated that adding 10 to 100 pg/ml of IL-6 significantly increased the formation of multinucleate osteoclasts in cultures. Use anti-human IL-1 inhibited the increase of multinucleate osteoclasts stimulated by IL-6. Furthermore, adding IL-6 in culture increased the elevated level of IL-lβ. These results suggested that IL-6 stimulated the formation of multinucleate osteoclasts is mediated by induction of release of IL-1β (Kurihara et al., 1990). TNF-α is a multifunctional cytokine produced by activated macrophages. It was found that TNF-α together with IL-1 induced osteoclast differentiation and mediated bone resorption (Wei et al., 2005).

Osteoclastic bone resorption is controlled systemically by four main hormones: parathyroid hormone (PTH), 1,25-Dihydroxycholecalciferol ($1,25(OH)_2D_3$), calcitonin and oestrogen. PTH is a potent stimulator of osteoclast function by binding to its receptors on osteoblasts and bone marrow stromal cells. This activates expression of MCSF and RANKL, thereby indirectly stimulating osteoclastic bone resorption (McSheehy and Chambers, 1986a, McSheehy and Chambers, 1986b). On the other hand, there has been evidence that PTH could be directly stimulating osteoclast-like cell formation from hemopoietic blast cells (HSCs) (Sugimoto et al., 1993). It has been postulated that PTH also stimulates the production of 1,25-Dihydroxycholecalciferol ($1,25(OH)_2D_3$) from a circulating inactive precursor. 1,25-Dihydroxycholecalciferol ($1,25(OH)_2D_3$) positively regulates bone resorption indirectly, which increases RANKL and M-CSF expression (McSheehy and Chambers, 1987). Calcitonin hormone binds to its receptors that are expressed on osteoclasts and inhibits osteoclastic resorption directly (Zaidi et al., 2002). Estrogens have an important function in the skeletal system in female, in with they act as a bone-sparing hormone. Estrogens bind to receptors

expressed on both osteoclasts and osteoblasts causing osteoclast apoptosis (Nakamura et al., 2007b, Krum et al., 2008). Nakamura et al (2007) demonstrated that activated osteoclastic estrogen receptor α (ERα) by estrogen induced apoptosis for osteoclasts through activation of the Fas/Fas ligand (FasL) system, in which oestrogen up-regulated FasL expression in osteoclasts. In vivo, ERα ablation in transgenic mice induced trabecular bone loss in females, but not males (Nakamura et al., 2007b). Krum et al (2008) demonstrated that oestrogen induced FasL expression in osteoblasts and not in osteoclasts *in vitro* and *in vivo*. Osteoclasts do not undergo oestrogen-induced apoptosis unless osteoblasts were added. Co-cultures of osteoblasts and ERαKO bone marrow-derived osteoclasts mediated osteoclast apoptosis suggesting oestrogen protects bone by inducing FasL in osteoblasts to regulate osteoclast survival (Krum et al., 2008).

#### *1.1.4.2 Regulation of osteoblast activity*

The differentiation of osteoblasts is controlled by key signaling systems Wnt, Dickkopf (DKK), BMPs and Insulin-like growth factors (IGFs). The Wnt signaling pathway is a network of proteins that has an important role in postnatal bone formation and bone turnover. Wnt stimulates osteoblast proliferation, function and survival though binding to Frizzled that subsequently binds to lipoprotein receptor related protein-5/6 (LRP-5/6) (Westendorf et al., 2004). Gong et al (2001) demonstrated that expression of LRP-5 by osteoblasts *in situ* can transduce Wnt signalling *in vitro*. In addition, a mutant-secreted form of LRP-5 can reduce bone thickness in mouse *in vivo* (Gong et al., 2001). Tamai et al (2000) demonstrated that LRP-6 binds to Wnt-1 to activate Wnt signalling in Xenopus embryos. Furthermore, LRP6 mutant lacking the carboxyl intracellular domain blocked Wnt signalling indicating that LRP-6 may be a component of the Wnt receptor complex (Tamai et al., 2000). Day et al (2005) demonstrated that controlling Wnt/β-catenin signalling is essential to control osteoblast and chondrocyte (cells found in healthy cartilage) differentiation. Wnt/β-catenin signalling enhanced osteoblast differentiation, ossification and suppressed chondrocyte formation. In contrast, inactivation of β-catenin caused chondrocyte differentiation *in vitro* (Day et al., 2005).

Wnt antagonist, (DKK), plays an important role in regulation of osteoblast activity. Four members of the DKK family; DKK-1, DKK-2, DKK-3 and DKK-4 have been identified. Wnt/β-catenin pathway can be inhibited by DKK-1 and DKK-2 by binding to LRP-5/6 and single transmembrane protein, Kremen, preventing their interaction with Wnt, which is essential for osteoblast activation (Niehrs, 2006). Mao et al (2001) demonstrated that LRP-6 is required for Wnt/β-catenin signaling in drosophila, xenopus and mouse. Dkk-1 and Dkk-2 interact with domains of LRP-6 that are required for Wnt/Frizzled interaction and blocks Wnt/β-catenin signaling (Mao et al., 2001). Furthermore, Mao et al (2002) demonstrated that transmembrane proteins Kremen-1 and Kremen-2 are high-affinity Dkk-1 receptors inducing rapid endocytosis and removal of the Wnt receptor LRP-6 from the plasma membrane. This result suggested Kremen-1 and Kremen-2 are modulating canonical Wnt signaling through LRP-6 in vertebrates (Mao et al., 2002).

BMPs are a group of growth factors that belong to TGF-β superfamily initially identified by their ability to induce bone development. BMPs are stored in the bone matrix and released during bone resorption, stimulating osteoblast proliferation and skeletogenesis by binding to two different types of serine-threonine kinase receptors, termed type I and type II receptors. Activities of BMPs are regulated by BMP-binding proteins; Noggin and Chordin (Kawabata et al., 1998, Yamaguchi et al., 2000). King et al (1994) demonstrated that BMP-5 was expressed in the early stage of skeletal development and that it was expressed in some soft tissues suggesting that BMP-5 is a signal for both skeletal and soft tissue development (King et al., 1994). Lyons et al (1995) demonstrated that BMP-2 and BMP-7 were expressed in midgestation embryos suggesting their roles during skeletal development (Lyons et al., 1995). Yamaguchi et al (1996) demonstrated that BMP-2, BMP-4 and BMP-6 stimulated the differentiation of osteoblast cell lines, ST2 and MC3T3-G2/PA6 *in vitro*. BMP-2, BMP-4 and BMP-6 stimulated ALP activity, induced PTH and generated mineralized bone in these osteoblastic cells suggesting that BMPs induce differentiation of bone marrow stromal cells into osteoblasts (Yamaguchi et al., 1996).

The insulin-like growth factor (IGF) signalling system is comprised of two receptors (IGF1R and IGF2R), two ligands (IGF-1 and IGF-2) and six binding proteins (IGFBP-1 to IGFBP-6). It was found that IGFs stimulate osteoblast activity and increase bone formation, and bone matrix mineralization. Overexpression of IGF-1 in transgenic mice indicated increased trabecular bone volume compared with control mice (Zhao et al., 2000a). Osteoblast-specific knockout of IGF receptor gene induced decrease in cancellous bone volume, trabecular number and decrease in the rate of mineralization of osteoid (Zhang et al., 2002).

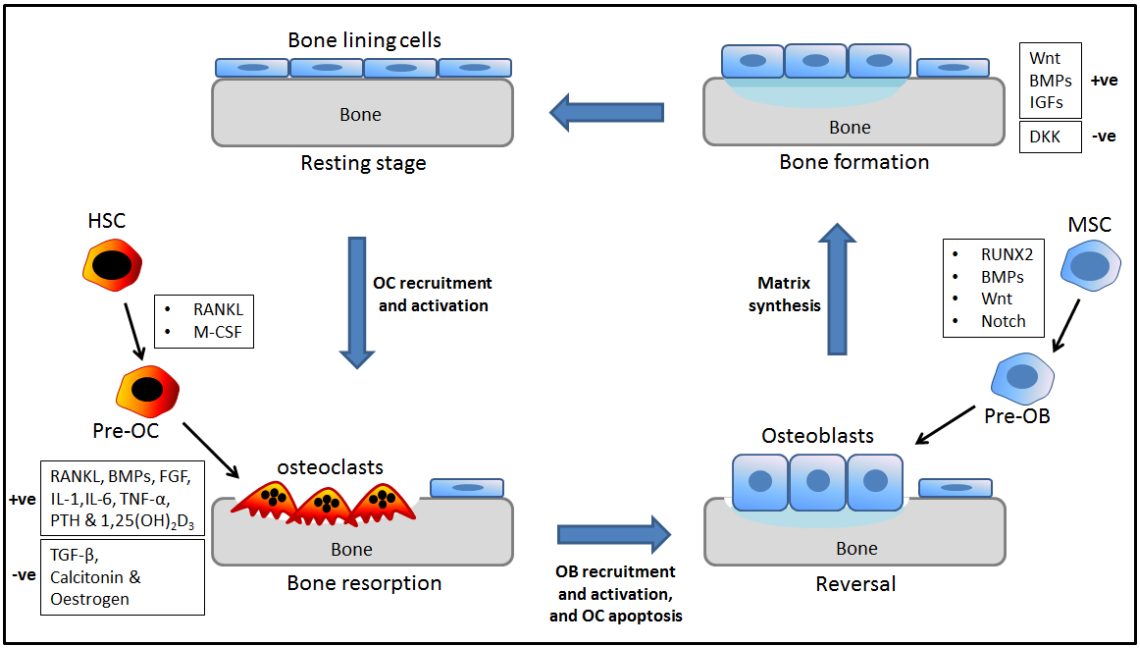


**Figure 1.3: Diagrammatic summary of bone remodeling cycle.** Bone remodeling is regulated by a couple of bone cells; osteoclasts and osteoblasts. Remodeling cycle firstly starts with activation phase; receptor activator of nuclear factor kappa-B ligand (RANKL) and Macrophage colony-stimulating factor (M-CSF) activate and recruit osteoclasts. Secondly bone resorption phase; the activity of osteoclasts and bone resorption controlled by RANKL, FGF, IL-1, IL-6, TNF-α, PTH, $1,25(OH)_2D_3$, TGF-β, BMPs, calcitonin and oestrogens. Thirdly reversal phase; osteoclasts are removed and osteoblasts are activated and recruited by Runx2, BMPs, Wnt and Notch. Fourthly bone formation phase; osteoblasts secrete new bone matrix which mineralized to generate new bone. The bone formation is regulated by Wnt, BMPs and IGFs.

## 1.2 Multiple myeloma

### 1.2.1 Epidemiology of multiple myeloma

Multiple myeloma (MM) is the second most common hematologic cancer after non-Hodgkin lymphoma and represents 10% of all hematologic malignancies and 1% of all deaths caused by cancers (British Committee for Standards in Haematology, 2001). 2,223 new cases of MM in men and 1,817 new cases of MM in women were reported in 2007 in the United Kingdom. The five year survival rates for MM patients are approximately 20% (Collins, 2005, Raab et al., 2009).

### 1.2.2 Pathophysiology of multiple myeloma

MM is a plasma cell malignancy of the B lymphocytes that secrete antibodies. Proliferation of B cells and antibody secretion are processes controlled by the immune system, which can be lost when chromosomes and genes are damaged. B cells are generated in the bone marrow (BM) in the form of precursors and differentiated into immature B cells. Immature B cells that express functional surface IgM exit the bone marrow into secondary lymphoid tissues and differentiated into mature B cells. Interaction of mature B cells with antigen results in the generation of short-lived plasma cells, which usually secrete IgM. Some mature B cells differentiated into memory B cells or plasma cells and are retained back into the BM as long-lived plasma cells. Complex chromosomal abnormalities and some genetic events are likely to be responsible for MM disease when B cells are at the secondary lymphoid tissues (Kuehl and Bergsagel, 2002). For example, a chromosomal translocation between the immunoglobulin heavy chain gene leads to dysregulation of oncogenes at translocation partner regions (*cyclin D1* at 11q13, *FGFR3/MMSET* at 4p16.3, *c-MAF* at 16q23, and *cyclin D3* at 6p21) and is thought to be an important initiating event for MM. In addition, deletions of 13q14, the site of a putative tumour suppressor gene, are observed in about 50% of MM cases. Other molecular events, epigenetic changes and activation of oncogenes (mutations of *N-RAS* and *K-RAS,* and changes in *c-MYC*) have been

reported to be associated with disease progression (Seidl et al., 2003, Kyle and Rajkumar, 2004). Furthermore, imbalances between RANKL and osteoprotegerin in addition to some osteoclastic activity factors (in particular macrophage inflammatory protein-1α (MIP-1α) and interleukin-3 (IL-3)) are major factors responsible for the development of myeloma bone disease (Croucher et al., 2001, Choi et al., 2000, Lee et al., 2004).

### 1.2.3 Homing of multiple myeloma cells to bone marrow

The mechanisms of MM cells trafficking or homing to the BM are not well understood. The most studied factors shown to regulate MM cells homing to the BM are C-X-C chemokine receptor type 4 (CXCR-4), hypoxia and E-cadherin. During the differentiation of B cells, plasma cells become increasingly sensitive to C-X-C chemokine ligand 12 (CXCL12). It was found that MM cells in the peripheral blood express high levels of CXCR-4, but this expression level decreased in the BM suggesting that this receptor-cytokine system important in homing of MM cells to the BM, but less involved in retention of cells. The CXCR-4 inhibitor, AMD3100, and the anti-CXCR4 antibody, MAB171, inhibited the migration of MM cells *in vitro* and the homing of MM cells to the BM *in vivo* (Alsayed et al., 2007). In addition, CXCR-4 knockdown demonstrated that CXCL12/CXCR4 is a critical regulator of MM migration and homing was regulated by the phosphatidylinositide 3-kinases (PI3K) and mitogen-activated protein kinases/ extracellular signal-regulated kinases (MAPK/ERK) pathways but not by p38 MAPK (Alsayed et al., 2007). In another study, it was found that hypoxia increased the expression of CXCR-4 in MM cells resulting in increased the migration and homing of MM cells from the peripheral blood to the BM (Azab et al., 2012). E-cadherin is adhesion molecule that may have role in homing of MM cells into the BM. Azab et al 2012 demonstrated that the expression of E-cadherin decreased in MM cells isolated from MM patients with tumour progression. In addition, it was found that MM cells circulated in peripheral blood expressed low level of E-cadherin compared with MM cells in the BM in mice (Azab et al., 2012).

### 1.2.4 Multiple myeloma bone disease

MM is predominantly a malignancy of bone marrow, but tumour is observed in non-skeletal sites such as spleen and liver in end stage disease demonstrating that myeloma is not necessarily dependent on the BM in the later stages. Within bone, myeloma induces a 'vicious cycle' resulting in osteolytic bone lesions in multiple skeletal locations, including long bones, vertebrae and calvariae. It was reported that 90% of MM patients develop osteolytic bone lesions and 60% of these patients develop pathologic fractures over the course of the disease (Kyle and Rajkumar, 2004, Esteve and Roodman, 2007). Healthy bone is regulated and coordinated by bone remodeling cycle, bone formation and bone resorption throughout the skeleton. As stated above, one of the most important consequences of myeloma bone disease is the induced imbalance in bone remodelling between osteoblasts and osteoclasts affecting bone resorption and bone formation, which is eventually responsible for the formation of osteolytic bone lesions (Figure 1.4). This appears to be mediated at a cellular level with increased numbers of osteoclasts and decreased numbers of osteoblasts. This imbalance between osteoclasts and osteoblasts is responsible for an increase in bone resorption and a reduction in bone formation resulting in osteolytic bone lesions (Heider et al., 2006, Esteve and Roodman, 2007, Datta et al., 2008, Edwards et al., 2008).

#### *1.2.4.1 Multiple myeloma induced bone resorption*

The identification of MM signalling pathways and their interactions with the surrounding BM microenvironment are providing insights into the molecular mechanisms which govern tumour–host interactions. Croucher et al (2001) demonstrated that 5T2MM cells express RANKL and suggested that this was at least in part responsible for the development of osteolytic bone lesions in C57BL/KaLwRij mice. Carrying this model for myeloma treatment of mice with OPG protein prevented osteolytic bone lesions and increased bone mineral density (BMD) in femoral, tibial, and vertebral bones, suggesting that RANKL/RANK/OPG system may play a potential therapeutic target to prevent osteolytic bone disease in MM (Croucher et al., 2001).

Another factor found to induce increased bone resorption is MIP-1α. Uneda et al (2003) demonstrated that MIP-1a mRNA was expressed in freshly purified myeloma cells *in vitro*. Immunohistochemical staining showed that MIP-1a expressed in the cytoplasm of myeloma cells. In patients, mRNA expression of MIP-1a was detected in relation to inducing bone lesions (Uneda et al., 2003). In addition, Choi et al (2001) demonstrated that this chemokine stimulated osteoclast formation *in vivo* in SCID mice. Blocking MIP-1α activity in human MM-derived cell line ARH cells, by transfection with an antisense construct to MIP-1α (AS-ARH) demonstrated that both bone lesion and tumour burden were significantly decreased in mice treated with AS-ARH, suggesting that MIP-1α may have an important role in mediating both myeloma cell growth and myeloma bone disease (Choi et al., 2000).

Bone resorption is also induced by the activity of interleukin-3 (IL-3). Lee et al (2004) demonstrated that MM cell line ARH-77 and MM.IS express IL-3 and MIP-1α *in vitro*. IL-3 mRNA and protein were increased in $CD138^{+}$ myeloma cells isolated from MM patients. Also, it was found that IL-3 in combination with RANKL or MIP-1α significantly increased osteoclast formation and bone resorption comparing with RANKL or MIP-1α alone in culture. Targeting IL-3 by anti-IL-3 neutralising antibodies inhibited the formation of osteoclasts from mononuclear cells derived from MM patients growing *in vitro* suggesting that IL-3 may have an important role in mediating myeloma growth and bone disease (Lee et al., 2004).

#### 1.2.4.1.1 Targeting increased bone resorption in MM bone disease

In addition to targeting the factors discussed previously; RANKL, MIP-1α and IL-3 as a treatment to supress the increase in bone resorption in myeloma bone disease, other therapies can also be used to generally suppress bone resorption in myeloma. In particular various bisphosphonates have been used. Croucher et al (2003) investigated the effect of the bisphosphonate zoledronic acid on osteolytic tumour-bone disease.

C57BL/KaLwRij mice were injected with 5T2MM cells, resulting in induced osteolytic bone lesions. Treatment of mice with zoledronic acid prevented the formation of lytic bone lesions and bone loss as well as reducing tumor burden (Croucher et al., 2003).

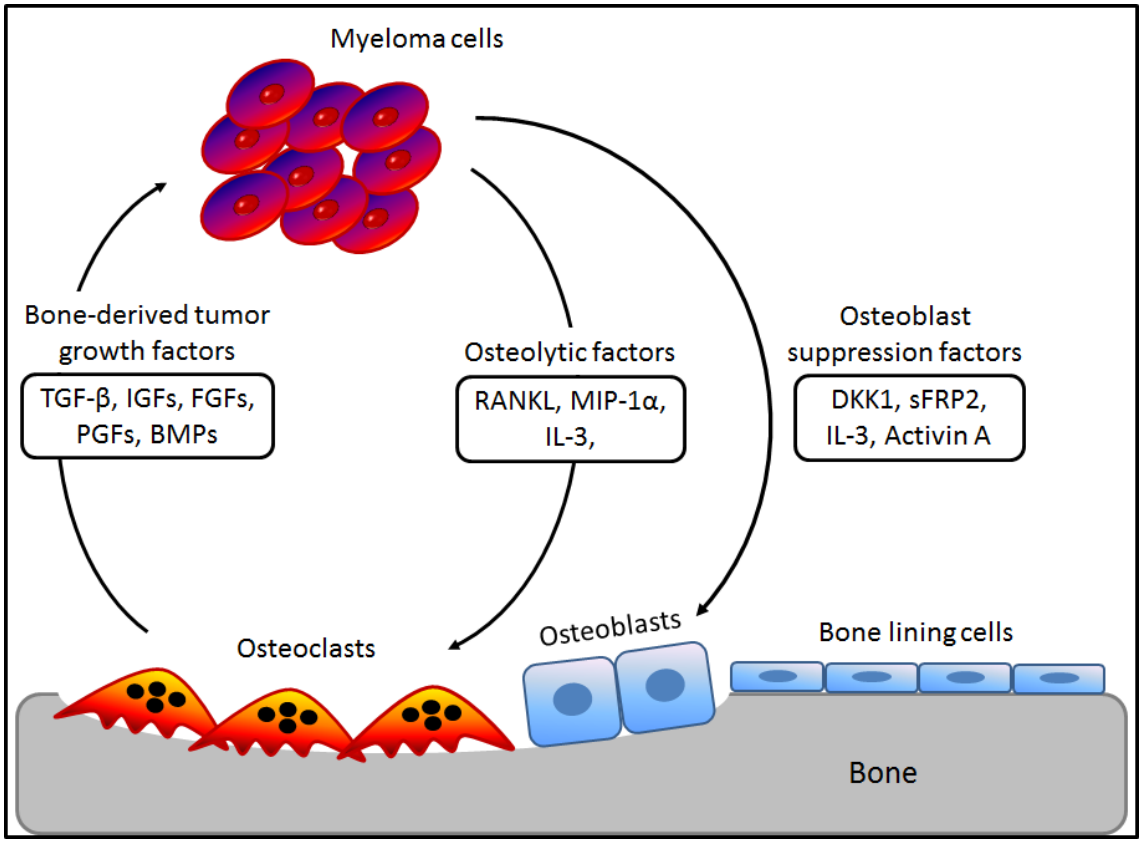


**Figure 1.4: Mechanisms responsible for multiple myeloma bone disease.** Imbalance in bone remodelling between osteoblasts and osteoclasts in the latter stage of MM induces more bone resorption. During bone resorption, growth factors such as TGF-β, IGFs, FGFs, PGFs and BMPs released by osteoclast cells permit myeloma cell survival. Important factors such as RANKL, IL-3 and MIP-1α released by MM cells activate osteoclasts. In addition, some factors such as Dkk1, sFRP-2, IL-3 and activin A released by MM cells suppress osteoblasts. These together induce osteolytic bone lesions in the late stage disease. Picture adapted from (Roodman, 2007).

#### *1.2.4.2 Multiple myeloma suppress bone formation*

As mentioned before, Wnt signaling pathway has an important role in postnatal bone formation and bone turnover. Wnt signalling pathway has a critical role in the proliferation, expansion and survival of osteoblasts though binding to Frizzled that subsequently binds to lipoprotein receptor related protein-5/6 (LRP-5/6). Binding of Wnt with its receptor complexes stimulates phosphorylation of LRP5/6, which subsequently degrade β-catenin inducing osteoblast differentiation (Westendorf et al., 2004). It was found that MM cells produce high level of Dkk1, Wnt signalling antagonist, in patients with multiple myeloma compared with control (Tian et al., 2003). Heath et al (2009) showed 5T2MM cells expressed Dkk1 an osteoblastogenesis inhibitory factor and proposed that this contributed to the development of osteolytic bone lesions in C57BL/KaLwRij mice. Targeting Dkk1 by anti-Dkk1 antibody (BHQ880, 10 mg/kg) demonstrated a reduction in the development of osteolytic bone lesions supporting the suggestion that Dkk1 plays a role in bone formation in myeloma (Heath et al., 2009). In addition, Fowler et al (2012) showed that there was an increase in the host-derived Dkk1 in myeloma-permissive KaLwRij mice resulting in a significant reduction in trabecular bone volume. Knockdown of Dkk1 in bone marrow stromal cells (BMSCs) demonstrated a reduction in the development of osteolytic bone lesions in mice suggesting that novel roles of BMSC-derived Dkk1 in bone formation in myeloma *in vivo* (Fowler et al., 2012).

As mentioned before, Wnt signalling has important roles in the mediation of osteoblast differentiation and induces bone development. Qiang et al (2008) demonstrated that Wnt signalling is necessary to promote BMP-2-mediated osteoblast differentiation. This study suggested that overexpression of Dkk1 inhibit osteoblast differentiation inducing myeloma bone disease (Qiang et al., 2008). MM cells produce another Wnt signalling antagonist factor, soluble frizzle-related protein-2 (sFRP-2). Oshima et al (2005) demonstrated that primary MM cells from patients with advanced bone lesion and human MM cell lines, RPMI8226 and U266 expressed the Wnt antagonist sFRP2 *in*

*vitro*. This study also showed that sFRP2 suppressed osteoblast differentiation and significantly inhibited mineralised nodule formation in osteoblast cell line MC3T3-E1 cells *in vitro* suggesting that sFRP2 has a role in the impairment of bone formation induced by myeloma cells (Oshima et al., 2005).

Another factor found to supress bone formation is IL-3. Ehrlich et al (2005) demonstrated that human and murine osteoblasts express IL-3 receptor (IL-3R) *in vitro*, which may allow these cells to respond to IL-3 produced by osteoblast precursors. Furthermore, it was found that the levels of IL-3 were increased in the bone marrow of myeloma patients compared with healthy controls. This study demonstrated that 100 pg/ml of IL-3 significantly inhibited osteoblast differentiation in both primary human and murine culture, but not in MC3T3-E1 cells or C2C12 cells *in vitro*. Targeting IL-3 using anti-IL-3 demonstrated partial inhibition in the suppression of osteoblast differentiation induced by bone marrow plasma from patients with high IL-3. This study suggests that IL-3 may play an indirectly role in the impairment of bone formation in MM bone disease, in addition to stimulating osteoclasts (Ehrlich et al., 2005).

The TGF-β superfamily is intimately increased an osteoblast differentiation in bone loss in myeloma. Activin A is a member of the TGF-β superfamily expressed abundantly in bone. Activin A inhibits osteoblast differentiation in MM bone disease. Activin A is increased in MM patients with osteolytic disease potentially inhibiting osteoblast differentiation via activation of mothers against decapentaplegic homolog 2 (SMAD2). Vallet et al (2010) demonstrated that inhibiting activin A with a soluble receptor, RAP-011, increased osteoblast differentiation and inhibited tumour growth. These results suggest that inhibition of activin A have potential new therapeutic strategy in tumour-related bone disease (Vallet et al., 2010). In addition, Chantry et al (2010) demonstrated that treatment of animals with an activin receptor type IIA fusion protein, ActRIIA.muFc, could increase osteoblast differentiation, bone formation and bone mass *in vivo* (Chantry et al., 2010).

## 1.3 Mouse models of multiple myeloma

### 1.3.1 History and characterisation of the 5TMM series

To support our understanding of MM bone disease, preclinical mouse models have been developed. C57BL/KalwRij mice develop a high frequency of monoclonal proliferative B-cell disorders. Most of C57BL/KalwRij mice have monoclonal gammopathy of undetermined significance (MGUS) similar to humans. 5TMM series of myeloma models originate from spontaneously developed MM in aging C57BL/KalwRij mice and have many of the features of the disease in humans. Several murine models of MM exist, but 5T2, 5T33 and 5TGM1 are the best characterized and used in most recent studies. 5TMM series of models share some common features including the selective localization of MM cells in the BM, presence of serum M-component, expression of LFA-1, CD44, VLA-4 and VLA-5 adhesion molecules, and some induce osteolytic bone disease similar to the human disease (Radl et al., 1978, Radl et al., 1979, Vanderkerken et al., 1997).

### 1.3.2 5T2 multiple myeloma model

5T2MM model originated from spontaneously developed myeloma in aging mice and represents a model for the most common forms of human MM. These cells only grow slowly *in vivo* and are mainly localised in the BM in addition to spleen. C57BL/KalwRij mice injected with 5T2MM cells develop high levels of tumour-related monoclonal immunoglobulins in their serum with reduction in the level of normal polyclonal immunoglobulins. Radiography and histology show 5T2MM cells induce osteolytic bone lesion similar to the human disease. Treatment of tumour bearing animals with bisphosphonate zoledronic acid significantly reduced the production of osteolytic bone lesions and decrease tumour burden in bone in 5T2MM-bearing mice (Radl et al., 1985, Vanderkerken et al., 1997, Asosingh et al., 2000b, Croucher et al., 2003).

### 1.3.3 5T33 multiple myeloma model

5T33MM model originated from a spontaneously developed myeloma in aging mice. These cells can grow *in vitro* as well as *in vivo*. In culture, 5T33MM cells grow as non-adherent single cells or in small loosely adherent clusters. 5T33MM grow rapidly in C57BL/KaLwRij mice and mainly localised in the BM in addition to spleen and liver. 5T33MM cells cause myeloma disease in inoculated C57BL/KaLwRij mice after 5-8 weeks of injection with $10^5$ marrow cells of 5T33 myeloma mice. C57BL/KalwRij mice post injected with 5T33MM cells develop high levels of tumour-related monoclonal immunoglobulins in their serum with reduction in the level of normal polyclonal immunoglobulins similar to 5T2MM cells. In contrast to human disease, radiography and histology show 5T33MM cells do not induce osteolytic bone lesions (Manning et al., 1992, Vanderkerken et al., 1997, Asosingh et al., 2000b).

### 1.3.4 5TGM1 multiple myeloma model

5TGM1 model was derived from the 5T33 model. 5T33MM cells were passaged in mice, and cells were then obtained from the marrow of 5T33MM-bearing mice cultured and cloned. These cells have all the features of human disease including the characteristic lytic bone lesions, in contrast to 5T33MM cells that do not induce osteolytic bone lesions in mice. 5TGM1 cells grow rapidly *in vitro* as well as *in vivo*. In culture, 5TGM1 cells grow as non-adherent single cells or in small loosely adherent clusters. C57BL/KalwRij mice injected with 5TGM1 cells develop high levels of tumour-related monoclonal immunoglobulins in their serum similar to 5T2MM cells and 5T33MM cells. Radiography and histology shows that 5TGM1 cells produce osteolytic bone lesions similar to the human disease. The bisphosphonate ibandronate has been shown significantly reduce the osteolytic bone lesions in 5TGM1-bearing mice (Garrett et al., 1997, Dallas et al., 1999).

## 1.4 The early stages of multiple myeloma disease and the myeloma niche

The general localisation of myeloma to the skeleton and recent studies suggest that the early stages of myeloma development are dependent on the surrounding BM microenvironment, however the characteristics of the early stage 'BM-dependent' microenvironment remains unknown. In contrast, in late stage disease; the myeloma cells are not BM microenvironment dependent, but appear to survive and grow interdependent of the bone (Pagnucco et al., 2004, Damiano et al., 1999, Hideshima et al., 2002, Damiano and Dalton, 2000). It is unclear whether myeloma cells attach to sites of bone formation, quiescent bone lining cells or remain close to a collagen matrix, a known store of growth factors. The effects of colonising myeloma cells on the adjacent micro-anatomical sites post-attachment are also unknown. Despite the present therapeutics there is an urgent clinical need for new therapies, and one such strategy targets the early stages of disease including myeloma cell colonisation and survival, where myeloma is more dependent on the bone microenvironment. Characterising the putative 'myeloma niche' (a myeloma permissive microenvironment) may offer novel therapeutic targets to treat patients. It is not unfeasible that colonising myeloma cells may retain the molecular machinery of haematopoietic stem cells (HSCs) and modify the HSC niche into a myeloma permissive niche or exploit the HSC niche to establish disease. These following sections will describe HSCs and the HSC niche, and evaluate the potential mechanisms colonising myeloma cells may exploit to establish colonies within the BM microenvironment.

### 1.4.1 The haematopoietic stem cell niche

The marrow cavity within bone is the main site of haematopoiesis in adult human. Adult BM comprises of ECM, HSCs, MSCs, blood cells and their precursors, osteoblasts, osteoclasts, fibroblasts, endothelial cells, and adipocytes (Fliedner, 1998, Wang et al., 2006, Muguruma et al., 2006). Stem cells are defined as the earliest undifferentiated cell types characterised by extensive capacity for self-renewal and the ability to differentiate into a range of specialized cell types (Zhang et al., 2003). HSCs differentiate into blood

progenitor cells and all blood cell types that have characteristic morphologies and specialized functions including myeloid; monocytes, granulocytes, erythrocytes and megakaryocytes, lymphoid cells; natural killer cells, T-cells and B-cells (Figure 1.5) (Akashi et al., 2000, Kondo et al., 1997). HSCs can be divided into two groups: long-term reconstituting (LTR) cells, which are seen frequently at the bone-lining osteoblastic cell surface and the short-term reconstituting (STR) cells. The LT-HSCs are characterised by their ability to support haematopoiesis for more than six months while ST-HSCs are characterised by their ability to repopulate blood elements for several weeks (Harrison and Zhong, 1992, Zhong et al., 1996, Zhao et al., 2000b).

The term 'niche' was firstly described by Schofield in 1978, who proposed HSCs are associated with bone by cell-cell contacts providing a microenvironment for HSCs self-renewal, proliferation and preventing their differentiation (Schofield, 1978). The HSC niche is defined as a specific regulatory microenvironment in adult bone marrow, which acts as a soil for HSCs where these stem cells are housed and maintained by self-renewal. Outside this niche HSCs cannot self-renew, but differentiate to large numbers of progeny as well as to other cell types and ultimately produce mature blood cells (Wilson and Trumpp, 2006, Yin and Li, 2006). The HSC niche is composed of the osteoblastic niche (endosteum) and vascular niche (sinusoidal vessels) (Figure 1.6). Zhang et al (2003) showed that an increase in trabecular bone and/or trabecular N-cadherin$^{+}$ osteoblasts correlated to an increase in HSCs (Zhang et al., 2003). Subsequently, Visnjic et al (2004) identified a reduction of HSCs can be observed in the bone marrow following ablation of osteoblast-lineage cells in transgenic mice. Extramedullary hematopoiesis was found in alternative sites such as spleen and liver (Visnjic et al., 2004). These together provide strong evidence that osteoblastic niche supports hematopoiesis in the HSC niche.

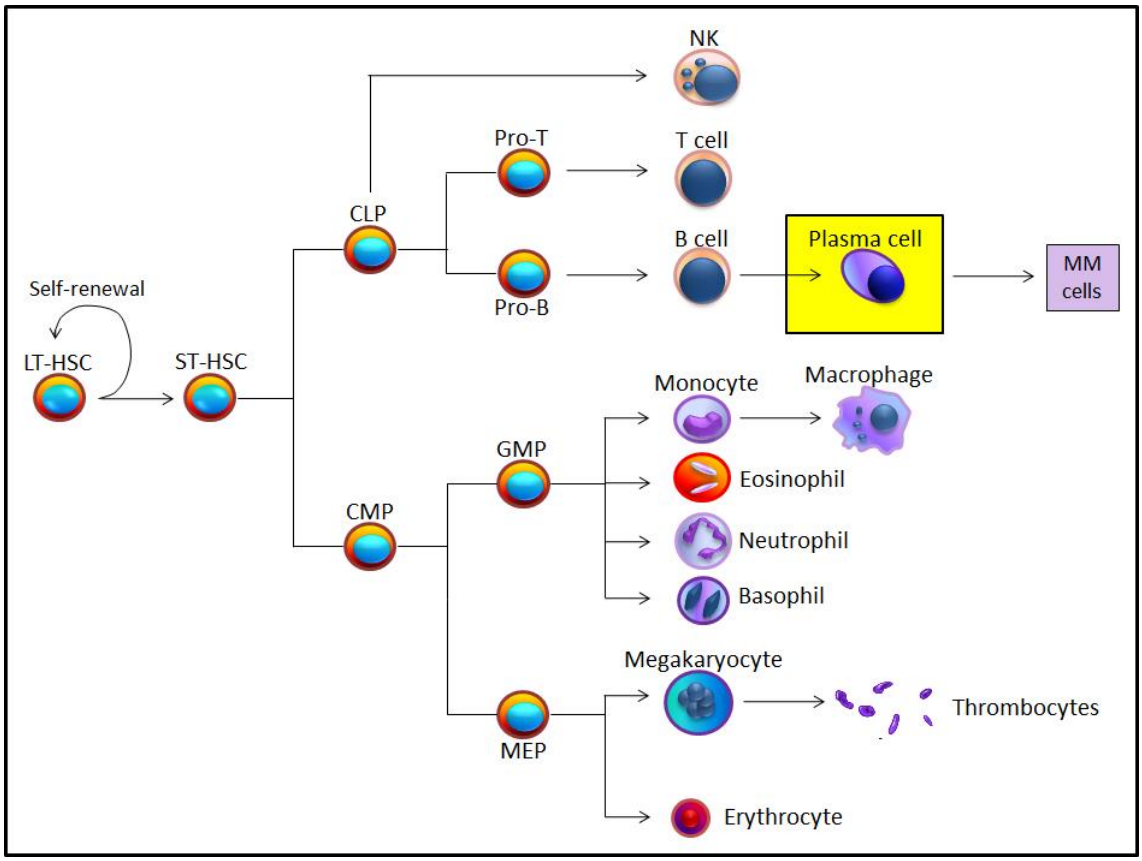


**Figure 1.5: Differentiation of HSCs in bone marrow.** ST-HSCs differentiate to CLP (common lymphoid progenitor) and CMP (common myeloid progenitor). GMP (granulocyte-macrophage precursor) and MEP (megakaryocyte-erythrocyte precursor) are progeny of the CMP, generating monocytes, granulocytes megakaryocytes and erythrocytes respectively. On the other hand, pro-T cell and pro-B cell are the progeny of the CLP, generating T-cells and B-cells, which differentiation into plasma cells in lymph nodes. MM cells are terminal plasma B cell malignancy derived from bone marrow plasma cells. Picture adapted from (Huntly and Gilliland, 2005).

Zhang et al (2003) used immunohistochemistry technology to identify the HSC niche. It was found that LT-HSCs reside in the osteoblastic niche (Figure 1.5) and were only attached to the N-cadherin$^{+}$ osteoblasts (Zhang et al., 2003). Xie et al (2009) developed new ex vivo real-time imaging technology. Green fluorescent protein expressing (GFP$^{+}$) HSCs homed through the vascular niche to the osteoblastic niche and attached to N-cadherin$^{+}$ osteoblast cells in irradiated mice (Xie et al., 2009). Lo Celso et al (2009)

used a combination of high resolution confocal microscopy and two-photon video imaging technology that allowed observation of homing of individual HSC in calvarial bone marrow of living mice in real time. HSCs have been observed closer to bone and osteoblasts in irradiated and *c-Kit*-receptor-deficient recipient mice (Lo Celso et al., 2009). It is only by using modern microscope that has permitted researchers to identify the stem cells in the niche. In relation to MM disease, no study has shown the location of colonising myeloma cells in relation to osteoblasts on the endosteal surface. It is unclear if MM cells have the ability to adhere to N-cadherin$^{+}$ osteoblasts.

Another specialized microenvironment used by HSC is the vascular niche, sinusoid vessels. Sinusoid endothelial cells are differentiated from the MSCs. The vascular niche together with osteoblastic niche support the HSCs in the HSC niche, in which the vascular niche promotes HSCs proliferation and further differentiation. It was reported that the sinusoid vessels are surrounded by endothelial cells secreting a high amount of CXCL12 chemokine. This chemokine is required for the maintenance of HSCs in the vascular niche as well as the maintenance of sinusoidal adjacent HSCs (Sugiyama et al., 2006). Alsayed et al (2007) showed CXCR4 expressed on MM cells are responsible for migration and homing of the MM to BM in response to high levels of SDF-1 (CXCL12). Targeting CXCR4 by specific inhibitor (AMD3100) and anti-CXCR4 antibody (MAB171) have been shown to inhibit MM cells migration *in vitro* (Alsayed et al., 2007). Ding et al (2012) showed that Stem cell factor (SCF) was primarily expressed by perivascular cells throughout the BM. knock-out SCF from both endothelial and receptor-expressing perivascular cells resulting in HSCs lost from BM suggesting that HSCs reside in a perivascular niche (Ding et al., 2012). More recently, Ding et al (2013) showed that showed that CXCL12 was primarily expressed by perivascular stromal cells. Deletion of CXCL12 from endothelial cells and/or from perivascular stromal cells, but not from osteoblasts depleted HSCs from BM and mobilized these cells into circulation (Ding and Morrison, 2013).

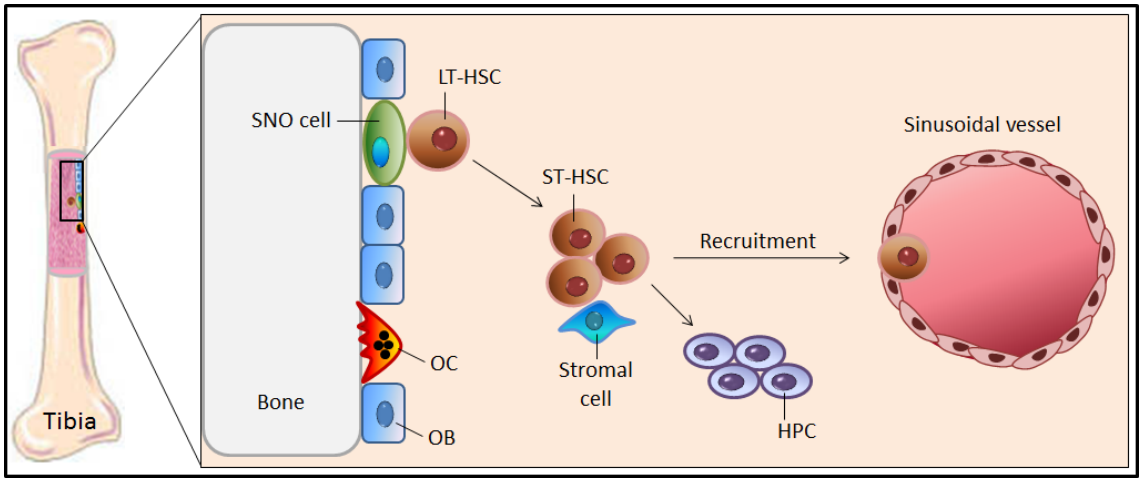


**Figure 1.6: N-cadherin$^+$ osteoblasts are required to maintain quiescent hematopoietic stem cells.** Hematopoietic stem cells (HSCs) line the endosteal bone surfaces. Spindle-shaped N-cadherin$^+$ osteoblasts serve as HSC docking sites, which maintain quiescent cells and prevent their differentiation (Zhang et al., 2003). In response to injury, HSCs leave the osteoblastic niche and are recruited to the vascular niche. HSCs outside their niche become active and differentiate to large numbers of cell progeny as well as to other cell types and ultimately produce mature blood cells. Picture adapted from (Yin and Li, 2006).

### 1.4.2 Cellular and molecular crosstalk in the HSC niche

The cellular interactions in the HSC niche occur between HSCs and osteoblasts at endosteal surfaces to maintain HSCs quiescence. The endosteal surface is enriched for primary HSCs indicating a potential important role of the osteoblastic niche to support hematopoiesis and regulate HSC niche (Calvi et al., 2003, Zhang et al., 2003, Wu et al., 2009). Passegué et al (2005) demonstrated that LT-HSCs are maintained as quiescent or slowly cycling cells comparing with ST-HSCs, which are maintained as active cycling cells. This result suggests that LT-HSCs require osteoblasts to remain quiescent in the niche (Passegue et al., 2005). In contrast, in response to higher levels of stromal cell-derived factor 1 (SDF-1) and fibroblast growth factor-4 (FGF-4) LT-HSCs exit the osteoblastic niche and migrate towards the central marrow or toward the vascular niche (Zhang et al., 2003, Xie et al., 2009, Askmyr et al., 2009, Lo Celso et al., 2009).

Several molecules are expressed and secreted by HSCs and osteoblasts that have been identified in their interactions. These molecular interactions appear to maintain the HSCs quiescent in the niche. Interacting molecular pairs include Notch/jagged 1 (Jag1), angiopoietin-1 (Ang-1)/tyrosine kinase receptor 2 (Tie2), osteopontin (OPN)/CD44, N-cadherin/N-cadherin and CXCR4/CXCL12 (Figure 1.7). It is possible that colonizing myeloma cells may retain the molecular machinery present in HSCs to hijack the HSC niche (Calvi et al., 2003, Arai et al., 2004, Nilsson et al., 2005, Stier et al., 2005, Zhang et al., 2003, Xie et al., 2009). This would allow a subpopulation of myeloma cells to remain quiescent or dormant and escape the effect of the potent agents directed at cycling cells.

Notch signalling has an essential supporting role in HSC proliferation and expansion. It was found that activating PTH/PTHrP receptors (PPRs) stimulated the production of high levels of Notch ligand, jagged 1 (Jag1) resulting in an increase in the number of HSCs *in vivo*. This study suggested that Notch/Jag1 signalling supports the HSC niche (Calvi et al., 2003). Jundt et al (2004) demonstrated the expression of Notch1 and Notch2 proteins as well as their ligand, Jag1 in MM cells (Jundt et al., 2004). Together these studies suggest that Notch/Jag1 mediated cell-cell interactions between MM cells and their microenvironment inducing proliferation of multiple myeloma cells.

Osteoblasts express Ang-1 that binds to tyrosine kinase receptor 2 (Tie-2), which is expressed in HSCs. Ang-1/Tie-2 activity plays an important role for HSCs in maintaining quiescence in the niche as well as inducing adhesion between HSCs and osteoblastic cells (Arai et al., 2004). Giuliani et al (2003) demonstrated that human myeloma cell lines; RPMI 8226, U266, OPM-2, XG-1 and XG-6 expressed Ang-1. In addition, human myeloma cell lines; XG-1 and XG-6 also expressed Tie-2. Moreover, it was found that Ang-1 and Tie-2 was expressed in patients with MM, suggesting a possible role in inducing angiogenesis in MM (Giuliani et al., 2003). On the other hand,

expression of Tie-2 by MM cells is a potential mechanism to establish colonies in the HSC niche via interactions with Ang-1 expressed by osteoblast cells.

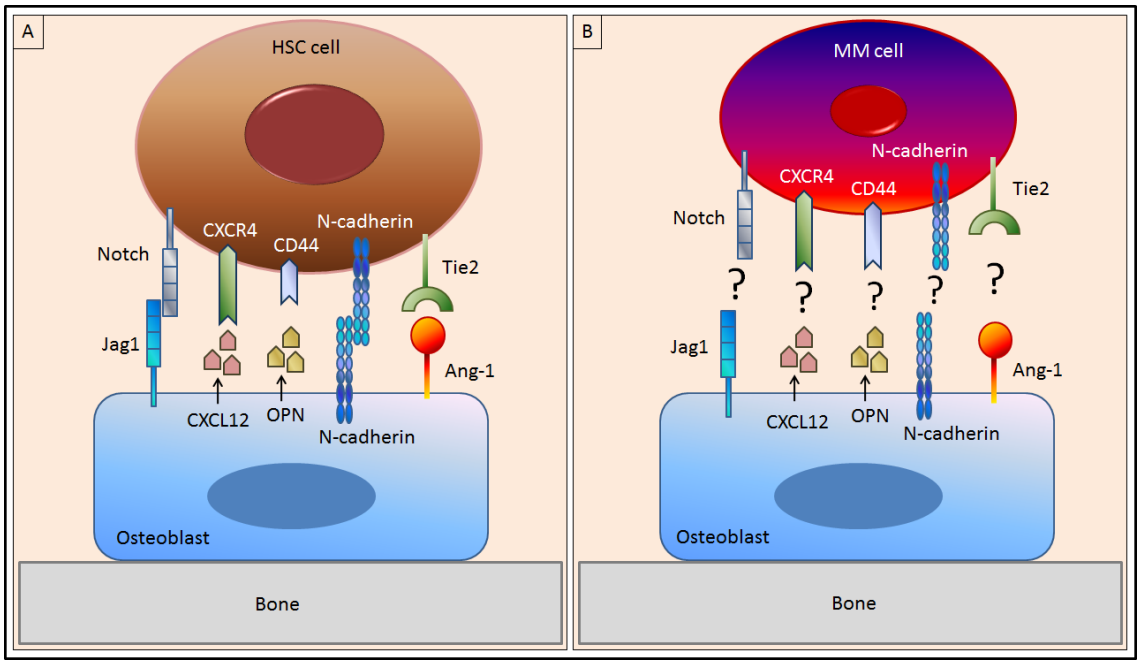


**Figure 1.7: Opportunities of multiple myeloma cells to colonise the hematopoietic stem cell niche.** (A) Interactions between HSCs and osteoblasts are mediated by several secreted factors and receptors expressed on both cells types including; Notch/jagged 1 (Jag1), angiopoietin-1 (Ang-1)/tyrosine kinase receptor 2 (Tie2), osteopontin (OPN)/CD44 N-cadherin/N-cadherin and C-X-C chemokine receptor type 4 (CXCR4)/ C-X-C chemokine ligand 12 (CXCL12). HSCs require osteoblasts to be quiescent in the niche. Interactions between osteoblasts and colonising MM cell in the putative MM niche are unknown. (B) Potential interactions between MM cells and osteoblasts to establish the colonization of MM cells into the bone. Picture adapted from (Wilson and Trumpp, 2006).

One mechanism by which HSCs are regulated in the HSC niche is via OPN, an acidic glycoprotein, expressed by osteoblasts. It was shown that OPN expression on the endosteal surface resulted in migration of HSCs toward the endosteal region (Nilsson et al., 2005). In addition, data from OPN-deficient mice demonstrated an increase in the number of HSCs in bone marrow microenvironment and a reduction in their apoptosis.

Therefore, this data provides evidence that OPN is a negative regulator for HSC proliferation in the HSC niche (Stier et al., 2005). Asosingh et al (2000) showed CD44 is expressed in the 5T33MM cell line and contributes to adherence of myeloma cells to BM stromal cells (Asosingh et al., 2000a). Vincent and Mechti (2004) showed CD44 has an important role in MM cell survival (Vincent and Mechti, 2004). In relation to early stage MM disease, CD44 may be exploited to establish MM cells in the HSC niche via interactions with OPN expressed by osteoblast cells.

HSCs express CXCR4 which binds to CXCL12 for the maintenance and migration of HSCs in the BM. It was reported that CXCR4-CXCL12 signaling play an important role in the regulation of HSCs in both vascular and endosteal niches. Sugiyama et al (2006) demonstrated that HSCs contact with the cells that express high amounts of CXCL12 called CXCL12-abundant reticular in vascular niche as well as in at the endosteum (Sugiyama et al., 2006). Broxmeyer et al (2010) demonstrated that blocking the interaction of CXCL12 and CXCR4 by AMD3100, a CXCR4 antagonist results in a rapid mobilization of HSCs from the BM into the peripheral blood. This result showed that CXCR4-CXCL12 signaling retains HSCs in the BM microenvironment (Broxmeyer et al., 2005). In relation to MM, Azab et al (2009) showed that using AMD3100 inhibited the migration of MM cells *in vitro* and inhibited the homing of MM cells to the BM *in vivo* (Azab et al., 2009).

N-cadherin is an adhesion molecule expressed by both HSCs and osteoblasts. Puch et al (2001) showed human $CD34^+$ HSCs express N-cadherin. Treatment of these cells with monoclonal anti-N-cadherin antibodies resulted in a reduction in the colony formation, which suggested a direct interaction between osteoblasts and HSCs via N-cadherin (Puch et al., 2001). *In vitro*, Aria and Suda showed enhancements of both HSCs and stromal cell adhesion and inhibition of cell division of HSCs by enforced N-cadherin expression suggesting a key role of N-cadherin-mediated adhesion and maintaining HSCs quiescence in the osteoblastic niche (Arai and Suda, 2007). Using gene array

studies Dring et al (2004) showed N-cadherin is expressed in t(4;14) MM cases (Dring et al., 2004). However, no publication has addressed the blocking of N-cadherin in myeloma cells. In addition, it was found that N-cadherin allows HSCs to localize to osteoblasts on endosteal bone surfaces in the HSC niche (Zhang et al., 2003, Xie et al., 2009). Expression of N-cadherin may be exploited by myeloma cells to establish the HSC niche via interactions with N-cadherin expressed by osteoblasts.

## 1.5 N-cadherin

### 1.5.1 Structure of N-cadherin cell-cell adhesion molecule

N-cadherin is a member of a $Ca^{2+}$-dependent cell-cell adhesion receptor family known as cadherin 2, containing extracellular domain, transmembrane domain and cytoplasmic domain (Figure 1.8). The extracellular domain of N-cadherin contains five extracellular repeats of ~110 amino acids each. The cytoplasmic domain directly binds to p120 catenin, β-catenin and α-catenin cleaved by γ-secretase protein and translocate the carboxy-terminal fragment of N-cadherin with β-catenin to the nucleus (Figure 1.9). Cleaved N-cadherin mediates signalling pathway following cell-cell adhesion (Miyatani et al., 1992, Gumbiner, 2005).

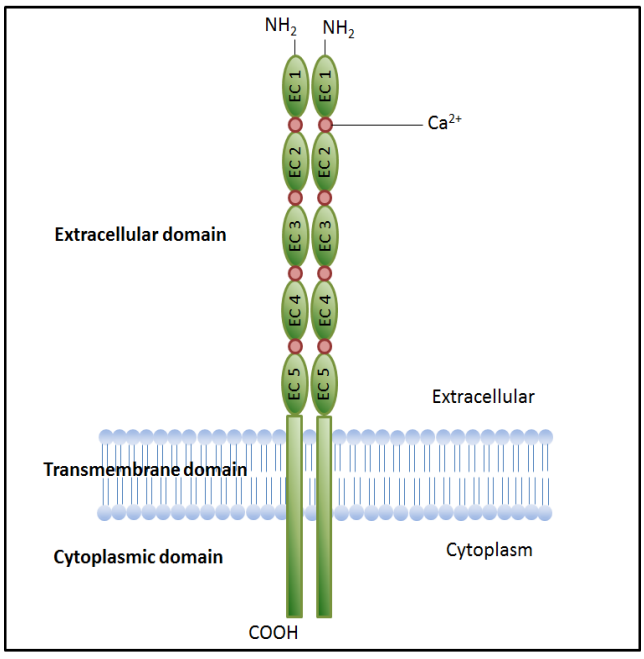


**Figure 1.8: The structure of N-cadherin.** N-cadherin is a member of the $Ca^{2+}$-dependent cell-cell adhesion receptor family containing extracellular domain, transmembrane domain and cytoplasmic domain. The extracellular domain of N-cadherin contains five extracellular repeats of ~110 amino acids each. Picture adapted from (Gumbiner, 2005).

### 1.5.2 N-cadherin expression in bone cells

Within the skeleton there are four basic types of bone cells; osteoclasts, osteoblast, bone lining cells and osteocytes. Mbalaviele et al (1995) showed that E-cadherin was expressed by osteoclasts, but no expression of N-cadherin was detected in these cells (Mbalaviele et al., 1995). In osteoblasts, Ferrari et al (2000) demonstrated that N-cadherin was expressed and this was increased during osteoblastogenesis. This study suggested a role for N-cadherin in the late stage of osteoblast differentiation (Ferretti et al., 2002). Kawaguchi et al (2001) also showed that N-cadherin was expressed by osteoblasts and this expression was increased during osteoblastogenesis (Kawaguchi et al., 2001). Marie (2002) demonstrated that the marked increases in expression of N-cadherin during osteoblast differentiation was correlated with increased cell-cell interactions in mature osteoblasts (Marie, 2002). In bone lining cells, Zhange et al (2003) demonstrated that N-cadherin was expressed by spindle-shaped osteoblasts (bone lining cells) and has an important role in maintaining HSCs quiescence in the HSC niche (Zhang et al., 2003). Ferrari et al (2000) demonstrated that N-cadherin was not expressed by osteocytes (Ferrari et al., 2000). Kawaguchi et al (2001) also showed that N-cadherin was not expressed by the osteocyte-like cell line MLO-Y4 (Kawaguchi et al., 2001). There studies showed that osteoblasts and bone lining cells, but not osteoclasts and osteocytes express N-cadherin.

### 1.5.3 N-cadherin interacts with FGFR mediating signalling

Fibroblast growth factor receptor (FGFR) has an important role in neurogenesis, cell migration and cell differentiation. Recent evidence has pointed to an interaction between N-cadherin and FGFR that might be able to serve as replacement ligands and/or receptor-binding partners that modulate signalling by the conventional ligands. Williams et al (2001) demonstrated that N-cadherin interacted with FGFR and was required for axonal growth. Blocking N-cadherin by antibody inhibited the neurite outgrowth response stimulated by N-cadherin (Williams et al., 2001). Suyama et al (2002) demonstrated that N-cadherin binds to FGFR-2 in breast cancer cells and this

binding increase migration, invasion, and secretion of extracellular proteases in breast cancer cells (Suyama et al., 2002). Sanchez-Heras et al (2006) showed that N-cadherin interacts with FGFR and this interaction is dependent on the presence of the acid box motif that can be found in the linker region between D1 and D2 (Sanchez-Heras et al., 2006). These studies produced some evidence for the possibility that N-cadherin binds to FGFR and mediates signalling.

### 1.5.4 N-cadherin mediates the interaction of HSCs with osteoblasts or bone lining cells in the niche

As stated previously in this chapter, Zhang et al (2003) demonstrated that HSCs home into the endosteal surfaces and attach to N-cadherin$^{+}$ osteoblasts. This attachment maintains the HSCs in a quiescent state in the HSC niche (Zhang et al., 2003). In addition, Xie et al (2009) tracked the HSCs by using high resolution microscopy and demonstrated that HSCs home to an osteoblastic niche and attach to N-cadherin$^{+}$ osteoblasts (Xie et al., 2009). Hosokawa et al (2010) showed that overexpression of N-cadherin inhibited the division of HSCs. In addition, knockdown of N-cadherin in HSCs reduced the long-term engraftment of HSCs *in vivo* and reduced the adhesion of HSCs onto the bone surfaces (Hosokawa et al., 2010). These studies showed that N-cadherin has an important role as N-cadherin is utilized in the location of HSCs to healthy bone.

### 1.5.5 N-cadherin interacts with Axin and LRP5a and negatively regulate Wnt/β-catenin signalling and bone formation

Canonical Wnt signalling plays an important regulatory role in the maintenance of bone mass and in bone formation. The canonical wnt signalling pathway is mediated by binding of wnt3a to LRP5 and frizzled. This binding activates dishevelled family proteins; axin, adenomatous polyposis coli protein (APC), Frat1, glycogen synthase kinase 3β (GSK3β) and ultimately β-catenin to reach the nucleus, promoting

osteoblastogenesis (Rawadi and Roman-Roman, 2005). Current evidence indicated some extracellular natural antagonists; SFRPs, connective tissue growth factor (CTGF), Wnt-inhibitory factor 1 (WIF1), Cerberus, Wise, Dkk and sclerostin that regulate the Wnt canonical signalling pathway (Kawano and Kypta, 2003, Rawadi and Roman-Roman, 2005). Hay et al (2009) demonstrated that N-cadherin interacts with LRP5 and axin in addition to directly binding with β-catenin to regulate osteoblastogenesis. The data showed N-cadherin-axin-LRP5 interactions increased β-catenin degradation resulting in negatively regulation of wnt signalling and decreased osteoblast differentiation (Hay et al., 2009a). Moreover, data from murine MC3T3-E1 osteoblastic cells and N-cadherin transgenic mice, demonstrated that over-expression of N-cadherin inhibited osteoblast proliferation and survival through increasing β-catenin degradation by N-cadherin-axin-LRP5 interactions *in vitro* and *in vivo* (Hay et al., 2009b).

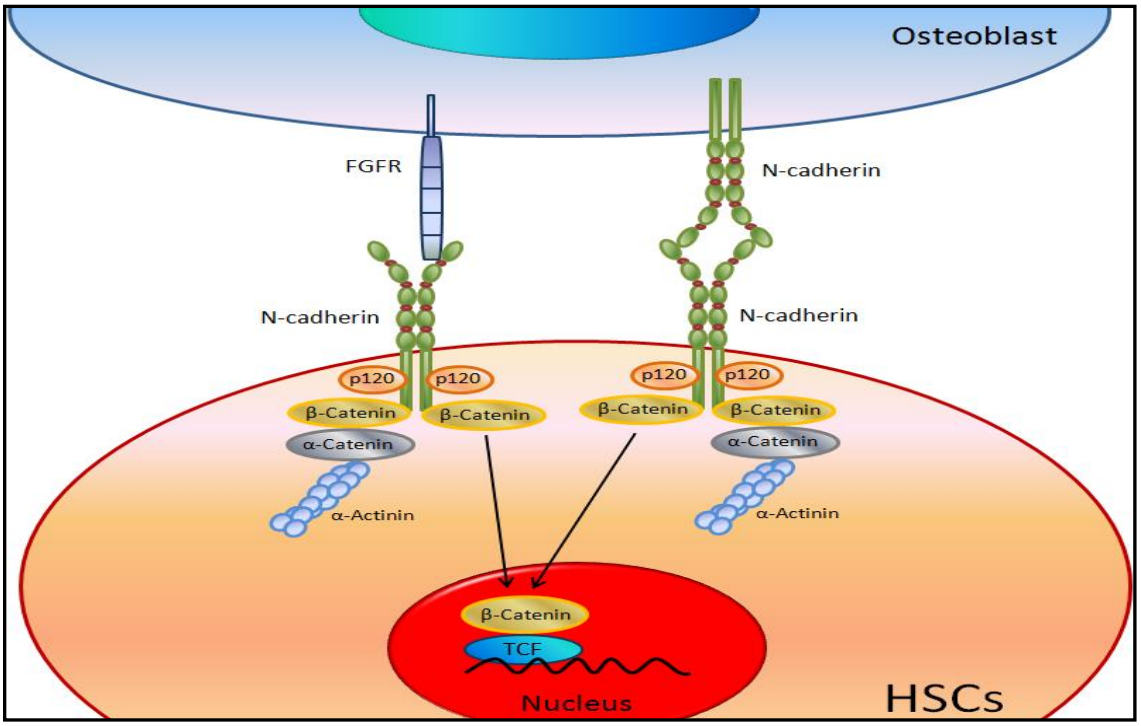


**Figure 1.9: The N-cadherin signalling pathways.** During cells-cell interactions, N-cadherin associates with N-cadherin and/or FGF receptors family. The cytoplasmic domain is cleaved and translocate the carboxy-terminal fragment of N-cadherin with β-catenin to the nucleus mediates the signalling following cell-cell adhesion. Picture adapted from (Christofori, 2006).

### 1.5.6 N-cadherin may established the colonisation of MM cell in the HSC niche

N-cadherin is a key component promoting quiescent HSCs and is expressed during osteoblast differentiation. Blaschuk et al (1990) reported that extracellular-1 of extracellular domain contain His-Ala-Val (HAV) motif sequence (Figure 1.10), which play an important role in N-cadherin functions (Blaschuk et al., 1990). ADH-1, N-Ac-CHAVC-NH2, is an agent targeting the HAV motif on extracellular-1 of N-cadherin was recently used as an anticancer agent (Shintani et al., 2008). During tumour progression, the invasion and metastatic properties acquired by cancer cells are initially linked to expression of adhesion molecules. Changes in expression of adhesion molecules mediate the interaction of cancer cells from their primary site to establish new interactions with the surrounding microenvironment. N-cadherin is expressed in several type of cancer including melanoma, breast cancer, prostatic cancer, gastric carcinoma, bladder carcinoma, overian carcinoma and pancreatic cancer mediating tumour cell invasion and metastasis (Li et al., 2001, Augustine et al., 2008, Hazan et al., 2004, Tanaka et al., 2010, Yanagimoto et al., 2001, Lascombe et al., 2006, Sarrio et al., 2006, Shintani et al., 2008).

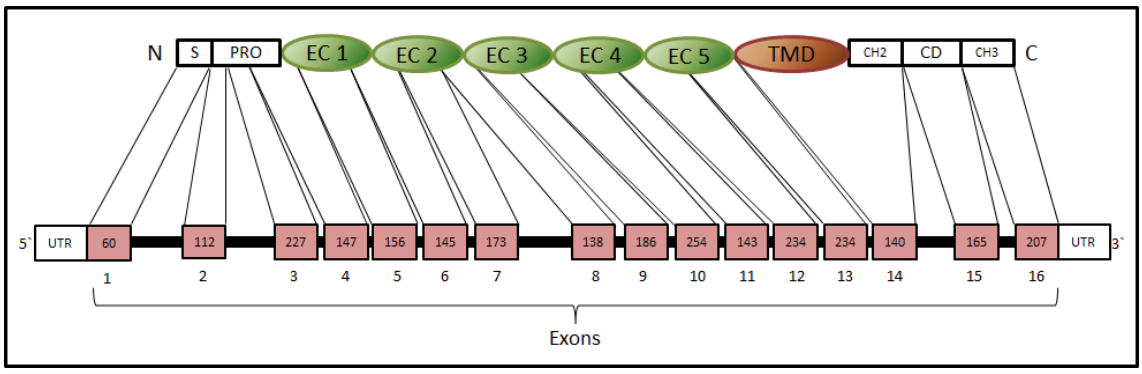


**Figure 1.10: Schematic of Mus musculus N-cadherin.** N-cadherin consists of 16 exons. The extracellular (EC) domain is encoded from exon 1 to exon 13 whereas the transmembrane domain (TMD) and cytoplasmic domain (CD) are encoded with exon 14 to exon 16. EC1 of cadherin contains His-Ala-Val (HAV) motif sequence, which play an important role in cadherin functions. C is carboxy-terminal; N is amino-terminal; PRO is propeptide; S is signal peptide; UTR is untranslated region.

## 1.6 Aim of the study

Multiple myeloma is a plasma cell malignancy that causes extensive osteolytic bone disease. Present treatments target end stage disease but understanding how tumours in bone are initiated may offer new approaches to prevent/suppress colonization. It is clear that myeloma cells form specific interactions with the bone microenvironment, where they can remain dormant and protected from current therapy to eventually proliferate and cause disease progression (Roodman, 2007). N-cadherin is an adhesion molecule that allows HSCs to localize to osteoblasts on endosteal bone surfaces in the HSC niche (Zhang et al., 2003, Xie et al., 2009). During tumour progression in solid tumours, the invasion and metastatic properties acquired by cancer cells have been linked to expression of N-adhesion molecules and cadherin switching from E-cadherin to N-cadherin (Li et al., 2001, Lascombe et al., 2006, Gravdal et al., 2007). Little was known at the start of my studies about N-cadherin expression, cell surface distribution or formation in MM. The hypothesis is that myeloma cells locate close to bone surfaces which is where the various bone cells are found. In addition, as N-cadherin is expressed by osteoblasts, but not by osteoclasts or osteocytes (Mbalaviele et al., 1995, Ferrari et al., 2000, Kawaguchi et al., 2001), the hypothesis that "**myeloma cells utilise N-cadherin to adhere to osteoblasts *in vitro* and *in vivo* during colonization of bone**" has been tested in this study.

The hypothesis of my study was addressed through four objectives.

1. Determine whether the stem cell marker N-cadherin is expressed by myeloma cells and osteoblasts (**chapter 3**).

2. Determine whether the expression of N-cadherin mediates attachment of osteoblasts/myeloma cells *in vitro* (**chapter 4**).

3. Determine whether different calvarial bones; frontal, parietal and interparietal contain different bone microenvironments (**chapter 5**).

4. Determine whether the expression of N-cadherin is important in the attachment of osteoblasts/myeloma cells *in vivo* (**chapter 6**).

# 2 Chapter 2: Materials and Methods

## 2.1 Materials

### 2.1.1 General chemicals and reagents

All chemicals, reagents and buffers used in this project were purchased from Sigma® Chemical company Ltd (UK), unless otherwise stated. Trizol®, chloroform and isopropanol were purchased from Invitrogen (UK). Oligonucleotides were purchased from Invitrogen (UK). Deoxynucleoside triphosphates (dNTPs) were purchased from Promega (UK). Agarose and ethidium bromide used for gel electrophoresis were purchased from Invitrogen (UK).

A 100-1500 bp DNA Ladder was purchased from Invitrogen (UK). The TaqMan Universal master Mix II and TaqMan® gene expression assays were purchased from Applied Biosystems (UK). QIAquick Gel Extraction Kit was purchased from QIAGEN Ltd (UK). UltraPure™ DNase/RNase-free distilled water was purchased from Invitrogen (UK). Quant-iT™ PicoGreen ® dsDNA Reagent and Kits used to normalise ALP activity with DNA content were purchased from Invitrogen (UK).

### 2.1.2 Immunofluorescence reagents and antibodies

Rabbit monoclonal anti-N-cadherin antibody (Catalogue No. 04-1126) used as a primary antibody (C-terminus of mouse N-cadherin) was purchased from Millipore (UK). Normal rabbit IgG was used as an isotype negative control (Catalogue No. AB-105-C) and Northern Lights™ donkey anti-rabbit IgG-NL637 used as secondary antibody (Catalogue No. NL005) were purchased from R&D systems (UK). ProLong® Gold reagent contains DAPI nuclear stain (Catalogue No. P-36931) was purchased from Invitrogen (UK).

### 2.1.3 Immunohistochemistry reagents and antibodies

A rabbit monoclonal anti-N-cadherin antibody (Catalogue No. 04-1126) used as a primary antibody (C-terminus of mouse N-cadherin) was purchased from Millipore (UK). Normal rabbit IgG was used as an isotype negative control (Catalogue No. AB-105-C) was purchased from R&D systems (UK). VECTASTAIN Elite ABC kit (Catalogue No. PK-6101) containing; normal rabbit serum, biotinylated anti-rabbit secondary antibody and VECTASTAIN® Elite® ABC reagent was purchased from Vector laboratories (UK). ImmPACT™ DAB kit (Catalogue No. SK-4105) was purchased from Vector laboratories (UK).

### 2.1.4 Flow cytometry reagents and antibodies

A mouse monoclonal anti-N-cadherin antibody (Catalogue No. 04-1126) was used as a primary antibody (N-terminus of mouse N-cadherin) was purchased from Sigma (UK). Mouse IgG antibody (Catalogue No. I-2000) used as an isotype negative control was purchased from Vector Laboratories (UK). Lightning-Link™ Atto637 conjugation kit (Catalogue No. 746-0010) used to label both mouse monoclonal anti-N-cadherin antibody and mouse IgG antibody was purchased from Innova Biosciences (UK).

### 2.1.5 Enzymes

DNase I was purchased from Invitrogen (UK). SuperScript™ III reverse transcriptase kit and Platinum *Taq DNA* polymerase kit and Collagenase II were purchased from Invitrogen (UK).

### 2.1.6 Tissue culture materials

Tissue culture media; RPMI1640 medium and Minimum Essential Medium (MEM) alpha were purchased from Invitrogen (UK). Fetal calf serum (FCS) was purchased from Invitrogen (UK). Penicillin/Streptomycin, amphotericin B, sodium pyruvate ($Na_2PO_3$) and non-essential amino acids (NEAA) were purchase from Invitrogen (UK). β-glycerophosphate, ascorbic acid and dexamethasone were purchased from Sigma (UK).

### 2.1.7 Cell lines

#### *2.1.7.1 5T33 myeloma cell line*

5T33MM model originates from a spontaneously developed myeloma in aging mice. These cells can grow *in vitro* as well as *in vivo*. In culture, 5T33MM cells grow as non-adherent single cells or in small loosely adherent clusters. 5T33MM is a highly aggressive form of MM with rapid tumour growth in C57BL/KaLwRij mice and is mainly localised in the BM in addition to spleen and liver. 5T33MM cells cause myeloma in inoculated C57BL/KaLwRij mice after 5-8 weeks of injection with $10^5$ of 5T33MM cells isolated from mice bone marrow. C57BL/KalwRij mice post injected with 5T33MM cells develop high levels of tumour-related monoclonal immunoglobulins in their serum with reduction in the level of normal polyclonal immunoglobulins similar to 5T2MM cells. In contrast to human disease, radiography and histology show 5T33MM cells do not induce osteolytic bone lesions (Manning et al., 1992, Vanderkerken et al., 1997, Asosingh et al., 2000b).

#### *2.1.7.2 5TGM1 myeloma cell line*

The 5TGM1 model was derived from the 5T33 model. 5T33MM cells were passaged in mice, and then obtained from the marrow of 5T33MM-bearing mice cultured and cloned. 5TGM1 cells have all the features of human disease including the production of characteristic osteolytic bone lesions in mice, in contrast to 5T33MM cells that do not induce osteolytic bone lesions in mice. 5TGM1 cells grow rapidly *in vitro* as well as *in vivo*. In culture, 5TGM1 cells grow as non-adherent single cells or in small loosely adherent clusters. C57BL/KalwRij mice after injection with 5TGM1 cells develop high levels of tumour-related monoclonal immunoglobulins in their serum similar to 5T2MM cells and 5T33MM cells. Radiography and histology show 5TGM1 cells induce osteolytic bone lesion similar to the human disease. Use of the bisphosphonate, ibandronate, demonstrated significantly reduced osteolytic bone lesions in 5TGM1-bearing mice (Garrett et al., 1997, Dallas et al., 1999).

### 2.1.8 Cell culture

All cell culture was performed using sterile equipment in a microbiological class II safety cabinet (Walker, UK) and cultures were incubated in a humidified atmosphere at 37 °C and 5% $CO_2$. All media were warmed in a water bath (37 °C) and filtered through a 0.2µM membrane before use. 5T33MM cells were a kind gift from Dr. Karin Vanderkerken (Free University Brussels, Belgium). 5TGM1 cells were a kind gift from Dr. Claire Edwards (University of Oxford, UK). These myeloma cells were cultured separately *in vitro* in RPMI1640 medium (Invitrogen, UK) containing 10% FCS, 100 units/ml Penicillin / 100 µg/ml of Streptomycin, 1% Na2PO3 and 1% non-essential amino acids (NEAA). Medium was changed every 2 days (Manning et al., 1992).

### 2.1.9 Mouse primary osteoblast preparation and culture

As N-cadherin is expressed by osteoblasts, but not by osteoclasts or osteocytes (Mbalaviele et al., 1995, Ferrari et al., 2000, Kawaguchi et al., 2001), osteoblasts were extracted as in previous standard published methods (Garcia et al., 2002, Hay et al., 2009a). Calvarial bones were obtained from 2-4 day old C57Bl/6J mice to extract mouse primary osteoblasts. Calvariae were dissected into small pieces and then digested with trypsin-ethylene-diaminetetraacetic acid (EDTA) for 10 minutes at 37°C with shaking then centrifuged at 1100 rpm for 1 min after which the supernatant was discarded. Tissues were incubated with 0.5% of 280 units/mg collagenase II in PBS, 0.15g of collagenase II was added into 30ml of PBS containing 100 units/ml Penicillin / 100 µg/ml of Streptomycin and 1.36 µg/mL of amphotericin B, for 10 minutes then centrifuged at 1100 rpm for 1 min after which the supernatant was discarded. Tissues were incubated with 0.5% of 280 units/mg collagenase II in PBS for 10 minutes then centrifuged at 1100 rpm for 1 min after which the supernatant was collected. This step was repeated 4 times and then the cells were pooled and re-suspended in MEM alpha containing 10% FCS, 100 units/ml Penicillin / 100 µg/ml of Streptomycin and 1.36 µg/mL of amphotericin B. After 6 hours, osteoblasts adhered to the bottom of the flasks while other cells floated in the medium. In addition, 10 mM of β-glycerophosphate and 50 µg/ml of ascorbic acid were added into the medium to promote cells to differentiate into osteoblasts, other cells (being dead) floated in the medium during the time. Medium with floated cells were discarded and replaced with new medium. Alkaline phosphatase activity and alizarin red staining were used as osteoblastogenesis markers.

### 2.1.10 Animals

Male C57BL/KalwRiJHsD mice, aged 5 weeks, were purchased from Harlan, Netherlands and from University of Leeds, UK. Mice were housed by University of Sheffield biological services laboratory. All animals were provided with food and water

*ad libitum,* light and all procedures were carried out under project license (402901). Live animals were by me, personal license (40/10118).

## 2.2 Methods

### 2.2.1 Cell counting using haemocytometer

Using a haemocytometer is a practical method to determine cell numbers. The Hemacytometer consists of two chambers, each of which consists of nine large, 1 x 1 mm (1 $mm^2$) squares (Figure 2.1). To count cells 15 µl of cell suspension was mixed with 15 µl of 0.4% w/v trypan blue. 10 µl of mix was loaded to each chamber of the Hemacytometer. To determine cell numbers, cells were counted in four 1$mm^2$ areas of the counting chamber. Each 1 $mm^2$ contains $1X10^{-4}$ ml. Therefore, to obtain cells/ml the final multiplication factors is $10^4$. A light microscope was used to count cells. The number of cells was calculated as following example (Table 2.1):

Table 2.1: Counting cell number: Example calculation

| Total cells counted in 4 X 1 $mm^2$ | Divided by 4 = cells/$mm^2$ | Multiply dilution factor (x2) (trypan blue) | = cells/ml |
|---|---|---|---|
| 100 | 25 | 50 | 50 x $10^4$ |

### 2.2.2 Passaging the cells

Primary osteoblasts are adherent cells that attach to the bottom of flasks. $6x10^3$ cells/$cm^2$ cells were seeded into T75 flasks containing 10 ml of MEM alpha (Invitrogen, UK) with 10% FCS, 100 units/ml Penicillin / 100 µg/ml of Streptomycin and 1.36 µg/mL of amphotericin B to grow. 3 days later flasks were sub-confluent. Medium was discarded and cells washed twice with PBS. Cells were incubated with 2 ml of 0.25% trypsin-EDTA at °C for 2 minutes and floating cells were observed under the microscope. 5 ml of MEM alpha (Invitrogen, UK) was added to cells and transferred

into 50 ml tube. Cells were centrifuged at 1000 rpm for 5 minutes at room temperature. Cells were re-suspended in 10 ml of MEM alpha (Invitrogen, UK) with 10% FCS, 100 units/ml Penicillin / 100 µg/ml of Streptomycin and 1.36 µg/mL of amphotericin B and seeded into several new T75 flasks in 6000 cells/$m^2$ density.

Myeloma cells, 5T33MM and 5TGM1 cells grow as non-adherent single cells or in small loosely adherent clusters. $10^5$ of myeloma cells were seeded into T75 flasks containing 10 ml of RPMI1640 medium (Invitrogen, UK) with 10% FCS, 100 units/ml Penicillin / 100 µg/ml of Streptomycin, 1% Na2PO3 and 1% NEAA. 3 days later flasks were sub-confluent. Medium containing myeloma cells was transferred into a 50 ml tube and centrifuge at 1000 rpm for 5 minutes at room temperature. Cells were re-suspended in 10 ml of MEM alpha (Invitrogen, UK) with 10% FCS, 100 units/ml Penicillin / 100 µg/ml of Streptomycin, 1% Na2PO3 and 1% NEAA and seeded into 5 new T75 flasks at $10^5$ cells/flask density. Medium was changed every 2 days.

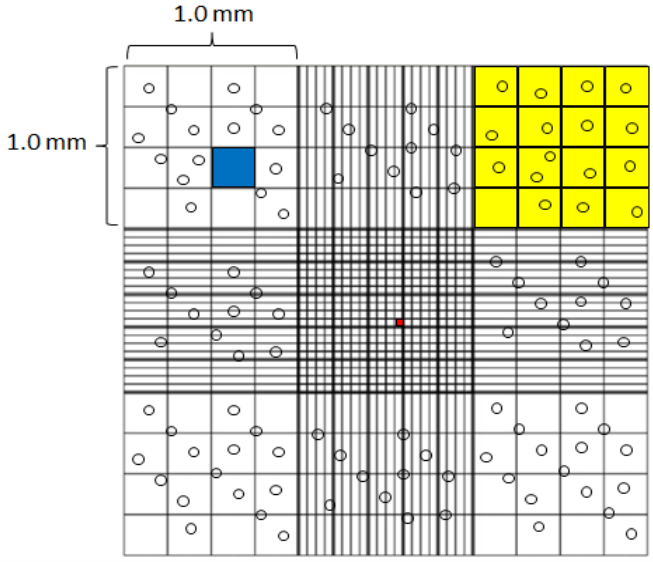


**Figure 2.1: Schematic overview of a haemocytometer under the microscope to count the cells.** The Haemocytometer consists of nine large, 1$mm^2$ squares. Cells were counted in four corners 1$mm^2$ squares and divided by four. Cell numbers were determined as described in table1. Yellow square = 1 $mm^2$, blue square = 0.0625 $mm^2$, red square = 0.0025 $mm^2$.

### 2.2.3 Cell viability tests using Trypan Blue

Cell viability was assessed by staining cells with Trypan Blue: live cells possess intact cell membranes and exclude the Trypan Blue dye, dead cells do not exclude Trypan Blue dye and stain blue. 15 µl of cell suspension was mixed with 15 µl of 0.4% w/v trypan blue. Cells were examined and counted as described in section 2.2.1. The percentages of viable and non-viable cells present in the samples were determined using Phase contrast microscopy.

### 2.2.4 Osteoblast differentiation

Osteoblasts were differentiated into mature functional osteoblasts, mineralised osteoblasts, to study the differences between immature osteoblasts and mature functional osteoblasts (Bancroft et al., 2002, Xiao et al., 2006, Garcia et al., 2002). $6x10^3$ cells/$cm^2$ of mouse primary osteoblasts *was* seeded *in vitro* into flasks for 2 days. When confluent after 2 days osteogenic media were added and osteoblasts were differentiated for 4 weeks into mature functional osteoblasts using osteogenic media; MEM alpha (Invitrogen, UK) containing 10 mM of β-glycerophosphate, 50 µg/ml of ascorbic acid and $10^{-8}$ M of dexamethasone in addition to 10% FCS, 100 units/ml Penicillin / 100 µg/ml of Streptomycin and 1.36 µg/mL of amphotericin B. Medium was changed every 2 days. Alkaline phosphatase [ALP] activity and alizarin red staining were used to analyse osteoblast differentiation. 2000 cells/well were seeded in 96 well plates for ALP activity assay. 12,000 cells/well were seeded in 24 well plates for the alizarin red staining assay. 150,000 cells/well were seeded in T25 for molecular biology assays. 4400 cells/well were seeded in 8 chamber slides for immuno-staining.

#### *2.2.4.1 Alkaline phosphatase activity assay*

p-Nitrophenyl phosphate (pNPP) (Sigma, UK) is a soluble substrate used for the detection of alkaline phosphatase activity (Xiao et al., 2006). $6x10^3$ cells/$cm^2$ of primary

osteoblasts were seeded in 96 well plates in MEM alpha containing 10% FCS, 100 units/ml Penicillin / 100 µg/ml of Streptomycin and 1.36 µg/mL of amphotericin B. Cells were washed twice with ice cold phosphate buffered saline (PBS) and permeabilised with 20 µl of 0.1% triton with agitating for 20 minutes at room temperature. One pNPP tablet and one tris buffer tablet were dissolved in 20 ml of water and 200 µl was carefully added to cells. ALP activity was determined by reading the absorbance at $A_{405}$ every 5 minutes for 90 minutes (Figure 2.2) and using the following formula; $OD_{(t1)}$, last optical density; $OD_{(t0)}$, start optical density; ε, constant; path length, length of 200 volume of sample in 96 well plate.

$$\text{ALP activity} = \frac{(OD_{(t1)} - OD_{(t0)}) \text{ X } 1000 \text{ X Total volume}}{\text{Time X } \varepsilon \text{ (18.75) X Path length (0.639) X Sample volume}}$$

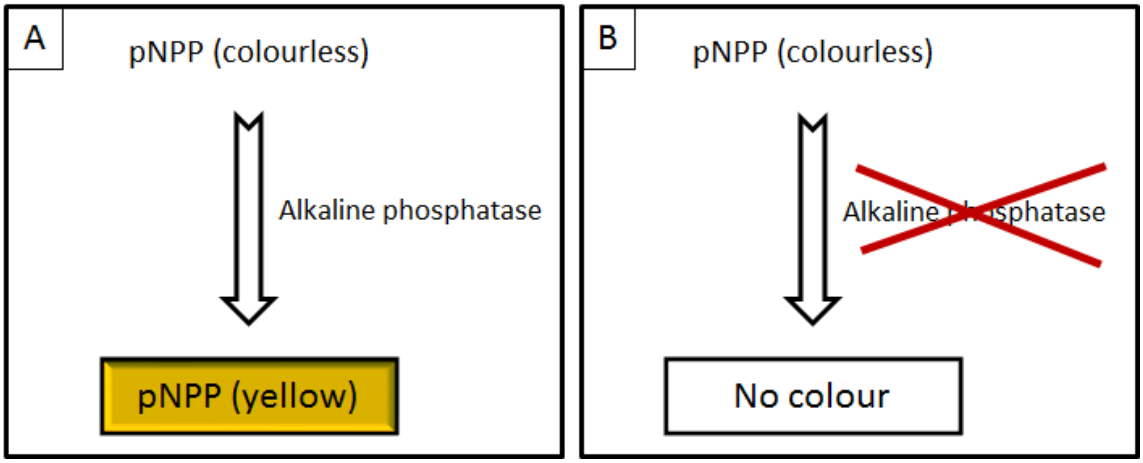


**Figure 2.2: Determining alkaline phosphatase activity during osteoblast differentiation.** p-Nitrophenyl phosphate was used as a soluble substrate to detect alkaline phosphatase activity. One pNPP tablet and one Tris Buffer tablet were dissolved in 25ml tap water. ALP hydrolyses colourless pNPP to a coloured product. The colour intensity was determined by reading the absorbance at $A_{405}$. The more ALP activity correlates with more yellow product. Panel A shows a yellow product is formed in the presence of ALP. Panel B shows no yellow product was formed in the absence of ALP. ALP activity is expressed as U/ml/min/ug DNA.

### *2.2.4.2 PicoGreen assay*

ALP activity was normalised with osteoblast DNA concentration using the picogreen assay. PicoGreen® double-stranded DNA (dsDNA) quantitation reagent (Invitrogen, UK) is a fluorescent nucleic acid stain used to quantify dsDNA (Xiao et al., 2006). 100µl of 1X TE buffer (10 mM Tris-HCl, 1 mM EDTA, pH 7.5) was added to standards and unknown DNA concentration of the osteoblasts in a 96 well plate. 100 µl of 1:200 dilutions of PicoGreen reagent was added to each standard and unknown sample, and incubated in the dark at room temperature for 5 minutes. Quantitation of DNA was determined by exciting samples at 485 nm and detecting fluorescence emission intensity at 530 nm.

### *2.2.4.3 Alizarin red staining*

Alizarin red staining is a dye used as an *in vitro* mineralisation marker, in which alizarin red dye binds to calcium in matrix deposited by osteoblasts (Xiao et al., 2006). $6x10^3$ cells/$cm^2$ of primary mouse osteoblasts were seeded in 24 well plates in MEM alpha containing 10% FCS, 100 units/ml penicillin / 100 µg/ml of streptomycin and 1.36 µg/mL of amphotericin B. Cells were washed twice with ice cold PBS and fixed with 1 ml of ice cold 70% ethanol for 1 hour at 4°C. Cells were rehydrated with water for 5 minutes before 1 ml of 1% alizarin red (pH 4.2) was added to each well for 10 minutes, washed 5 times with water and dried overnight to at 25°C. ImageJ software was used to quantify the red colour of alizarin red staining. Colour images were converted into 8 bit images (255 grey levels) and the intensity of objects and pixel value of white/black was calculated (Figure 2.3).

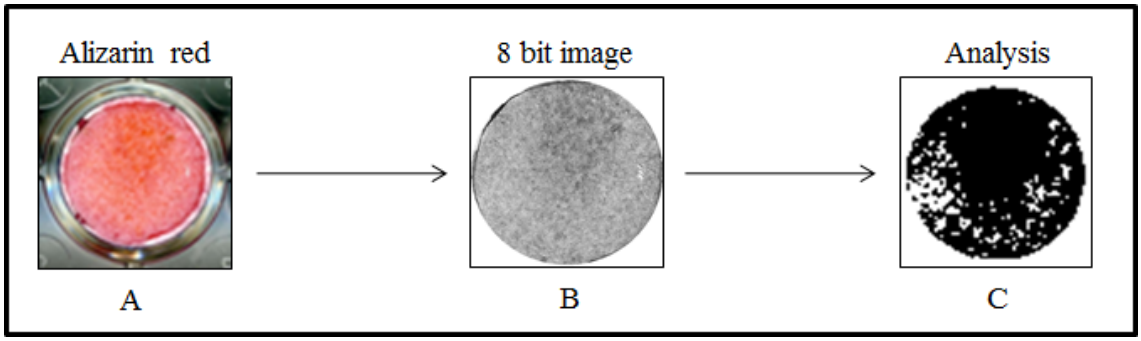


**Figure 2.3: Determining alizarin red staining as a marker of osteoblast activity.** Wells containing alizarin red stained osteoblasts from 24 well plates were digitally scanned to capture alizarin red staining (A). Captured colour digital images were processed using imageJ software to generate 8 bit images (B) with 0-255 gray levels. 8 bit images were converted into binary images (C). The pixel value of equal binary areas osteoblasts in each stained well was derived. Results were expressed by intensity 0-255. Pixel values of 0 = white represented minimum intensity alizarin red staining whereas pixel values of 255 were maximum intensity alizarin red staining.

### 2.2.5 Molecular biology

#### *2.2.5.1 RNA extraction*

RNA was extracted from 5T33MM cells, 5TGM1 cells and mouse calvarial primary osteoblasts. According to manufacturer's instructions homogenised tissues/cells were washed in phosphate buffered saline (PBS) and Trizol® (Invitrogen, UK) and chloroform was added. The solution was centrifuged for 12000rpm at 4°C for 10 minutes. RNA in aqueous phase was removed, and 2 volumes of isopropanol added to precipitate the RNA in -20ºC for 24 hour. The solution was thawed and centrifuged for 12000rpm at 4°C for 10 minutes. The resultant RNA pellet was re-suspended in RNase and DNase free $H_2O$ and stored at -20°C. Samples were stored for no more than 6 weeks.

### *2.2.5.2 RNA and DNA quantitation*

NanoDrop ND 1000 Spectrophotometer (NanoDrop Technologies, USA) was used to quantify total RNA and DNA in the solution. RNA and/or DNA solutions were centrifuged for 12000rpm at 4°C for 10 minutes and pellets washed twice in 70% ethanol to precipitate RNA and/or DNA. The resultant RNA and/or DNA pellet was re-suspended in 10 µl of DNase/RNase-free distilled water. The purity of the RNA and/or DNA with respect to protein contamination was estimated by 280 nm and 260/280 nm ratio.

### *2.2.5.3 RNA agarose gel electrophoresis*

The quality of the purified RNA was verified with 1% Agarose gel electrophoresis of RNA samples. 2g agarose (Invitrogen, UK) was dissolved in 200 ml 1X Tris-Borate-EDTA buffer (TBE) preparing 1% (w/v) agarose gels. The gel mixture was boiled and allowed to cool to ambient temperature. 2 µl of ethidium bromide (Fluka, Switzerland), a fluorescent tag that permits visualisation of bands under ultraviolet light was added. Agarose was poured into a casting tray containing a multi-well comb. RNA samples were added and mixed with 3 µl of loading buffer (X2 TBE, 0.25% bromophenol blue (BPB)/ 30% glycerol) and loaded into wells for electrophoresis and run in 1X TBE buffer with BIO-RAD Power PAC300 at 120 volts (constant voltage) for 40 minutes. After electrophoresis, bands were visualized under UV light using ultraviolet transilluminator (Bio-Rad Gel Doc 2000 using Quantity One v4.5.1 software). Images were saved as tiff files. Good quality RNA was judged to have clean 28S and 18S ribosomal RNA bands, little or no fluorescence at the bottom of the gel and a smear or fluorescent fragments above the 28S and 18S ribosomal bands.

#### *2.2.5.4 cDNA synthesis*

According to manufacturer's instructions (Invitrogen, UK), a known concentration of RNA was treated with DNase I to remove any genomic DNA contamination. SuperScript™ II reverse transcriptase (Invitrogen, UK) was used to reverse transcribes mRNA to cDNA. The resultant solution was incubated at 50°C for an hour and made up to 50 µl, with DNase/RNase-free distilled water, as a cDNA template for amplification in PCR. Control samples (water only) were used to ensure there is no false positives or negative in subsequent RT-PCR (Figure 2.4).

#### *2.2.5.5 Bioinformatics and primer design*

National Center for Biotechnology Information (NCBI), UCSC (University of California Santa Cruz) and Ensemble were searched against N-cadherin, NM_007664.4 mouse RefSeq gene and GAPDH (control), NM_008084.2 mouse RefSeq gene. Exon spanning primers, on separate exons, were designed (Table 2.2) with PCR product sizes of approximately 560 bp and 354 bp to cover coding region of N-cadherin and GAPDH, respectively (Figure 2.5). All primers were manually designed with 20 bases in length, melting temperatures of 60ºC (annealing at 55ºC), containing 50% G or C, and containing GC clamp at the 3' end. BLAST software was used to determine the specificity of PCR primers.

#### *2.2.5.6 Polymerase chain reaction*

Platinum *Taq DNA* polymerase kit (Invitrogen, UK) was used to amplify N-cadherin using 1µl of cDNA template according to manufacturer's instructions (Invitrogen, UK). 16.05 µl of water was mixed with 2.5 µl of 10X PCR buffer, 0.75 µl of 1.5 mM $MgCl_2$, 1 µl of 10 mM deoxynucleoside triphosphates (dNTPs), 0.5 µl of each primer (final concentration = 0.2 µM), and 0.2 µl Platinum *Taq* polymerase (5 U/µl stock). Using DNA Engine (MJ Research PTC200 Thermo Cycler (BC-MJPC200)) PCR reaction was

started with heating at 94ºC for 3 minutes followed by cycles of denaturation at 94 ºC for 30 seconds, annealing at 55ºC for 30 seconds, and extension at 72ºC for 30 seconds, performed for 30 cycles for N-cadherin and 20 cycles for GAPDH.

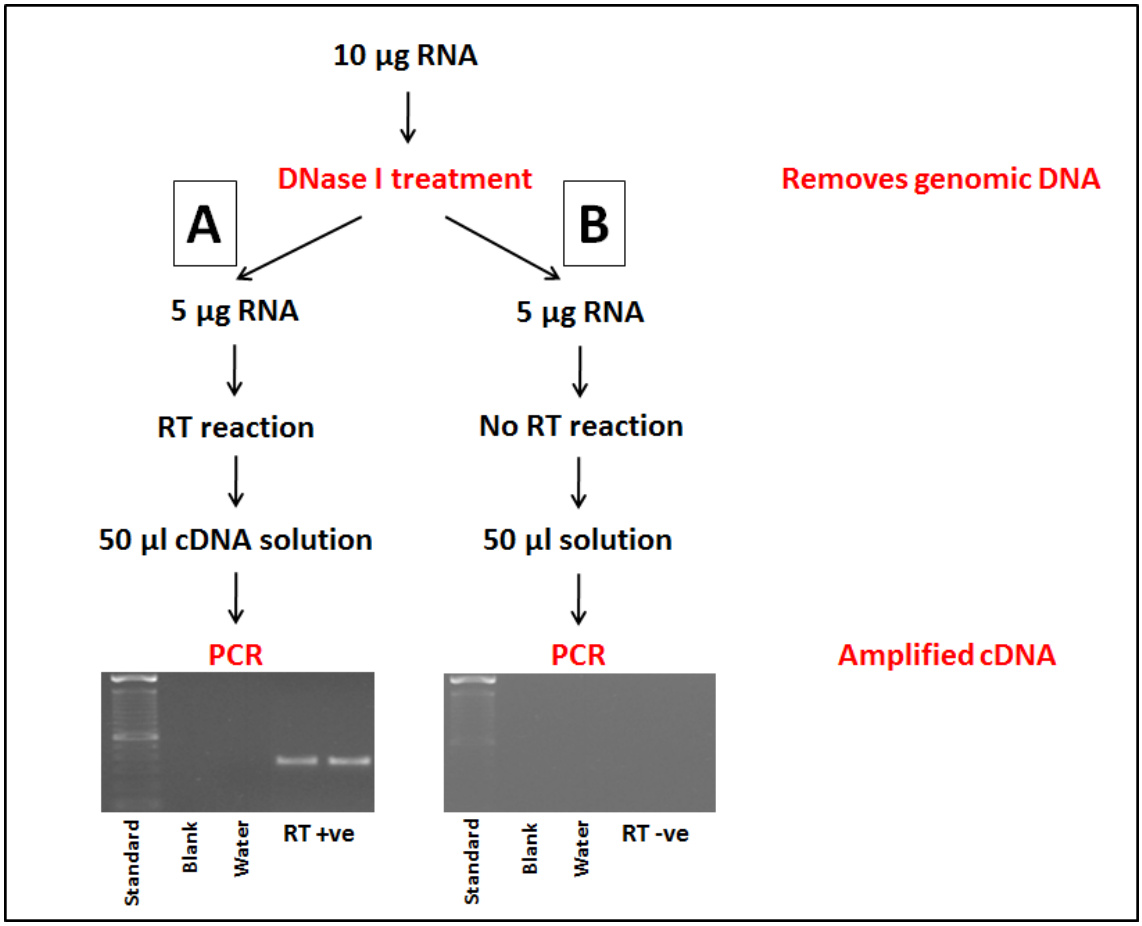


**Figure 2.4: Gene expression analysis using reverse transcriptase-polymerase chain reaction (RT-PCR) to synthesise cDNA from RNA and amplify specific gene transcripts using PCR.** Total RNA was treated with DNase I to remove genomic DNA prior to reverse transcription. PCR was performed using 1µl cDNA template (A) and 1µl no cDNA template (B). Housekeeping gene GAPDH primers were used as an internal control for each sample showing successful cDNA synthesis. PCR products were electrophoretically separated by size using ethidium bromide/agarose gel demonstrating no genomic contamination in the RT-ve samples. Expected size of GAPDH products = 354 bp.

Table 2.2: Primers designed and used to amplify target genes

| Gene | Accession number | Forward 5`- 3` | Reverse 5`- 3` | Expected size |
|---|---|---|---|---|
| N-cad | NM_007664.4 | CAGGTAGCTGTAAACCTGAG | CCATTCAGGGCATTTGGATC | 560 bp |
| GAPDH | NM_008084.2 | TTGTCAGCAATGCATCCTGC | GCTTCACCACCTTCTTGATG | 354 bp |

### *2.2.5.7 cDNA agarose gel electrophoresis*

Agarose gel electrophoresis was used to separate the amplified nucleic acids by length. 2g agarose (Invitrogen, UK) was dissolved in 200 ml 1X Tris-Borate-EDTA buffer (TBE) preparing 1% (w/v) agarose gels. The gel mixture was boiled and allowed to cool to ambient temperature. 2 µl of ethidium bromide (Fluka, Switzerland), a fluorescent tag that binds to dsDNA permits visualisation of bands under ultraviolet light. Agarose was poured into a casting tray containing a multi-well comb. PCR samples were added and mixed with 3 µl of loading buffer (X2 TBE, 0.25% bromophenol blue (BPB)/ 30% glycerol) and loaded into wells for electrophoresis and run in 1X TBE buffer with BIO-RAD Power PAC300 at 120 volts (constant voltage) for 40 minutes. After electrophoresis, bands were visualised under UV light using ultraviolet transilluminator (Bio-Rad Gel Doc 2000 using Quantity One v4.5.1 software).

### *2.2.5.8 DNA extraction from the gel using Qiaquick gel extraction Kit*

This QIAquick Gel Extraction kit was used according to manufacturer's instructions (QIAGEN Ltd, UK) to extract and purify DNA fragments from agarose gels. PCR samples were added and mixed with 3 µl of loading buffer (0.25% bromophenol blue (BPB)/ 30% glycerol) and loaded into wells for electrophoresis and run in 1X TBE buffer with BIO-RAD Power PAC300 at 120 volts (constant voltage) for 40 minutes. The position of the fragment of interest was excised from the agarose gel with a clean,

sharp scalpel under the UV light and placed in a 1.5 ml Eppendorf tube. 600 µl of buffer QC (contains guanidine thiocyanate, buffer composition is proprietary, pH ≤7.5) was added to the gel in the tube. Samples were incubated at 50°C until the gel slice had completely dissolved and the colour of buffer changed to yellow. Samples were mixed every 2 minutes to help the gel to dissolve. The products were transferred into a QIAquick spin column and centrifuged at 13,000 rpm for 1 minute. The flow-through was discarded to remove all traces of agarose. 0.5 ml of buffer QC was added to the membrane of QIAquick spin column and centrifuged at 13,000 rpm for 1 minute. The flow-through was discarded and 0.7 ml of buffer PE (containing 80% (v/v) ethanol, while the composition of the buffer was proprietary) was added to the membrane of QIAquick spin column to wash the column. Samples were centrifuged at 13,000 rpm for 1 minute and the flow-through was discarded. The column was then transferred to a clean 1.5 ml Eppendorf tube and 50 µl of DNase/RNase-free distilled water was added to the QIAquick spin column membrane and allowing the column to stand for 1 minute in room temperature. DNA was recovered by centrifugation the QIAquick spin column at 13,000 rpm for 1 minute and quantitated as described in section 2.2.5.2.

#### *2.2.5.9 Sequencing*

DNA samples were sequenced in the DNA Sequencing Core Facility housed within the University of Sheffield Medical School (http://genetics.group.shef.ac.uk/dna-sequencing.html). 10 µl of purified PCR product (50 ng/µl) was supplied to the core facility for sequencing along with the appropriate primers for N-cadherin (1 pmol/µl) (Table 2.2). Samples were sequenced in both directions using an ABI 3730 DNA capillary sequencer (Applied Biosystems). FinchTV software was used in analysing the output sequence after receiving from the Sequencing Core Facility.

#### *2.2.5.10 TaqMan analysis*

TaqMan is a method used to quantify gene expression (Holland et al., 1991). According to manufacturer's instructions (Invitrogen, UK) TaqMan Universal master Mix II (Applied biosystems, UK) was mixed with cDNA templates. According to manufacturer's instructions (Applied Biosystems, UK) 10 µl of TaqMan Universal Master Mix II was mixed with 1 µl of TaqMan assay and 9 µl of cDNA. Runx2 (Mm00501580_m1), COL1A2 (Mm00483888_m1), osteocalcin (Mm03413826_mH), N-cadherin (Mm01162497_m1) and β-actin (Mm00607939_s1) assays were used. ABI PRISM > 900 sequence detector was used to quantify gene expression. Expression was normalised with housekeeping genes.

### 2.2.6 Immuno-detection of N-cadherin

#### *2.2.6.1 Immunofluorescence detection of N-cadherin in osteoblasts*

Immunofluorescence is a technique used to detect specific antigens using specific antibodies. Rabbit monoclonal anti-N-cadherin antibody (Millipore, UK) and donkey anti-rabbit IgG antibodies (R&D systems, UK) were used as primary and secondary antibodies. $6x10^3$ cells/$cm^2$ of osteoblasts were seeded in chamber slides (BD, UK) and cultured in MEM alpha containing 10% FCS, 100 units/ml penicillin / 100 µg/ml of streptomycin and 1.36 µg/mL of amphotericin B. Cells were washed twice with ice cold PBS and fixed with 300 µl of 4% fresh paraformaldehyde in PBS for 10 minutes in 4°C. Cells were permeablized with 0.1% triton in PBS for 10 minutes at room temperature. Osteoblasts were washed twice with room temperature PBS, blocked with 1% normal donkey serum for 30 minutes at room temperature.

In optimising antibody concentration, osteoblast were incubated overnight at 4°C with 300 µl of 25-125 µg/ml anti-N-cadherin antibody (Millipore, UK) in different dilutions in PBS (1:50), (1:100), and (1:500). 300 µl of 100 µg/ml normal rabbit IgG antibody

(R&D systems, UK) was used with (1:50), (1:100), and (1:500) dilution of isotype in PBS as a negative controls. Cells were washed twice with 300 µl of PBS and incubated with 300 µl of donkey anti-rabbit IgG secondary antibody, (1:200) (R&D systems, UK) for 1 hour at room temperature, then washed twice with 300 µl of PBS. to remove unbound antibody, and incubated with 300 µl of donkey anti-rabbit IgG secondary antibody, (1:200), labelled with fluorochrome northern light (NL637) (R&D systems, UK) for 1 hour at room temperature, then washed twice with PBS. Slides were mounted using prolong mounting medium containing DAPI stain (Invitrogen, UK), DAPI stain was used to stain nuclei. Images were acquired using a Zeiss 510 microscope.

After optimal concentration of antibody determined, osteoblasts incubated overnight at 4°C with 300 µl of 25-125 µg/ml anti-N-cadherin antibody (Millipore, UK) using 1:50 dilution. 300 µl of 100 µg/ml normal rabbit IgG antibody (R&D systems, UK) was used with 1:50 dilution as a negative control. Cells were washed twice with PBS to remove unbound antibody, and incubated with 300 µl of donkey anti-rabbit IgG secondary antibody, (1:200), labelled with fluorochrome northern light (NL637) (R&D systems, UK) for 1 hour at room temperature, then washed twice with PBS. Slides were mounted using prolong mounting medium containing DAPI stain (Invitrogen, UK), DAPI stain was used to stain nuclei. Images were acquired using a Zeiss 510 microscope.

#### *2.2.6.2 Immunofluorescence detection of N-cadherin in 5T33MM cell line*

$1x10^6$ cells/ml were re-suspended in 4% paraformaldehyde and fixed for 10 minutes. 250 µl of this suspension was added to the funnel in assembled cytospin cassette and centrifuged in cytospin for 5 minutes at 500 rpm. Slides were removed from cytospin cassette. Cells were permeablized with 0.1% triton in PBS for 10 minutes at room temperature, washed twice with PBS, blocked with 1% normal donkey serum for 30 minutes at room temperature and incubated overnight at 4°C with 300 µl of 25-125 µg/ml anti-N-cadherin antibody (Millipore, UK), 1:50 dilutions. 300 µl of 100 µg/ml

normal rabbit IgG antibody (R&D systems, UK) was used with 1:50 dilution as a negative control. Cells were washed twice with room temperature PBS to remove unbound antibody, and incubated with 300 µl of donkey anti-rabbit IgG secondary antibody, (1:200 dilution), labelled with fluorochrome northern light (NL637) (R&D systems, UK) for 1 hour at room temperature, then washed twice with PBS. Slides were mounted using Prolong mounting medium containing DAPI stain (Invitrogen, UK), DAPI stain was used to stain nuclei. Images were acquired using a Zeiss 510 microscope.

#### *2.2.6.3 Immunocytochemistry detection of N-cadherin in 5T33MM and 5TGM1MM cell lines*

$1x10^6$ cells/ml were re-suspended in 4% paraformaldehyde and fixed for 10 minutes. 250 µl of this stock was added to funnel in assembled cytospin cassette and centrifuged in cytospin for 5 minutes at 500 rpm. Slides were removed from cytospin cassette. Cells were permeablized with 0.1% triton in PBS for 10 minutes at room temperature, washed twice with PBS, blocked with 1% normal donkey serum for 30 minutes at room temperature and incubated overnight at 4°C with 300 µl of 25-125 µg/ml anti-N-cadherin antibody (Millipore, UK), 1:50 dilutions in PBS. 300 µl of 100 µg/ml normal rabbit IgG antibody (R&D systems, UK) was used with 1:50 dilution of isotype in PBS as a negative control. Cells were washed twice with 300 µl of PBS to remove unbound antibody, and incubated with 300 µl of biotinylated anti rabbit IgG secondary antibody, (1:200 dilution), for 30 minutes at room temperature. Cells were washed twice again with PBS, and incubated with 300 µl of avidin-biotin complex (ABC) for 30 minutes at room temperature. Cells were washed twice again with PBS, and incubated with 300 µl of DAB for 5 minutes at room temperature. Cells were washed with water for 5 minutes, and counter stained with haematoxyline for 20 seconds to stain nuclei. Slides were mounted and covered using cover slip. Images were acquired using an Osteomeasure software version 4.10 (Osteomerics Incorporated, Atlanta, USA).

### 2.2.7 Flow cytometry

#### *2.2.7.1 Antibody labelling*

Lightning-Link™ Atto637 conjugation kit (Innova Biosciences, UK) was used for labelling the anti-N-cadherin antibody, GC-4 (Sigma, UK) and the mouse IgG antibody (Vector laboratories, UK). The kit contains 3 glass vials of Lightning-Link™ mix, each suitable to label 100-200 µg of antibody. 10 µl of LL-Modifier reagent was added to 100 µl of 2 mg/ml anti-N-cadherin, GC-4, antibody (Sigma, UK) and added to 100 µl of 2 mg/ml mouse IgG antibody (Vector laboratories, UK). Each antibody was added to separate glass vial of Lightning-Link™ mix and incubated overnight at 4°C before used.

#### *2.2.7.2 Cell preparation*

Mouse primary osteoblasts adhere to the bottom of flasks. Medium was discarded and cells were washed twice with room temperature PBS. Four different methods were used to harvest cells to determine the expression of N-cadherin protein by flow cytometry including; 0.25% trypsin-EDTA, scrape cells gently using cell scrapers (Thermo Scientific, UK), 1X sodium citrate (Sigma, UK) and 1% of 280 units/mg collagenase II (Invitrogen, UK) in 1X sodium citrate (Sigma, UK).

#### *2.2.7.3 Detection of N-cadherin protein in osteoblasts and myeloma cell lines; 5T33MM and 5TGM1*

Flow cytometry is a technique used to separate and detect sub-population of cells or particles, such as cell surface antigens, protein expression and enzymatic activity based on fluorescence detection and/or bio-physiology, such as size and granularity of cells. Flow cytometry is routinely used in basic research, clinical practice and the diagnosis of health disorders, such as blood cancers (Barlogie et al., 1983). In this study, flow cytometry was used to detect the specific cell surface antigen, N-cadherin, using

specific fluorescent antibodies. Mouse monoclonal anti-N-cadherin, GC-4 antibody (Sigma, UK) was used as primary antibody. Mouse IgG (Vector Laboratory, UK) was used as a negative control. $5x10^5$ of mouse primary osteoblasts, 5T33MM cells and 5TGM1 cells were re-suspended in 1 ml of 4% paraformaldehyde and fixed at 4°C for 10 minutes. Cells were washed twice with PBS, blocked with 1 ml of 1% normal FCS for 30 minutes at room temperature. Cells were incubated with 1 ml of 2 mg/ml anti-N-cadherin GC-4 antibody labeled by Lightning-Link™ Atto637 (1:200 dilution in 1% normal FCS) for 30 minutes at 4°C in dark. 1 ml of 2 mg/ml mouse IgG antibody labeled by Lightning-Link™ Atto637 was used (1:200 dilution in 1% normal FCS) for 30 minutes at 4°C in dark as a negative control. Cells were washed twice with room temperature PBS to remove unbound antibody and resuspended in 300 µl in 1% normal FCS. Results were acquired using FACSCalibur.

### 2.2.8 Western blot

#### *2.2.8.1 Protein extraction using NP40 buffer*

Proteins were extracted from cells using Nonylphenoxypolyethoxylethanol (NP40) reagent (Fluka). 1mL of NP40 buffer (1.0%NP40 reagent (Fluka) +150 mM sodium chloride +50 mM Tris, pH 8.0) was added to the ~80% confluent of pre-osteoblasts and mature osteoblasts and to $1x10^6$ of 5T33MM cells and 5TGM1 cells. Then, 1X of Protease Inhibitor Cocktail set 1 (CALBIOCHEM) was added to prevent protein degradation.

#### *2.2.8.2 Bicinchoninic acid (BCA) protein assay*

BCA protein assay is a biochemical assay for determining the total concentration of protein in a solution (Smith et al., 1985). Peptide bonds in the proteins reduced the copper sulphate(II) to copper sulphate(I). The amount of copper sulphate(II) reduced is propotional to the amount of proteins in the sample. The BCA protein assay detects the

copper sulphate(I). In this study, 10µl of each standard protein concentration, 1000 µg/ml, 800 µg/ml, 600 µg/ml, 400 µg/ml, 200 µg/ml, 100 µg/ml and 0 µg/ml was added into 96 well plates. 10µl of the un-known sample was added in duplicate in the same 96 well plate. 200 µl of BCA working reagent (50 part of BCA reagent A : 1 part of BCA reagent B) was added into each standard and samples. Plates were read on a plate reader (DYNEX technologies, MRX II) at 562nm.

#### *2.2.8.3 Sodium-Dodecyl-Sulphate Poly-Acrylamide Gel Electrophoresis (SDS-PAGE)*

This technique allows the separation of proteins based on their size. SDS is applied to denature the protein and imparts a uniform negative charge to linearized proteins. The separation of proteins is done by the acrylamide/bis-acrylamide matrix on the basis of molecular weight. 12% resolving gel was prepared by a mixture of 4 ml of Acrylamide 30% (Total), 2.5 ml of resolving gel buffer (1.5 M Tris), 3.3 ml of water, 100 µl of 10% SDS, 100 µl of 10% ammonium persulphate (APS) and 4 µl of Tetramethylethylenediamine (TEMED) (BIORAD). This was loaded between the spacer plates 1.5 mm apart and kept for 30 – 40 minutes to polymerise. 15% resolving gel was prepared by a mixture of 5 ml of Acrylamide 30% (Total), 2.5 ml of resolving gel buffer (1.5 M Tris), 2.3 ml of water, 100 µl of 10% SDS, 100 µl of 10% APS and 4 µl of Tetramethylethylenediamine (TEMED) (BIORAD). This was loaded between the spacer plates 1.5 mm apart and kept for 30 – 40 minutes to polymerise. 3% stacking gel was prepared by mixing of 180 µl of Acrylamide 30% (Total), 600 µl of stacking gel buffer 0.5 M Tris, 1.57 ml of water, 24 µl of 10% SDS, 24 µl of 10% APS and 2.4 µl of TEMED. These were loaded onto the resolving gel after it had polymerised.

Sample buffer was prepared by diluted 250 µl of 4X SDS in 750 µl water that gave a 1X SDS solution. 25 mg of DTT was then dissolved in 1X SDS and used as sample buffer. 1X SDS running buffer was prepared by diluted 100 ml of 10X Tris/Glycine/SDS running buffer in 900 ml water that gave a 1X SDS running buffer (pH 8.3).

In this procedure, SDS/polyacrylamide-gel electrophoresis was done in slab gels containing 12% (w/v) total acrylamide and 3% stacking gels for N-cadherin and 15% (w/v) total acrylamide and 3% stacking gels for β-actin, where proteins were separated by molecular mass. 25 µl of degraded proteins was mixed with 25 µl of the sample buffer. The samples were then boiled for 5 minutes at 100 °C and allowed to cool to ambient temperature for 5 minutes. 40 µl of each sample were then loaded into the gel slots for electrophoresis and run in 1X running buffer at 200 volts (constant voltage) for 1 hour surrounded by ice.

#### *2.2.8.4 Proteins transfer*

The SDS-PAGE gels were placed into a transfer manifold. The transfer apparatus was purchased from BioRad (Mini Trans-Blot Electrophoretic Transfer Cell). Polyvinylidene fluoride (PVDF) membrane was re-hydrated by successive washing in MeOH, dH2O and transfer buffer. The transfer apparatus was assembled as described in figure 2.5 and the cassette placed in the transfer cell filled with cooled transfer buffer. For keeping the buffer cold during the horizontal protein transfer to the PVDF membrane, a stirrer and an ice container were placed in the transfer cell. Electrophoresed gel was placed on the top of PVDF membrane, which was kept on the cathode side. The transfer manifold allowed transfer at 100V for 600 min in a tank containing transfer buffer (25mM Tris base, 200mM glycine, 20% (v/v) methanol) and was cooled using an ice block.

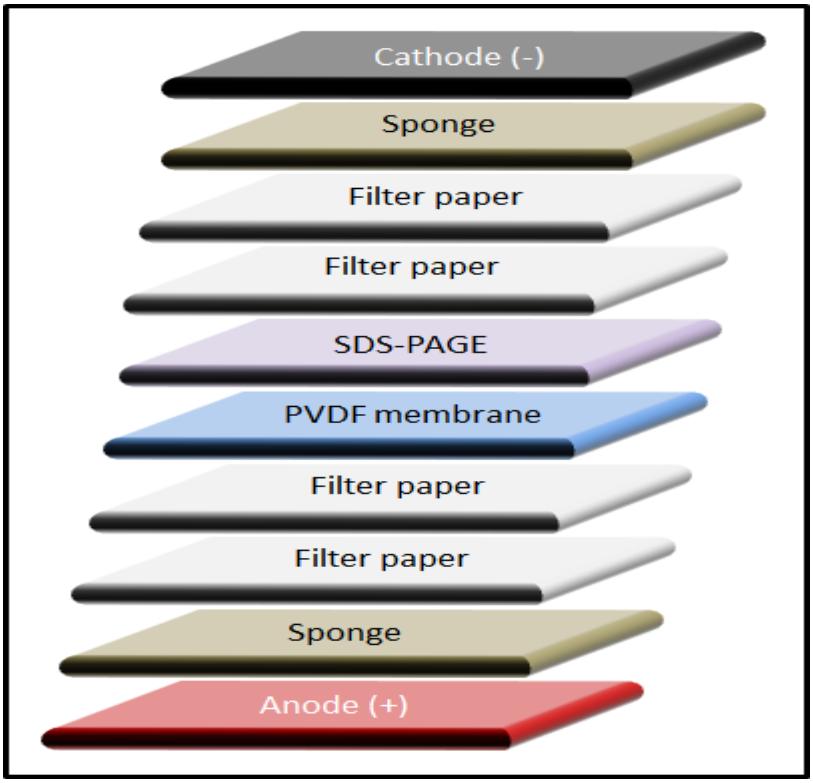


**Figure 2.5: A diagram showing the transfer apparatus for western blotting.** The transfer apparatus (Mini Trans-Blot Electrophoretic Transfer Cell, Bio Rad) is assembled in following order: cassette (red/anode), scouring pad (sponge), 2X filter paper, PVDF membrane, acrylamide gel, 2X filter paper, scouring pad, cassette (black/cathode). When the electric field is applied, proteins, which are negatively charged with SDS, migrate to the positive pole and are captured by the PVDF membrane at 100V for 600 min in a tank containing transfer buffer.

#### *2.2.8.5 Immuno-detection of N-cadherin on western blot*

After the transfer, the membrane was blocked using 5% non-fat powder milk (Marvel) in TBS (0.136M NaCl, 2.68mM KCl, 24.7mM Tris base, adjusted to pH 7.4 using HCl) for 1 hour. After the blocking, the membrane was incubated on a rotary shaker overnight at 4˚C with 10 ml of anti-N-cadherin antibody (Millipore, UK) (1:1000 dilution) in 1% milk solution. Membranes were washed 4 times for 10 minutes in PBS-T on a rotary shaker and incubated with anti-rabbit IgG, horseradish peroxidase-linked species-specific (GE Healthcare, UK) at a 1:2000 dilution in 1% milk solution for 1 hour on a rotary shaker. Membranes were washed 3 times for 10-15 minutes in PBS-T on a rotary shaker followed by 3 times washes with distilled water for 10-15 minutes. Membranes were dipped in enhanced chemiluminescent substrate (SuperSignal®West Dura Extended Duration Substrate, Thermo Scientific) for 15-30 seconds for detecting horseradish peroxidase, in which horseradish peroxidase cleave the chemiluminescent and produces luminescence in proportion to amount of protein. Films (Hyperfilm™, Amersham) were developed using AGFA Curix 60 in the dark room.

### 2.2.9 Cell adhesion assay

#### *2.2.9.1 Determining the incubation time and concentration of recombinant N-cadherin for adherence of myeloma cells*

96 well plates were coated overnight at 4°C with different concentrations of recombinant N-cadherin/Fc chimera (R&D Systems). Optimal incubation period was determined by incubating $1x10^5$ cells/ml of myeloma cells with 1 µg/ml of recombinant N-cadherin/Fc chimera at 37°C for different times; 0, 4, 8, 10, 15, 20, 30 and 60 minutes. Optimal N-cadherin concentration was detected by incubating $1x10^5$ cells/ml of myeloma cells with 0, 0.1, 0.5, 1, 2, 5, 10 µg/ml of recombinant N-cadherin/Fc chimera (R&D Systems) at 37°C for 20 minutes. Plates were washed 5 times using PBS. Adherent cells were fixed with 4% PFA and counted. Results were presented as percentage of adhered myeloma cells out of the total number of myeloma cells.

### *2.2.9.2 Blocking N-cadherin using anti-N-cadherin (GC-4) antibody: blocking myeloma interaction with recombinant N-cadherin/Fc chimera*

To block N-cadherin, myeloma cells, 5T33MM and 5TGM1, were incubated with anti-N-cadherin antibody (10 µg/ml) (Sigma, UK) at 37°C for 30 minutes (Figure 2.6). Mouse IgG1 antibody (Dako, Denmark) (10 µg/ml) was used as a negative control. Cells were mixed every 5 minutes. After 30 minutes, myeloma cells were centrifuged at 1000 rpm for 4 minutes, washed twice with PBS to remove non-binding antibody and re-suspended in MEM alpha media (Groen et al., 2011). After blocking, $1x10^5$ cells/ml of myeloma cells were plated and incubated with recombinant N-cadherin/Fc chimera at 37°C for 20 minutes. Plates were washed 5 times using PBS. Adherent cells were fixed with 4% PFA and counted using phase contrast microscopy. Results were presented as percentage of adhered myeloma cells out of the total number of myeloma cells.

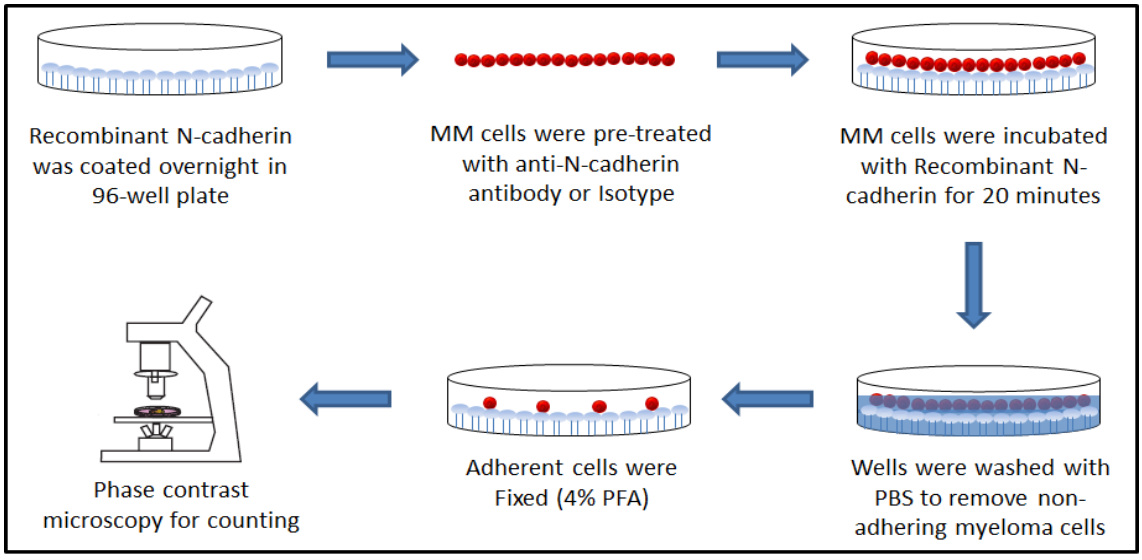


**Figure 2.6: A diagram showing the process of an adhesion assay of myeloma cells on N-cadherin-coated wells.** 96 well plates were coated overnight at 4°C with different concentrations of recombinant N-cadherin/Fc chimera (R&D Systems). $1x10^5$ cells/ml of myeloma cells were pre-treated with anti-N-cadherin antibody or isotype control for 30 minutes at 4ºC. Myeloma cells were plated and incubated with 1 µg/ml recombinant N-cadherin/Fc chimera at 37°C for 20 minutes. Plates were washed 5 times using PBS. Adherent cells were counted using phase contrast microscopy. Results were presented as percentage of adhesion out of the total number

### 2.2.10 Co-culture myeloma cells with osteoblasts

$6x10^3$ cells/$cm^2$ of primary osteoblasts were seeded in 24 well plates for 2 days in MEM alpha media (Invitrogen, UK) containing 10% FCS. When confluent, after 2 days, osteogenic media was added and osteoblasts were differentiated for 4 weeks to mature functional osteoblasts using osteogenic media; MEM alpha (Invitrogen, UK) containing 10 mM of β-glycerophosphate, 50 µg/ml of ascorbic acid and $10^{-8}$ M of dexamethasone (day 15 – day 28) in addition to 10% FCS, 100 units/ml Penicillin / 100 µg/ml of Streptomycin and 1.36 µg/mL of amphotericin B. Medium was changed every 2 days. Non-adherent 5T33MM and 5TGM1MM cells were cultured separately in RPMI1640 medium (Invitrogen, UK) containing 10% FCS, 100 units/ml Penicillin / 100 µg/ml of Streptomycin, 1% $Na_2PO_3$ and 1% non-essential amino acids (NEAA) and incubated in a humidified atmosphere at 37°C and 5% $CO_2$. Medium was changed every 2 days.

$6x10^3$ cells/$cm^2$ of mouse primary osteoblasts were seeded in 35mm glass bottom dishes. $5x10^4$ cells/ml of myeloma cells, 5T33MM-GFP and 5TGM1-GFP, were plated and incubated with osteoblasts at 37°C for 20 minutes. Plates were washed 5 times with 1ml of PBS and fixed with 300 µl of 4% fresh paraformaldehyde in PBS for 10 minutes in 4°C. Cells were permeablized with 0.1% triton in PBS for 10 minutes at room temperature and washed twice using PBS. Rabbit monoclonal anti-N-cadherin antibody (Millipore, UK) (1:50 dilution) was used. Cells were washed twice with 1ml of PBS to remove unbound antibody, and incubated with 300 µl of donkey anti-rabbit IgG secondary antibody, (1:200), labelled with fluorochrome northern light (NL637) (R&D systems, UK) for 1 hour at room temperature, then washed twice with PBS. Slides were mounted using Prolong mounting medium containing DAPI stain (Invitrogen, UK), DAPI stain was used to stain nuclei. Images were acquired using a Zeiss 510 microscope. Myeloma cells can be clearly identified in these cultures, as they are $GFP^+$ (green fluorescence) cells.

To block N-cadherin, myeloma cells, 5T33MM and 5TGM1, were incubated with anti-N-cadherin antibody (10 µg/ml) (Sigma, UK) at 37°C for 30 minutes (Figure 2.7). Mouse IgG1 antibody (Dako, Denmark) (10 µg/ml) was used as a negative control. Cells were mixed every 5 minutes. After 30 minutes, myeloma cells were centrifuged at 1000 rpm for 4 minutes, washed twice with PBS to remove non-binding antibody and re-suspended in MEM alpha (Groen et al., 2011). After blocking, $1x10^6$ cells/ml of myeloma cells were plated and incubated with immature osteoblasts (day 7) and mature functional osteoblasts (day 28) at 37°C for 20 minutes (Figure 2.6). Plates were washed 5 times using PBS. Adherent cells were fixed with 4% PFA and counted using phase contrast microscopy. Results were presented as percentage of adhered myeloma cells out of the total number of myeloma cells.

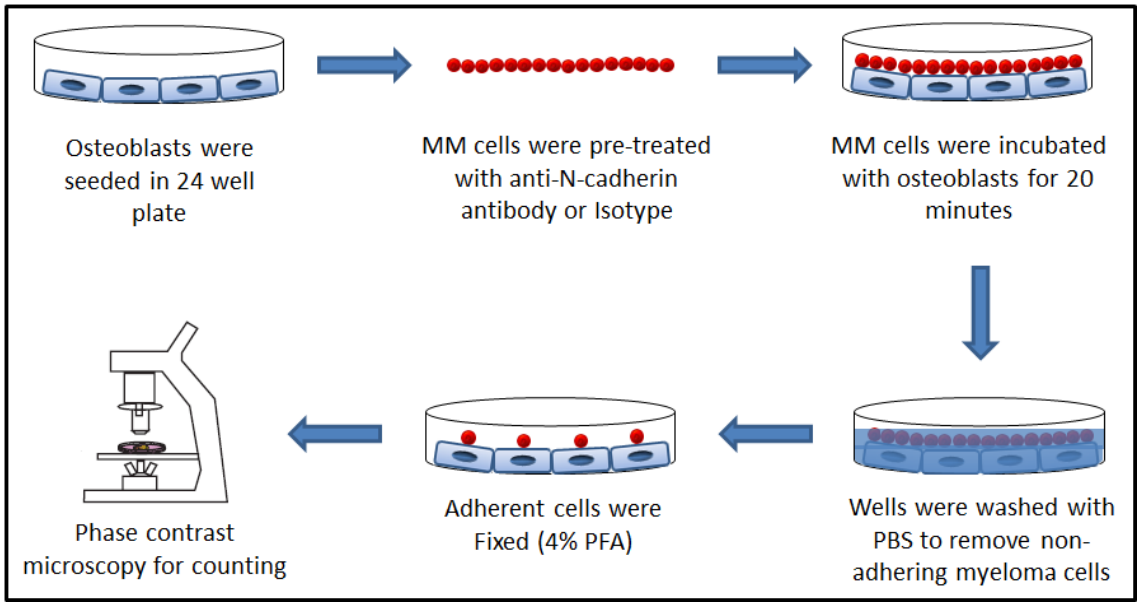


**Figure 2.7: A diagram showing the process of a co-culture of myeloma cells with osteoblasts.** Primary osteoblasts were seeded in 24 well plates and differentiated for 4 weeks from pre-osteoblasts to mature osteoblasts. $1x10^6$ cells/ml of myeloma cells were pre-treated with anti-N-cadherin antibody or isotype control for 30 minutes at 4ºC. Myeloma cells were plated and incubated with osteoblasts at 37°C for 20 minutes. Plates were washed 5 times using PBS. Adherent cells were counted using phase contrast microscopy. Results were presented as percentage of adhesion out of the total number of cells.

### 2.2.11 Cell labelling with DiD and blocking using anti-N-cadherin antibody

Myeloma cells ($1x10^6$ cells/ml) were re-suspended in RPMI1640 medium (Invitrogen, UK) containing 10% FCS. 5 µl of 1 µg/ml DiD (Invitrogen, UK) was added to each $1x10^6$ cells/ml and incubated at 37°C for 20 minutes. Cells were mixed every 5 minutes. After 20 minutes, myeloma cells were centrifuged at 1000 rpm for 4 minutes, washed twice with PBS to remove excessed DiD dye and re-constituted in RPMI medium containing 10% FCS. Figure 2.8 shows myeloma cells after labelling under the Zeiss 510 multiphoton laser scanning microscope. To block N-cadherin, myeloma cells, 5T33MM and 5TGM1, were incubated with anti-N-cadherin 40 µg/ml antibody (Sigma, UK) for 30 minutes at 37 °C (Ciolczyk-Wierzbicka et al., 2004). Mouse IgG1 antibody (Dako, Denmark) was used as a negative control. Cells were mixed every 5 minutes. After 30 minutes, myeloma cells were centrifuged at 1000 rpm for 4 minutes, washed twice with PBS to remove the non-adherent antibody and re-suspended in 1 ml PBS. Cells were counting (see section 2.2.1) to determine the percentage of dead and live cells after blocking.

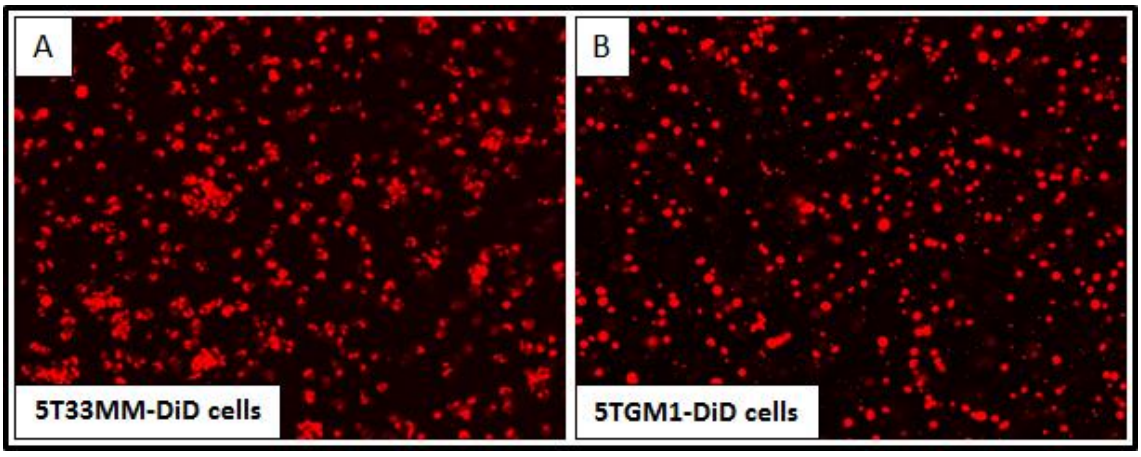


**Figure 2.8: Zeiss 510 multiphoton laser scanning microscope analysis of myeloma cells labelled with DiD.** 5T33MM-DiD cells (A) and 5TGM1-DiD cells (B) were visualised using Zeiss 510 multiphoton laser scanning microscope.

### 2.2.12 Inoculation of MM cells into mice

4-6 week old male C57BL/KaLwRij mice were used. Mice were handled carefully. Mice were put in rodent restrainer, a plastic that hold mice body and keep their tails free for induction, and their tails were anesthetized using EMLA$^{TM}$ cream 5% (AstraZeneca, UK). After 5 minutes, 200 µl of MM cell lines: 5T33MM and 5TGM1 ($2x10^6$ cells/200 µl) were inoculated into each mouse via their tail veins. Mice were harvested after various times according to the aims of each study.

### 2.2.13 Harvesting calvarial tissues

#### *2.2.13.1 Excise calvarial tissue*

Bone formation occurs through two unique mechanisms: intramembranous ossification and endochondral ossification. Nakashima et al (2003) showed that in calvarial mice, MSCs differentiate into osteoprogenitor cells then differentiate into osteoblasts that differentiate into osteocytes, which become embedded within the bone matrix in process called intramembranous ossification. In this case cells participated in bone formation include: MSCs, osteoprogenitor cells, osteoblasts and osteocytes. In contrast, in long bone, MSCs differentiate into chondrocytes forming the cartilage anlagen. Cells from the perichondrium of cartilage anlagen differentiate into osteoblasts, and the periphery of the cartilage anlage becomes hypertrophic. Finally, the matrix surrounding these hypertrophic chondrocytes calcifies and longitudinal growth is stimulated as cartilaginous matrix. In this case cells that participate in bone formation include: MSCs, perichondrium, chondrocytes, periosteum, hypertrophic chondrocytes, osteoclasts osteoblasts and osteocytes (Nakashima and de Crombrugghe, 2003). As we were interested in osteoblasts, we expected to see more osteoblasts compared to other cells in the calvariae. Therefore, we decided to use calvariae in this study.

The calvariae of mice consists of five bones; two frontal, two parietal and one interparietal bone (Figure 2.7). Calvariae of the mice were dipped in dilute embedding medium for frozen tissue specimens (Cryo-M-Bed) and snap frozen in liquid nitrogen. Samples were transferred and stored at -80 °C for multiphoton microscopy scanning. For cellular distribution C57BL/KalwRiJHsD calvariae were excised carefully and stored in 10% of neutral buffered formalin (NBF) for a minimum of three days and decalcified in EDTA for 14 days (Fisher Scientific, UK). Bones were washed with distilled water to remove EDTA and through graded alcohols to remove water. Sections of frontal, parietal and interparietal bones were taken for three levels every 200µM using a Leica microsystems microtome RM 2265 (Figure 2.8). Sections were floated for 30 minutes in a 45°C water bath, transferred onto glass slides, dried for 30 minutes on a 45°C hotplate (Raymond A Lamb Blockmaster II), incubated overnight at 37°C, and stored at 4°C until staining. Osteoclasts, osteoblasts and bone lining cells frequency were determined from 1.5 mm of both right and left side in the endo-cortical and trabecular surfaces of calvariae (Figure 2.9).

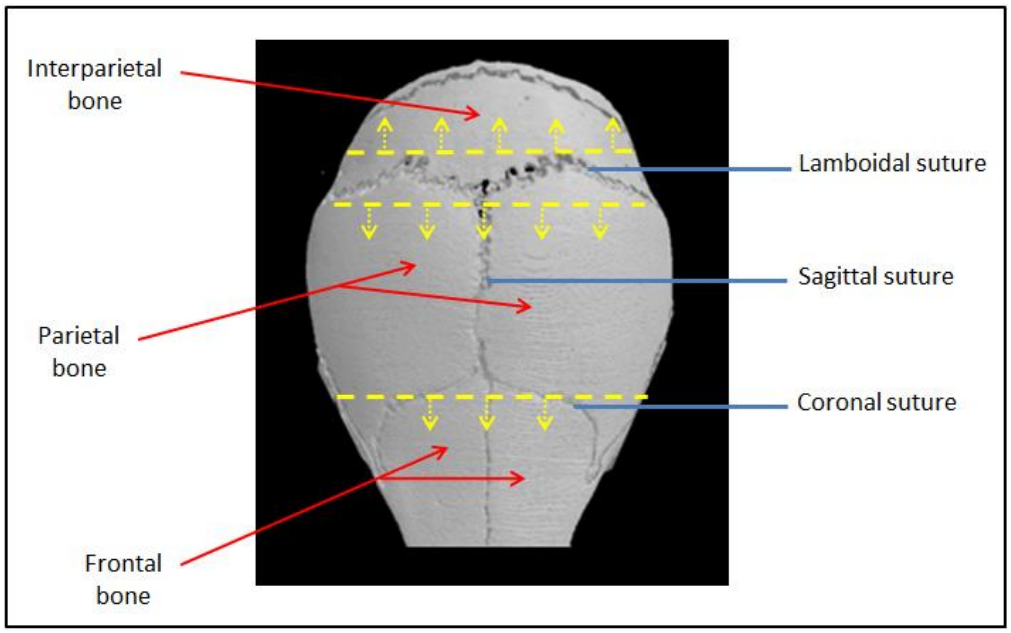


**Figure 2.7: A three-dimensional microCT reconstruction of a mouse skull demonstrating calvariae bones and dissected sections.** Calvariae of mice consist of five bones; two frontal, two parietal and one interparietal bone (red arrows).

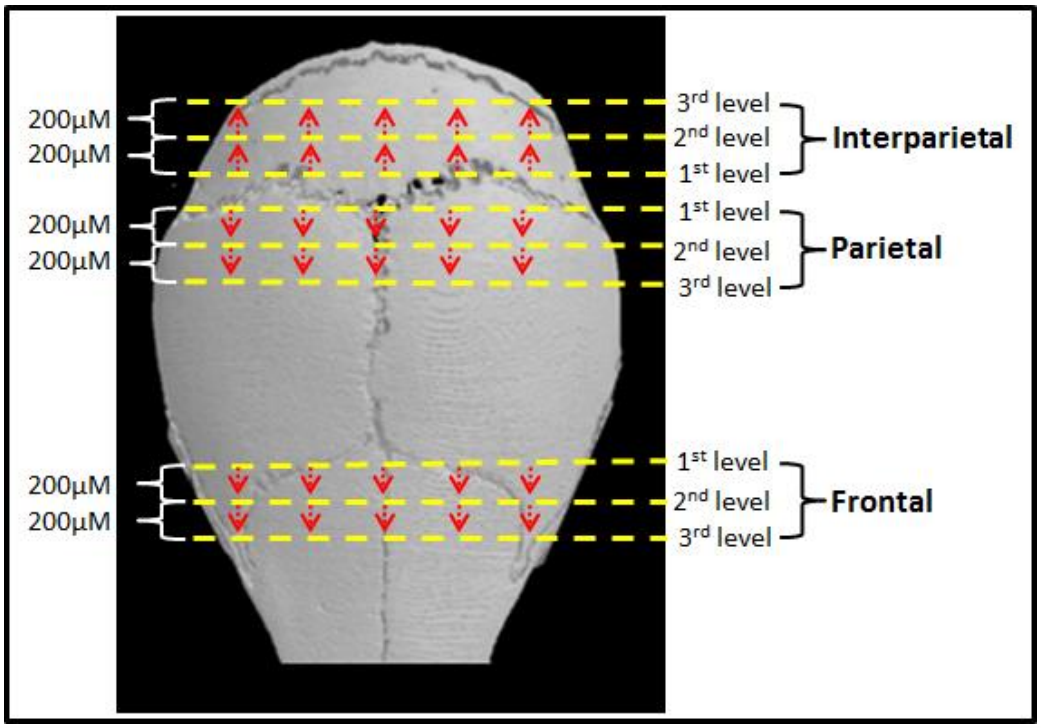


**Figure 2.8: A microCT three-dimensional reconstruction of C57BL/KaLwRijHsd calvariae.** Frontal, parietal, and interparietal bones were carefully dissected, as denoted by yellow arrows and the sections were taken for 3 levels every 200µM. Sections were stained with TRAP for determining the distribution of osteoclasts and stained with hematoxylin and eosin for determining the distribution of osteoblasts and quiescent bones.

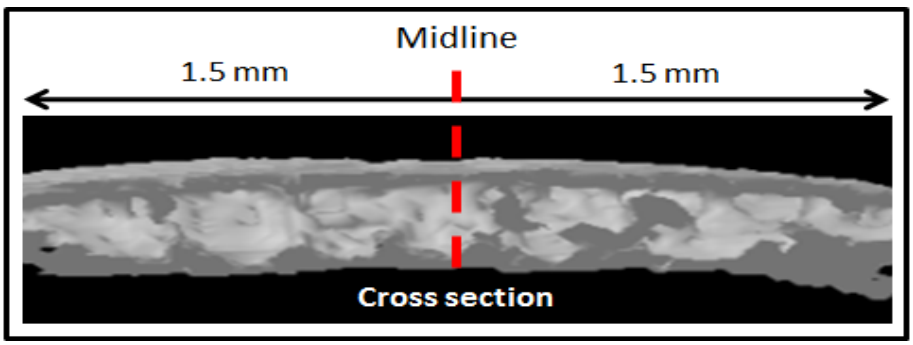


**Figure 2.9: A microCT cross section of calvarial bone.** Osteoclasts, osteoblasts and bone lining cells were determined in 3 mm from the middle.

### *2.2.13.2 TRAP staining*

Tartrate-resistant acid phosphatase (TRAP) is an isoenzyme of acid phosphatase found to be highly expressed by osteoclasts. TRAP is usually detected as a marker of osteoclast function (Minkin, 1982, Filgueira, 2004). The enzyme present within the tissue reacts with the substrate naphthol AS-BI phosphate to give a primary reaction product. This product then reacts with the diazonium salt (hexazotised pararosaniline) to form the final reaction product which is seen as a red deposit within the bone osteoclast cytoplasm. Bone sections were dipped twice in xylene for 5 minutes to remove wax and re-hydrated twice in absolute alcohol, 95% alcohol and 70% alcohol for 5 minutes and washed briefly in water. Sections were incubated in solution A, 50ml acetate-tartrate buffer (Sigma, UK) in 1ml naphthol/dimethylformamide (Sigma, UK), for 30 minutes at 37°C. After that, sections were incubated in 2.5ml of hexazotised solution (Sigma, UK), 2ml pararosaniline stock (Sigma, UK) with 2ml of 4% sodium nitrite solution (Sigma, UK), to 50ml acetate-tartrate buffer (VWR, UK) for 15 mins at 37°C. Sections were rinse twice gently in running tap water, counterstain for 20 seconds in Gill's haematoxylin (VWR, UK) by washing gently in running tap water. Sections were de-hydrated through 70% alcohol for 10 seconds, 95% alcohol for 10 seconds and twice in absolute alcohol for 30 seconds each. Xylene was used for 1 minute to remove alcohol and 3 minutes for clearance. Slides were mounted and covered using coverslips (VWR, UK). In endo-cortical and trabecular surfaces of calvariae the nuclei were stained blue and osteoclasts stained bright red/pink.

### *2.2.13.3 Hematoxylin and eosin staining*

Hematoxylin and eosin stain (H&E) is a standard staining method in histological studies. Hemalum is formed from aluminium ions and oxidized haematoxylin stains nuclei with blue colour whereas eosin stains cytoplasm and extracellular matrix with varying degrees of pink staining (Fischer et al., 2008, Llewellyn, 2009). Bone sections were dipped twice in xylene for 5 minutes to remove wax and re-hydrated twice in absolute alcohol, 95% alcohol and 70% alcohol for 5 minutes and washed briefly in

water. Gill's II haematoxylin (VWR, UK) was used for 120 seconds to stain nuclei. Sections were washed in water. 1% aqueous eosin (VWR, UK) with 1% calcium carbonate (Sigma, UK) was used for 5 minutes to stain cytoplasm. Sections were de-hydrated through 70% alcohol for 10 seconds, 95% alcohol for 10 seconds and twice in absolute alcohol for 30 seconds each. Xylene was used for 1 minute to remove alcohol and 3 minutes for clearance. Slides were mounted and covered using coverslips (VWR, UK). In endo-cortical and trabecular surfaces of calvariae the nuclei were stained blue, cytoplasm and extracellular matrix stained pink.

#### *2.2.13.4 Immunohistochemistry detection of N-cadherin in calvariae*

Bone sections were dipped twice in xylene for 5 minutes to remove wax and re-hydrated twice in absolute alcohol, 95% alcohol and 70% alcohol for 5 minutes and washed briefly in water. Sections were incubated in 3% hydrogen peroxide in water for 15 minutes to block the endogenous peroxidase activity. Sections were washed in water. For antigen retrieval sections were incubated with 10 mM of tri-sodium citrate (pH6) for 25 minutes at 80 ºC and cooled for 10 minutes. Sections were washed twice with PBS-Tween, blocked with 1% normal donkey serum for 30 minutes at room temperature, and followed by an incubation overnight at 4°C with 100 µl of 25-125 µg/ml anti-N-cadherin antibody (Millipore, UK) (1:200 dilution in PBS). 100 µl of 100 µg/ml normal rabbit IgG antibody (R&D systems, UK) was used as a negative control (1:200 dilution in PBS). Cells were washed twice with room temperature to remove unbound antibody, and incubated with 100 µl of biotinylated anti rabbit secondary antibody, (1:200 dilution), for 30 minutes at room temperature. Cells were washed twice again with PBS, and incubated with 300 µl of ABC for 30 minutes at room temperature. Cells were washed twice again with PBS, and incubated with 300 µl of Immpact DAB for 5 minutes at room temperature. Cells washed with water for 5 minutes, counter stained with haematoxyline for 20 seconds to stain nuclei, and washed again with water for 5 minutes. Bone sections were de-hydrated in 70% alcohol for 5 minutes, 95%

alcohol, twice in absolute alcohol for 5 minutes each and dipped twice in xylene for 5 minutes to remove alcohol. Slides were mounted and covered using cover slip.

### 2.2.14 Microscopy

#### *2.2.14.1 Multiphoton microscopy*

A Zeiss 510 Multiphoton Laser Scanning Microscopy was used to visualise fluorescence. Images included 2D X/Y plane, 2D tiled stacks and 3D z stacks to analyze imaging in more depth. Zeiss 510 Microscope is connected to the computer were used to capture images. The fluorochrome northern light (NL637) of the secondary antibody was excited at 633 nM and detected at 658 nM. Blue fluorescence of DAPI stain, which stains cells nuclei, is excited at 740 nM and detected at 360 nM. The bone was excited at 900 nM and detected at 450 nM. Red fluorescence of DiD stain was excited at 633 nM and detected at 658 nM. Images included 2D X/Y plane, 2D tiled stacks and 3D z stacks to analyze imaging in more depth.

#### *2.2.14.2 Leitz DMRB microscopy*

Osteomeasure software version 4.10 (Osteomerics Incorporated, Atlanta, USA) was used with a Leitz DMRB microscope and a drawing tablet, (CalComp Drawing Broad III) to quantify the cellular on endo-cortical and trabecular surfaces of calvariae. In addition, this microscopy was used to visualized non-florescence cells and sections.

### 2.2.15 Lightools image analysis system

All calvariae were analysed using Fluorescence Cheda Lightools Illumatools System (LT-9900 Bright Light System) in the University of Sheffield biological services laboratory. The Lightools image analysis system used to visualise $GFP^+$ tumour in

calvarial BM. The GFP-tumour was exited at 470 nm and detected at 515 nm with a MagnaFire SP cooled color charge-coupled device (CCD) camera.

### 2.2.16 High-resolution micro–computed tomography (µCT)

High resolution µCT scanner (model 1172; Skyscan, Belgium) is a non-destructive technique that provides three-dimensional micro-structure of bone (Laib et al., 2000, van Lenthe et al., 2007). µCT scanner was used to scan calvarial bones. Image captured every 0.35° through a 360° rotation with 4.1 pixel size. Scanned images were reconstructed using Skyscan NRecon software (version 1.5.1.3, Skyscan, Belgium) and analysed using Skyscan CT analysis software (version 1.8.1.2, Skyscan, Belgium). Cortical volume, trabecular volume, trabecular thickness and trabecular number were evaluated in a standardized region of interest. All cortical and trabecular bone within this region was quantitated.

### 2.2.17 Study to determine the distribution of osteoclasts, osteoblasts and quiescent bone in C57BL/KaLwRijHsd calvariae

C57BL/KaLwRijHsd calvariae were excised carefully from 5 male mice, 6 weeks of age and stored in formalin. Frontal, parietal, and interparietal bones were carefully dissected and sections of each calvarial part were cut for 3 levels. Each level cut after 200µM from previous (Figure 2.8). TRAP staining was used to determine the distribution of osteoclasts in the endo-cortical and trabecular surfaces of calvariae as described in section 2.2.11.3. Haematoxylin and eosin staining was used to determine the frequency of osteoblasts and non-osteoclast/osteoblast lined surfaces, quiescent bones in the endo-cortical and trabecular surfaces of calvariae in section 2.2.11.4. Osteomeasure software version 4.10 (Osteomerics Incorporated, Atlanta, USA) was used to analyse the sections. Osteoclasts, osteoblasts and bone lining cells frequency were determined in section 2.2.13.1 (see figure 2.9).

### 2.2.18 Study to determine the distribution of new bone formation in C57BL/KaLwRijHsd calvariae

4 male C57BL/KaLwRijHsd mice, 6 weeks of age, were injected with 200µl of calcein-GFP (3 mg/ml in PBS) each at day 0 (Figure 2.10). After 3 days, mice were sacrificed and calvariae were excised carefully, dipped in 1:2 diluted OCT and stored in -80 ºC. Zeiss 510 multiphoton laser scanning microscope was used to determine the new bone formation in different part of calvariae bones: frontal, parietal and interparietal.


**Figure 2.10: Experiment design to determine the bone formation rate.** 4 x 6 week old male, C57BL/KaLwRijHsd mice were injected with 200µl of 3 mg/ml calcein-GFP each at day 0. At day 3 mice sacrificed and calvarial bone were analysed under the Zeiss 510 multiphoton laser scanning microscope.

### 2.2.19 Study to determine if myeloma tumour can grow in C57BL/KaLwRijHsd calvarial BM

9 male C57BL/KaLwRijHsd mice, 6 weeks of age, were used in this experiment and separated to 3 groups (Figure 2.11). The first group contained 3 mice used as a control, no myeloma injected. The second group contained 3 mice that were inoculated with 5T33MM-GFP cells ($2x10^6$ cells/mouse) at day 0. The third group contained 3 mice that were inoculated with 5TGM1-GFP cells ($2x10^6$ cells/mouse) at day 0. After 21 days all mice were sacrificed. Calvariae were excised carefully and analysed under the Lightools system to obtain optical images of fluorescent tumour growth in calvarial BM.


**Figure 2.11: Experiment design to determine the tumour growth in calvarial bone marrow.** 3 x 6 week old male, C57BL/KaLwRijHsd mice were injected with 200µl of PBS as control mice at day 0 (group 1). 3 x 6 week old male, C57BL/KaLwRijHsd mice were injected with 200µl of $2x10^6$ cells/mouse 5T33MM-GFP cells at day 0 (group 2). 3 x 6 week old male, C57BL/KaLwRijHsd mice were injected with 200µl of $2x10^6$ cells/mouse 5TGM1-GFP cells at day 0 (group 3). At day 21 all mice sacrificed and calvarial bone were analysed under the light tool.

### 2.2.20 Study to determine the single cell numbers arriving in C57BL/KaLwRijHsd calvarial BM

12 male C57BL/KaLwRijHsd mice, 6 weeks of age, were used in this experiment and separated into 4 groups (Figure 2.12). The first group contained 3 mice were injected with 5T33MM-DiD cells ($2x10^6$ cells/mouse) at day 0. The second group contained 3 mice were injected with 5TGM1-DiD cells ($2x10^6$ cells/mouse) at day 0. After 3 days groups 1 and 2 mice were sacrificed to determine the single cell numbers in calvarial BM in the early stage of disease. The third groups contained 3 mice were injected with 5T33-DiD cells ($2x10^6$ cells/mouse) at day 0. The fourth group contained 3 mice were injected with 5TGM1-DiD cells ($2x10^6$ cells/mouse) at day 0. After 21 days groups 3 and 4 were sacrificed to determine the quiescent cell numbers in calvarial BM in the late stage of disease. Zeiss 510 multiphoton laser scanning microscope was used to determine the cell numbers in C57BL/KalwRij calvarial BM.

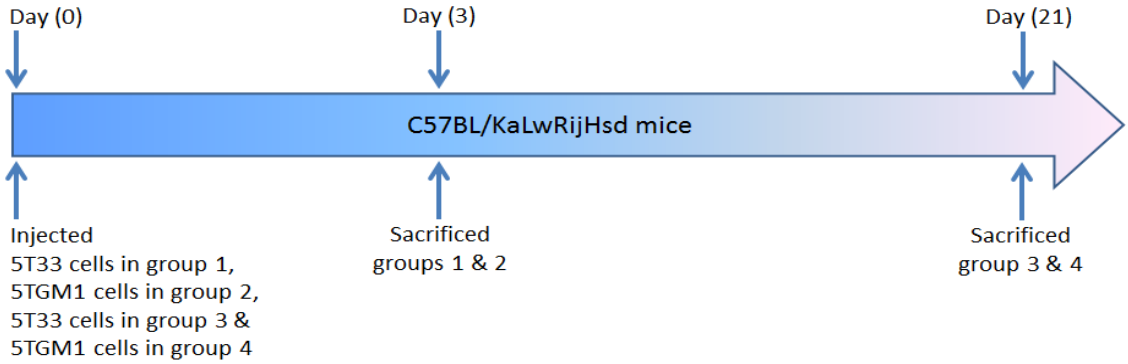


**Figure 2.12: Experiment design to determine single cell numbers in calvarial bone marrow.** 3 x 6 week old male, C57BL/KalwRij mice were injected with 200µl of $2x10^6$ cells/mouse 5T33MM-DiD cells at day 0 (group 1). 3 x 6 week old male, C57BL/KalwRij mice were injected with 200µl of $2x10^6$ cells/mouse 5TGM1-DiD cells at day 0 (group 2). At day 3 groups 1 and 2 mice were sacrificed and calvarial bone were analysed under the Zeiss 510 multiphoton laser scanning microscope. 3 x 6 week old male, C57BL/KalwRij mice were injected with 200µl of $2x10^6$ cells/mouse 5T33MM-DiD cells at day 0 (group 3). 3 x 6 week old male, C57BL/KalwRij mice were injected with 200µl of $2x10^6$ cells/mouse 5TGM1-DiD cells at day 0 (group 4). After 21 groups 3 and 4 mice were sacrificed and calvarial bone were analysed under the Zeiss 510 multiphoton laser scanning microscope.

### 2.2.21 Assessment of the cellular distribution of N-cadherin *in vivo*

9 male C57BL/KaLwRijHsd mice, 6 weeks of age, were used in this experiment and separated to 3 groups (Figure 2.13). The first group contained 3 mice and were inoculated with PBS at day 0 as a negative control. The second group contained 3 mice and were inoculated with 5T33MM cells ($2x10^6$ cells/mouse) at day 0. The third group contained 3 mice and were inoculated with 5TGM1 cells ($2x10^6$ cells/mouse) at day 0. After 7 days all mice were sacrificed. Calvariae were excised and sections of interparietal bones of calvariae were dissected for immunohistochemistry. Bone sections were de-waxed in xylene and re-hydrated twice in absolute alcohol, 95% alcohol and 70% alcohol. Sections were incubated in 3% hydrogen peroxide in water for 15 minutes to block the endogenous peroxidase activity. For antigen retrieval sections were incubated with 10 mM of tri-sodium citrate (pH6) for 25 minutes at 80 ºC and cooled for 10 minutes. Rabbit monoclonal anti-N-cadherin antibody (Millipore, UK) and donkey anti-rabbit IgG antibodies (R&D systems, UK), isotype negative control were used as described in section 2.2.11.5.


**Figure 2.13: Experiment design to determine the cellular distribution of N-cadherin *in vivo*.** 9 x 6 week old male, C57BL/KaLwRijHsd mice were inoculated with 200µl of PBS or myeloma cells ($2x10^6$ cells/mouse) at day 0. At day 7 mice sacrificed and calvarial bones were carefully dissected for immunohistochemistry.

### 2.2.22 Study to determine the effect of blocking N-cadherin on myeloma colonization in bone *in vivo*

18 male C57BL/KaLwRijHsd mice, 6 weeks of age, were used in this experiment and separated to 3 groups (Figure 2.14). The first group containing 6 mice were inoculated with 5T33MM-DiD labelled cells, second group containing 6 mice were inoculated with 5T33MM-DiD labelled cells pre-treated with isotype control antibody and third group containing 6 mice were inoculated with 5T33MM-DiD labelled cells pre-treated with anti-N-cadherin antibody ($2x10^6$ cells/mouse) at day 0. After 3 days these mice were sacrificed to determine the effect of blocking N-cadherin on myeloma arrival and colonization in calvariae. Calvariae were excised and sections of frontal, parietal, and interparietal bones were dissected (Figure 2.15). Sections were analysed under Zeiss 510 multiphoton laser scanning microscope to determine the myeloma cell numbers and the distance of myeloma cells to bone between different groups in C57BL/KalwRij calvarial BM: frontal, parietal and interparietal.

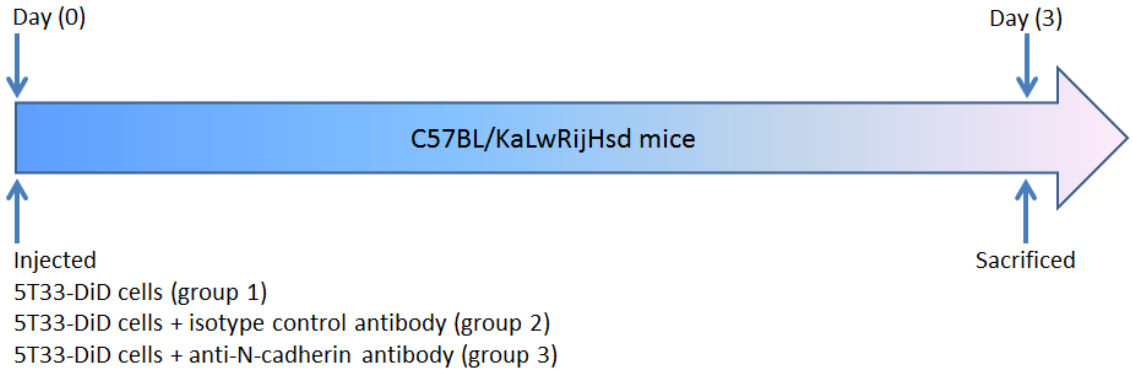


**Figure 2.14: Experiment design to determine the effect of blocking N-cadherin on myeloma colonisation in bone *in vivo*.** 6 x 6 week old male, C57BL/KalwRij mice were inoculated with 200µl of $2x10^6$ cells/mouse 5T33MM-DiD cells, 6 x 6 week old male, C57BL/KalwRij mice were inoculated with 200µl of $2x10^6$ cells/mouse 5T33MM-DiD cells pre-treated with isotype control antibody and 6 x 6 week old male, C57BL/KalwRij mice were inoculated with 200µl of $2x10^6$ cells/mouse 5T33MM-DiD cells pre-treated with anti-N-cadherin antibody at day 0. At day 3 mice were sacrificed and calvarial bone were analysed under the Zeiss 510 multiphoton laser scanning microscope.

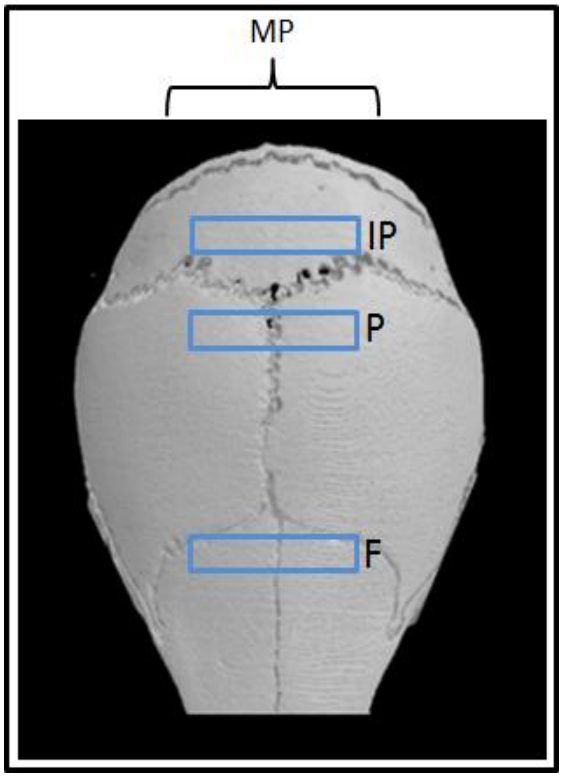


**Figure 2.15: A microCT three-dimensional reconstruction of C57BL/KaLwRijHsd calvariae showing areas selected for multiphoton (MP) analysis.** Frontal (F), parietal (P), and interparietal (IP) bones were carefully dissected, as denoted by blue oblongs. Section were analysed under Zeiss 510 multiphoton laser scanning microscope to determine the myeloma cell numbers and the distance of myeloma cells to the bone between different groups: 5T33MM, 5T33MM pre-treated with isotype control antibody. 5T33MM pre-treated with anti-N-cadherin antibody.

### 2.2.23 Study to determine the effect of blocking N-cadherin on myeloma bone disease *in vivo*

9 male C57BL/KaLwRijHsd mice, 6 weeks of age, were used in this experiment and separated into 3 groups (Figure 2.16). The first group containing 3 mice were inoculated with 5TGM1-DiD labelled cells, second group containing 3 mice were inoculated with 5TGM1-DiD labelled cells pre-treated with isotype control antibody and third group containing 3 mice were inoculated with 5TGM-DiD labelled cells pre-treated with anti-N-cadherin antibody ($2x10^6$ cells/mouse) at day 0. After 21 days these mice were sacrificed and calvariae examined to determine the effect of blocking N-cadherin on myeloma bone disease *in vivo*. Calvariae were excised and sections of frontal, parietal, and interparietal bones were dissected (Figure 2.17). Sections (left side) were analysed under Zeiss 510 multiphoton laser scanning microscope to determine the quiescent myeloma cell numbers and the distance of quiescent myeloma cells to bone between different groups in C57BL/KalwRij calvarial BM. Sections (right side) were analysed using the µCT to determine the bone disease.

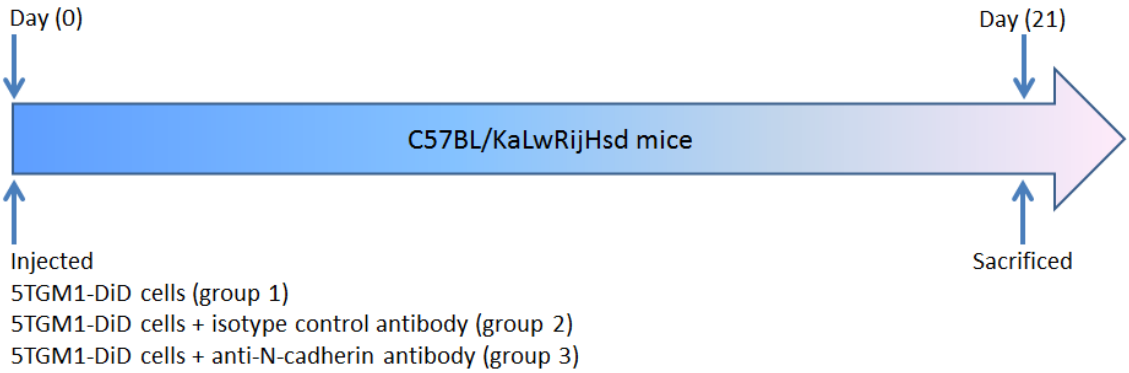


**Figure 2.16: Experiment design to determine the effect of blocking N-cadherin on myeloma bone disease *in vivo*.** 3 x 6 week old male, C57BL/KalwRij mice were inoculated with 200µl of $2x10^6$ cells/mouse 5TGM1-DiD cells, 3 x 6 week old male, C57BL/KalwRij mice were inoculated with 200µl of $2x10^6$ cells/mouse 5TGM1-DiD cells pre-treated with isotype control antibody and 3 x 6 week old male, C57BL/KalwRij mice were inoculated with 200µl of $2x10^6$ cells/mouse 5TGM1-DiD cells pre-treated with anti-N-cadherin antibody at day 0. At day 21 mice were sacrificed and calvarial bone were analysed.

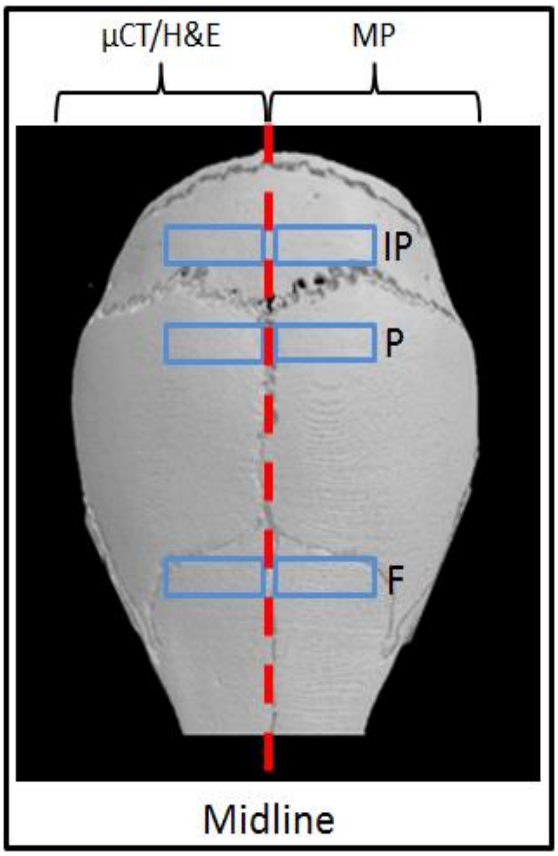


**Figure 2.17: A microCT three-dimensional reconstruction of C57BL/KaLwRijHsd calvariae showing areas selected for µCT, histology and MP analysis.** Frontal (F), parietal (P), and interparietal (IP) bones were dissected, as denoted by blue oblongs. Sections in left side were analysed under Zeiss 510 multiphoton laser scanning microscope to determine the quiescent myeloma cell numbers and the distance of quiescent myeloma cells to bone between different groups. Sections in right side were analysed using the µCT then stained with H&E to determine the bone disease and tumour burden, respectively, between different groups.

### 2.2.24 Statistical analysis

Statistical analyses were performed with the statistical software package, GraphPad Prism 5 version 5.04 for Windows. Firstly the data were checked if they were normally distributed or not by using the D'Agostino and Pearson normality test. The data were analysed using an ANOVA test (one-way analysis of variance) for more than two group comparisons or with *t* test for two group comparisons if the data was normally distributed. Tukey's test was used as post-hoc analysis when ANOVA test was used in normal distribution data. When data not normally distributed, ANOVA test (non-parametric Kruskal-Wallis test) was used for more than two group comparisons or non-parametric Mann–Whitney test was used for two group comparisons. Dunns test was used as post-hoc analysis when ANOVA test was used in not normally distributed data. Data were considered statistically significant when a p-value was equal to or less than 0.05. Results are expressed as mean ± values of standard deviation (SD).

# 3 Chapter 3: The stem cell marker N-cadherin is expressed by myeloma cells and osteoblasts

## 3.1 Introduction

Characterising the putative 'myeloma niche' (a myeloma permissive microenvironment) may offer novel therapeutic targets to treat patients. The concept of a specialised niche "HSC niche" has recently been described for HSCs. In the present project the hypothesis that colonising myeloma cells retain the molecular machinery of HSCs and modify the HSC niche to establish the myeloma bone disease has been considered. Several secreted factors and receptors have been shown to be expressed and may have functions in mediating the cellular interactions that occur between osteoblasts and HSCs. Notch, Tie2, CD44, N-cadherin and CXCR4 are molecules expressed by HSCs and bind with their complimentary ligands, Jag1, Ang-1, OPN, N-cadherin and CXCL12, respectively on the osteoblasts. These molecular associations: Notch/Jag1, Ang-1/ Tie2, OPN/CD44, N-cadherin/N-cadherin and CXCR4/CXCL12 are thought to maintain HSCs in a quiescent state in the HSC niche (Calvi et al., 2003, Arai et al., 2004, Nilsson et al., 2005, Stier et al., 2005, Zhang et al., 2003, Xie et al., 2009, Burger and Kipps, 2006). Colonizing myeloma cells may use one or some of these molecules, to bind to their complimentary ligands on the osteoblasts to hijack the HSC niche.

The present study focused on one of these molecules, N-cadherin, that has been identified as an important regulatory molecule in the HSC niche expressed by both HSCs and osteoblasts (Zhang et al., 2003, Xie et al., 2009) and also during tumour progression in solid tumours, in which the invasion and metastatic properties acquired by cancer cells have been linked to expression of N-adhesion molecules (Li et al., 2001, Lascombe et al., 2006, Gravdal et al., 2007). In addition, there is no current publication that addresses blocking of N-cadherin in myeloma cells. As N-cadherin is expressed by osteoblasts, but not by osteoclasts or osteocytes (Mbalaviele et al., 1995, Ferrari et al., 2000, Kawaguchi et al., 2001), this study focused on the expression of N-cadherin in myeloma cells and osteoblasts. As we were interested in osteoblasts, more osteoblasts compared to other cells were expected to be found in calvariae (Nakashima and de Crombrugghe, 2003).

Puch et al (2001) showed N-cadherin was expressed on a subpopulation of early hematopoietic progenitor cells, human $CD34^+$ HSCs using RT-PCR, western blot analysis and immunofluorescence staining. During the differentiation of $CD34^+$ HSCs, N-cadherin expression was lost. Treatment of $CD34^+$ HSCs with monoclonal anti-N-cadherin antibodies, GC-4, inhibited the formation of total (colony-forming unit-culture) CFU-C count. Furthermore, N-cadherin mediated the adhesion of HSCs within the bone marrow, which could be inhibited by using anti-N-cadherin antibodies. Together these data suggested a direct interaction of HSCs within the bone marrow microenvironment via N-cadherin (Puch et al., 2001). In addition, it was shown that HSCs home to and reside in the 'osteoblast niche' via attachment to N-cadherin$^+$ osteoblasts on the endosteal bone surface. Green fluorescent protein-expressing ($GFP^+$) HSCs were injected in irradiated mice. $GFP^+$ HSCs were monitored using *ex vivo* real-time imaging technology and immunoassay. It was found that HSCs tended to home to the endosteum near N-cadherin$^+$ pre-osteoblasts. In contrast, HSCs in the central marrow underwent active division suggesting that the endosteum formed a special zone to maintain HSCs quiescent (Xie et al., 2009). It is unclear whether myeloma cells attach to sites of bone formation, quiescent bone lining cells or remain close to a collagen matrix, a known store of growth factors.

In this chapter, primary mouse osteoblasts and myeloma cell lines, 5T33MM and 5TGM1 were used. In preliminary studies, the conditions for *in vitro* osteoblastogenesis were established. In addition, the expression of N-cadherin at different stages of osteoblastogenesis and in myeloma cell lines; 5T33MM and 5TGM1, was described and the potential mechanisms colonising myeloma cells may exploit to establish colonies within the BM microenvironment were evaluated.

## 3.2 Hypothesis and objectives of this chapter

### 3.2.1 Hypothesis:

The stem cell marker N-cadherin is expressed by myeloma cells and osteoblasts.

### 3.2.2 Objectives:

To test this hypothesis, I have:

1. Developed a model of mouse osteoblastogenesis.
2. Determined and quantified the relative expression of N-cadherin mRNA during osteoblastogenesis.
3. Immuno-localized N-cadherin protein in osteoblasts.
4. Determined the percentage and relative expression of N-cadherin protein during osteoblastogenesis.
5. Determined and quantified the relative expression of N-cadherin mRNA in myeloma cell lines, 5T33MM and 5TGM1.
6. Immuno-localized N-cadherin protein in myeloma cell lines, 5T33MM and 5TGM1.
7. Determined the percentage and relative levels of N-cadherin protein in myeloma cell lines, 5T33MM and 5TGM1.

## 3.3 Materials and methods

### 3.3.1 Cell culture

Non-adherent 5T33MM cells and 5TGM1 cells were cultured separately *in vitro* in RPMI1640 medium (Invitrogen, UK) containing 10% FCS, 100 units/ml Penicillin / 100 µg/ml of Streptomycin, 1% $Na_2PO_3$ and 1% non-essential amino acids (NEAA) in T75 flasks as described in section 2.1.7.1 and section 2.1.7.2. Mouse primary osteoblasts were obtained from calvarial bones of 2-4 day old C57Bl/6J mice, (Harlan, UK). Mouse primary osteoblasts were prepared and cultured *in vitro* in T75 flasks as described in section 2.1.9.

### 3.3.2 An *in vitro* model of mouse osteoblastogenesis

Osteoblastogenesis is a complex multi-step process, in which osteoblasts derived from MSCs, proliferate, maturate and lay down in a matrix which is then mineralised. These sequential actions may define unique subsets of osteoblasts residing in discreet pockets or niches within bone, depending on functional activity. These niches may maintain levels of a specific array of cytokines and growth factors that enable myeloma cell colonization. Mouse primary osteoblasts were obtained from calvarial bones of 2-4 day old C57Bl/6J mice as in previous published methods (Garcia et al., 2002, Hay et al., 2009a) and prepared as described in section 2.1.9. *In vitro*, cells were seeded in T75 flasks and passaged as described in section 2.2.2 to obtained the required number of cells. The cells were transferred to 96 well plates, 24 well plates, 8 chambers slides and T25 flasks, and differentiated for 4 weeks (28 days) in osteogenic medium to form mature functional osteoblasts (see figure 3.1). ALP activity, alizarin red staining, RT-PCR, TaqMan, flow cytometry, immuno-staining and western blot experiments were used to analysed osteoblastogenesis.

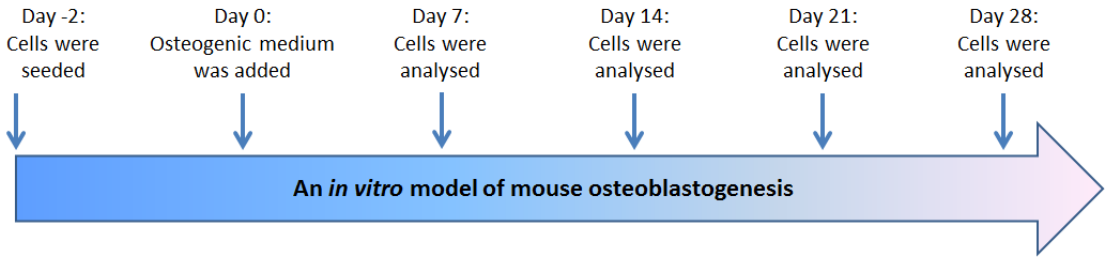


**Figure 3.1: Experiment design of mouse osteoblastogenesis.** Extracted osteoblasts from mouse calvariae were seeded in T-75 flasks for expansion of cell numbers. Cells were harvested from a nearly confluent flask by trypsinisation. Day 0; $6x10^3$ cells/$cm^2$ of mouse primary osteoblasts was re-suspended in 10% α-MEM medium and seeded in 96 well plates, 24 well plates, chamber slides and flasks. Cells were then incubated at 37 ˚C with 5% $CO_2$. Osteoblasts were differentiated using osteogenic medium. Day 2; α-MEM medium was replaced by osteogenic medium to start osteoblastogenesis process. Osteoblastogenesis was analyzed at days 7, 14, 21 and 28 using ALP activity, alizarin red staining, RT-PCR, TaqMan, flow cytometry, immuno-staining and western blot experiments. Medium was changed every 2 days.

### 3.3.3 Osteoblasts differentiation

$6x10^3$ cells/$cm^2$ of mouse primary osteoblasts were seeded and differentiated for to mature functional osteoblasts in osteogenic media as described in section 2.2.4. ALP activity for mouse primary osteoblasts was analysed as described in section 2.2.4.1. Total DNA content of primary osteoblasts was determined with a PicoGreen double-stranded DNA quantitation reagent as described in section 2.2.4.2 and these measurements used to normalise the ALP activity to cell DNA content. Matrix deposited by mouse primary osteoblasts was analysed as described in section 2.2.4.3 during differentiation. ImageJ software was used to quantify the red colour of alizarin red staining as described in section 2.2.4.3.

### 3.3.4 Determination of the effect of dexamethasone on osteoblastogenesis

Mouse primary osteoblasts were seeded at day -2, incubated with osteogenic media at day 0, and ALP activity and mineralization of primary osteoblasts were analyzed at days 7, 14, 21 and 28. Gilbert et al (2002) differentiated osteoblasts using α-MEM medium containing; 10% FCS, 10 mM of β-glycerophosphate and 50 µg/ml of ascorbic (Gilbert et al., 2002). However, Bancroft et al (2002) differentiated osteoblasts using α-MEM medium containing; 10% FCS, 10 mM of β-glycerophosphate, 50 µg/ml of ascorbic acid and $10^{-8}$ M of dexamethasone (Bancroft et al., 2002). Therefore, in my study different osteogenic medium were used to determine if adding $10^{-8}$ M of dexamethasone promotes the differentiation of osteoblasts. Cells were incubated in different formulations and regimens of osteogenic medium as described in the following table (Table 3.1).

Table 3.1: Different formulation and regimens of osteogenic medium

| Series | 1st formulation and regimens (Days 0-14) | 2nd formulation and regimens (Days 15-28) |
|---|---|---|
| 1 | α-MEM medium + 10% FCS + 10 mM of β-glycerophosphate + 50 µg/ml of ascorbic acid. | As 1st formulation |
| 2 | α-MEM medium + 10% FCS + 10 mM of β-glycerophosphate + 50 µg/ml of ascorbic acid. | α-MEM medium + 10% FCS + 10 mM of β-glycerophosphate + 50 µg/ml of ascorbic acid + **$10^{-8}$ M of dexamethasone**. |
| 3 | α-MEM medium + 10% FCS + 10 mM of β-glycerophosphate + 50 µg/ml of ascorbic acid + **$10^{-8}$ M of dexamethasone**. | As 1st formulation |
| 4 | α-MEM medium + 10% FCS, 10 mM of β-glycerophosphate, 50 µg/ml of ascorbic acid + **$H_2O$**. | As 1st formulation |

### 3.3.5 Molecular biology

#### *3.3.5.1 RNA isolation and quantitation*

For osteoblasts, nearly confluent T25 flasks were washed twice with PBS and total RNA was extracted from primary osteoblasts at different stages of development using TriZol. For myeloma cell lines 5T33MM and 5TGM1 cells around $1x10^6$ cells were washed twice with PBS and total RNA was extracted using TriZol. Total RNA was precipitated using isopropanol and re-suspended in RNase and DNase free $H_2O$ as described in section 2.2.5.1. NanoDrop ND 1000 Spectrophotometer (NanoDrop Technologies, USA) was used to quantify total RNA in the solution as described in section 2.2.5.2.

#### *3.3.5.2 cDNA synthesis*

According to the manufacturer's instructions (Invitrogen, UK), known concentrations of RNA were treated with DNase I to remove any genomic DNA contamination. RNAs were then transcribed to cDNA using SuperScript™ II reverse transcriptase (Invitrogen, UK) as described in section 2.2.5.4.

#### *3.3.5.3 RT-PCR and sequencing*

NCBI, UCSC and Ensemble were searched against N-cadherin, NM_007664.4 mouse RefSeq gene and GAPDH (control), NM_008084.2 mouse RefSeq gene. PCR primers used to amplify N-cadherin and GAPDH (see table 2.2 in materials and methods) in mouse primary osteoblasts, 5T33MM cells and 5TGM1 cells were designed as described in section 2.2.5.5. According to the manufacturer's instructions (Invitrogen, UK), RT-PCR was performed using Platinum *Taq DNA* polymerase kit (Invitrogen, UK) to amplify N-cadherin and GAPDH, a control (Hay et al., 2009b, Arai et al., 2012) as described in section 2.2.5.6. PCR products were run in a 1% agarose (Invitrogen,

UK) gel and stained with ethidium bromide (Fluka, Switzerland) as described in section 2.2.5.7. The QIAquick Gel Extraction kit was used according to the manufacturer's instructions (QIAGEN Ltd, UK) to extract and purify DNA fragments from agarose gels as described in section 2.2.8. DNA samples were sent into the DNA Sequencing Core Facility housed within the University of Sheffield, Medical School and sequenced (http://genetics.group.shef.ac.uk/dna-sequencing.html).

#### *3.3.5.4 TaqMan analysis*

Nearly confluent T25 flasks were washed twice with PBS and total RNA was extracted from primary osteoblasts at different stages of development and from myeloma cells, and cDNA was synthesised. N-cadherin mRNA, Runx2 mRNA, COL1A2 mRNA and osteocalcin mRNA primers (see table 2-3 in materials and methods) were used to quantify the expression of these molecules during mouse primary osteoblast differentiation and in myeloma cells using TaqMan. Universal master Mix II (Applied biosystems, UK) was used as described in section 2.2.5.10.

### 3.3.6 Immunofluorescence detection of N-cadherin protein in osteoblasts

Osteoblasts were seeded and differentiated as described in section 2.2.4. Cells were washed twice with PBS then fixed in 4% paraformaldehyde. Rabbit monoclonal anti-N-cadherin antibody (Millipore, UK) and donkey anti-rabbit IgG antibodies (R&D systems, UK), secondary antibody were used as described in section 2.2.6.1. Slides were mounted using prolong mounting medium containing DAPI stain (Invitrogen, UK), DAPI stain was used to stain nuclei. Images were acquired using a Zeiss 510 microscope.

### 3.3.7 Immunocytochemistry detection of N-cadherin protein in myeloma cells: 5T33MM and 5TGM1 cells

$1x10^6$ cells/ml of myeloma cells were re-suspended and fixed in 4% paraformaldehyde then spun onto slides using a cytospin cassette. Rabbit monoclonal anti-N-cadherin antibody (Millipore, UK) and biotinylated anti-rabbit IgG antibodies (R&D systems, UK), secondary antibody were used as described in section 2.2.6.3.

### 3.3.8 Microscopy

Osteomeasure software version 4.10 (Osteomerics Incorporated, Atlanta, USA) was used with a Leitz DMRB microscope and a drawing tablet, (CalComp Drawing Broad III) to determine the N-cadherin when biotinylated anti-rabbit IgG antibodies (R&D systems, UK), secondary antibody was used as described in section 2.2.14.2. A Zeiss 510 Multiphoton Laser Scanning Microscopy was used to visualise fluorescence as described in section 2.2.14.1.

### 3.3.9 Flow cytometry

Lightning-Link™ Atto637 conjugation kit (Innova Biosciences, UK) was used to label the anti-N-cadherin antibody, GC-4 (Sigma, UK) and the mouse IgG antibody (Vector laboratories, UK), isotype negative control as described in section 2.2.7.1. To determine the expression of N-cadherin protein by flow cytometry, adherent cells were harvested as described in section 2.2.7.2. $5x10^5$ of fixed primary osteoblasts, 5T33MM cells and 5TGM1 cells were stained as described in section 2.2.7.3.

### 3.3.10 Western blot

Proteins were extracted from ~80% confluent cells and quantified using the BCA protein assay. 10 μg of protein samples were separated on 12.5% SDS-PAGE for N-cadherin and 15% SDS-PAGE for β-actin, blotted on PVDF membranes and probed with anti-N-cadherin antibody and/or with anti-β-actin as housekeeping genes. Rabbit monoclonal anti-N-cadherin antibody (Millipore, UK) (1:1000 dilution) and donkey anti-rabbit IgG antibodies (R&D systems, UK) (1:1000 dilution), secondary antibody were used as described in methods in section 2.2.8.

### 3.3.11 Statistical analysis

The data were analysed using an ANOVA test (one-way analysis of variance) for more than two group comparisons or with *t* test for two group comparisons if the data was normally distributed. Tukey's test was used as post-hoc analysis when ANOVA test was used in normal distribution data. When data not normally distributed, ANOVA test (non-parametric Kruskal-Wallis test) was used for more than two group comparisons or non-parametric Mann–Whitney test was used for two group comparisons. Dunns test was used as post-hoc analysis when ANOVA test was used in not normally distributed data. Data were considered statistically significant when a p-value was equal to or less than 0.05. Results are expressed as mean ± values of standard deviation (SD).

## 3.4 Results

### 3.4.1 Optimising a model of mouse osteoblastogenesis

#### *3.4.1.1 ALP activity during osteoblast differentiation*

ALP activity was used as an early osteoblast differentiation marker. Figure 3.2 panel A shows ALP activity of primary osteoblasts incubated in the first series in which cells were incubated in α-MEM medium containing; 10% FCS, 10 mM of β-glycerophosphate and 50 μg/ml of ascorbic acid for 28 days. The result demonstrated statistically significant increases in ALP activity on day 14 compared to day 7 (60.03±8.50 versus 11.48±1.23, $p<0.001$) then a statistically significant decrease in ALP activity on day 21 and day 28.

Figure 3.2 panel B shows ALP activity of primary osteoblast incubated in the second series in which cells were incubated in α-MEM medium containing; 10% FCS, 10 mM of β-glycerophosphate and 50 μg/ml of ascorbic acid for 14 days and at day 15, $10^{-8}$ M of dexamethasone was added to the osteogenic medium to promote differentiation. The result demonstrated statistically significant increases in ALP activity on day 14 compared to day 7 (51.55±5.75 versus 12.10±1.07, $p<0.001$) then a statistically significant decrease on day 21 and day 28. Dexamethasone did not increase overall ALP activity in series 2.

Figure 3.2 panel C shows ALP activity of primary osteoblast incubated in the third series in which cells were incubated in α-MEM medium containing; 10% FCS, 10 mM of β-glycerophosphate, 50 μg/ml of ascorbic acid and $10^{-8}$ M of dexamethasone for 28 days. The result demonstrated statistically significant increases in ALP activity on day 14 compared to day 7 (67.33±8.68 versus 11.71±1.19, $p<0.001$) then a statistically significant decrease on day 21 and day 28. Dexamethasone did not increase overall ALP activity in series 3.

Figure 3.2 panel D shows ALP activity of primary osteoblast incubated in the fourth series in which cells were incubated in α-MEM medium containing; 10% FCS, 10 mM of β-glycerophosphate, 50 µg/ml of ascorbic acid and distilled water as a control for dexamethasone. The result demonstrated statistically significant increases in ALP activity on day 14 compared to day 7 (60.34±7.14 versus 11.05±0.97, $p<0.001$) then statistically significant decreased on day 21 and day 28.

#### *3.4.1.2 Alizarin red staining during osteoblast differentiation*

Alizarin red staining was used as a mineralization marker. Figure 3.3 panel A shows the graph of the mineralization marker in the first series in which cells were incubated in α-MEM medium containing; 10% FCS, 10 mM of β-glycerophosphate and 50 µg/ml of ascorbic acid for 28 days. The result demonstrated statistically significant increases in the mineralization marker on day 21 compared to day 7 (30.96±3.92 versus 2.37±1.38, $p<0.001$) and on day 28 compared to day 7 (71.27±2.80 versus 2.37±1.38, $p<0.001$).

Figure 3.3 panel B shows the graph of the mineralization marker in the second series in which cells were incubated in α-MEM medium containing; 10% FCS, 10 mM of β-glycerophosphate and 50 µg/ml of ascorbic acid for 14 days and at day 15, $10^{-8}$ M of dexamethasone was added to the osteogenic medium to promote differentiation. The result demonstrated statistically significant increases in the mineralization marker on day 21 compared to day 7 (48.35±5.06 versus 5.99±3.80, $p<0.001$) and on day 28 compared to day 7 (95.79±4.22 versus 5.99±3.80, $p<0.001$). Dexamethasone did not increase overall mineralization in series 2.

Figure 3.3 panel C shows the graph of mineralization marker in the third series in which cells were incubated in α-MEM medium containing; 10% FCS, 10 mM of β-glycerophosphate, 50 µg/ml of ascorbic acid and $10^{-8}$ M of dexamethasone for 28 days. The result demonstrated statistically significant increases in the mineralization marker on day 14 compared to day 7 (22.91±4.18 versus 4.34±0.53, $p<0.001$), day 21 compared to day 7 (69.44±4.55 versus 4.34±0.53, $p<0.001$) and on day 28 compared to day 7 (95.06±4.28 versus 4.34±0.53, $p<0.001$). Dexamethasone did not increase overall mineralization in series 3.

Figure 3.3 panel D shows the graph of mineralization marker in the fourth series in which cells were incubated in α-MEM medium containing; 10% FCS, 10 mM of β-glycerophosphate, 50 µg/ml of ascorbic acid and distilled water as a control for dexamethasone. The result demonstrated statistically significant increases in the mineralization marker on day 21 compared to day 7 (24.33±5.84 versus 1.13±0.21, $p<0.001$) and on day 28 compared to day 7 (61.55±5.39 versus 1.13±0.21, $p<0.001$).

Figure 3.4 shows that there was an increase in the mineralization in series 2 and series 3 compared to series 1 and series 4. However, the results of alizarin red analysis showed there are no differences between series 2 and series 3 (95.79±4.220 versus 95.06±3.026, $p>0.05$) of osteogenic medium on day 28 as osteoblasts are mature (see figure 3.4). Series 2 (10% FCS, 10 mM of β-glycerophosphate and 50 µg/ml of ascorbic acid for 14 days and at day 15, $10^{-8}$ M of dexamethasone was added) of osteogenic medium was chosen as a differentiation medium in this project.

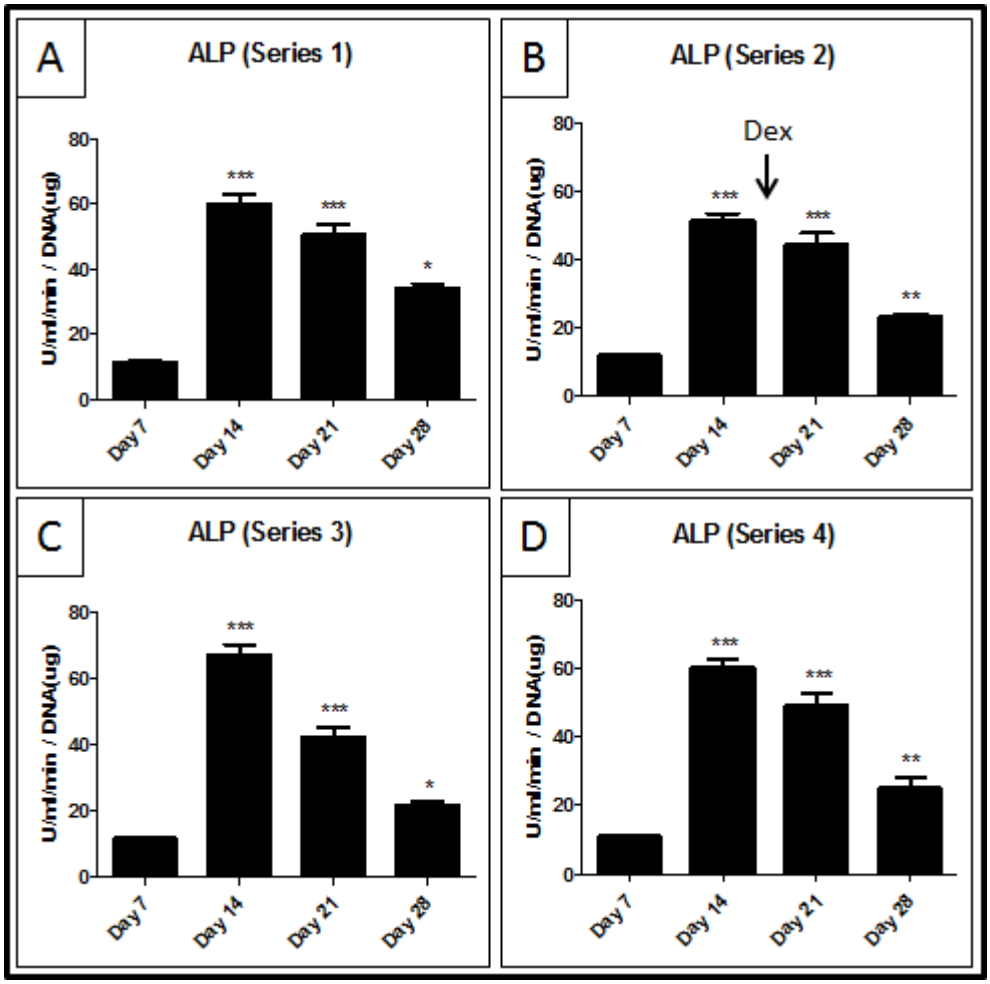


**Figure 3.2: ALP activity during osteoblast differentiation.** Primary osteoblasts were differentiated in four different osteogenic medium. Panel A shows the first series, 10% FCS, 10 mM of β-glycerophosphate and 50 µg/ml of ascorbic acid for 28 days. Panel B shows the second series, 10% FCS, 10 mM of β-glycerophosphate and 50 µg/ml of ascorbic acid for 14 days and at day 15, $10^{-8}$ M of dexamethasone was added. Panel C shows the third series, 10% FCS, 10 mM of β-glycerophosphate, 50 µg/ml of ascorbic acid and $10^{-8}$ M of dexamethasone for 28 days. Panel D shows the fourth series, 10% FCS, 10 mM of β-glycerophosphate, 50 µg/ml of ascorbic acid and distilled water as a control for dexamethasone. ALP activity data shows there are no differences between all conditions of osteogenic medium. *** = $p<0.001$. ** = $p<0.01$. * = $p<0.05$. ANOVA test was used. (n=3).

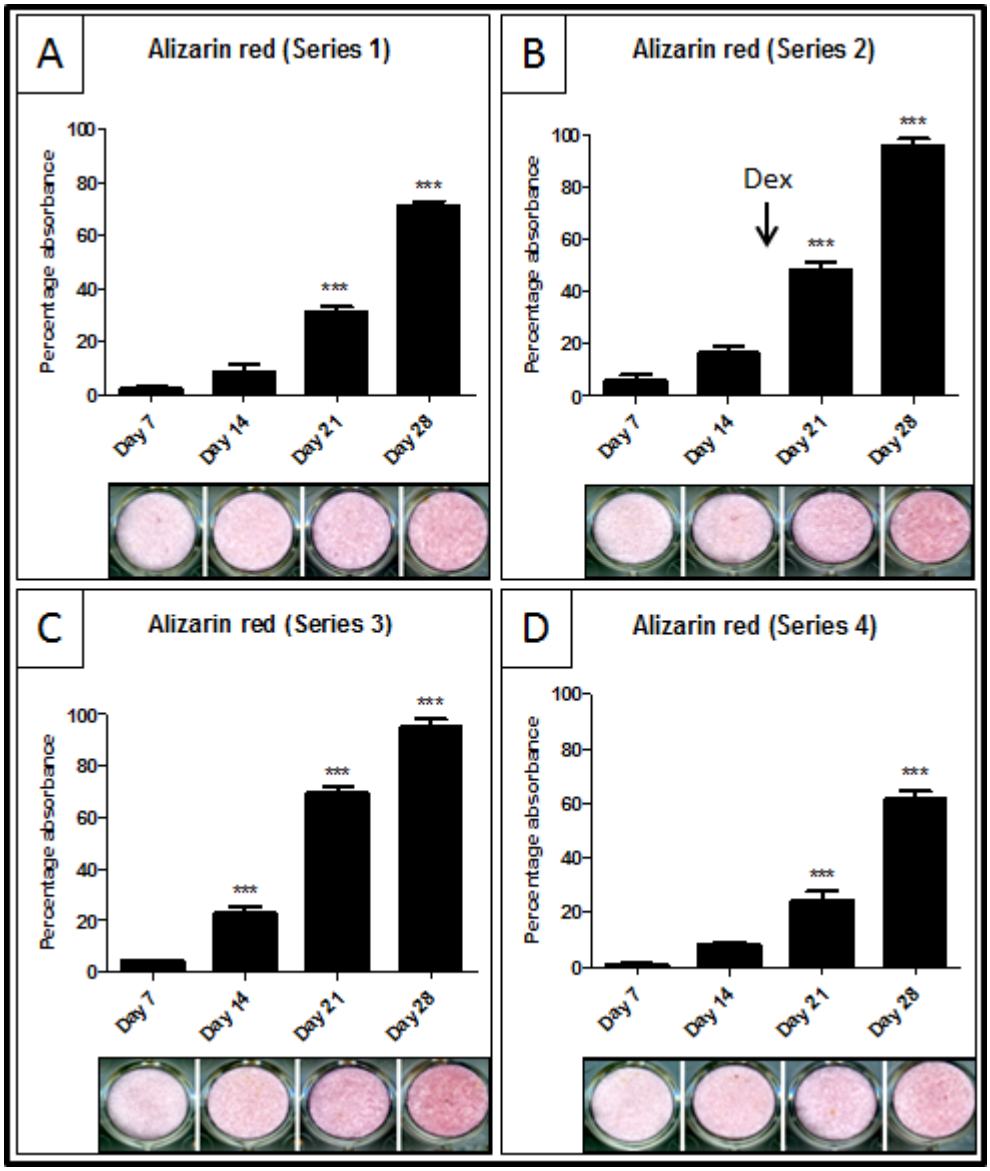


**Figure 3.3: Alizarin red staining during osteoblast mineralization.** Primary osteoblasts were differentiated in different osteogenic medium. Panel A shows the first series, 10% FCS, 10 mM of β-glycerophosphate and 50 µg/ml of ascorbic acid for 28 days. Panel B shows the second series, 10% FCS, 10 mM of β-glycerophosphate and 50 µg/ml of ascorbic acid for 14 days and at day 15, $10^{-8}$ M of dexamethasone was added. Panel C shows the third series, 10% FCS, 10 mM of β-glycerophosphate, 50 µg/ml of ascorbic acid and $10^{-8}$ M of dexamethasone for 28 days. Panel D shows the fourth series, 10% FCS, 10 mM of β-glycerophosphate, 50 µg/ml of ascorbic acid and distilled water as a control for dexamethasone Alizarin red staining data showed there is no difference between all series of osteogenic medium. *** = $p<0.001$. ANOVA test was used. (n=3).

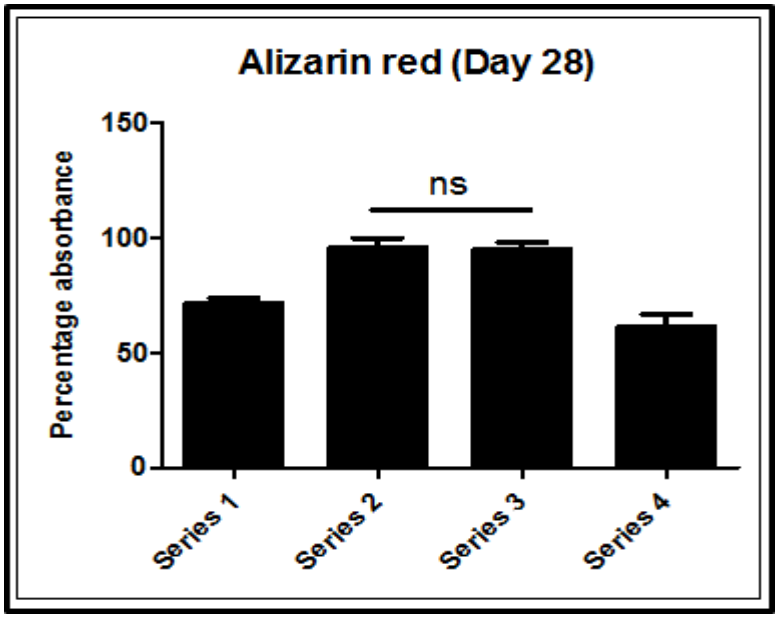


**Figure 3.4: Differences in the alizarin red staining between different series on day 28 as the osteoblasts are mature.** Primary osteoblasts were differentiated in different osteogenic medium. There are no differences between series 2 and series 3 (95793±4.220 versus 95.06±3.026, $p>0.05$) of osteogenic medium on day 28 as osteoblasts are mature. Series 2 (10% FCS, 10 mM of β-glycerophosphate and 50 µg/ml of ascorbic acid for 14 days and at day 15, $10^{-8}$ M of dexamethasone was added) of osteogenic medium was chosen as a differentiation medium in this project. ANOVA test was used. (n=3).

### 3.4.2 Evaluation of the expression of osteoblast differentiation markers

#### *3.4.2.1 ALP activity increased during osteoblast differentiation*

The early stage differentiation of mouse primary osteoblasts was analyzed using the ALP activity assay. Cells were seeded on day 0 and ALP activity was analyzed on days 7, 14, 21 and 28, respectively. Cells were incubated in osteogenic medium; α-MEM containing 10% FCS, 10 mM of β-glycerophosphate and 50 µg/ml of ascorbic acid for 14 days. At day 15, a $10^{-8}$ M concentration of dexamethasone was added to the osteogenic medium to promote differentiation. ALP activity was normalized to cell

DNA content. Figure 3.5 shows the results of ALP activity of primary osteoblasts in three independent experiments (n=3). The result demonstrated statistically significant increases in ALP activity of primary osteoblasts on day 14 compared to day 7 (78.65±13.70 versus 12.87±0.85, $p<0.001$) and on day 21 compared to day 7 (131.90±24.81 versus 12.87±0.85, $p<0.001$). On day 28, ALP activity was significantly decreased compared to ALP activity on day 21 (62.74±11.68 versus 12.87±0.85, $p<0.001$).

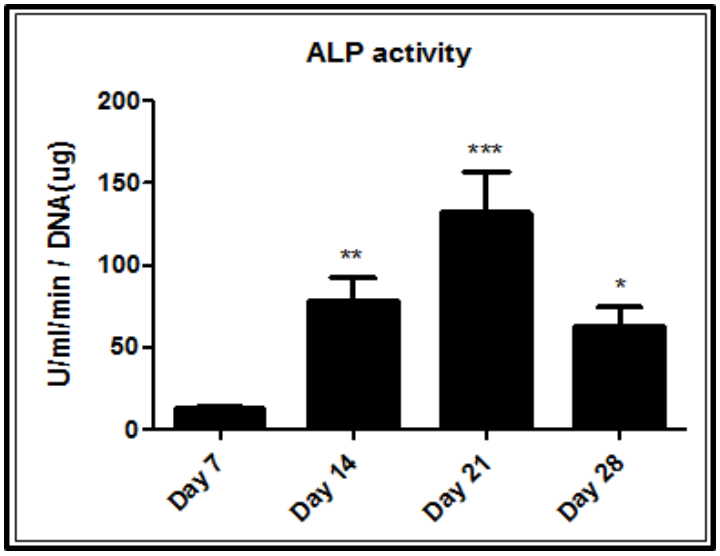


**Figure 3.5: ALP activity increased during culture of primary osteoblasts in osteogenic medium day 14, 21 and decreased day 28.** Primary osteoblasts were differentiated in osteogenic medium; 10 mM of β-glycerophosphate, 50 μg/ml of ascorbic acid from day 0 to day 14. $10^{-8}$ M dexamethasone was added to the osteogenic medium at day 15 to increase differentiation. ALP activity was normalised to cell DNA content. Data shows significant increases in the ALP activity of primary osteoblasts on day 14 and 21 comparing to day 7, and decreases on day 28. *** = $p<0.001$. ** = $p<0.01$. * = $p<0.05$. ANOVA test was used. (n=3).

#### *3.4.2.2 Alizarin red staining increased during osteoblasts differentiation*

The late stage differentiation of mouse primary osteoblasts was analyzed using alizarin red staining. Cells were seeded on day 0 and mineralization of primary osteoblasts was analyzed on days 7, 14, 21 and 28, respectively. Cells were incubated in osteogenic medium; α-MEM containing 10% FCS, 10 mM of β-glycerophosphate and 50 µg/ml of ascorbic acid for 14 days. On day 15, a $10^{-8}$ M concentration of dexamethasone was added to the osteogenic medium to promote differentiation. ALP activity was normalized to cell DNA content. Figure 3.6 shows the results of alizarin red staining, as a matrix mineralization marker in primary osteoblasts in three independent experiments (n=3) and demonstrated that there was a statistically significant increase during osteoblastogenesis. The results showed statistically significant increases in the mineralization marker on day 14 compared to day 7 (29.60±6.35 versus 1.26±0.58, $p<0.001$), day 21 compared to day 7 (52.58±4.38 versus 1.26±0.58, $p<0.001$) and on day 28 compared to day 7 (67.26±8.12 versus 1.26±0.58, $p<0.001$).

#### *3.4.2.3 Assessment of the quality of the mouse primary osteoblast purified RNAs and synthesized cDNAs*

Total RNA was extracted over 4 weeks differentiation of primary osteoblasts cultured *in vitro*. Figure 3.7 shows the electrophoresis of RNA isolated from primary osteoblasts during differentiation; days 7, 14, 21 and 28. Clear dens 28S and 18S bands, ribosomal RNAs, were present and little low molecular weight fragments indicating of good quality undamaged RNA. Figure 3.8 shows RT-PCR of GAPDH with expected size of 354 bp in differentiated mouse primary osteoblasts after reverse transcription (+RT) or no reverse transcription (-RT). Expression of GAPDH in +RT and not in -RT indicated that there was no genomic contamination in cDNA preparation.

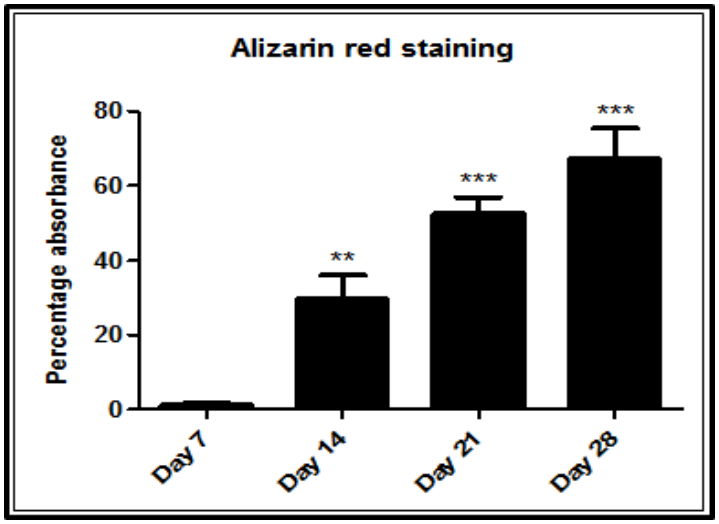


**Figure 3.6: Mineralisation increased during culture of primary osteoblasts in osteogenic medium.** Primary osteoblasts were differentiated in osteogenic medium; 10 mM of β-glycerophosphate, 50 µg/ml of ascorbic acid from day 0 to day 14. $10^{-8}$ M dexamethasone was added to the osteogenic medium on day 15 to help cells more differentiated. Data shows significant increases in the mineralisation of primary osteoblast during cells differentiation from day 0 to day 28. *** = $p<0.001$. ** = $p<0.01$. ANOVA test was used. (n=3).

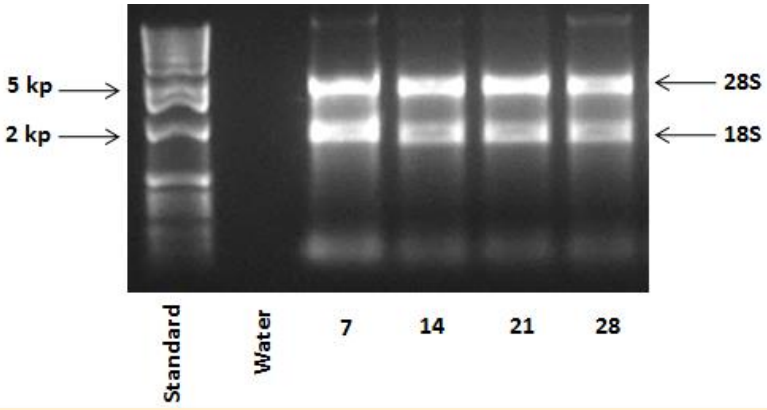


**Figure 3.7: Electrophoresis of total mRNA isolated from cells during osteoblastogenesis.** RNA was extracted from mouse primary osteoblasts at days 7, 14, 21 and 28. Clear 28S and 18S bands, ribosomal RNAs, were indicates of good quality and undamaged RNA. (n=3).

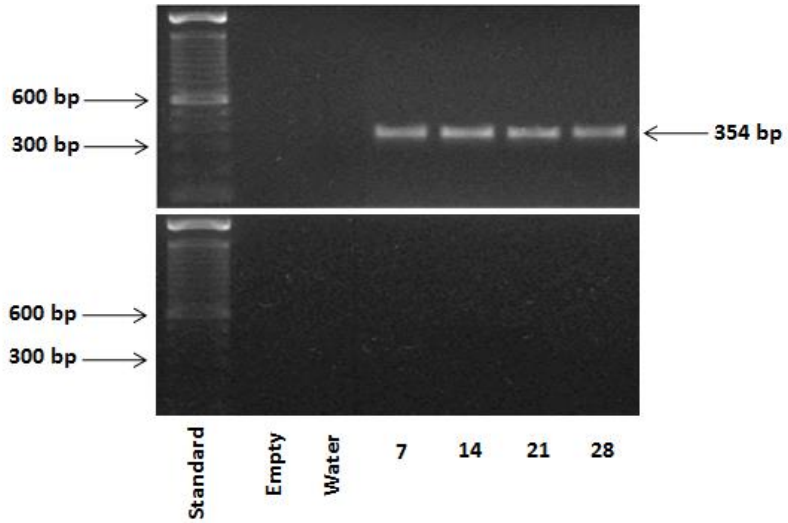


**Figure 3.8: RT-PCR analysis of GAPDH mRNA during osteoblastogenesis.** RNA was extracted from mouse primary osteoblasts at days 7, 14, 21 and 28. RT-PCR was performed using GAPDH, gene specific primers. GAPDH expression was detected in +RT with expected size of 354 bp and not in - RT demonstrating no genomic DNA contamination in prepared cDNAs. Water was used as a negative control. (n=3).

### *3.4.2.4 Assessment of the relative levels of expression of Runx2 mRNA, COL1A2 mRNA and osteocalcin mRNA*

The level of expression of osteoblast markers; Runx2, COL1A2 and osteocalcin genes were analysed using TaqMan. Expression of these genes was normalised to the expression of a housekeeping gene, β-actin. Figure 3.9 panel A shows that there was a positive correlation between increased Runx2 mRNA expression and primary osteoblast differentiation. Data showed statistically significant increases in the relative expression of Runx2 mRNA on day 28 compared to day 7 (169.10±46.74 versus 3.18±1.51, $p<0.01$). Figure 3.9 panel B shows that there was a positive correlation between increased COL1A2 mRNA expression and primary osteoblasts differentiation. There was a statistically significant increase in the relative expression of COL1A2 mRNA in day 28 compared to day 7 (734.60±283.80 versus 3.20±0.90, $p<0.01$). Figure 3.9

panel C shows the expression of Osteocalcin mRNA during primary osteoblasts differentiation. There was no statistically significant increase in the relative expression of Osteocalcin mRNA during osteoblastogenesis in these experiments.

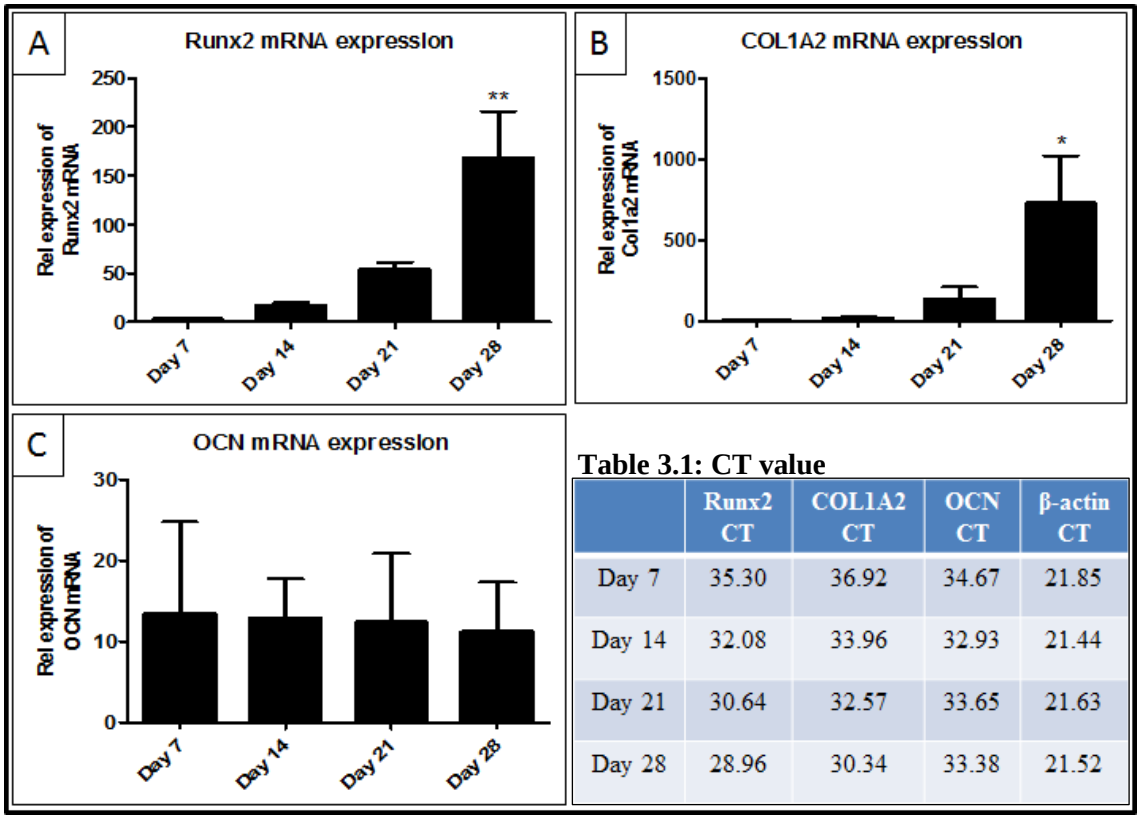


**Table 3.1: CT value**

| | Runx2 CT | COL1A2 CT | OCN CT | β-actin CT |
|---|---|---|---|---|
| Day 7 | 35.30 | 36.92 | 34.67 | 21.85 |
| Day 14 | 32.08 | 33.96 | 32.93 | 21.44 |
| Day 21 | 30.64 | 32.57 | 33.65 | 21.63 |
| Day 28 | 28.96 | 30.34 | 33.38 | 21.52 |

**Figure 3.9: TaqMan analysis of osteoblast marker genes; Runx2, COL1A2 and osteocalcin expression during mouse primary osteoblasts differentiation.** RNA was extracted from mouse primary osteoblasts at days 7, 14, 21 and 28. The relative expression of osteoblast marker genes was adjusted relative to expression of housekeeping gene, β-actin. Data shows significant increases in Runx2 mRNA and COL1A2 mRNA in mature osteoblasts (day 28) compared with the expression of these genes in pre-osteoblasts (day 7). However, data shows there is no difference in the relative expression of osteocalcin (OCN) mRNA during osteoblastogenesis. Table 3.1 shows the CT values of Runx2, COL1A2, osteocalcin (OCN) and β-actin. ** = $p<0.01$. * = $p<0.05$. ANOVA test was used. Table 3.1 shows the CT value of Runx2 mRNA, COL1A2 mRNA, OCN mRNA and β-actin mRNA. (n=3).

### 3.4.3 Determination and quantification of the relative expression of N-cadherin mRNA during osteoblastogenesis

#### *3.4.3.1 N-cadherin mRNA was expressed during osteoblast differentiation*

Total RNA were extracted and cDNAs were synthesised from mouse primary osteoblasts cultured *in vitro* and differentiated up to 4 weeks. Figure 3.10 shows that N-cadherin was expressed during mouse primary osteoblasts differentiation; days 7, 14, 21 and 28. End-point RT-PCR is not a quantitative technique and was only used initially to establish if N-cadherin specific mRNA was expressed in cells. Bands were excised and sent for sequencing (Figure 3.11) and gave 100% homology with GenBank (Figure 3.12). Real time PCR (TaqMan) was used to study the relative levels of expression of N-cadherin during mouse primary osteoblasts differentiation.

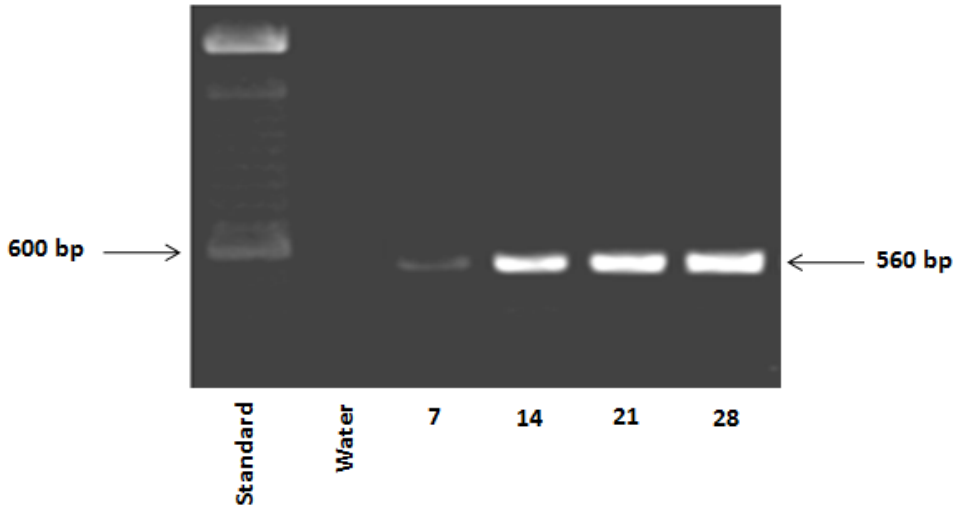


**Figure 3.10: RT-PCR analysis of N-cadherin mRNA during osteoblastogenesis.** RNA was extracted from mouse primary osteoblasts at days 7, 14, 21 and 28. RT-PCR was performed using N-cadherin, gene specific primers. Data shows N-cadherin was expressed in primary osteoblast during cells differentiation with expected size of 560 bp. (n=3).

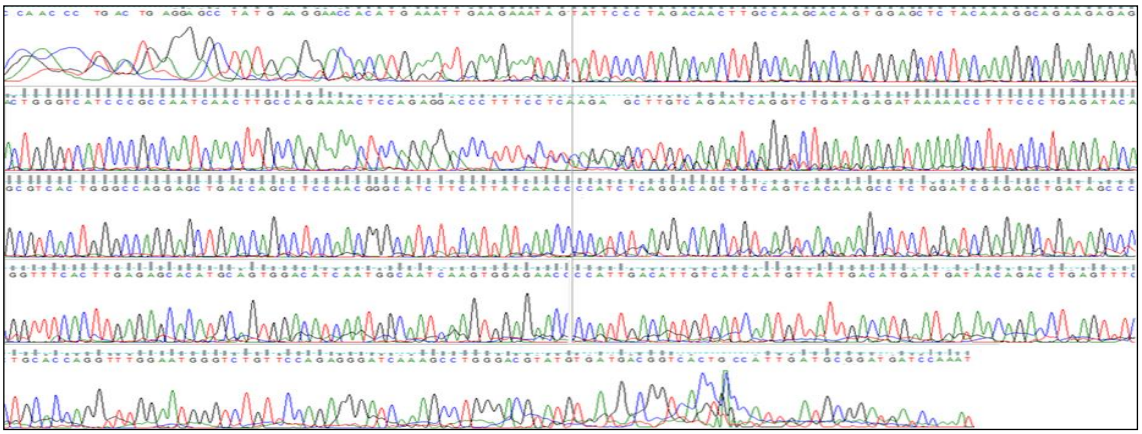

**Figure 3.11: N-cadherin cDNA sequencing.** RNA was extracted from mouse primary osteoblasts at days 7, 14, 21 and 28. RT-PCR was performed using N-cadherin, gene specific primers. Bands were sequenced in University of Sheffield Core Genomic Facility (http://genetics.group.shef.ac.uk/dna-sequencing.html). This sequence was received from the Core Genomic Facility. (n=3).

>ref|NM_007664.4| Mus musculus cadherin 2 (Cdh2), mRNA
Length=4646

GENE ID: 12558 Cdh2 | cadherin 2 [Mus musculus] (Over 100 PubMed links)

Score = 965 bits (522), Expect = 0.0
Identities = 522/522 (100%), Gaps = 0/522 (0%)
Strand=Plus/Plus

```
Query  1     CCAACCCTGACTGAGGAGCCTATGAAGGAACCACATGAAATTGAAGAAATAGTATTCCCT  60
             ||||||||||||||||||||||||||||||||||||||||||||||||||||||||||||
Sbjct  1028  CCAACCCTGACTGAGGAGCCTATGAAGGAACCACATGAAATTGAAGAAATAGTATTCCCT  1087

Query  61    AGACAACTTGCCAAGCACAGTGGAGCTCTACAAAGGCAGAAGAGAGACTGGGTCATCCCG  120
             ||||||||||||||||||||||||||||||||||||||||||||||||||||||||||||
Sbjct  1088  AGACAACTTGCCAAGCACAGTGGAGCTCTACAAAGGCAGAAGAGAGACTGGGTCATCCCG  1147

Query  121   CCAATCAACTTGCCAGAAAACTCCAGAGGACCCTTTCCTCAAGAGCTTGTCAGAATCAGG  180
             ||||||||||||||||||||||||||||||||||||||||||||||||||||||||||||
Sbjct  1148  CCAATCAACTTGCCAGAAAACTCCAGAGGACCCTTTCCTCAAGAGCTTGTCAGAATCAGG  1207

Query  181   TCTGATAGAGATAAAAACCTTTCCCTGAGATACAGCGTCACTGGGCCAGGAGCTGACCAG  240
             ||||||||||||||||||||||||||||||||||||||||||||||||||||||||||||
Sbjct  1208  TCTGATAGAGATAAAAACCTTTCCCTGAGATACAGCGTCACTGGGCCAGGAGCTGACCAG  1267

Query  241   CCTCCAACGGGCATCTTCATTATCAACCCCATCTCAGGACAGCTGTCAGTCACAAAGCCT  300
             ||||||||||||||||||||||||||||||||||||||||||||||||||||||||||||
Sbjct  1268  CCTCCAACGGGCATCTTCATTATCAACCCCATCTCAGGACAGCTGTCAGTCACAAAGCCT  1327

Query  301   CTGGATCGAGAGCTGATAGCCCGGTTTCACTTGAGAGCACATGCAGTGGACATCAATGGC  360
             ||||||||||||||||||||||||||||||||||||||||||||||||||||||||||||
Sbjct  1328  CTGGATCGAGAGCTGATAGCCCGGTTTCACTTGAGAGCACATGCAGTGGACATCAATGGC  1387

Query  361   AATCAAGTGGAGAACCCCATTGACATTGTCATCAATGTTATTGACATGAATGATAACAGA  420
             ||||||||||||||||||||||||||||||||||||||||||||||||||||||||||||
Sbjct  1388  AATCAAGTGGAGAACCCCATTGACATTGTCATCAATGTTATTGACATGAATGATAACAGA  1447

Query  421   CCTGAGTTTCTGCACCAGGTTTGGAATGGGTCTGTTCCAGAGGGATCAAAGCCTGGGACG  480
             ||||||||||||||||||||||||||||||||||||||||||||||||||||||||||||
Sbjct  1448  CCTGAGTTTCTGCACCAGGTTTGGAATGGGTCTGTTCCAGAGGGATCAAAGCCTGGGACG  1507

Query  481   TATGTGATGACGGTCACTGCCATTGATGCGGATGATCCAAAT  522
             |||||||||||||||||||||||||||||||||||||||||||
Sbjct  1508  TATGTGATGACGGTCACTGCCATTGATGCGGATGATCCAAAT  1549
```

**Figure 3.12: Using genomic website to identify the matching gene.** Sequence received from the Core Genomic Facility was blast in NCBI browser (http://blast.ncbi.nlm.nih.gov/Blast.cgi) gave 100% homology with GenBank. (n=3).

### *3.4.3.2 Relative expression of N-cadherin mRNA increased during osteoblast differentiation*

The quantitation expression of N-cadherin mRNA was analysed using TaqMan analysis. Expression of N-cadherin was normalised to expression of the housekeeping gene, β-actin. Figure 3.13 shows the relative expression of N-cadherin mRNA during the differentiation of primary osteoblasts. Data showed a statistically significant increase in the relative expression of N-cadherin mRNA on day 28, in mature osteoblasts, compared to day 7, pre-osteoblasts, (134.80±37.27 versus 5.53±3.75, $p<0.01$).

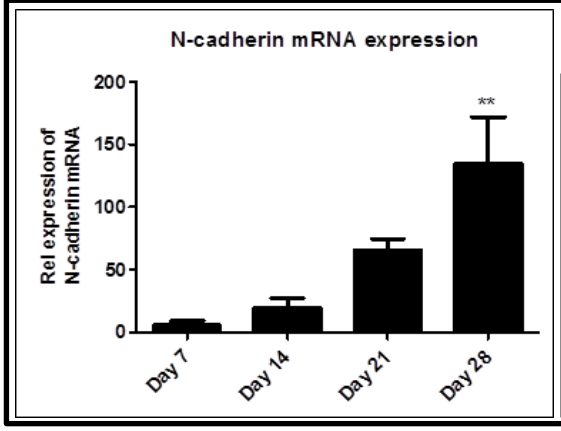


**Table 3.2: CT value**

| | N-cadherin CT | β-actin CT |
|---|---|---|
| Day 7 | 34.20 | 21.85 |
| Day 14 | 31.90 | 21.44 |
| Day 21 | 29.94 | 21.63 |
| Day 28 | 28.65 | 21.52 |

**Figure 3.13: N-cadherin mRNA expression increased during osteoblast differentiation.** RNA was extracted from mouse primary osteoblasts at days 7, 14, 21 and 28. Data shows significant increase in the relative expression of N-cadherin mRNA in mature osteoblasts (day 28) compared with pre-osteoblasts (day 7). ** = $p<0.01$. ANOVA test was used. Table 3.2 shows the CT value of N-cadherin mRNA and β-actin mRNA. (n=3).

### 3.4.4 Immuno-localization of N-cadherin protein on osteoblasts

#### *3.4.4.1 Determination of the optimal concentration of primary antibody required for immunofluorescent localization of N-cadherin*

A rabbit monoclonal, anti-N-cadherin antibody (Millipore, UK) and isotype control, normal rabbit IgG antibody (R&D systems, UK) were used in these studies. A donkey anti-rabbit IgG secondary antibody conjugated to fluorochrome northern light (NL637) was used for detection. Figure 3.14 panel A shows positive staining (red fluorescence) of N-cadherin when mouse primary osteoblasts were incubated with the primary rabbit monoclonal anti-N-cadherin antibody at a 1:50 dilution and no staining was observed with isotype control (Figure 3.14 panel B). Figure 3.14 panel C shows no red fluorescence staining was observed when mouse primary osteoblasts were incubated with rabbit monoclonal anti-N-cadherin antibody at a 1:100 dilution (Figure 3.14 panel D shows the negative control isotype at a dilution of 1:100). Therefore, 1:50 dilution was chosen as an optimal primary antibody concentration for immunofluorescence.

#### *3.4.4.2 Contiguous expression of N-cadherin was observed on the membranes of adjacent osteoblasts*

Rabbit monoclonal anti-N-cadherin antibody (Millipore, UK) or isotype control, normal rabbit IgG antibody (R&D systems, UK) were used to determine possible localisation of N-cadherin in osteoblast cultures. A donkey anti-rabbit IgG secondary antibody conjugated by fluorochrome northern light (NL637) was used for detection. Figure 3.15 panel A shows specific positive staining (red fluorescence) for N-cadherin and no staining with isotype control (Figure 3.15 panel B). Figure 3.15 panel C shows an enlarged picture illustrating contiguous expression of N-cadherin protein on the membranes of adjacent osteoblasts.

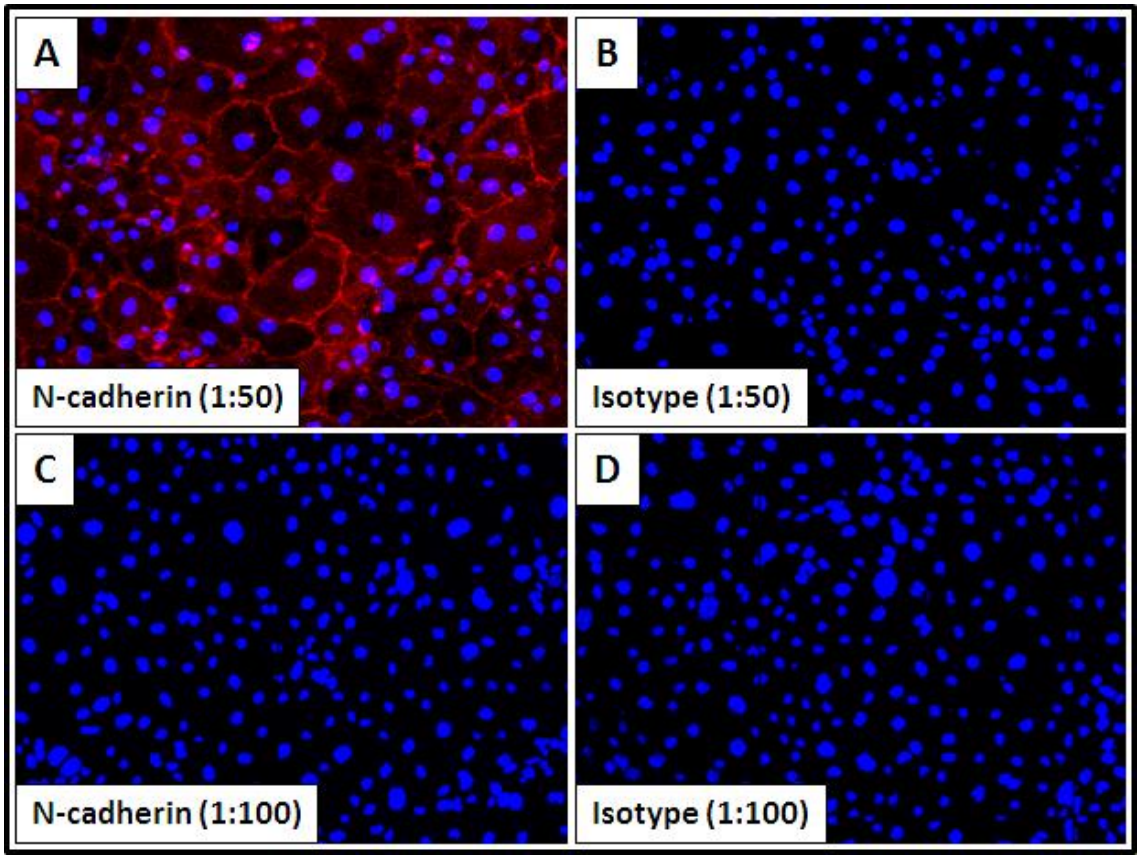


**Figure 3.14: Immunofluorescence optimization of N-cadherin protein in primary osteoblasts.** Fixed and permeabilized cells were stained with rabbit monoclonal anti-N-cadherin primary antibody or isotype control, normal rabbit IgG antibody. Nuclei were counterstained with DAPI (blue fluorescence). Cells were examined under Zeiss 510 multiphoton laser scanning microscope with 20x objective. Data shows there was no staining (red fluorescence) at 1:100 antibody dilution (panel C). Panel A shows the optimal antibody concentration (1:50 dilution) for N-cadherin (red fluorescence) around the cells and no staining with isotype control (panel D) using primary osteoblasts. (n=3).

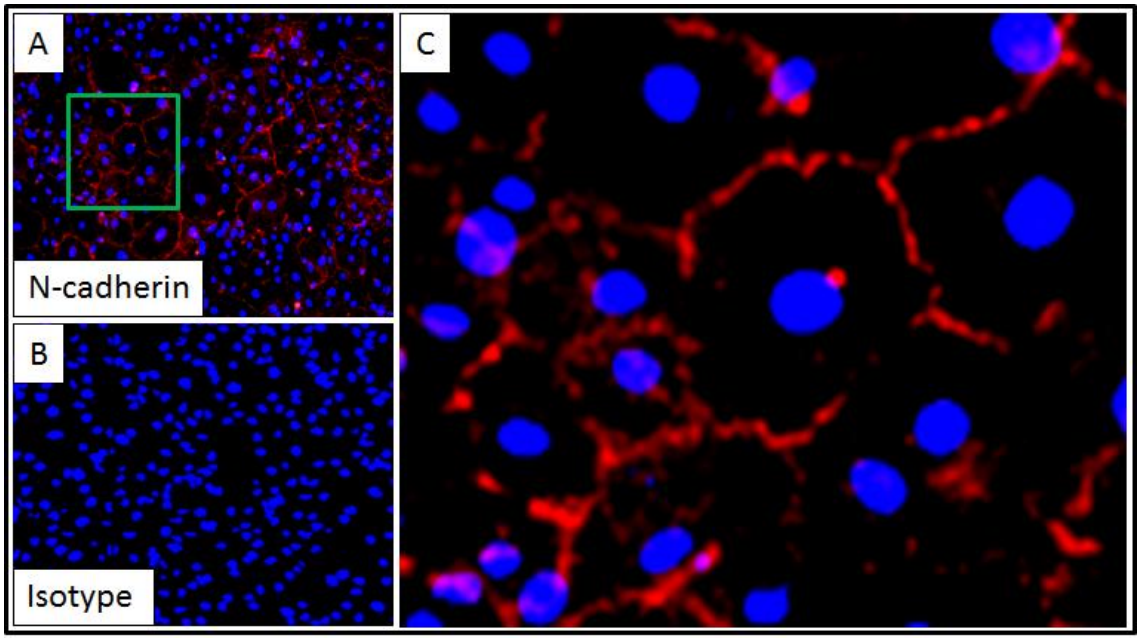


**Figure 3.15: N-cadherin protein expression in primary osteoblasts.** Fixed and permeabilized cells were stained with rabbit monoclonal primary anti-N-cadherin antibody or isotype control, normal rabbit IgG antibody. Nuclei were counterstained with DAPI (blue fluorescence). Cells were examined under Zeiss 510 multiphoton laser scanning microscope with 20x objective. Panel A shows the N-cadherin protein expression (red fluorescence) around most cells. Panel B shows isotype control with no staining. Panel C shows an enlarged picture illustrating contiguously expression of N-cadherin (red fluorescence) on the membranes of adjacent osteoblasts. (n=3).

### 3.4.5 Determination of the percentage and relative expression of N-cadherin protein during osteoblastogenesis

#### *3.4.5.1 Determination of the optimal procedures to harvest adherent osteoblasts*

Flow cytometry was performed using a mouse monoclonal primary anti-N-cadherin antibody (Sigma, UK) and an isotype control, mouse IgG antibody (Vector laboratories, UK). Anti-N-cadherin antibody (Sigma, UK) and mouse IgG antibody (Vector laboratories, UK) were labeled with Lightning-Link$^{TM}$ Atto637 (Innova Biosciences, UK). Four different methods were used to harvest and prepare cells for flow cytometry. Figure 3.16 panel A and B show N-cadherin positive cell populations and negative controls, respectively, generated using 0.25% trypsin-EDTA. Figure 3.16 panel C and D show N-cadherin positive cell populations and negative controls, respectively, generated using cell scrapers. Figure 3.16 panel E and F show N-cadherin positive cell populations and negative controls, respectively, generated using 1X sodium citrate. Figure 3.15 panel G and H show N-cadherin positive cell populations and negative controls, respectively, generated using 1% of 280 units/mg collagenase II in 1X sodium citrate.

The results demonstrated that using 1X sodium citrate and/or 1% of 280 units/mg collagenase II in 1X sodium citrate are the best ways to harvest osteoblasts and maintain N-cadherin positive populations. When 1X sodium citrate was used to harvest mature osteoblasts (day 21 and day 28), cells clumped together with the matrix and prohibited analysis by the flow cytometry machine due to the machine blocking. However, the use of 1% of 280 units/mg collagenase II in 1X sodium citrate is the only procedure to release and harvest the mature osteoblasts with generated matrix and maintain N-cadherin positive populations. Therefore, 1% of 280 units/mg collagenase II in 1X sodium citrate was chosen to harvest osteoblasts for flow cytometry.

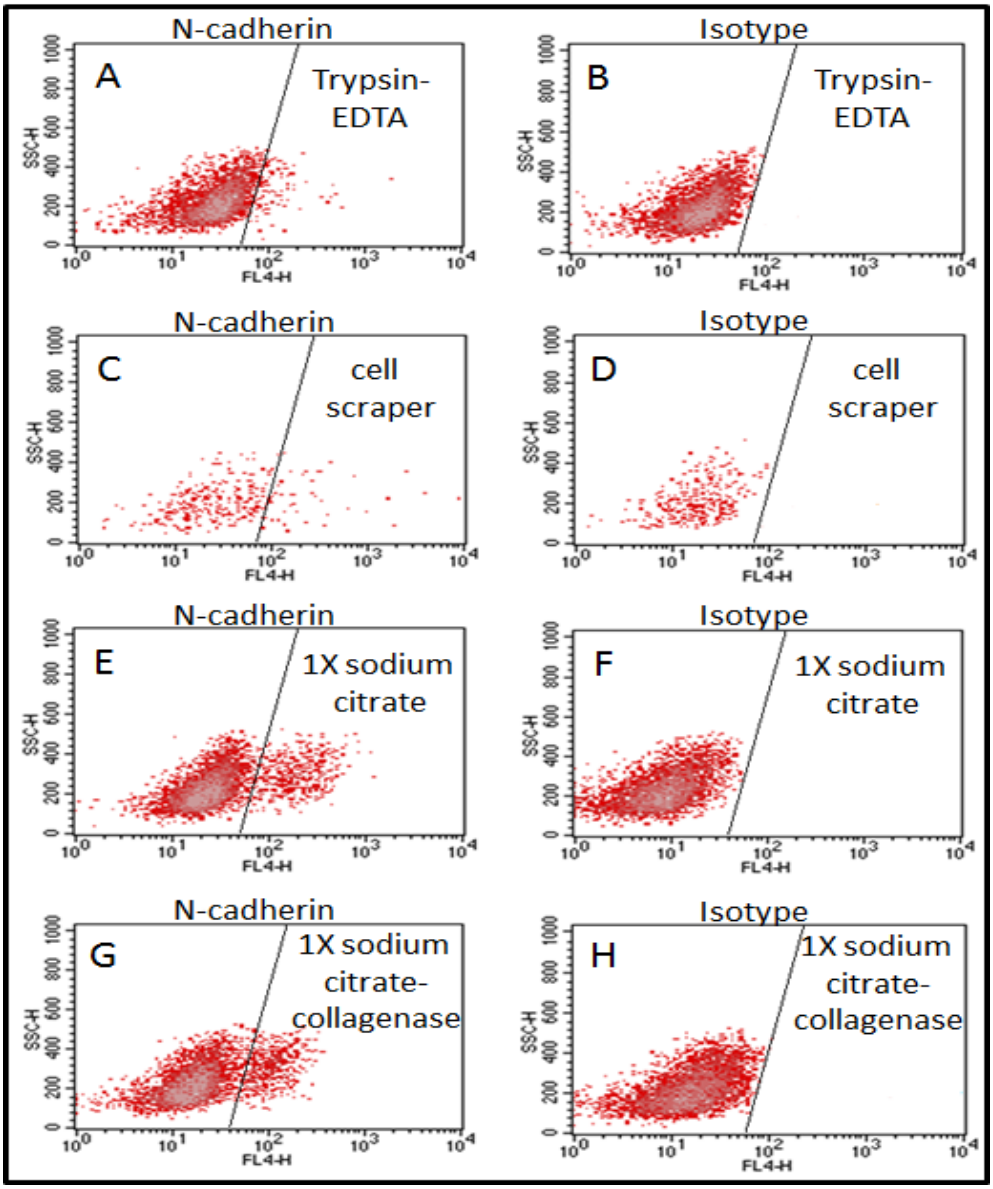


**Figure 3.16: Optimising different ways to harvest adherent cells; primary osteoblasts.** Four different methods were used to harvest and prepare cells for flow cytometric experiment before cells stained with mouse monoclonal anti-N-cadherin antibody or isotype control, mouse IgG antibody. Cells were analyzed using FACS Calibur. Data shows using 0.25% trypsin-EDTA (panel A) or cell scrapers (panel C) lead do loose the N-cadherin molecules. Using 1X sodium citrate (panel E) and using 1% of 280 units/mg collagenase II in 1X sodium citrate (panel G) are the best ways to harvest adherent cells. However, when 1X sodium citrate was used to harvest mature osteoblasts (day 21 and day 28), cells clumped together with the matrix and prohibited analysis by the flow cytometry machine to avoid blocking. Panel B, D, F and H show the negative control, mouse IgG. (n=3).

### *3.4.5.2 Determination of the optimal concentration of anti-N-cadherin antibody used for flow cytometry*

Flow cytometry was performed using a mouse monoclonal anti-N-cadherin antibody (Sigma, UK) and an isotype control, mouse IgG antibody (Vector laboratories, UK). Anti-N-cadherin antibody (Sigma, UK) and mouse IgG antibody (Vector laboratories, UK) were labeled by Lightning-Link$^{TM}$ Atto637 (Innova Biosciences, UK). Figure 3.17 panels A, C, E and G show N-cadherin positive populations (red dots) in mouse primary osteoblast cultures using anti-N-cadherin antibody at 1:100, 1:200, 1:400 and 1:800 dilutions, respectively, in the right half of the FACS plots. However, the positive populations in 1:400 and 1:800 dilutions were not clearly defined compared to the negative population. Figure 3.17 panels B, D, F and H show no positive red populations in the right half of the FACS plots with isotype control at 1:100, 1:200, 1:400 and 1:800 dilutions, respectively. Therefore, 1:200 dilution was chosen as an optimal antibody concentration for flow cytometry because the positive population can be clearly defined from to the negative population with using a minimum volume of antibody.

### *3.4.5.3 Percentage of N-cadherin$^{+}$ osteoblast, as measured by FACS, did not change during osteoblast differentiation*

A mouse monoclonal anti-N-cadherin antibody (Sigma, UK) and an isotype control, mouse IgG antibody (Vector laboratories, UK) were used in these experiments. Both antibodies were labeled with Lightning-Link$^{TM}$ Atto637 (Innova Biosciences, UK). Figure 3.18 panel A shows the percentage of N-cadherin positive cells in immature osteoblast populations, and no positive cells in the isotype controls (Figure 3.18 panel B). The data demonstrated that 10% of immature osteoblasts expressed N-cadherin. Figure 3.18 panel C shows the percentage of N-cadherin positive cells in mature osteoblast populations, and no positive cells with isotype control (Figure 3.18 panel D). Again, the data demonstrated 10% of mature osteoblasts expressed N-cadherin.

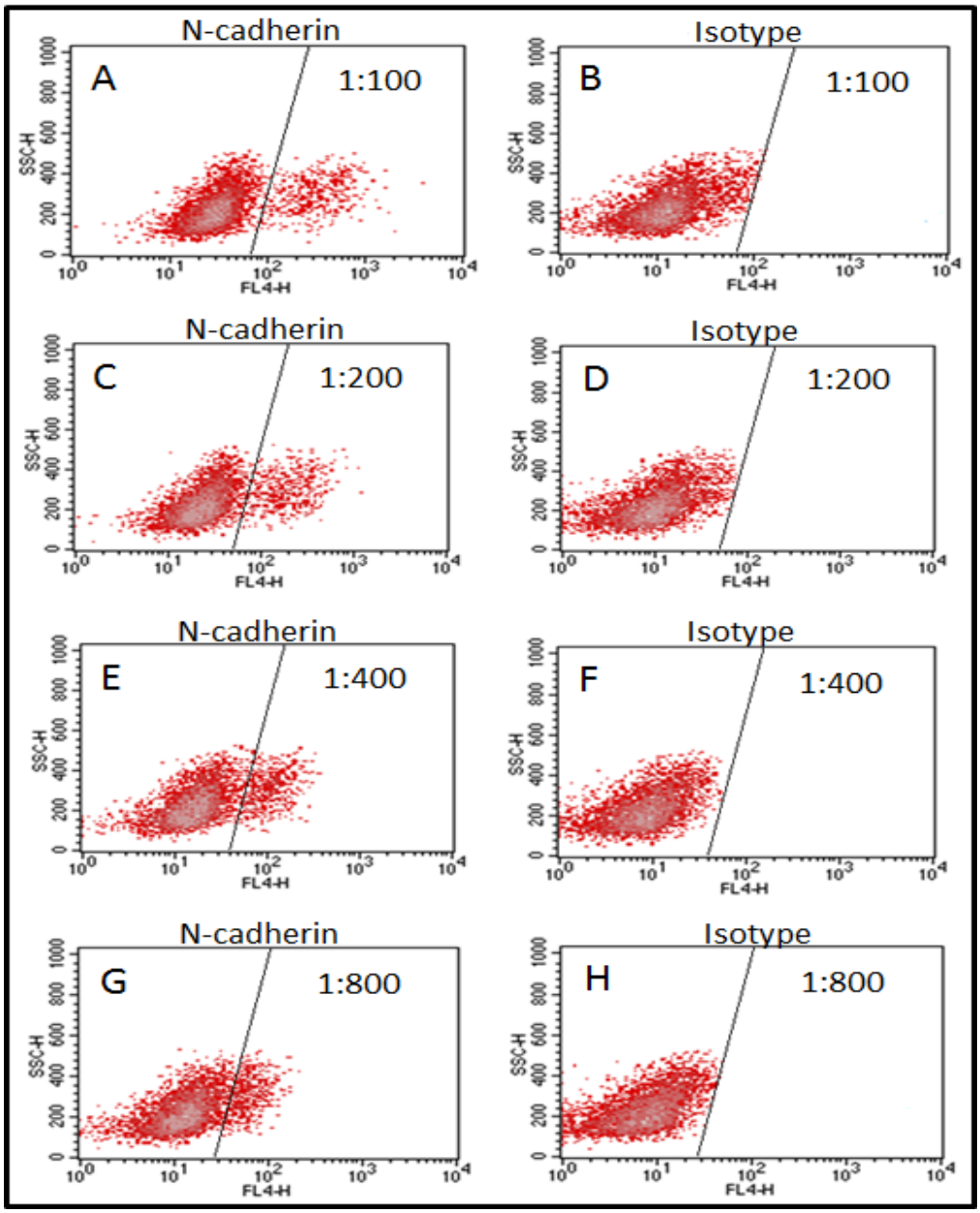


**Figure 3.17: Optimising the concentration of anti-N-cadherin antibody using flow cytometry.** Four different dilutions; 1:100, 1:200, 1:400 and 1:400 were used to stain cells with mouse monoclonal anti-N-cadherin antibody or isotype control, mouse IgG antibody. Cells were analyzed using FACS Calibur. Data shows that 1:200 dilution is the optimal concentration that clearly determines the N-cadherin positive cells because the positive population can be clearly defined from to the negative population with using a minimal antibody. Panel B, D, F and H show the negative control, mouse IgG isotype. (n=3).

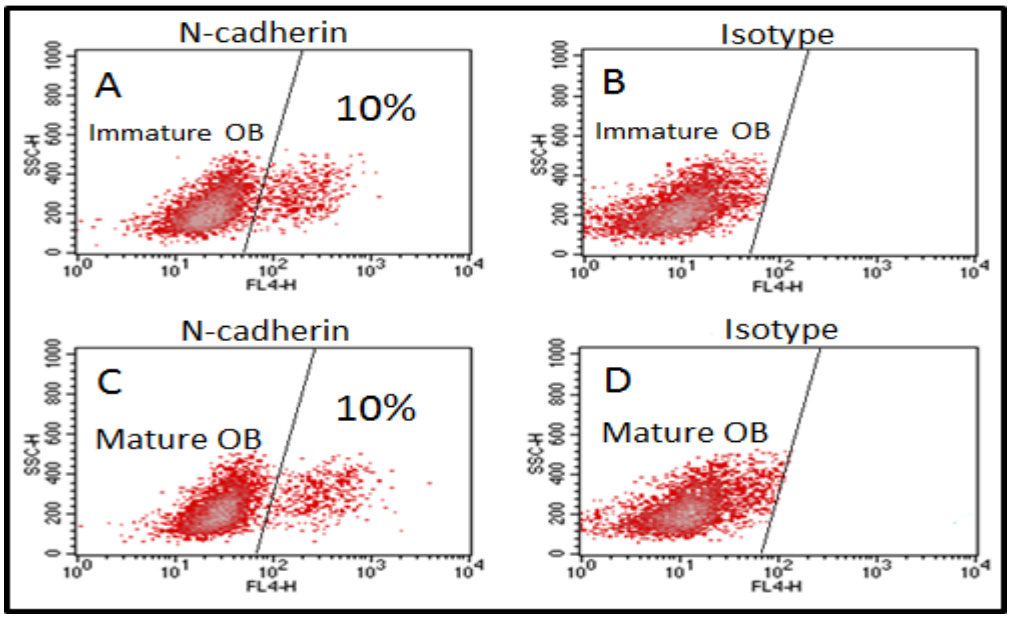


**Figure 3.18: The percentage of N-cadherin$^{+}$ osteoblasts did not change during osteoblast differentiation.** Live cells were stained with a mouse monoclonal anti-N-cadherin antibody or an isotype control, mouse IgG antibody. Cells were analyzed using FACs Calibur. Panel A shows 10% of immature osteoblasts express N-cadherin (red fluorescence in the right half). Panel B shows isotype control. Panel C shows 10% of mature osteoblasts express N-cadherin (red fluorescence in the right half). Panel D shows the isotype control. (n=3).

### *3.4.5.4 The relative expression of N-cadherin protein increased during osteoblast differentiation using immunofluorescence*

Fixed and permeablilized osteoblasts were stained using a rabbit monoclonal anti-N-cadherin antibody (Millipore, UK). A normal rabbit IgG isotype control antibody (R&D systems, UK) was used. Figure 3.19 panel A shows the relative staining of N-cadherin in immature osteoblast and mature osteoblasts. Data showed statistically significant increase in the amount of N-cadherin protein in cultures of day 28, mature osteoblasts, compared to day 7, immature osteoblasts, (70.00±2.49 versus 2.56±0.69, $p<0.001$). Figure 3.19 panels B and C show positive staining (red fluorescence) of N-cadherin in pre-osteoblasts and mature osteoblasts during osteoblastogenesis, respectively.

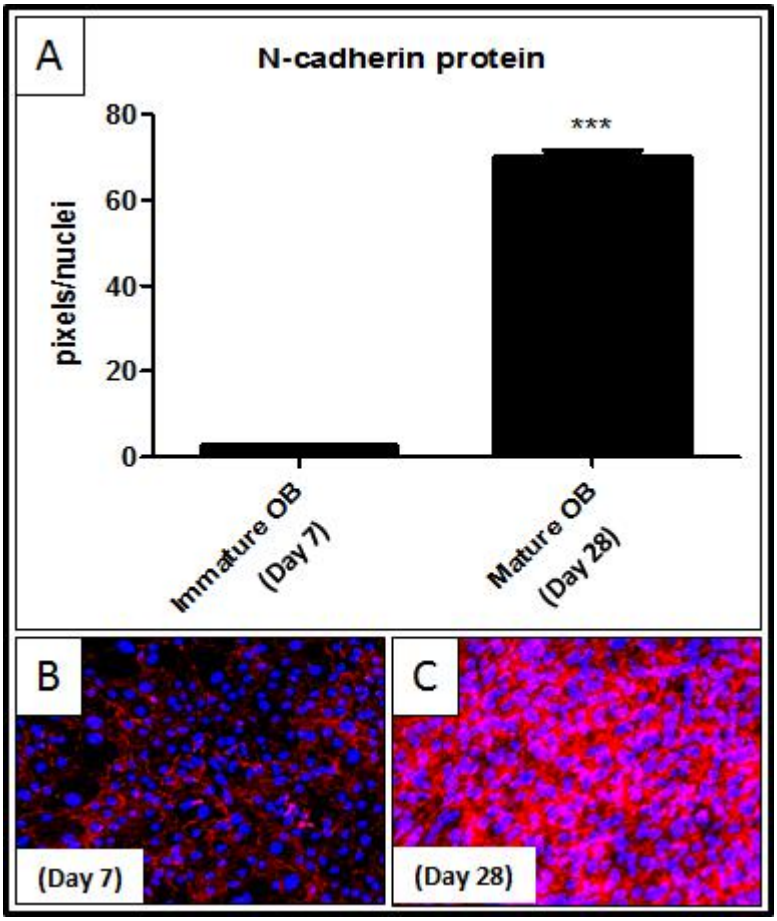


**Figure 3.19: N-cadherin protein expression increased during osteoblast differentiation using immunofluorescence.** Fixed and permeabilized cells were stained with rabbit monoclonal anti-N-cadherin antibody or an isotype control, normal rabbit IgG antibody. Panel A shows significant increase in the relative expression of N-cadherin protein in mature osteoblasts (day 28) compared with immature osteoblasts (day 7). Panel B and C show representative images of N-cadherin protein expression (red fluorescence) in immature osteoblasts and mature osteoblasts. *** = $p<0.001$. *t* test was used. (n=3).

#### *3.4.5.5 The relative expression of N-cadherin protein increased during osteoblast differentiation using western blot*

A rabbit monoclonal anti-N-cadherin antibody (Millipore, UK) and donkey anti-rabbit IgG antibodies (R&D systems, UK) (1:1000 dilution), secondary antibody were used to detect N-cadherin protein during osteoblastogenesis by western blot. Figure 3.20 panel A shows the N-cadherin protein levels in immature osteoblasts and mature osteoblasts. It was found that an osteocyte-like cell line, MLO-Y4 was not expressed N-cadherin (Kawaguchi et al., 2001). Therefore, MLO-Y4 was used as a negative control to determine if there is a positive false expression and brain rat used as a positive control to determine if there is a negative false expression. Figure 3.20 panel B shows that a significant increase was observed in the relative expression of N-cadherin protein in day 28, mature osteoblasts, compared to day 7, immature osteoblasts ($68.24 \pm 13.10$ versus $23.95 \pm 7.13$, $p<0.001$). Figure 3.20 panel C shows the expression of the positive control, β-actin.

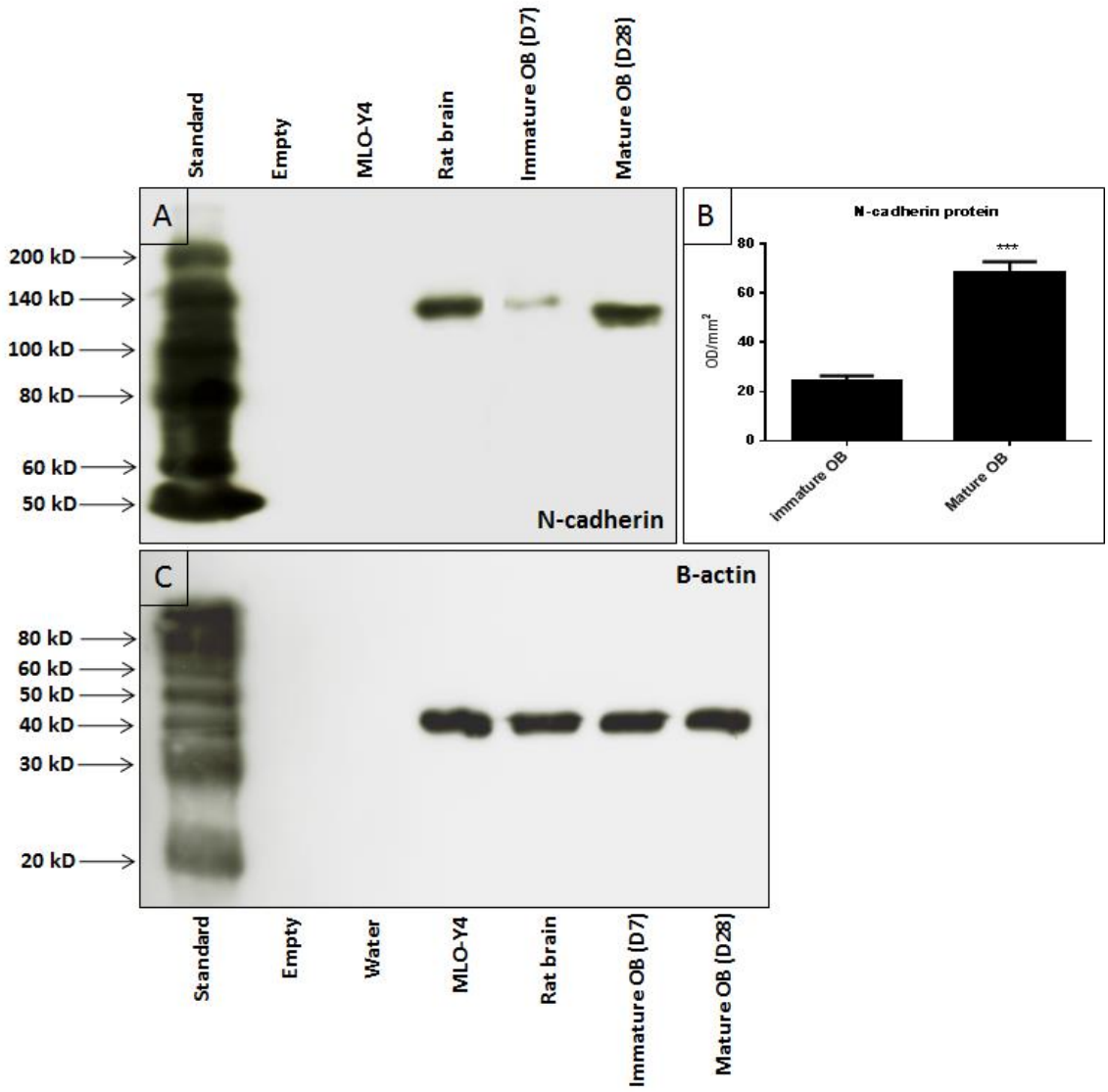


**Figure 3.20: N-cadherin protein expression increased during osteoblast differentiation using western blot.** Whole cell lysis preparation electrophoresed in 12.5% SDS PAGE gels for N-cadherin and 15% SDS PAGE gels for β-actin, and transferred to PVDF membranes were probed with a rabbit monoclonal anti-N-cadherin antibody and donkey anti-rabbit IgG antibodies (R&D systems, UK) (1:1000 dilution), secondary antibody. Panel A shows N-cadherin protein expression during osteoblastogenesis. The osteocyte-like cell line, MLO-Y4 used as negative control and brain rat used as positive control. Panel B shows a significant increase in the relative expression of N-cadherin protein in mature osteoblasts (day 28) compared with immature osteoblasts (day 7). Panel C shows the expression of β-actin control. *** = $p<0.001$. Mann Whitney test was used. (n=3).

### 3.4.6 Determination of the relative expression of N-cadherin mRNA in myeloma cell lines, 5T33MM and 5TGM1

#### *3.4.6.1 Determination of the quality of the purified RNAs and synthesized cDNAs*

RNAs were extracted from 5T33MM cells and 5TGM1 cells cultured *in vitro*. Figure 3.21 shows the electrophoresis of RNA isolated from 5T33MM cells and 5TGM1 cells. Clear 28S and 18S bands, ribosomal RNAs, are observed, indicating good quality and undamaged RNA. Figure 3.22 shows RT-PCR of GAPDH with expected size of 354 bp in RNA isolated from myeloma cells after reverse transcription (+RT) or no reverse transcription (-RT). Expression of GAPDH in +RT and not in -RT demonstrated no genomic contamination was present in cDNAs preparation.

#### *3.4.6.2 N-cadherin mRNA was expressed in Myeloma cell*

RNAs were extracted from 5T33MM cells and 5TGM1 cells cultured *in vitro* and cDNAs were synthesised. Figure 3.23 shows that N-cadherin was expressed in 5T33MM cells and 5TGM1 cells. End-point RT-PCR is not a quantitative technique and was used to establish if N-cadherin specific mRNAs were expressed in cells. Bands for specific products were sent for sequencing (Figure 3.24) and gave 100% homology with GenBank (Figure 3.25). Therefore, TaqMan was used to study the relative levels of expression of N-cadherin in myeloma cells.

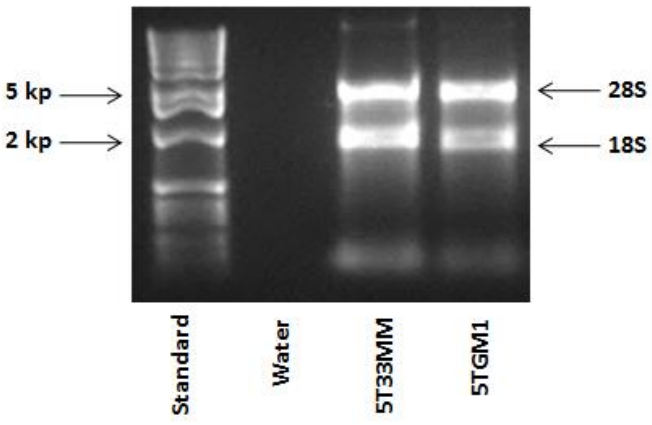


**Figure 3.21: Electrophoresis of total RNA isolated from myeloma cells.** RNA was extracted from myeloma cell lines; 5T33MM and 5TGM1MM. Clear 28S and 18S bands, ribosomal RNAs were indicate of good quality and undamaged RNA. (n=3).

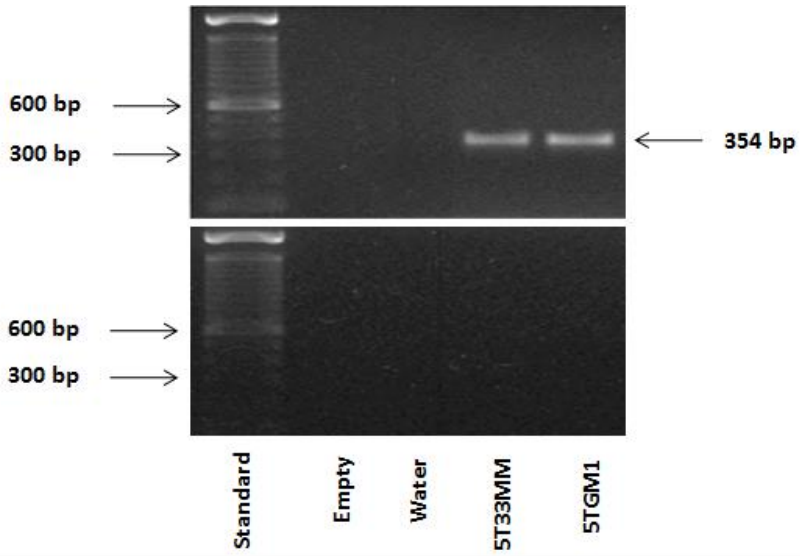


**Figure 3.22: RT-PCR analysis of GAPDH mRNA in myeloma cell lines; 5T33MM and 5TGM1MM.** RNA was extracted from myeloma cell lines; 5T33MM and 5TGM1MM. RT-PCR was performed using GAPDH, gene specific primers. Data shows GAPDH expressed in +RT with expected size of 354 bp and not in - RT demonstrating no genomic DNA contamination in prepared cDNAs. Water was used as a negative control. (n=3).

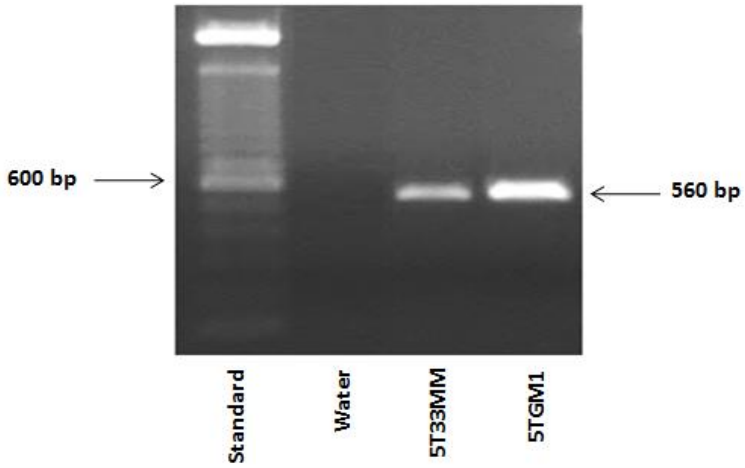


**Figure 3.23: RT-PCR analysis of N-cadherin mRNA in myeloma cells; 5T33MM and 5TGM1.** RNA was extracted from myeloma cell lines; 5T33MM and 5TGM1MM. RT-PCR was performed using N-cadherin, gene specific primers. Data shows N-cadherin was expressed in myeloma cells with expected size of 560 bp. (n=3).

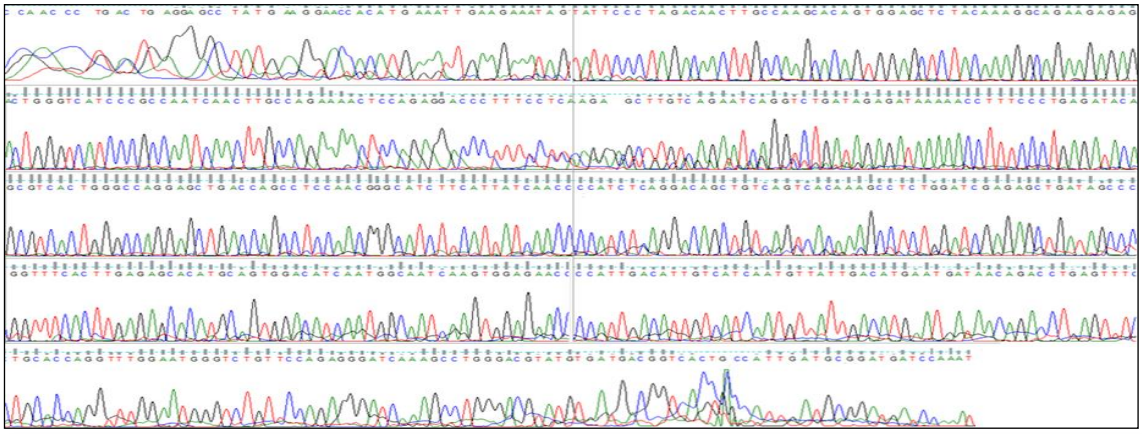

**Figure 3.24: N-cadherin cDNA sequencing.** RNA was extracted from myeloma cells. RT-PCR was performed using N-cadherin, gene specific primers. Bands were sequenced in University of Sheffield Core Genomic Facility (http://genetics.group.shef.ac.uk/dna-sequencing.html). This sequence was received from the Core Genomic Facility. (n=3).

>ref|NM_007664.4| Mus musculus cadherin 2 (Cdh2), mRNA
Length=4646

GENE ID: 12558 Cdh2 | cadherin 2 [Mus musculus] (Over 100 PubMed links)

Score = 965 bits (522), Expect = 0.0
Identities = 522/522 (100%), Gaps = 0/522 (0%)
Strand=Plus/Plus

```
Query  1     CCAACCCTGACTGAGGAGCCTATGAAGGAACCACATGAAATTGAAGAAATAGTATTCCCT  60
             ||||||||||||||||||||||||||||||||||||||||||||||||||||||||||||
Sbjct  1028  CCAACCCTGACTGAGGAGCCTATGAAGGAACCACATGAAATTGAAGAAATAGTATTCCCT  1087

Query  61    AGACAACTTGCCAAGCACAGTGGAGCTCTACAAAGGCAGAAGAGAGACTGGGTCATCCCG  120
             ||||||||||||||||||||||||||||||||||||||||||||||||||||||||||||
Sbjct  1088  AGACAACTTGCCAAGCACAGTGGAGCTCTACAAAGGCAGAAGAGAGACTGGGTCATCCCG  1147

Query  121   CCAATCAACTTGCCAGAAAACTCCAGAGGACCCTTTCCTCAAGAGCTTGTCAGAATCAGG  180
             ||||||||||||||||||||||||||||||||||||||||||||||||||||||||||||
Sbjct  1148  CCAATCAACTTGCCAGAAAACTCCAGAGGACCCTTTCCTCAAGAGCTTGTCAGAATCAGG  1207

Query  181   TCTGATAGAGATAAAAACCTTTCCCTGAGATACAGCGTCACTGGGCCAGGAGCTGACCAG  240
             ||||||||||||||||||||||||||||||||||||||||||||||||||||||||||||
Sbjct  1208  TCTGATAGAGATAAAAACCTTTCCCTGAGATACAGCGTCACTGGGCCAGGAGCTGACCAG  1267

Query  241   CCTCCAACGGGCATCTTCATTATCAACCCCATCTCAGGACAGCTGTCAGTCACAAAGCCT  300
             ||||||||||||||||||||||||||||||||||||||||||||||||||||||||||||
Sbjct  1268  CCTCCAACGGGCATCTTCATTATCAACCCCATCTCAGGACAGCTGTCAGTCACAAAGCCT  1327

Query  301   CTGGATCGAGAGCTGATAGCCCGGTTTCACTTGAGAGCACATGCAGTGGACATCAATGGC  360
             ||||||||||||||||||||||||||||||||||||||||||||||||||||||||||||
Sbjct  1328  CTGGATCGAGAGCTGATAGCCCGGTTTCACTTGAGAGCACATGCAGTGGACATCAATGGC  1387

Query  361   AATCAAGTGGAGAACCCCATTGACATTGTCATCAATGTTATTGACATGAATGATAACAGA  420
             ||||||||||||||||||||||||||||||||||||||||||||||||||||||||||||
Sbjct  1388  AATCAAGTGGAGAACCCCATTGACATTGTCATCAATGTTATTGACATGAATGATAACAGA  1447

Query  421   CCTGAGTTTCTGCACCAGGTTTGGAATGGGTCTGTTCCAGAGGGATCAAAGCCTGGGACG  480
             ||||||||||||||||||||||||||||||||||||||||||||||||||||||||||||
Sbjct  1448  CCTGAGTTTCTGCACCAGGTTTGGAATGGGTCTGTTCCAGAGGGATCAAAGCCTGGGACG  1507

Query  481   TATGTGATGACGGTCACTGCCATTGATGCGGATGATCCAAAT  522
             |||||||||||||||||||||||||||||||||||||||||||
Sbjct  1508  TATGTGATGACGGTCACTGCCATTGATGCGGATGATCCAAAT  1549
```

**Figure 3.25: Using genomic website to identify the matching gene.** Sequence received from the Core Genomic Facility was blast in NCBI browser (http://blast.ncbi.nlm.nih.gov/Blast.cgi) gave 100% homology with GenBank. (n=3).

### *3.4.6.3 The relative expression of N-cadherin mRNA was higher in 5TGM1 cells compared to 5T33MM cells*

cDNAs were synthesised from myeloma cell lines; 5T33MM and 5TGM1 cultured *in vitro* and N-cadherin mRNA expression analysed by real time PCR using TaqMan. Expression of N-cadherin was normalised to the expression of the housekeeping gene, β-actin. Figure 3.26 shows the relative expression of N-cadherin mRNA in 5T33MM cells and 5TGM1 cells. Data showed statistically significant high relative expression of N-cadherin mRNA in 5TGM1 cells compared to 5T33MM cells (169.20±50.60 versus 5.09±1.66, $p<0.001$).

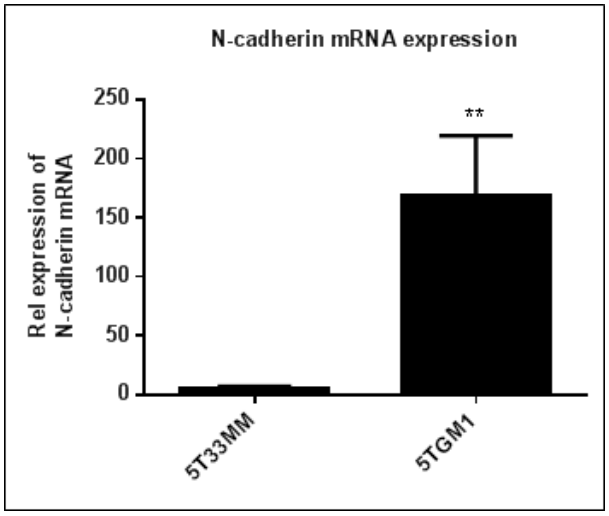


**Table 3.3: CT value**

| | N-cadherin CT | β-actin CT |
|---|---|---|
| 5T33MM | 34.65 | 22.25 |
| 5TGM1 | 28.60 | 22.46 |

**Figure 3.26: Relative expression of N-cadherin mRNA was increased in 5TGM1 cells compared with 5T33MM cells.** cDNAs were synthesised from 5T33 cells and 5TGM1 cells cultured *in vitro* and N-cadherin mRNA expression analysed using TaqMan. Expression of N-cadherin was normalized to expression of housekeeping gene, β-actin. Data shows significant increase in the relive expression of N-cadherin mRNA in 5TGM1 cells compared to 5T33MM cells. *** = $p<0.001$. *t* test was used. (n=3).

### 3.4.7 Immuno-localization of N-cadherin protein in myeloma cell lines, 5T33MM and 5TGM1

A rabbit monoclonal anti-mouse-N-cadherin antibody (Millipore, UK) and an isotype control, normal rabbit IgG antibody (R&D systems, UK) were used to determine possible localization of N-cadherin in 5T33MM and 5TGM1 myeloma cells. Northern light anti-rabbit IgG (NL637) antibody, (secondary antibody for immunofluorescence) or biotinylated anti-rabbit IgG antibody, (secondary antibody for immunocytochemistry) was used for detection of primary antibody. Figure 3.27 panel A shows positive staining (red fluorescence) of N-cadherin in 5T33MM cells and no staining with isotype control (Figure 3.27 panel B). Data determined that the distribution of N-cadherin was focal on 5T33MM cells using immunofluorescence. Figure 3.27 panel C shows positive staining (brown staining) of N-cadherin on the membrane of 5T33MM cells and no staining with isotype control (Figure 3.27 panel D). This results also demonstrated that N-cadherin is focal on the myeloma cell line, 5T33MM. Figure 3.27 panel E shows positive staining (brown staining) of N-cadherin on the membrane of 5TGM1 cells and no staining with isotype control (Figure 3.27 panel F). This result demonstrated that N-cadherin was also focal on 5TGM1 cells.

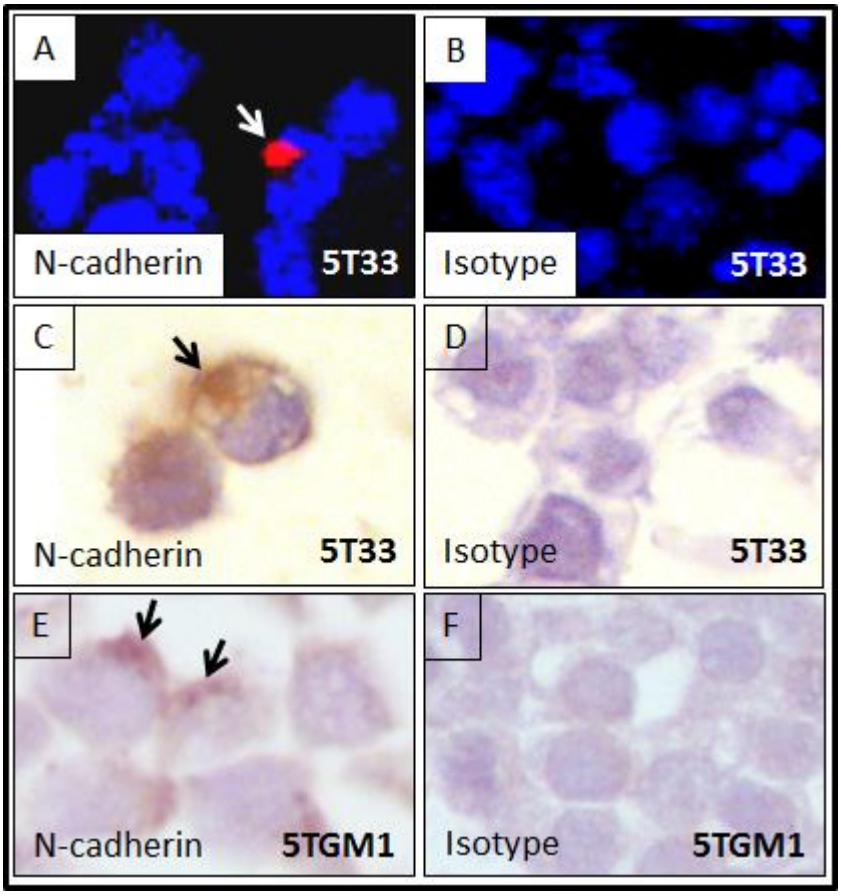


**Figure 3.27: N-cadherin protein expression in myeloma cell lines; 5T33MM and 5TGM1MM.** Fixed and permeabilized cells were stained with rabbit monoclonal anti-N-cadherin antibody or isotype control, normal rabbit IgG antibody. Nuclei were counterstained with DAPI (blue fluorescence) or hematoxylin (blue staining). Cells were examined under Zeiss 510 multiphoton laser scanning microscope or Leitz DMRB microscope. Panel A shows focal staining of N-cadherin (red) in 5T33MM cells. Immunocytochemistry using rabbit monoclonal anti-N-cadherin antibody also shows focal staining of N-cadherin (brown) on the membranes of 5T33MM cells.. Panel E shows focal expression of N-cadherin (brown staining) on the membranes of 5TGM1 cells using immunocytochemistry. Panel B, D and F show the isotype control for these experiments. (n=3).

### 3.4.8 Determination of the percentage and relative expression of N-cadherin protein in myeloma cell lines, 5T33MM and 5TGM1

#### *3.4.8.1 The frequency of N-cadherin positive cells was higher in 5TGM1 cells than in 5T33MM cells*

A mouse monoclonal anti-N-cadherin antibody (Sigma, UK) and an isotype control, mouse IgG antibodies (Vector laboratories, UK) were used to determine the percentage of N-cadherin positive on myeloma cells using flow cytometry. Figure 3.28 shows the percentage of N-cadherin positive myeloma cells in populations, and no positive cells in the isotype controls. The data demonstrated that 1% of 5T33MM cells and 6% of 5TGM1 cells expressed N-cadherin. Figure 3.29 shows the percentage of N-cadherin positive 5T33MM cells and N-cadherin positive 5TGM1 cells. Data showed statistically significant higher relative frequency of N-cadherin positive cells in 5TGM1 cells compared to 5T33MM cells using flow cytometry (5.00±0.20 versus 1.00±0.14, $p<0.05$).

#### *3.4.8.2 The relative levels of N-cadherin protein was higher in 5TGM1 cells than to 5T33MM cells compared by western blot*

A rabbit monoclonal anti-N-cadherin antibody (Millipore, UK) was used to detect N-cadherin protein in 5T33MM cells and 5TGM1 cells analysed by western blot. Figure 3.30 panel A shows the N-cadherin protein levels in 5T33MM cells and 5TGM1 cells. It was found that an osteocyte-like cell line, MLO-Y4 was not expressed N-cadherin (Kawaguchi et al., 2001). Therefore, MLO-Y4 was used as a negative control. Figure 3.30 panel B shows significant increase in the relative levels of N-cadherin protein in 5TGM1 cells compared to 5T33MM cells (38.17±10.52 versus 13.07±1.57, $p<0.001$). Figure 3.28 panel C shows the expression of the positive control, β-actin.

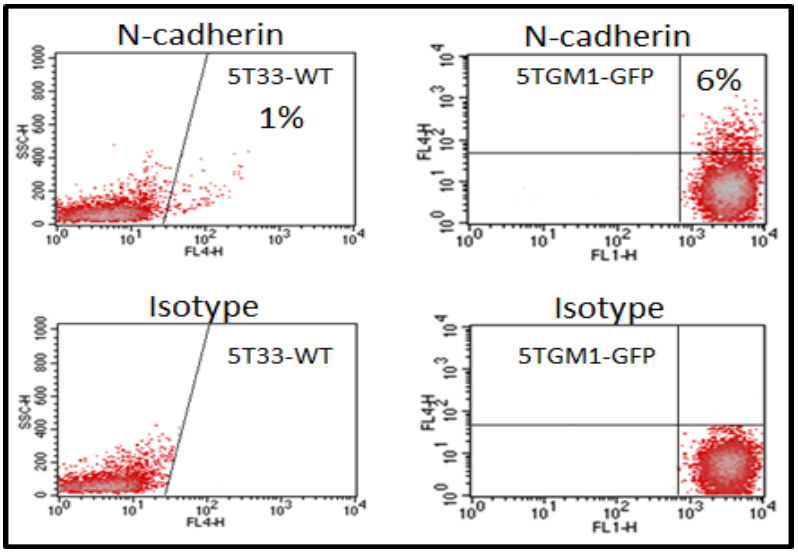


**Figure 3.28: The percentage of N-cadherin$^{+}$ myeloma cells.** Live cells were stained with a mouse monoclonal anti-N-cadherin antibody or an isotype control, mouse IgG antibody. Cells were analyzed using FACs Calibur. Data shows 1% of 5T33MM cells and 5% of 5TGM1 cells express N-cadherin (red fluorescence in the right half). Panel B shows isotype control. (n=3).

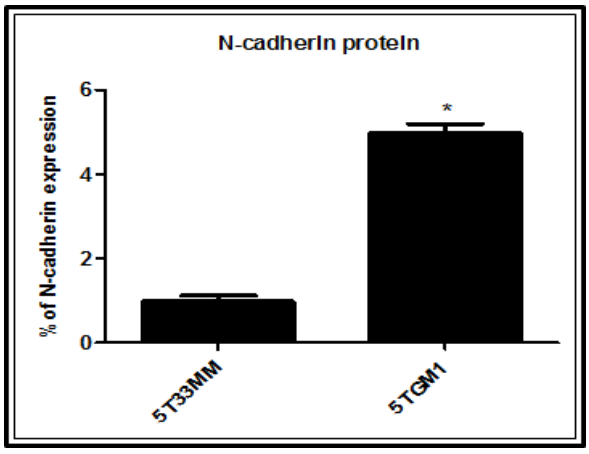


**Figure 3.29: Relative level of N-cadherin protein on 5TGM1 cells compared with 5T33MM cells using flow cytometry.** Data shows significant highest relative levels of N-cadherin protein in 5TGM1 cells compared to 5T33MM cells (n=4). * = $p<0.05$. Mann Whitney test was used. (n=3).

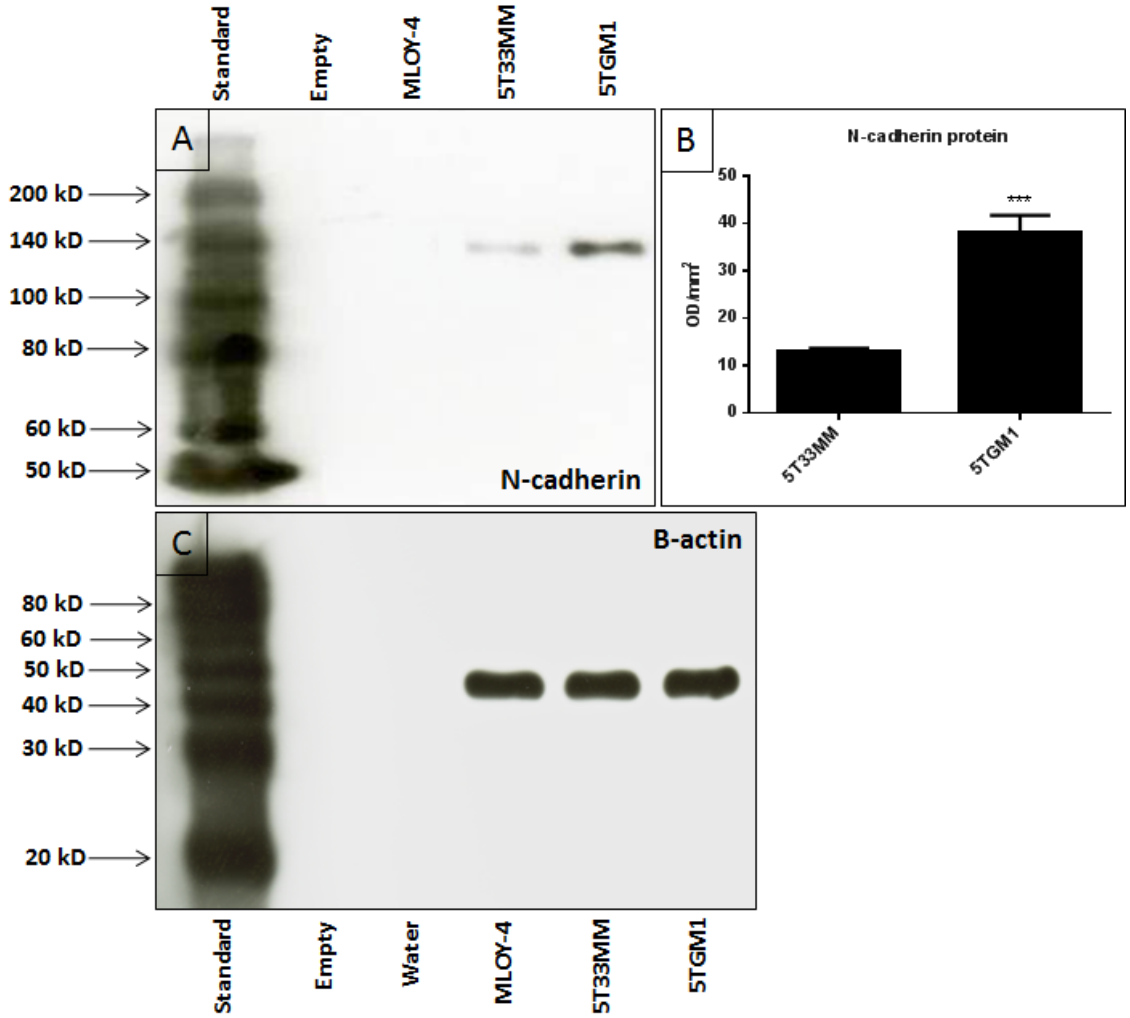


**Figure 3.30: Relative expression of N-cadherin protein was highest in 5TGM1 cells compared with 5T33MM cells using western blot.** Whole cell lysis preparation electrophoresed in 12.5% SDS PAGE gels for N-cadherin and 15% SDS PAGE gels for β-actin, and transferred to PVDF membranes were probed with a rabbit monoclonal anti-N-cadherin antibody or an isotype control, normal rabbit IgG antibody. Panel A shows N-cadherin protein levels in 5T33MM cells and 5TGM1 cells. The osteocyte-like cell line, MLO-Y4 was used as a negative control. Panel B shows significant highest relative levels of N-cadherin protein in 5TGM1 cells compared with 5T33MM cells. Panel C shows the expression of β-actin control. *** = $p<0.001$. Mann Whitney test was used. (n=3).

### 3.4.9 A comparison in the expression of N-cadherin between myeloma cells and osteoblasts

cDNAs were synthesised from myeloma cell lines, 5T33MM and 5TGM1, and mouse primary osteoblasts cultured *in vitro* and N-cadherin mRNA expression analysed by real time PCR using TaqMan. Expression of N-cadherin was normalised to the expression of the housekeeping gene, β-actin. Figure 3.31 shows the relative expression of N-cadherin mRNA in 5T33MM cells, 5TGM1 cells, immature osteoblasts (day 7) and mature osteoblasts (day 28). In addition, a rabbit monoclonal anti-N-cadherin antibody (Millipore, UK) was used to detect N-cadherin protein in myeloma cells and osteoblasts analysed by western blot. GS-710 calibrated imaging densitometer was used to measure the density of bands. Figure 3.32 shows the relative levels of N-cadherin protein in 5T33MM cells, 5TGM1 cells, immature osteoblasts and mature osteoblasts.

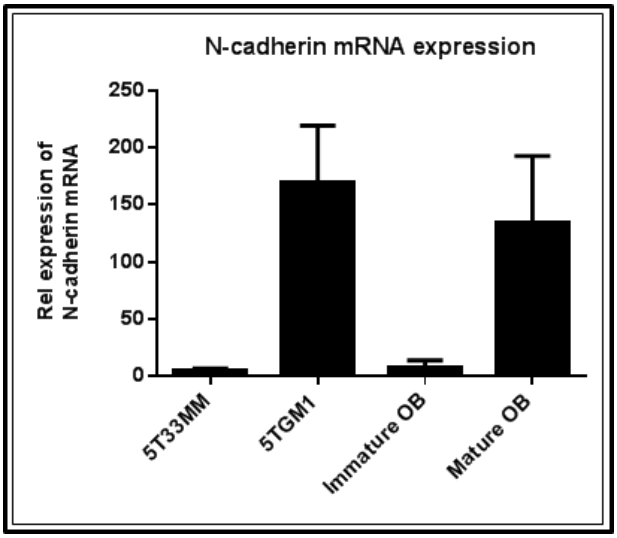


**Figure 3.31: Relative expression of N-cadherin mRNA in myeloma cells and osteoblasts.** cDNAs were synthesised from 5T33MM cells, 5TGM1 cells, immature osteoblasts and mature osteoblasts cultured *in vitro* and N-cadherin mRNA expression analysed using TaqMan. Expression of N-cadherin was normalized to expression of housekeeping gene, β-actin. Data show high expression of N-cadherin mRNA in 5TGM1 cells and mature osteoblasts compared to 5T33MM cells and immature osteoblasts. (n=3).

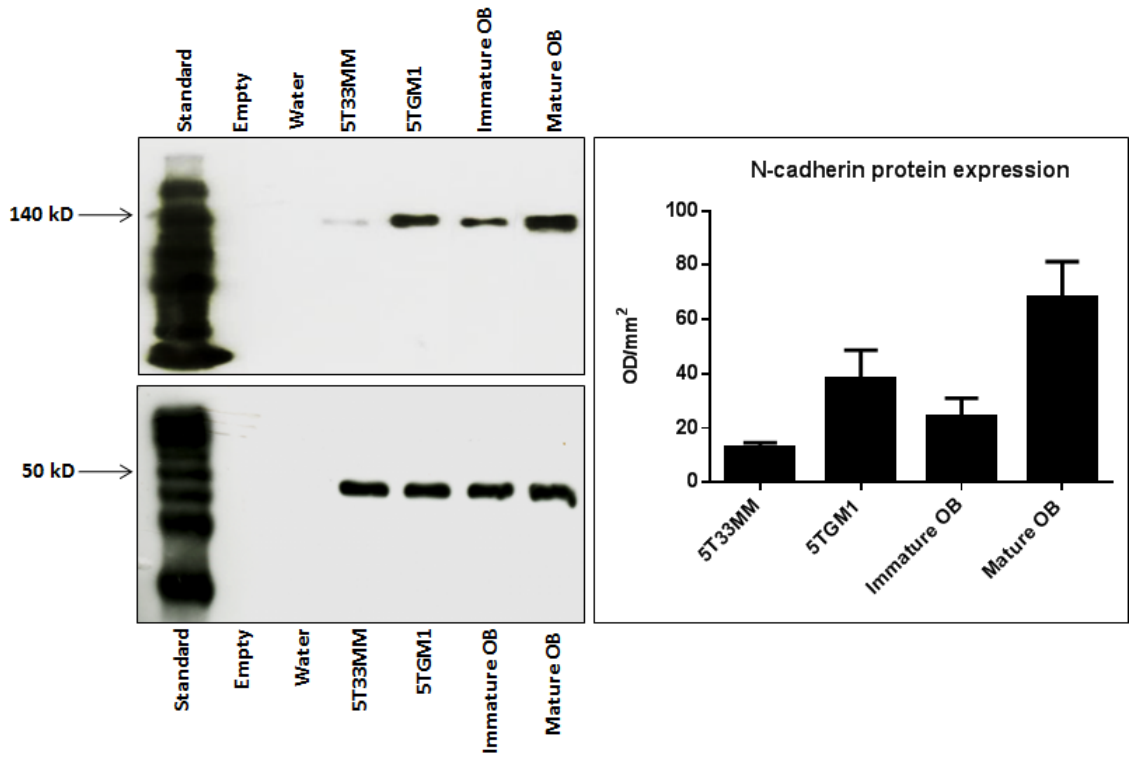


**Figure 3.32: Relative expression of N-cadherin protein in myeloma cells and osteoblasts using western blot.** Whole cell lysis preparation electrophoresed in 12.5% SDS PAGE gels for N-cadherin and in 15% SDS PAGE gels for β-actin. Data show high expression of N-cadherin protein in 5TGM1 cells and mature osteoblasts compared to 5T33MM cells and immature osteoblasts. (n=3).

## 3.5 Discussion

In this chapter an *in vitro* model of mouse osteoblastogenesis was developed. The expression of N-cadherin mRNA and the levels of N-cadherin protein at different stages of osteoblastogenesis were determined. Primary cultures of calvarial mouse osteoblasts were differentiated to mature functional osteoblasts using different osteogenic medium to address the effect of dexamethasone on osteoblastogenesis. Gilbert et al (2002) differentiated osteoblasts to mature osteoblasts using α-MEM medium containing; 10% FCS, 10 mM of β-glycerophosphate and 50 µg/ml of ascorbic (Gilbert et al., 2002). However, Bancroft et al (2002) differentiated osteoblasts to mature osteoblasts using α-MEM medium containing; 10% FCS, 10 mM of β-glycerophosphate, 50 µg/ml of ascorbic acid and $10^{-8}$ M of dexamethasone (Bancroft et al., 2002). Therefore, in my study different osteogenic medium were used to determine if adding $10^{-8}$ M of dexamethasone promotes the differentiation of osteoblasts.

In the first series, cells were incubated in α-MEM medium containing; 10% FCS, 10 mM of β-glycerophosphate and 50 µg/ml of ascorbic acid for 28 days. In the second series, cells were incubated in α-MEM medium containing; 10% FCS, 10 mM of β-glycerophosphate and 50 µg/ml of ascorbic acid for 14 days and at day 15, $10^{-8}$ M of dexamethasone was added to the osteogenic medium to promote differentiation. In the third series, cells were incubated in α-MEM medium containing; 10% FCS, 10 mM of β-glycerophosphate, 50 µg/ml of ascorbic acid and $10^{-8}$ M of dexamethasone for 28 days. In the fourth series, cells were incubated in α-MEM medium containing; 10% FCS, 10 mM of β-glycerophosphate, 50 µg/ml of ascorbic acid and water for 28 days. The results demonstrated that osteoblasts can be differentiated to mature functional osteoblasts with and without using $10^{-8}$ M of dexamethasone. However, the results of alizarin red analysis showed that there was an increase in the mineralization of cells on day 28 when $10^{-8}$ M of dexamethasone was added into the osteogenic medium. The data also demonstrated that there was no difference in the mineralization of cells on day 28 between the second series, when $10^{-8}$ M of dexamethasone was added into the

osteogenic medium at day 15, and the third series, when $10^{-8}$ M of dexamethasone was added into the osteogenic medium at day 0. In my study the second series, α-MEM medium containing; 10% FCS, 10 mM of β-glycerophosphate and 50 μg/ml of ascorbic acid was used for 14 days and at day 15, $10^{-8}$ M of dexamethasone was added to the osteogenic medium, and used as a medium for the osteoblastogenesis *in vitro* to promote cell differentiation. This was because I wanted to examine cells in less well differentiation versus well differentiated states and series 2 appeared to alter lower differentiation on day 7 to higher differentiated states on day 28. This allows clearer distinction between differentiating and differentiated cell types.

ALP activity and alizarin red staining were used as an osteoblast differentiation and mineralization markers. Xiao et al (2006) demonstrated that ALP activity and alizarin red staining increased during mouse osteoblastogenesis (Xiao et al., 2006). In addition, Hay et al also showed that ALP activity and alizarin red staining increased during mouse osteoblastogenesis (Hay et al., 2009a). In this study, ALP activity and alizarin red staining were also used as osteoblast differentiation and mineralization markers. My experiments also showed the ALP activity and alizarin red staining increased during mouse osteoblastogenesis.

In this study, the quantification of relative levels of expression of Runx2 mRNA and COL1A2 mRNA was analysed to determine the relevance between osteoblast markers, Runx2 and COL1A2, and osteoblastogenesis. Runx2 is a transcriptional activator necessary for bone formation and osteoblast differentiation in mice (Ducy et al., 1997). Runx2-null mice resulted in a complete lack of bone formation and suggested that Runx2 plays an essential role in osteoblastogenesis in mice (Komori et al., 1997). My experiments demonstrated that the relative expression of Runx2 mRNA significantly increased during osteoblastogenesis. COL1A2 gene encodes one of the chains for type I collagen and mutations in this gene produced an osteogenesis imperfecta a type IV phenotype (Wenstrup et al., 1988). Both Runx2 and COL1A2 are induced at an early

stage in osteoblast differentiation (Sila-Asna et al., 2007). My experiments demonstrated that the relative expression of COL1A2 mRNA significantly increased during osteoblastogenesis. Therefore, this study showed that not only ALP activity and alizarin red staining are useful as osteoblast differentiation and mineralization markers, but also the relative expression of Runx2 mRNA and COL1A2 mRNA can be used as markers for mouse osteoblastogenesis. I found that there were some limitations in this experiment, in which some variability in the tissue cultures of osteoblast differentiation *in vitro* between experiments. This variability could be due to the differences in the age of mice used to obtain osteoblasts. In published protocols, Hay et al, (2009) obtained primary osteoblasts of calvarias from 2-5 day old mice (Hay et al., 2009a). Subramaniam et al (2005) obtained primary osteoblasts of calvarias from 1-3 day old mice (Subramaniam et al., 2005). Mukherjee et al (2010) obtained primary osteoblasts of calvarias from 2-7 day old mice (Mukherjee et al., 2010). In this study osteoblasts obtained from 2-4 day old C57Bl/6J mice due to the policy of arriving time and the policy of The University of Sheffield biological services laboratory. Although there was variability, I can say that in week one and two the osteoblasts are in the differentiating phase but in week three and four the osteoblasts are fully differentiated.

N-cadherin$^{+}$ osteoblasts are a key cell type to which HSCs home to on the endosteal bone surface (Xie et al., 2009). The authors offered that N-cadherin$^{+}$ cells were probably pre-osteoblasts, osterix$^{+}$ cells, however, Nakashima et al (2002) have shown osterix to be expressed in all subsets of osteoblasts; pre-osteoblasts and mature osteoblasts (Nakashima et al., 2002). Previously, Wennberg et al (2000) showed that N-cadherin is expressed in mouse primary osteoblasts (Wennberg et al., 2000). In this study specific primers and an antibody against N-cadherin were used to analyze the relative expression of N-cadherin mRNA and the levels of N-cadherin protein, respectively, during osteoblastogenesis. TaqMan analysis of primary calvarial osteoblasts cDNA demonstrated an increase in the expression of N-cadherin mRNA during osteoblastogenesis from day 7 to day 28. The data showed a significant increase in the N-cadherin mRNA expression in mature osteoblasts (day 28) compared with

immature osteoblasts (day 7). Flow cytometry demonstrated that there was no difference in the levels of N-cadherin protein between immature osteoblasts and mature osteoblasts. This was unexpected and could be because the osteoblasts were separated from each other when prepared for flow cytometry. Alternatively, it may be that the flow cytometry underscored the levels of N-cadherin due to general issues of the antibody sensitivity. However, immunofluorescence and western blot showed a significant increase in the levels of N-cadherin protein in mature osteoblasts (day 28) compared to immature osteoblasts (day 7) and this suggested a low levels of N-cadherin expression in immature osteoblasts and relatively high levels of N-cadherin expression in mature osteoblasts during osteoblastogenesis. The approach taken to controlling the loading of protein was to run 2 gels: that for N-cadherin analysis designed for higher molecular weight (50-200 kD) and that for the loading control (β-actin) for lower molecular weight (20-100 kD). These gels were run simultaneously with the same samples and this allowed good resolution over the expected target molecular weights for the 2 proteins analyzed.

These observations are supported by previous work performed by Ferrari et al (2000) and by Kawaguchi et al (2001). Ferrari et al (2000) showed that N-cadherin mRNA expression was increased during osteoblastogenesis of the human cell line, SaOS-2, rat cell line, ROS, and primary osteoblast cells prepared from fetal rat calvariae. This study supported the role of N-cadherin in the late stage of osteoblast differentiation (Ferrari et al., 2000). Kawaguchi et al (2001) showed that the mouse osteoblast cell line, MC3T3-E1, expressed N-cadherin and this expression was increased during MC3T3-E1 cell differentiation (Kawaguchi et al., 2001). In contrast, Greenbaum et al (2012) demonstrated a decrease in the relative expression of N-cadherin during osteoblastogenesis using western blot. In this published study, osteoblasts were originated from the differentiation of bone marrow stromal cells using $Cdh2^{flox/flox}$ mice, backcrossed to more than 99% congenic with the C57BL/6 background. In addition, for differentiation they used α-MEM (Invitrogen) with 20% FCS, 50 μM ascorbic acid and 10 μM β-glycerophosphate (Greenbaum et al., 2012). These discrepancies may be due

to differences in culture conditions and N-cadherin analysis methods. My data clearly showed an increase in the relative levels of N-cadherin mRNA and protein during osteoblastogenesis in culture using TaqMan analysis, immunofluorescence and western blot, and although the flow cytometric analysis data did not show increased percentage in N-cadherin labelled cells this may have been due to the culture disruption and underscoring issues.

The flow cytometry analysis may underscore the actual levels of N-cadherin positivity within a population. Resolving of this could be by generating a new anti-N-cadherin antibody with high affinity to the extracellular domain of N-cadherin for flow cytometry. The antibody used in this project for flow cytometry is anti-N-cadherin antibody, GC-4 (Sigma, UK). To date, the flow cytometry analysis of N-cadherin as a surface molecule are extremely limited. Wein et al (2010) used anti-N-cadherin antibody, GC-4 (Sigma, UK) and anti- N-cadherin antibody (MNCD2) for flow cytometry to detect the N-cadherin in human hematopoietic progenitor cells (HPCs). They demonstrated that the percentage of N-cadherin$^{+}$ HPC varied between different samples from 5% to 50% between different samples and this might be due to the available antibodies (Wein et al., 2010). More recently, Groen et al (2011) used anti-N-cadherin antibody, GC-4 (Sigma, UK) for flow cytometry and anti-N-cadherin, clone 32 (BD Biosciences, Erembodegem, Belgium) for immuno-staining and western blot to detect the N-cadherin in myeloma cells. They demonstrated that there were some differences in the expression of N-cadherin in myeloma cells when western blotting and flow cytometry were used. It was found that N-cadherin expression in NCI-H929 and LME-1 myeloma cells was high by western blot whereas N-cadherin expression by flow cytometry in the same cells was found to be low (Groen et al., 2011). Although, this issue has been raised for the anti-N-cadherin antibody, to date anti-N-cadherin antibody, GC-4 (Sigma, UK) is used by resent publication for flow cytometry. Therefore, this antibody was used in this study for flow cytometry. In western blot and immuno-staining I used another antibody, rabbit monoclonal, anti-N-cadherin antibody (Millipore, UK).

Dring et al (2004) demonstrated that N-cadherin was expressed in t4;14 MM patients using gene array studies (Dring et al., 2004). In addition, Groen et al (2011) demonstrated that N-cadherin was expressed in myeloma cell lines; OPM-1, NCI-H929 and LME-1 as well as in primary MM using western blot, immunocytochemistry and immunohistochemistry (Groen et al., 2011). These support my observation, in which N-cadherin is expressed in murine myeloma cell lines; 5T33MM and 5TGM1. A novel finding in my study was that N-cadherin distribution in 5T33MM and 5TGM1 cells was focal using immunofluorescence and immunocytochemistry, similar to N-cadherin expression in mouse HSCs (Xie et al., 2009) and human HSCs (Wein et al., 2010). Flow cytometriy data demonstrated that 1% of 5T33MM cells expressed N-cadherin whereas 5% of 5TGM1 cells express N-cadherin. Western blot data showed higher levels of N-cadherin protein in 5TGM1 cells compared with 5T33MM cells. In addition, TaqMan analysis demonstrated higher expression of N-cadherin in 5TGM1 cells compared with 5T33MM cells. Taken together these findings suggest that N-cadherin expression and surface levels of N-cadherin are higher in 5TGM1 cells than in 5T33MM cells.

Alizarin red staining is a dye used as an *in vitro* mineralisation marker by binding to calcium in matrix deposited by osteoblasts (Xiao et al., 2006). N-cadherin is a member of the $Ca^{2+}$-dependent cell-cell adhesion receptor family (Miyatani et al., 1992, Gumbiner, 2005). My study showed that there was a correlation between N-cadherin expression and bone mineralisation. My data demonstrated a significant increase in the expression of N-cadherin in correlation to a significant increase in alizarin red staining in mature osteoblast (day 28), this could be because of the presence of calcium. Potentially, colonising N-cadherin$^{+}$ myeloma cell bind to a population of osteoblast expressing high level of N-cadherin, mature osteoblast, initiating the formation of the myeloma niche and tumour cells growth.

In conclusion, this chapter demonstrated that I had generated a consistent *in vitro* model for osteoblast differentiation using primary osteoblast lineage cells derived from mouse calvariae. My studies showed that N-cadherin was expressed at increasing levels during differentiation in this model. Studies with the 5T33MM and 5TGM1 cells showed that these cells produced N-cadherin and that this was focally distributed on the surface of these cells. 5TGM1 cells appeared to produce more N-cadherin than 5T33MM cells. These findings indicate the potential for interactions between myeloma cells and osteoblasts mediated via N-cadherin, and these will be investigated in the next chapter.

# 4 Chapter 4: N-cadherin mediates the interaction of myeloma cells with osteoblasts *in vitro*

## 4.1 Introduction

### 4.1.1 N-cadherin maintains the HSCs quiescent in the HSC niche

One of the regulatory molecules in the HSC niche is N-cadherin, which is expressed by both HSCs and osteoblasts mediating their association (Zhang et al., 2003, Xie et al., 2009). N-cadherin is a member of a $Ca^{2+}$-dependent cell-cell adhesion receptor family known as cadherin 2, and contains an extracellular domain, transmembrane domain and a cytoplasmic domain that interacts with catenins and mediates signalling pathway following cell-cell adhesion (Gumbiner, 2005).

Puch et al (2001) showed human $CD34^+$ HSCs express N-cadherin. It was shown that treatment of these cells with monoclonal anti-N-cadherin antibodies resulted in a reduction in colony formation when HSCs were injected into experimental animals, which suggested a direct interaction between osteoblasts and HSCs via N-cadherin (Puch et al., 2001). Zhang et al (2003) demonstrated that there is a correlation between an increase in the number of spindle-shaped N-$cadherin^+CD45^-$ osteoblastic cells and an increase in the number of HSCs. In addition, it was found that persistent HSCs attached to SNO cells via N-cadherin and β-catenin (Zhang et al., 2003). *In vitro,* Aria and Suda (2007) showed enhancements of both HSCs and stromal cell adhesion and inhibition of cell division of HSCs by enforced N-cadherin expression, suggesting a key role of N-cadherin-mediated adhesion in maintaining HSCs quiescence in the osteoblastic niche (Arai and Suda, 2007). Using a new technology, *ex vivo* real-time imaging, and immunoassaying found that HSCs home to the 'osteoblast niche' via attachment to N-$cadherin^+$ osteoblasts on endosteal bone surfaces (Xie et al., 2009). Recently, Hosokawa et al (2010) showed that N-cadherin is expressed in LT-HSCs and in the osteoblasts mediating cell adhesion in the HSC niche. Knockdown of N-cadherin showed an enhanced cell division and reduced long-term engraftment activity of HSCs in the BM *in vivo* (Hosokawa et al., 2010).

### 4.1.2 N-cadherin molecular interactions may be exploited to establish multiple myeloma cell colonisation in the HSC niche

#### *4.1.2.1 Cadherin switching in tumours*

During tumour progression in solid tumours, the invasion and metastatic properties acquired by cancer cells have been linked to expression of N-adhesion molecules and cadherin switching from E-cadherin to N-cadherin. Changes in expression of adhesion molecules mediate the interaction of cancer cells from their primary site to establish new interactions with the surrounding microenvironment. In melanoma, Li et al (2001) showed that expression of N-cadherin increased invasion, metastasis and promoted survival of melanoma cells (Li et al., 2001). In bladder cancer, Lascombe et al (2006) demonstrated that N-cadherin expression was absent in normal urothelium. During tumour progression or invasive increased N-cadherin expression was observed in association with loss of E-cadherin expression suggesting that N-cadherin is a prognostic marker of progression in urothelial tumours (Lascombe et al., 2006). In prostate cancer, Gravdal et al (2007) demonstrated that cadherin switch from E-cadherin to N-cadherin, increased N-cadherin and reduced E-cadherin expression, increased invasion and metastasis of the cancer cells, and associated with shorter survival times in prostate cancer progression patient. Loss of E-cadherin in a member of epithelial to mesenchymal transition a process that increase invasion of tumour cells in progress of prostate cancer (Gravdal et al., 2007).

#### *4.1.2.2 Role of N-cadherin in tumours*

N-cadherin is expressed in several cancers including melanoma, prostate, breast, gastric carcinoma, bladder carcinoma and overian carcinoma. Expression of N-cadherin in cancer cells mediates the invasion and interaction of cancer cells from their primary site to establish new interactions with the surrounding microenvironment (Hazan et al., 2004, Yanagimoto et al., 2001, Lascombe et al., 2006, Sarrio et al., 2006). Shintani et al (2008) demonstrated that using a cyclic pentapeptide, ADH-1, targeting N-cadherin,

significantly reduced growth and metastasis of pancreatic cancer cells in transgenic mice (Shintani et al., 2008).

In melanoma, Augustine et al (2008) showed that N-cadherin was expressed in human melanoma-derived cell lines. Targeting N-cadherin with ADH-1 pentapeptide in combination with chemotherapy drug (Melphalan) was used as a novel therapeutic approach and significantly reduced tumour growth and enhanced the antitumor activity to treat melanoma (Augustine et al., 2008). Clinically, Beasley et al (2009) demonstrated that ADH-1 at a dose of 4000 mg in combination with melphalan on days 1 and 8 was safe and well tolerated by patients in phase I studies and was a potential novel targeted therapy approach in melanoma (Beasley et al., 2009).

In prostate cancer, Tanaka et al (2010) demonstrated that prostate cancer metastasis and castration resistance are mainly caused by N-cadherin. Targeting N-cadherin using monoclonal antibodies against N-cadherin resulted in a reduction in proliferation, adhesion and invasion of prostate cancer cells *in vitro* and delayed the castration resistance progression *in vivo*. In addition, Tanaka et al (2010) indicated the possibility of using N-cadherin as a marker for castration-resistant stem cells in prostate cancer, in which N-cadherin$^{+}$ cells were tumourigenic. Moreover, Tanaka et al (2010) demonstrated that N-cadherin was expressed by small proportion of human primary tumours (Tanaka et al., 2010).

In myeloma, using gene array studies, Dring et al (2004) showed that N-cadherin was expressed in t(4;14) chromosomal translocation MM patients cases. The t(4;14) are cases of MM that represent about 10–20% of MM patients and it has been suggested that this subset have poor prognosis. 127 genes were identified with significant differences between t(4;14) and non-t(4;14) cases by using global gene expression. N-cadherin (CDH2) was one of these genes with significant mean different, p value =

0.04, (Dring et al., 2004). More recently, Groen et al (2011) showed that myeloma cells express N-cadherin. The expression of N-cadherin directly mediated the bone marrow localization/retention of myeloma cells *in vivo*. In addition, it was found that expression of N-cadherin facilitated the interaction of myeloma cells with N-cadherin$^{+}$ osteoblasts (Groen et al., 2011). This chapter will examine whether N-cadherin expression mediates the interaction of myeloma cells with osteoblasts *in vitro* as a potential mechanism used by colonising myeloma cells to establish the colonising on bone.

## 4.2 Hypothesis and objectives of this chapter

### 4.2.1 Hypothesis

Expression of N-cadherin mediates the adhesion of myeloma cells to osteoblasts *in vitro*.

### 4.2.2 Objectives

To test this hypothesis, I have determined:

1. The incubation time required for myeloma cells to adhere to recombinant N-cadherin.
2. The optimal concentration of recombinant N-cadherin required for myeloma cell adhesion.
3. Whether expression of N-cadherin mediates adhesion of myeloma cells *in vitro*.
4. Whether treating cultures with an anti-N-cadherin antibody blocks myeloma cells from adhering to recombinant N-cadherin *in vitro*.
5. Whether expression of N-cadherin mediates the interaction of myeloma cells with osteoblasts *in vitro*.
6. Whether treating cultures with an anti-N-cadherin antibody blocks myeloma cells from adhering to osteoblasts *in vitro*.

## 4.3 Materials and Methods

### 4.3.1 Cell culture

Non-adherent 5T33MM and 5TGM1 cells were cultured separately *in vitro* in RPMI1640 medium (Invitrogen, UK) containing 10% FCS, 100 units/ml Penicillin / 100 µg/ml of Streptomycin, 1% $Na_2PO_3$ and 1% non-essential amino acids (NEAA). Mouse primary osteoblasts were prepared as described in section 2.1.9 and cultured *in vitro* in MEM alpha containing 10% FCS, 100 units/ml Penicillin / 100 µg/ml of Streptomycin and 1.36 µg/mL of amphotericin B. Both media were changed every 2 days.

### 4.3.2 Osteoblast differentiation

Mouse primary osteoblasts were differentiated for 4 weeks to mature functional osteoblasts in osteogenic media; MEM alpha (Invitrogen, UK) containing 10 mM of β-glycerophosphate and 50 µg/ml of ascorbic acid in addition to 10% FCS, 100 units/ml Penicillin / 100 µg/ml of Streptomycin and 1.36 µg/mL of amphotericin B. medium was changed every 2 days.

### 4.3.3 Cell adhesion assay

#### *4.3.3.1 Determining the incubation times*

96 well plates were coated overnight at 4°C with PBS containing 1 µg/ml recombinant N-cadherin/Fc chimera. $1x10^5$ cells/ml of myeloma cells were plated and incubated with recombinant N-cadherin at 37°C for different times; 0, 4, 8, 10, 15, 20, 30 and 60 minutes to determine the incubation time required for myeloma cells to adhere to N-cadherin (see section in 2.2.9.1 materials and methods).

#### *4.3.3.2 Determining the concentration of recombinant N-cadherin*

96 well plates were coated overnight at 4°C with PBS containing different concentrations of recombinant N-cadherin/Fc chimera (R&D Systems); 0, 0.1, 0.5, 1, 2, 5, 10 µg/ml. $1x10^5$ cells/ml of myeloma cells were plated and incubated with these different recombinant N-cadherin concentration at 37°C for 20 minutes to determine the effect of increasing the concentration of recombinant N-cadherin required for myeloma cell adhesion (see section in 2.2.9.1 materials and methods).

#### *4.3.3.3 Blocking N-cadherin using anti-N-cadherin GC-4 antibody*

To block N-cadherin, cells were incubated with anti-N-cadherin 10 µg/ml GC-4 antibody (Sigma, UK) at 37°C for 30 minutes. After blocking, $1x10^5$ cells/ml of myeloma cells were plated and incubated with recombinant N-cadherin at 37°C for 20 minutes to determine the effect of blocking N-cadherin on the adhesion of myeloma cells (see section 2.2.9.2).

### 4.3.4 Co-culture of myeloma cells with osteoblasts

$6x10^3$ cells/$cm^2$ of mouse primary osteoblasts were seeded in 35mm glass bottom dishes. $5x10^4$ cells/ml of myeloma cells, 5T33MM-GFP and 5TGM1-GFP, were plated and incubated with osteoblasts as described in section 2.2.10. To block N-cadherin, cells were incubated with anti-N-cadherin GC-4 antibody (see section 2.2.10). $GFP^+$ expression allowed the identification of myeloma cells versus osteoblasts in these cultures.

### 4.3.5 Microscopy

Osteomeasure software version 4.10 (Osteomerics Incorporated, Atlanta, USA) was used with a Leitz DMRB microscope and a drawing tablet, (CalComp Drawing Broad III) to determine the adhesion of myeloma cells with N-cadherin coated plates or PBS coated plates as described in section 2.2.14.2. A Zeiss 510 Multiphoton Laser Scanning Microscopy was used to visualise fluorescence as described in section 2.2.14.1.

### 4.3.6 Statistical analysis

The data were analysed using an ANOVA test (one-way analysis of variance) for more than two group comparisons or with *t* test for two group comparisons if the data was normally distributed. Tukey's test was used as post-hoc analysis when ANOVA test was used in normal distribution data. When data not normally distributed, ANOVA test (non-parametric Kruskal-Wallis test) was used for more than two group comparisons or non-parametric Mann–Whitney test was used for two group comparisons. Dunns test was used as post-hoc analysis when ANOVA test was used in not normally distributed data. Data were considered statistically significant when a p-value was equal to or less than 0.05. Results are expressed as mean ± values of standard deviation (SD).

## 4.4 Results

### 4.4.1 Determination of the incubation time required for myeloma cells to adhere to recombinant N-cadherin

5T33MM cells and 5TGM1 cells ($1X10^5$ cells/100 µl) were plated and incubated with 1 µg/ml of recombinant N-cadherin coated plates (Groen et al., 2011). Cells were incubated at 37°C for different times; 0, 4, 8, 10, 15, 20, 30 and 60 minutes. Figure 4.1 shows the adherence of myeloma cells; 5T33MM and 5TGM1 to recombinant N-cadherin over times. The data clearly demonstrated an increase in the number of myeloma cells; 5T33MM and 5TGM1 that were adherent to recombinant N-cadherin from 0 minutes to 20 minutes and after 20 minutes the adherent numbers were reduced. Therefore, 20 minutes was chosen as an optimal incubation time to incubated myeloma cells with recombinant N-cadherin or with osteoblasts.

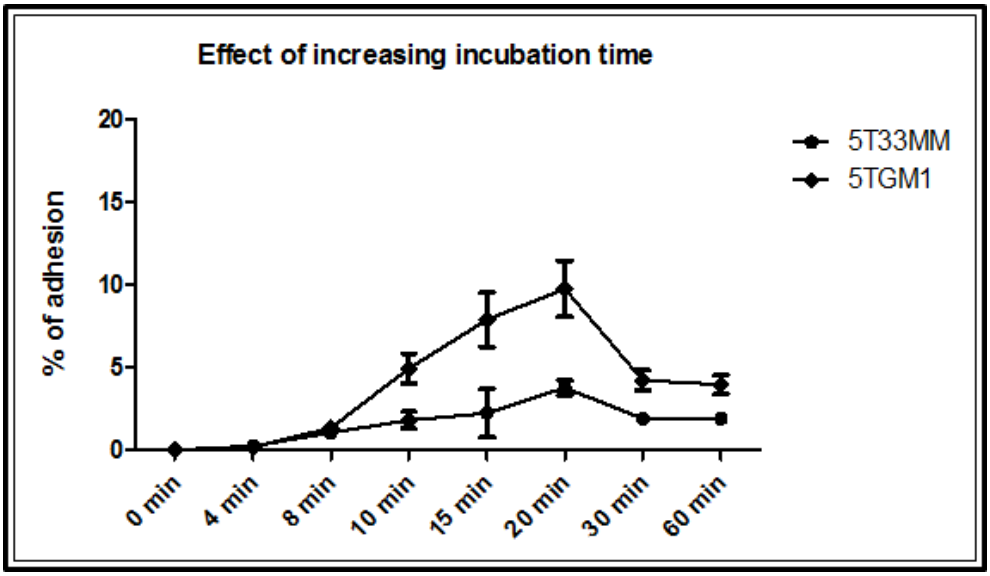


**Figure 4.1: Effect of increasing incubation time.** 96-well plates were coated overnight with recombinant N-cadherin. 5T33MM cells and 5TGM1 cells were incubated with recombinant N-cadherin coated plates at 37°C for 0, 4, 8, 10, 15, 20, 30 and 60 minutes. Wells were washed with PBS to remove non-adhering myeloma cells. Adherent cells were fixed and counted. 20 minutes was an optimal incubation time to incubated myeloma cells with recombinant N-cadherin or with osteoblasts. (n=4).

### 4.4.2 Determination the effect of increasing the concentration of recombinant N-cadherin required for myeloma cell adhesion

5T33MM cells and 5TGM1 cells ($1X10^5$ cells/100 µl) were plated and incubated in plates coated with different concentration of recombinant N-cadherin; 0, 0.1, 0.5, 1, 2, 5 and 10 µg/ml at 37°C for 20 minutes. Figure 4.2 shows the adherence of myeloma cells; 5T33MM and 5TGM1, to different concentrations of recombinant N-cadherin. The data clearly demonstrated an increase in the number of myeloma cells; 5T33MM and 5TGM1 that were adherent to recombinant N-cadherin from 0 µg/ml to 2 µg/ml and this did not change with higher concentrations. 1 µg/ml was chosen as an effective concentration to incubate myeloma cells with recombinant N-cadherin as it was used in published protocol (Groen et al., 2011).

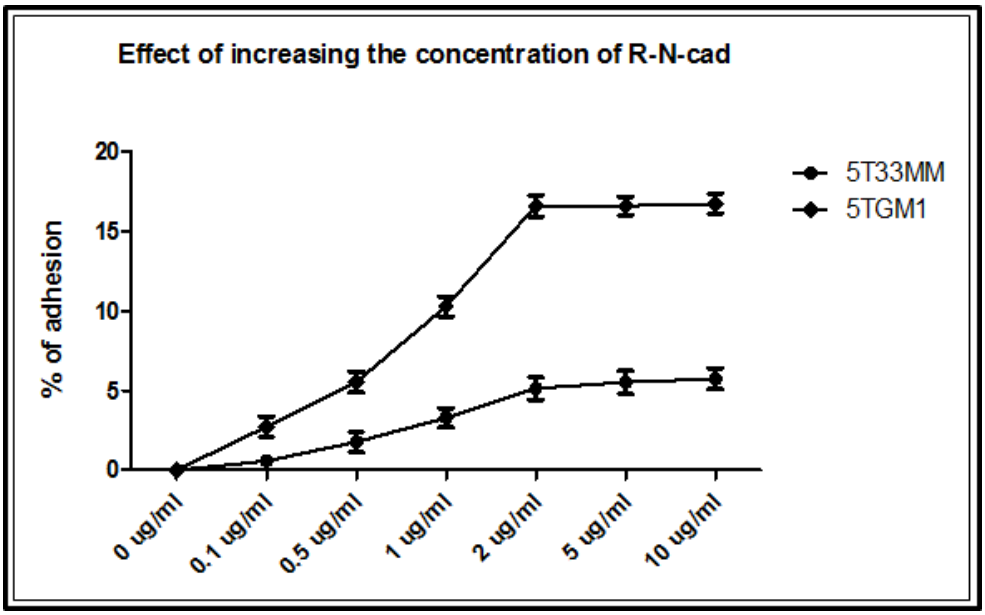


**Figure 4.2: Effect of increasing the concentration of recombinant N-cadherin concentration.** 96-well plates were coated overnight with 0, 0.1, 0.5, 1, 2, 5 and 10 µg/ml of recombinant N-cadherin. 5T33MM cells and 5TGM1 cells were incubated with recombinant N-cadherin at 37°C for 20 minutes. Wells were washed with PBS to remove non-adhering myeloma cells. Adherent cells were fixed and counted. 1 µg/ml concentration was used as a concentration of recombinant N-cadherin. (n=4).

### 4.4.3 Myeloma cells: 5T33MM and 5TGM1 adhere to N-cadherin coated plates *in vitro*

5T33MM cells and 5TGM1 cells ($1X10^5$ cells/100 µl) were plated and incubated with recombinant N-cadherin at 37°C for 20 minutes. Figure 4.3 panel A shows the N-cadherin-positive 5T33MM cells specifically adhered to recombinant N-cadherin compared to PBS-coated plates as a negative control (2.45±0.24 versus 0.23±0.079, $p<0.001$). Figure 4.3 panel B shows the N-cadherin-positive 5TGM1 cells specifically adhered at higher frequency to recombinant N-cadherin compared to PBS-coated plates as a negative control (10.06±0.98 versus 0.42±0.17, $p<0.001$). In addition, data showed that there is some non-specific binding of myeloma cells with PBS-coated plates. However, these non-specific bindings represent less than 1%.

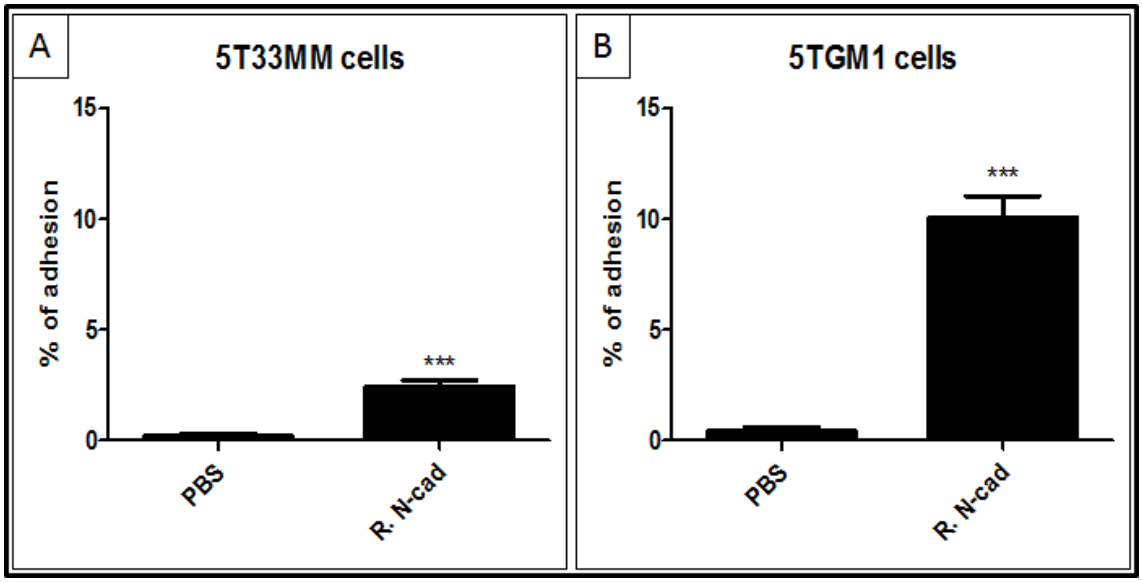


**Figure 4.3: N-cadherin specifically increased the adhesion of myeloma cells: 5T33MM and 5TGM1 *in vitro*.** 96-well plates were coated overnight with recombinant N-cadherin. 5T33MM cells and 5TGM1 cells were incubated in plates with recombinant N-cadherin or PBS as a negative control at 37°C for 20 minutes. Wells were washed with PBS to remove non-adhering myeloma cells. Adherent cells were fixed (4% PFA) and counted using a light microscope. Results demonstrated N-cadherin-positive myeloma cells specifically adhered to recombinant N-cadherin coated plates compared to PBS-coated plates. *** = $p<0.001$. *t* test was used. (n=4).

### 4.4.4 Blocking N-cadherin significantly reduced the adhesion of myeloma cells: 5T33MM and 5TGM1 to recombinant N-cadherin *in vitro*

5T33MM cells or 5TGM1 cells were firstly treated with 10 μg/ml of anti-N-cadherin antibody (Sigma, UK) to block N-cadherin, or with 10 μg/ml of mouse IgG1 antibody (Dako, Denmark) as a negative control. $1X10^5$ cells/100 μl were plated and incubated with recombinant N-cadherin coated plates at 37°C for 20 minutes. Figure 4.4 panel A shows a statistically significant decrease in the adhesion of 5T33MM cells to recombinant N-cadherin when N-cadherin was blocked by anti-N-cadherin antibody compared with isotype control (0.51±0.20 versus 2.50±0.24, $p<0.001$). Figure 4.4 panel B shows a statistically significant decrease in the adhesion of 5TGM1 cells to recombinant N-cadherin when N-cadherin blocked by anti-N-cadherin antibody compared with isotype control (1.76±0.46 versus 10.36±0.75, $p<0.001$).

In addition, figure 4.4 A and B also show that binding in the absence of N-cadherin was not affected by antibody treatment (Column 1 and 2). Myeloma cells, 5T33MM and 5TGM1, were pre-treated with 10 μg/ml of anti-N-cadherin antibody or with 10 μg/ml of mouse IgG1 antibody and then plated onto plates incubated with PBS. The data showed that non-specific binding represent less that 1%. In addition, the data showed that when N-cadherin was blocked in myeloma cells with 10 μg/ml of anti-N-cadherin antibody, GC-4, the adhesion of non-specific binding was not affected compared with myeloma cells treated with 10 μg/ml of mouse IgG1 antibody plated onto plates incubated with PBS.

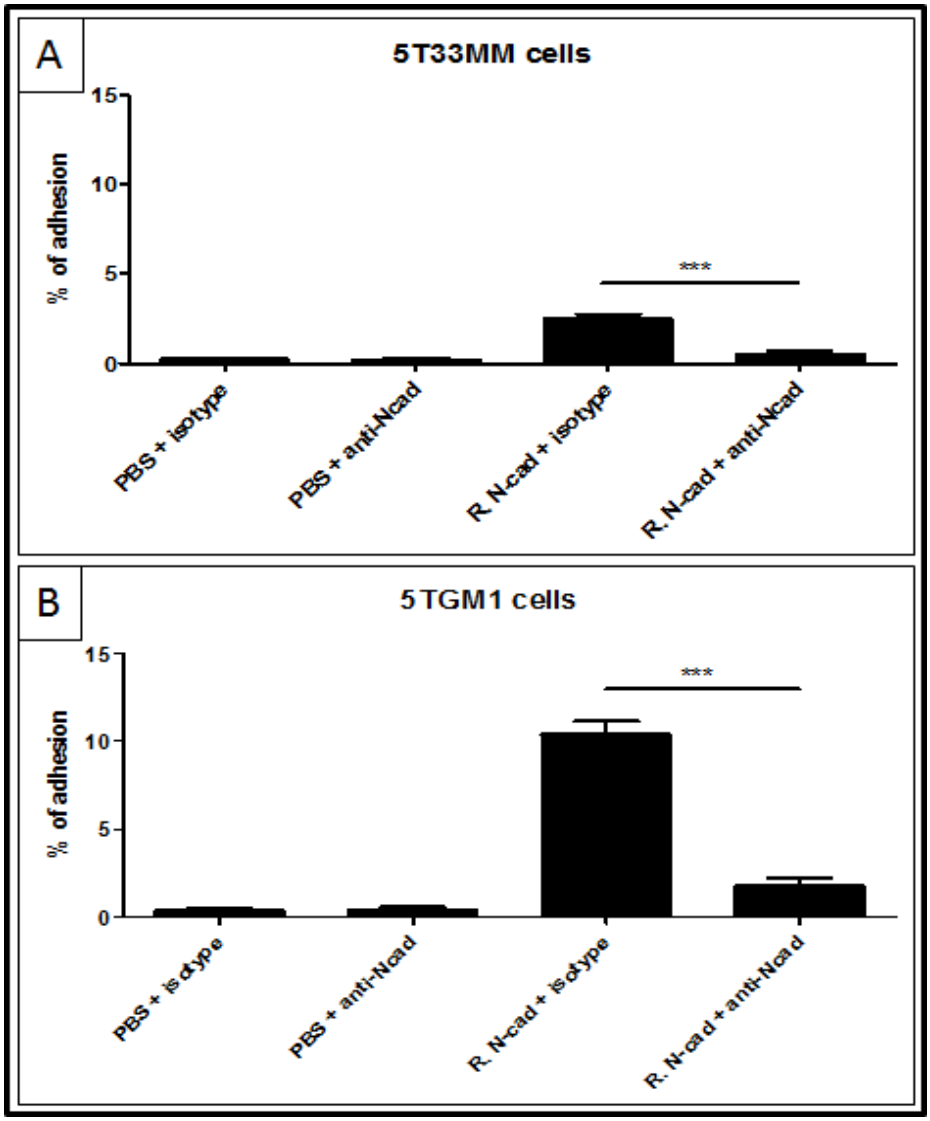


**Figure 4.4: Myeloma cells adherence to recombinant N-cadherin coated plates was blocked using an anti-N-cadherin antibody.** 96-well plates were coated overnight with recombinant N-cadherin or PBS. 5T33MM cells and 5TGM1 cells were pre-treated with 10 µg/ml of anti-N-cadherin antibody or 10 µg/ml of mouse IgG1 antibody as a negative control and incubated with recombinant N-cadherin or PBS as a negative control at 37°C for 20 minutes. Wells were washed with PBS to remove non-adhering myeloma cells. Adherent cells were fixed (4% PFA) and counted using light microscopy. Results demonstrated significant decrease in the adhesion of 5T33MM cells (panel A) and 5TGM1 cells (panel C) when N-cadherin blocked by anti-N-cadherin antibody. PBS coated plates were used as negative control for the adhesion of 5T33MM cells and 5TGM1 cells, in which treated myeloma cells were plated and incubated with PBS coated plates. *** = $p<0.001$. ANOVA was used. (n=4).

### 4.4.5 N-cadherin was present in the attachment of myeloma cells: 5T33MM and 5TGM1 to osteoblasts *in vitro*

#### *4.4.5.1 N-cadherin expression was observed at the junction of adherent myeloma cells and osteoblasts using immunofluorescence in vitro*

$6X10^3$ cells/$cm^2$ of mouse primary osteoblasts were seeded and differentiated for 7 days as the level of N-cadherin expression is low. $5x10^4$ cells/ml of 5T33MM-GFP cells and 5TGM1-GFP cells were plated and incubated with immature osteoblasts (day 7) at 37°C for 20 minutes. The adhesion of myeloma cells with osteoblasts was determined by using immunofluorescence microscopy for GFP and immunostaining for N-cadherin (red). Figure 4.5 panel A shows the co-culture of 5T33MM cells with immature osteoblasts. Figure 4.5 panel B shows that N-cadherin is present in the interaction of adherent 5T33MM cells with osteoblasts. Figure 4.5 panel C shows the co-culture of 5TGM1 cells with immature osteoblasts. Figure 4.5 panel D shows that N-cadherin is present in the interaction of adherent 5TGM1 cells with osteoblasts.

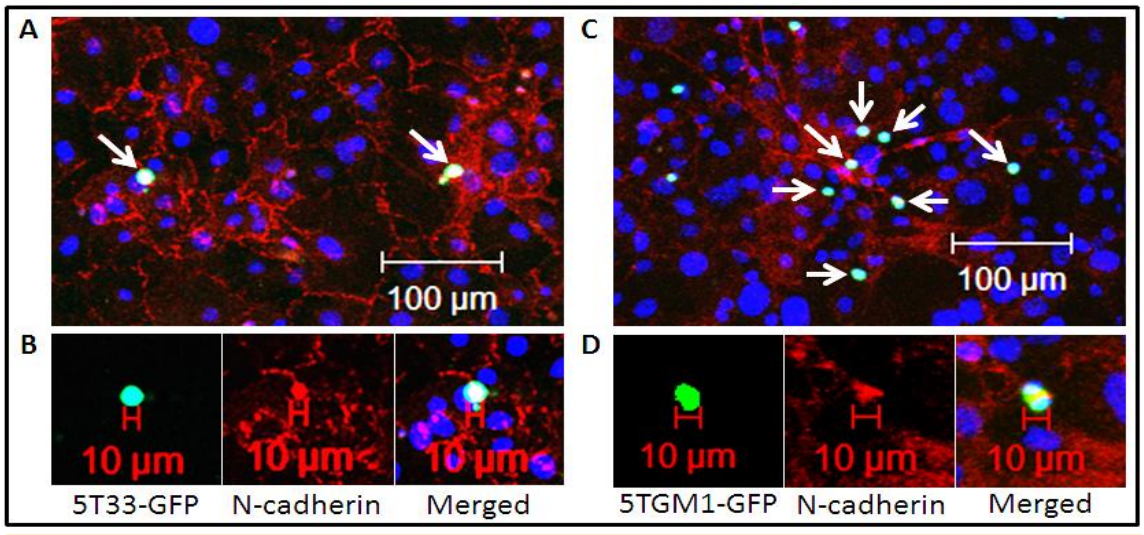


**Figure 4.5: N-cadherin expression was observed at the junction of myeloma cells and osteoblasts.** Mouse primary osteoblasts were seeded and differentiated for 7 days. Myeloma cells were plated and incubated with osteoblasts (day 7) at 37°C for 20 minutes. Panel A and B show co-culture of 5T33MM-GFP cells with osteoblasts. Panel C and D show co-culture of 5TGM1-GFP cells with osteoblasts. (n=4).

### *4.4.5.2 Increased adhesion of myeloma cells, 5T33MM and 5TGM1, was observed with mature osteoblasts compared to pre-osteoblasts*

$6X10^3$ cells/$cm^2$ of mouse primary osteoblasts were seeded and differentiated for 4 weeks in osteogenic media. $1X10^6$ cells/ml of 5T33MM cells and 5TGM1 were plated and incubated separately with pre-osteoblasts (day 7) and mature osteoblasts (day 28) at 37°C for 20 minutes. Figure 4.6 panel A shows that adhesion of 5T33MM cells was significantly increased in co-cultures with mature osteoblasts compared to immature osteoblasts (4.70±0.70 versus 1.35±0.10, $p<0.001$). Figure 4.6 panel C shows that adhesion of 5TGM1 cells was significantly increased in co-culture with mature osteoblasts compared to immature osteoblasts (9.26±1.52 versus 2.95±0.30, $p<0.001$).

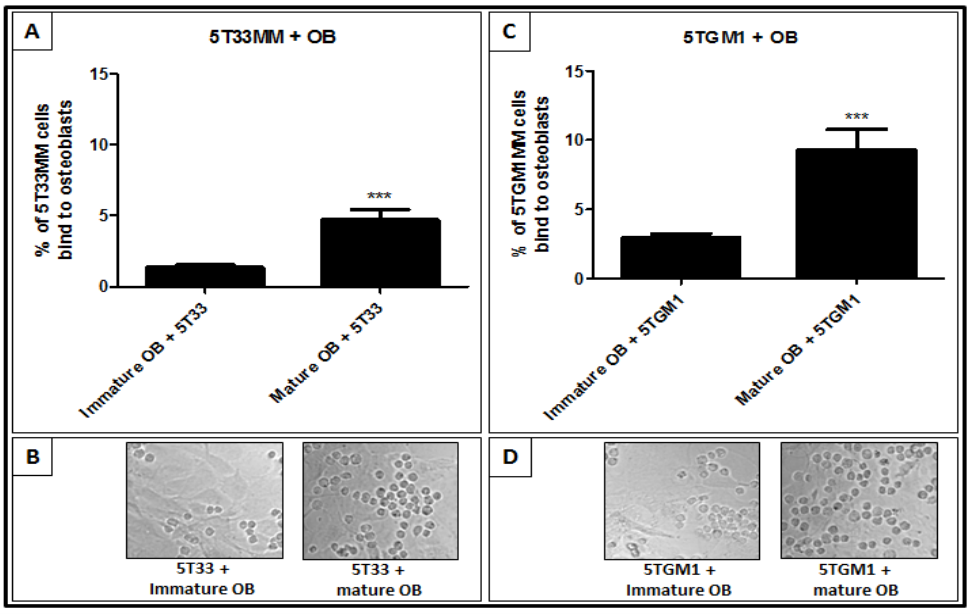


**Figure 4.6: Increased adhesion of myeloma cells with mature osteoblasts compared to immature osteoblasts.** Mouse primary osteoblasts were seeded and. $1X10^6$ cells/ml of myeloma cells were plated and incubated with immature osteoblasts (day 7) and mature osteoblasts (day 28) at 37°C for 20 minutes. Wells were washed with PBS to remove non-adhering myeloma cells. Adherent cells were fixed and counted. Panel A shows significant increase in the adhesion of 5T33MM cells with mature osteoblasts compared with immature osteoblasts. Panel C shows significant increase in the adhesion of 5TGM1 cells with mature osteoblasts compared with immature osteoblasts. Panel B and D show representative images of the co-culture of myeloma cells with osteoblasts. *** = $p<0.001$. *t* test was used. (n=4).

#### *4.4.5.3 Anti-N-cadherin antibody blocked the adhesion of myeloma cells: 5T33MM and 5TGM1 co-cultured with osteoblasts in vitro*

$6X10^3$ cells/$cm^2$ of mouse primary osteoblasts were seeded and differentiated for up to 4 weeks from immature osteoblasts to mature functional osteoblasts in osteogenic media. 5T33MM cells and 5TGM1 cells were pre-treated using 10 μg/ml of anti-N-cadherin antibody (Sigma, UK) to block N-cadherin, or 10 μg/ml of mouse IgG1 antibody (Dako, Denmark) as a negative control. $1X10^6$ cells/100 μl of myeloma cells were plated and incubated with osteoblasts at 37°C for 20 minutes. Figure 4.7 panel A shows that adhesion of 5T33MM cells with immature osteoblasts (day 7) was significantly decreased when cells were treated with anti-N-cadherin antibody compared to untreated cells (0.60±0.09 versus 1.35±0.16, $p<0.001$) and cells treated with isotype control (0.60±0.09 versus 1.38±0.28, $p<0.001$). Figure 4.7 panel C shows a similar significant decrease in the adhesion of 5T33MM cells to mature osteoblasts (day 28) when cells were treated with anti-N-cadherin antibody compared to untreated cells (2.26±0.49 versus 4.70±0.70, $p<0.001$) and cells treated with isotype control (2.26±0.49 versus 4.76±0.60, $p<0.001$). Figure 4.7 panel B and D shows representative images of the co-culture of 5T33MM cells with immature osteoblasts (day 7) and mature osteoblasts (day 28), respectively, with and without treatment.

Figure 4.8 panel A shows that adhesion of 5TGM1 cells to immature osteoblasts (day 7) was significantly decreased when cells were treated with anti-N-cadherin antibody compared to untreated cells (1.17±0.11 versus 2.95±0.30, $p<0.001$) and cells treated with isotype control (1.17±0.11 versus 3.00±0.23, $p<0.001$). Figure 4.8 panel C shows a similar significant decrease in the adhesion of 5TGM1 cells to mature osteoblasts (day 28) when cells treated with anti-N-cadherin antibody compared to untreated cells (4.45±1.01 versus 9.26±1.52, $p<0.001$) and cells treated with isotype control (4.45±1.01 versus 9.62±0.60, $p<0.001$). Figure 4.8 panel B and D shows representative images of the co-culture of 5TGM1 cells with immature osteoblasts (day 7) and mature osteoblasts (day 28), respectively, with and without treatment.

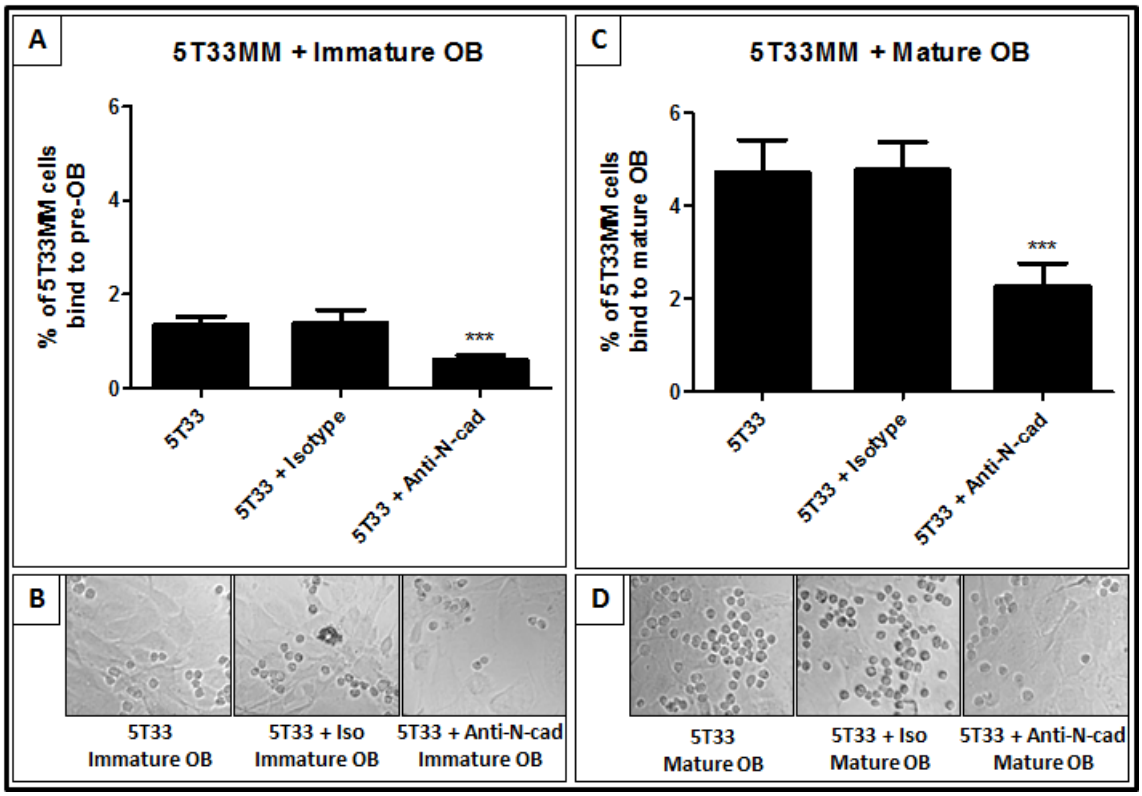


**Figure 4.7: 5T33MM cells adherence to osteoblasts was blocked using an anti-N-cadherin antibody.** 6X10$^3$ cells/cm$^2$ of mouse primary osteoblasts were seeded and differentiated for 4 weeks from immature osteoblasts to mature functional osteoblasts in osteogenic media. 5T33MM cells were pre-treated with 10 µg/ml of anti-N-cadherin antibody or 10 µg/ml of mouse IgG1 antibody as a negative control and incubated with osteoblasts at 37°C for 20 minutes. Wells were washed with PBS to remove non-adhering myeloma cells. Adherent cells were fixed (4% PFA) and counted using light microscope. Results demonstrated significant decrease in the adhesion of 5T33MM cells with immature osteoblasts (panel A) and with mature osteoblasts (panel C) when N-cadherin blocked by anti-N-cadherin antibody. Panel B and D show representative images of the co-culture of 5T33MM cells with immature osteoblasts and mature osteoblasts with and without treatment. *** = $p<0.001$. ANOVA was used. (n=4).

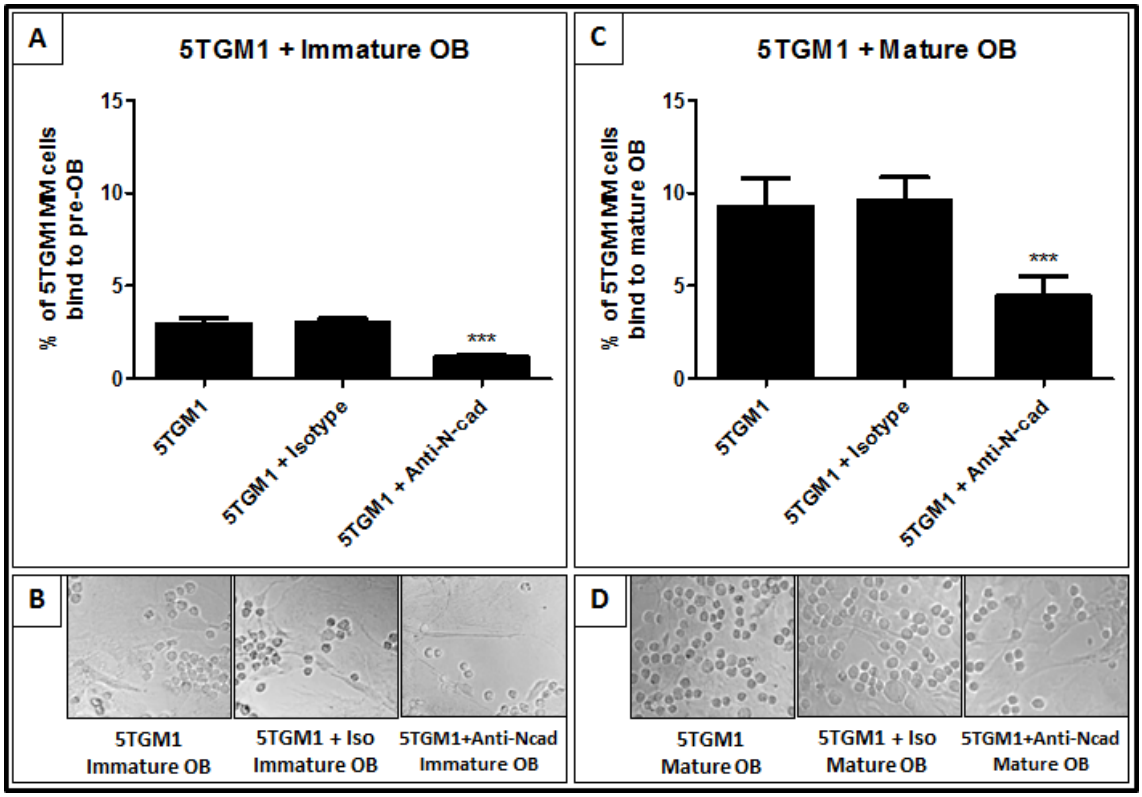


**Figure 4.8: 5TGM1 cells adherence to osteoblasts was blocked using an anti-N-cadherin antibody.** $6X10^3$ cells/$cm^2$ of mouse primary osteoblasts were seeded and differentiated for 4 weeks from immature osteoblasts to mature functional osteoblasts in osteogenic media. 5TGM1 cells were pre-treated with 10 µg/ml of anti-N-cadherin antibody or 10 µg/ml of mouse IgG1 antibody as a negative control and incubated with osteoblasts at 37°C for 20 minutes. Wells were washed with PBS to remove non-adhering myeloma cells. Adherent cells were fixed (4% PFA) and counted using light microscope. Results demonstrated significant decrease in the adhesion of 5TGM1 cells with immature osteoblasts (panel A) and with mature osteoblasts (panel C) when N-cadherin blocked by anti-N-cadherin antibody. Panel B and D show representative images of the co-culture of 5TGM1 cells with immature osteoblasts and mature osteoblasts with and without treatment. *** = $p<0.001$. ANOVA was used. (n=4).

## 4.5 Discussion

In this chapter I developed and optimized a co-culture system to study the interactions of MM cells with the osteoblasts via adhesion molecule, N-cadherin, *in vitro*. 5T33MM cells and 5TGM1 cells were cultured separately *in vitro* as described in methods. Mouse primary osteoblasts were obtained from calvarial bones of 2-4 day old C57Bl/6J mice, (Harlan, UK) and cultured *in vitro* as described in methods. Osteoblasts were differentiated into mature functional osteoblasts using an *in vitro* model of osteoblastogenesis, discussed in **chapter 3**. In co-cultures, myeloma cells were re-suspended in 1 ml of RPMI media and seeded onto osteoblasts cultured in 24 well plates with each well containing 1 ml of α-MEM media.

Increasing evidence indicates that the expression of N-cadherin in solid tumour cells mediates the invasion, metastasis and interaction of cancer cells from their primary site to establish new interactions with the surrounding microenvironment (Li et al., 2001, Lascombe et al., 2006, Gravdal et al., 2007). Shintani et al (2008) demonstrated that using a cyclic pentapeptide (ADH-1, N-Ac-CHAVC-NH2), targeting the HAV motif on EC1 of N-cadherin, significantly reduced growth and metastasis of pancreatic cancer cells in transgenic mice (Shintani et al., 2008). In addition, Beasley et al (2009) demonstrated that ADH-1 at a dose of 4000 mg in combination with melphalan on days 1 and 8 was safe and well tolerated by patients in phase I studies and provided a novel targeted therapy approach in melanoma (Beasley et al., 2009). More recently, Tanaka et al (2010) demonstrated that prostate cancer metastasis and castration resistance are mainly caused by N-cadherin. Targeting N-cadherin using a monoclonal antibody against N-cadherin showed a reduction in proliferation, adhesion and invasion of prostate cancer cells *in vitro* and *in vivo* (Tanaka et al., 2010). Critically, no study has addressed blocking N-cadherin in myeloma.

Groen et al (2011) demonstrated that N-cadherin was expressed by myeloma cell lines, UM-1, OPM-1, NCI-H929 and LME-1, and primary myeloma cells. These cells specifically adhere to recombinant N-cadherin and this binding was showed to be specifically prevented by using an anti-N-cadherin antibody, GC-4 (10 μg/mL) (Groen et al., 2011). In this published protocol, myeloma cells were plated and incubated for 20 minutes with recombinant N-cadherin (1 μg/ml). However, the authors did not show the optimal incubation period of myeloma cells with the recombinant N-cadherin. In addition, the authors did not show the optimal concentration required by the recombinant N-cadherin for the adhesion. In my study, Recombinant N-cadherin/Fc chimera (R&D Systems) was used to determine the optimal incubation period and recombinant N-cadherin concentration required for myeloma cells binding. I observed 20 minutes to be the optimal incubation period of myeloma cells with recombinant N-cadherin or osteoblasts, with some loss of adherence after this. The reason for the latter are unclear but it may be that N-cadherin was lost from plastic surfaces with prolonged incubation, this needs to be evaluated. However, 20 minutes gave consistent, elevated rates of attachment and was a sufficient time frame for simple association to occur such as those provided by N-cadherin and was in line with other studies. In addition, I observed 2 μg/ml of recombinant N-cadherin is an effective concentration for adhesion assays. However, 1 μg/ml of recombinant N-cadherin was used in this study consistent with that used in published protocol (Groen et al., 2011). I also thought that higher levels of N-cadherin could be more difficult to block with antibodies in later experiments.

In the adhesion assay experiments, I observed significant specific adhesion of myeloma cells to recombinant N-cadherin coated plates compared with PBS coated plates. Blocking N-cadherin with 10 μg/ml of anti-N-cadherin antibody showed significant decrease in the adhesion of myeloma cells with the recombinant N-cadherin. This observation is supported with the more recent work done by Groen et al (2011) who demonstrated that adhesion of myeloma cells was prevented by using an anti-N-cadherin antibody, GC-4 (10 μg/mL) and suggests that N-cadherin is a specific

component of myeloma cell adhesion (Groen et al., 2011). In my adhesion assays some limitations were found. We showed non-specific binding of myeloma cells with PBS coated plates. However, this non-specific binding of myeloma cells with PBS coated plates represent approximately less that 1%. Additional controls were used to determine if this non-specific binding could be affected by anti-N-cadherin antibody. Myeloma cells, 5T33MM and 5TGM1, were pre-treated with 10 μg/ml of anti-N-cadherin antibody, GC-4, or with 10 μg/ml of mouse IgG1 antibody and plated onto plates incubated with PBS. The data showed that when N-cadherin was blocked in myeloma cells with 10 μg/ml of anti-N-cadherin antibody, GC-4, myeloma cells still bound to PBS coated plates and this binding was not prevented or decreased. These findings suggest that the non-specific binding was not affected by anti-N-cadherin antibody compared to mouse IgG1 antibody. In conclusion, since it was found that anti-N-cadherin antibody, GC-4, only decreased the adhesion of myeloma cells to recombinant N-cadherin compared with PBS, this showed the specificity of the antibody used to block N-cadherin in these assays.

I found that when N-cadherin was blocked in myeloma cells by 10 μg/ml of anti-N-cadherin antibody, GC-4, the adhesion of myeloma cells was significantly decreased but not completely prevented. This could be due to the fact that the concentration of antibody used to block N-cadherin in myeloma cells was not enough to block N-cadherin 100%. Groen et al (2011) demonstrated that 10 μg/ml of anti-N-cadherin antibody, GC-4, completely prevented the adhesion of myeloma cells, UM-1, OPM-1, NCI-H929, LME-1 and primary myeloma cells, with the recombinant N-cadherin (Groen et al., 2011). In contrast, Ciolczyk-Wierzbicka et al (2004) blocked N-cadherin in human melanoma cell lines using anti-N-cadherin antibody, GC-4, (40 μg/ml), a treatment which inhibited the migration of melanoma cells by about 40% *in vitro* (Ciolczyk-Wierzbicka et al., 2004). In addition, Wein et al (2010) blocked N-cadherin in human HSCs using anti-N-cadherin antibody, GC-4, (50 μg/ml), which significantly reduced the adhesion of HSCs to MSCs (Wein et al., 2010). It would be useful to know the concentration needed to completely block N-cadherin in cellular attachment and as

in the studies with recombinant N-cadherin. In future work different concentrations of anti-N-cadherin antibodies will need to be tested for the ability to block N-cadherin in myeloma cells to determine the effective antibody concentrations. It has been shown that myeloma cells use another molecule to bind to N-cadherin, as it was found that N-cadherin can bind to FGFR (Williams et al., 2001, Suyama et al., 2002, Sanchez-Heras et al., 2006). Future work might consider blocking both N-cadherin and FGFR in myeloma cells to completely prevent the adhesion of myeloma cells with recombinant N-cadherin. Earlier studies by Shintani et al (2008) demonstrated that using the cyclic ADH-1 pentapeptide, N-cadherin antagonist, significantly reduced growth and metastasis of pancreatic cancer cells in transgenic mice (Shintani et al., 2008). In addition, ADH-1 might be considered to effectively block N-cadherin in myeloma cells to completely prevent the adhesion of myeloma cells with recombinant N-cadherin.

A previous study by Groen et al (2011) demonstrated that myeloma cells adhere to osteoblasts, and this adhesion is prevented by using an N-cadherin blocking antibody, GC-4 (10 μg/mL) (Groen et al., 2011). However, the previous study did not investigate differences between adhesion of myeloma cells to immature osteoblasts compared to mature osteoblasts. My data showed that N-cadherin was expressed at the junction of myeloma cells with osteoblasts suggesting a direct interaction of myeloma cells with osteoblasts via N-cadherin. This was the first time this has been visualized as part of the attachment of myeloma cells to osteoblasts using immunocytochemistry and again suggests that N-cadherin is specifically involved in these interactions. When myeloma cells were co-cultured with immature osteoblasts (day 7), the level of N-cadherin expression was significantly lower than in mature osteoblasts, and this therefore allowed very specific associations between cells to be demonstrated with attachment shown only between adjacent osteoblasts when N-cadherin could be shown to be present.

My study also demonstrated that there was a significant increase in the adhesion of myeloma cells with mature osteoblasts compared to immature osteoblasts and this is due to the fact that the expression of N-cadherin is significantly increased in mature osteoblasts compared to immature osteoblasts as described in **chapter 3**. Blocking N-cadherin with 10 μg/ml of anti-N-cadherin antibody showed a significant decrease in the adhesion of myeloma cells to osteoblasts. These data suggest that colonising N-cadherin$^{+}$ myeloma cell can bind to both immature and mature osteoblasts and either may be involved in the formation of the myeloma niche *in vivo*. Colonising N-cadherin$^{+}$ myeloma cell could be more likely to attach to mature osteoblasts *in vivo* due to the higher N-cadherin expression in the these cells. However, the ubiquitous distribution of N-cadherin in the latter may not supply the specific positioning allowed by that provided by the junctions between immature osteoblasts, which association represent "niches" remains to be determined. When N-cadherin was blocked in myeloma cells by 10 μg/ml of anti-N-cadherin antibody, GC-4, the adhesion of myeloma cells with osteoblasts was significantly decreased but not completely prevented. This could be because the concentration of antibody used to block N-cadherin in myeloma cells was not enough to block N-cadherin 100%. Alternatively, interaction of N-cadherin with FGFR or the presence of other molecules could be contributing to these interaction (Williams et al., 2001, Suyama et al., 2002, Sanchez-Heras et al., 2006).

In summary, I can conclude that N-cadherin is at least part of the process of adherence of myeloma cells to osteoblasts. My observations may support a role for mature osteoblasts being likely niche components for myeloma cells since they express high levels of N-cadherin and bind more myeloma cells significantly *in vitro*. This may mean that the interactions of myeloma cells with mature functional osteoblasts are more likely *in vivo* and these will be investigated in the next chapter by determining different bone microenvironments in calvarial bones.

# 5 Chapter 5: Different calvarial bones; frontal, parietal and interparietal contain different bone microenvironments

## 5.1 Introduction

To support our understanding of MM bone disease, preclinical mouse models have been developed. C57BL/KaLwRijHsd mice develop a high frequency of monoclonal proliferative B-cell disorders. Cells within BM provide a microenvironment for myeloma cells survival and potentially for the development of drug resistance. Murine models of multiple myeloma have been developed over the last four decades. The 5TMM series of myeloma models originate from spontaneously developed MM in C57BL/KaLwRijHsd mice and have many of the human features of the disease (Radl et al., 1978, Radl et al., 1979, Vanderkerken et al., 1997). Several murine models of MM exist, but 5T2, 5T33 and 5TGM1 are the best characterized and used in most recent studies (Vanderkerken et al., 2000, Croucher et al., 2003, Alici et al., 2004, Van Valckenborgh et al., 2012, Olson et al., 2005, Edwards et al., 2009, Fowler et al., 2012). Oyajobi et al (2007) demonstrated the murine myeloma 5TGM1-GFP tumour was detectable in calvariae between 10-14 days post intravenous inoculation into animals suggesting that these cells home to calvarial BM (Oyajobi et al., 2007). However, this study lacked the imaging capability to study the arrival of single cells in calvarial BM. There are no publications that demonstrate the murine myeloma 5T33MM model can home to calvarial BM in C57BL/KaLwRijHsd mice.

The 5T2MM model originated from spontaneously developed myeloma in aging mice and represents a model of human MM disease with inducing osteolytic bone lesions (Radl et al., 1985, Vanderkerken et al., 1997, Asosingh et al., 2000b, Croucher et al., 2003). The 5T33MM model also originated from a spontaneously developed myeloma in aging mice and represents a model of human MM disease, but without inducing osteolytic bone lesions (Manning et al., 1992, Vanderkerken et al., 1997, Asosingh et al., 2000b). The 5TGM1 model was derived from the 5T33 model, in which 5T33MM cells were passaged in mice and the cells were then obtained from the marrow of 5T33MM-bearing mice, cultured and cloned. The 5TGM1 model represents a model of human MM disease that induces osteolytic bone lesions (Garrett et al., 1997, Dallas et

al., 1999). The 5T33MM and 5TGM1 models can grow *in vitro* as well as *in vivo* whereas the 5T2MM model only grows slowly *in vivo* and not *in vitro* (Radl et al., 1985, Vanderkerken et al., 1997, Garrett et al., 1997, Dallas et al., 1999). In this study, the 5T33MM model and 5TGM1 model have been used. The 5T2MM model was not used because I did not have an access to this model, which is restricted. Together the 5T33MM and 5TGM1 models offer advantages to address MM-bone interactions. The 5T33MM cell line is not osteolytic in character whereas the 5TGM1 is. Both use the same genetic background. Both grow in syngeneic immuno-completed hosts *in vivo*. Havening an intact immune system allows the induction of all potential interacting cell types in bone. This is not offered by xenograft models.

It was shown that in calvarial mice, MSCs differentiate into osteoprogenitor cells then differentiate into osteoblasts that differentiate into osteocytes, which become embedded within the bone matrix. In this case cells participating in bone formation include: MSCs, osteoprogenitor cells, osteoblasts and osteocytes. In contrast, in long bones, MSCs differentiate into chondrocytes forming the cartilage anlagen. Cells from the perichondrium of cartilage anlagen differentiate into osteoblasts, and the periphery of the cartilage anlage becomes hypertrophic. Matrix surrounding these hypertrophic chondrocytes calcifies and longitudinal growth is stimulated as cartilaginous matrix. In this case cells participating in bone formation include: MSCs, perichondrium, chondrocytes, periosteum, hypertrophic chondrocytes, osteoclasts osteoblasts and osteocytes (Nakashima and de Crombrugghe, 2003). As we are interested in osteoblasts, we expected to see more osteoblasts compared to other cells in the calvariae. In this chapter I focused on the calvarial bones of C57BL/KaLwRijHsd mice. C57BL/KaLwRijHsd mice were purchased from Harlan, Netherlands and housed by University of Sheffield Biological Services Laboratory. The calvariae of C57BL/KaLwRijHsd mice are composed of five bones: two frontal bones, two parietal bones and one interparietal bone (Figure 5.1). In preliminary studies I determined the distribution of osteoclasts, osteoblasts and bone lining cells in each part of calvariae: frontal, parietal and interparietal to determine if different calvarial bones contain

different bone microenvironments. Then, I used the 5T33MM and 5TGM1 models, where these cells were inoculated into C57BL/KaLwRijHsd mice via their tail veins. The aim of this chapter was to determine if different calvarial bones contain different bone microenvironments and to study single cell arrival in calvarial BM.

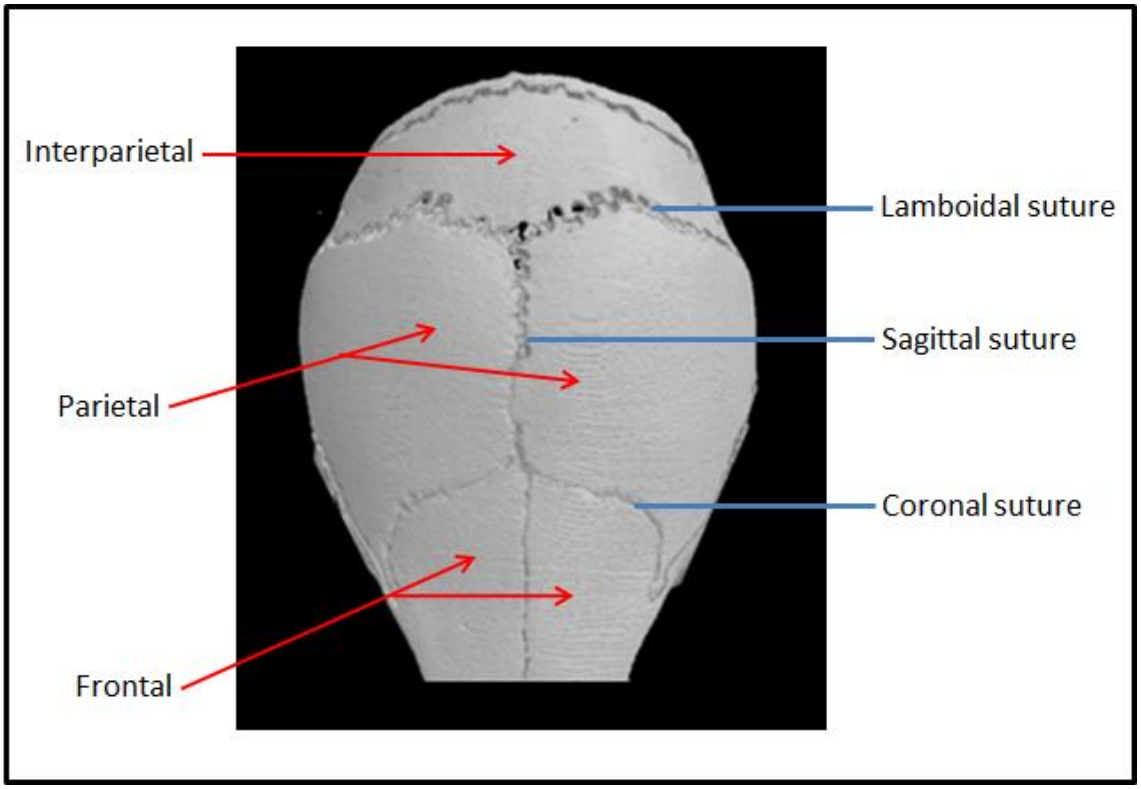


**Figure 5.1: A microCT three-dimensional reconstruction of C57BL/KaLwRijHsd mice calvarial bone.** microCT model of a murine skull showing calvariae are composed of two frontal bones, two parietal bones and one interparietal bone (red arrows). Frontal and parietal bones are separated longitudinally by sagittal suture. Coronal suture separates frontal bones from parietal bones. Lamboidal suture separates parietal bones from interparietal bone.

## 5.2 Hypothesis and objectives of this chapter

### 5.2.1 Hypothesis

Different calvarial bones; frontal, parietal and interparietal contain different bone microenvironments for the support of myeloma survival and growth.

### 5.2.2 Objectives

To test this hypothesis I have:

1. Determined the bone surface area and BM area in C57BL/KaLwRijHsd calvariae.
2. Determined the distribution of osteoclasts in C57BL/KaLwRijHsd calvariae.
3. Determined the distribution of osteoblasts in C57BL/KaLwRijHsd calvariae.
4. Determined the distribution of bone lining cells in C57BL/KaLwRijHsd calvariae.
5. Determined the new bone formation in C57BL/KaLwRijHsd calvariae.
6. Determined the growth of tumours in C57BL/KaLwRijHsd calvarial BM using 5T33MM and 5TGM1 models.
7. Determined the single myeloma cell number in C57BL/KaLwRijHsd calvarial BM using 5T33MM and 5TGM1 models.

## 5.3 Materials and Methods

### 5.3.1 Study to determine the distribution of osteoclasts, osteoblasts and quiescent bone in C57BL/KaLwRijHsd calvariae

C57BL/KaLwRijHsd calvariae were excised carefully from 5 male mice, 6 weeks of age and stored in formalin. Frontal, parietal, and interparietal bones were dissected to determine the bone microenvironment in calvariae as described in section 2.2.17. TRAP staining was used to determine the distribution of osteoclasts as described in section 2.2.13.1. Haematoxylin and eosin staining was used to determine the frequency of osteoblasts and bone lining cells as described in section 2.2.13.2. Osteomeasure software version 4.10 (Osteomerics Incorporated, Atlanta, USA) was used to analyse the sections.

### 5.3.2 Study to determine the distribution of new bone formation in C57BL/KaLwRijHsd calvariae

4 male C57BL/KaLwRijHsd mice, 6 weeks of age, were injected with 200µl of calcein-GFP (3 mg/ml in PBS) each at day 0. After 3 days, mice were sacrificed and calvariae were excised to determine the new bone formation in different part of calvariae bones: frontal, parietal and interparietal as described in section 2.2.18. Zeiss 510 multiphoton laser scanning microscope was used to analyse the new bone formation.

### 5.3.3 Study to determine if myeloma tumour can grow in C57BL/KaLwRijHsd calvarial BM

9 male C57BL/KaLwRijHsd mice, 6 weeks of age, were used in this experiment and separated to 3 groups to determine the myeloma tumour growth in calvarial BM as described in section 2.2.19. Lightools system used to obtain optical images of fluorescent tumour growth in calvarial BM.

### 5.3.4 Study to determine the single cell numbers arriving in C57BL/KaLwRijHsd calvarial BM

12 male C57BL/KaLwRijHsd mice, 6 weeks of age, were used in this experiment and separated into 4 groups to determine the single cell numbers in calvarial BM in the early and late stage of disease as described in section 2.2.20. Zeiss 510 multiphoton laser scanning microscope was used to determine the cell numbers in C57BL/KalwRij calvarial BM.

### 5.3.5 Cell labelling with DiD

5T33MM cells and 5TGM1 cells were labelled with DiD (Invitrogen, UK) to easily identified myeloma cells under fluorescent microscopy as described in section 2.2.11.

### 5.3.6 Inoculation of MM cells into C57BL/KaLwRijHsd mice

Myeloma cells for injection were re-suspended in PBS ($2x10^6$ cells/200 µl). C57BL/KaLwRijHsd mice were handled and their tails were anesthetized using EMLA$^{TM}$ cream 5% (AstraZeneca, UK) and myeloma cells were inoculated into mouse via their tail veins as described in section 2.2.12.

### 5.3.7 Microscopic examination

Osteomeasure software version 4.10 (Osteomerics Incorporated, Atlanta, USA) was used with a Leitz DMRB microscope and a drawing tablet, (CalComp Drawing Broad III) to determine the distribution of osteoclasts, osteoblasts and bone lining as described in section 2.2.14.2. A Zeiss 510 Multiphoton Laser Scanning Microscopy was used to visualise fluorescence as described in section 2.2.14.1.

### 5.3.8 Using the Lightools image analysis system to detect the tumour in C57BL/KaLwRijHsd mice

All calvariae were analysed using Fluorescence Cheda Lightools Illumatools System (LT-9900 Bright Light System) in the University of Sheffield biological services laboratory to determine the tumour growth in calvariae as described in section 2.2.15.

### 5.3.9 Statistical analysis

The data were analysed using an ANOVA test (one-way analysis of variance) for more than two group comparisons or with *t* test for two group comparisons if the data was normally distributed. Tukey's test was used as post-hoc analysis when ANOVA test was used in normal distribution data. When data not normally distributed, ANOVA test (non-parametric Kruskal-Wallis test) was used for more than two group comparisons or non-parametric Mann–Whitney test was used for two group comparisons. Dunns test was used as post-hoc analysis when ANOVA test was used in not normally distributed data. Data were considered statistically significant when a p-value was equal to or less than 0.05. Results are expressed as mean ± values of standard deviation (SD).

## 5.4 Results

### 5.4.1 Determination of the bone surface area and BM area in C57BL/KaLwRijHsd calvariae

The bone surface area and BM area in C57BL/KaLwRijHsd calvariae was determined (Figure 5.2). Histological analysis demonstrated statistically significant increases in the bone surface area in interparietal bones compared to frontal bones (1.3±0.17 versus 0.76±0.15, $p<0.001$) and parietal bones (1.3±0.17 versus 0.55±0.10, $p<0.001$) (Figure 5.3 A). Furthermore, data demonstrated statistically significant increases in the BM area in interparietal bones compared to frontal bones (2.55±0.48 versus 0.41±0.05, $p<0.001$) and parietal bones (2.55±0.48 versus 0.21±0.02, $p<0.001$) (Figure 5.3 B). The ratio of the volume of BM to the bone surface area was significant increases in the interparietal bones compared to frontal bones (1.85±0.31 versus 0.60±0.25, $p<0.001$) and parietal bones (1.85±0.31 versus 0.42±0.05, $p<0.001$) (Figure 5.3 C).

### 5.4.2 Determination of the percentage of osteoclast surfaces in C57BL/KaLwRijHsd calvariae

Cortical bone was identified as an outside solid bone with a regular structure whereas trabecular bone identified as a bone inside the BM with an irregular structure (see figure 5.2 B). Endo-cortical bone surface is a surface of the cortical bone inside the BM. The distribution of osteoclasts was determined on endo-cortical and trabecular surfaces in interparietal bones and on endo-cortical surfaces in frontal and parietal bones. No trabeculae were observed in frontal and parietal bones. Histological analysis demonstrated that there was no statistically significant difference in the percentage of bone surface covered by osteoclasts in the interparietal bones compared to frontal bones (15.61±6.42 versus 18.84±7.88, $p>0.05$) and parietal bones (15.61±6.42 versus 12.80±3.04, $p>0.05$) (Figure 5.4 A). Analysis did show there was a significant increase in the frequency of osteoclasts in the lower endo-cortical surfaces compared to the upper endo-cortical surfaces in frontal bones (32.77±14.19 versus 4.90±2.69, $p<0.05$)

(Figure 5.5 A) and in parietal bones (22.11±6.71 versus 3.94±1.73, $p<0.05$) (Figure 5.5 B). In interparietal bones there was a similar trend, but this was not significant, (19.19±10.97 versus 8.63±6.04, $p=0.07$) (Figure 5.5 C).

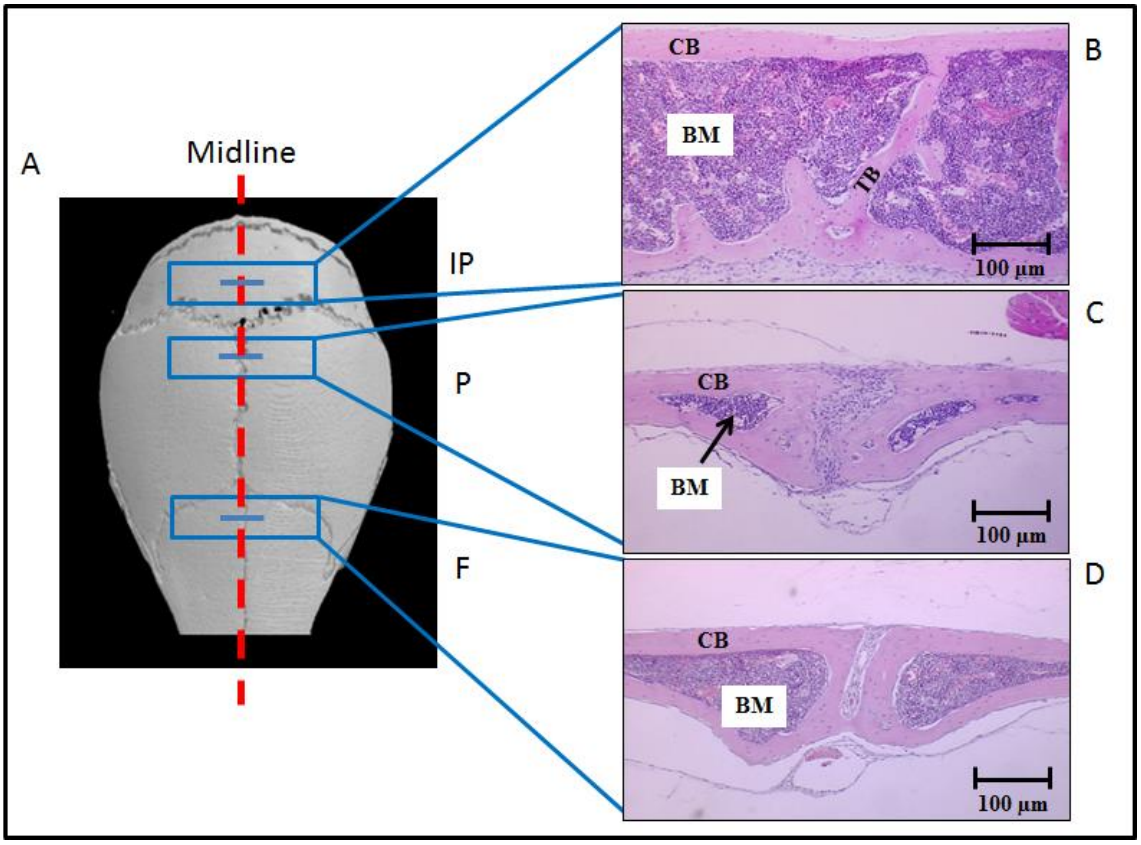


**Figure 5.2: Sectioning of calvarial bones across their regions of interest.** Panel A is microCT model of a murine skull showing calvariae are composed of frontal (F), parietal (P) and interparietal (IP) bones, respectively. Panels B, C and D show cross-sections of frontal, parietal and interparietal bones, respectively. BM is bone marrow, CB is cortical bone and TB is trabecular bone. (n=5).

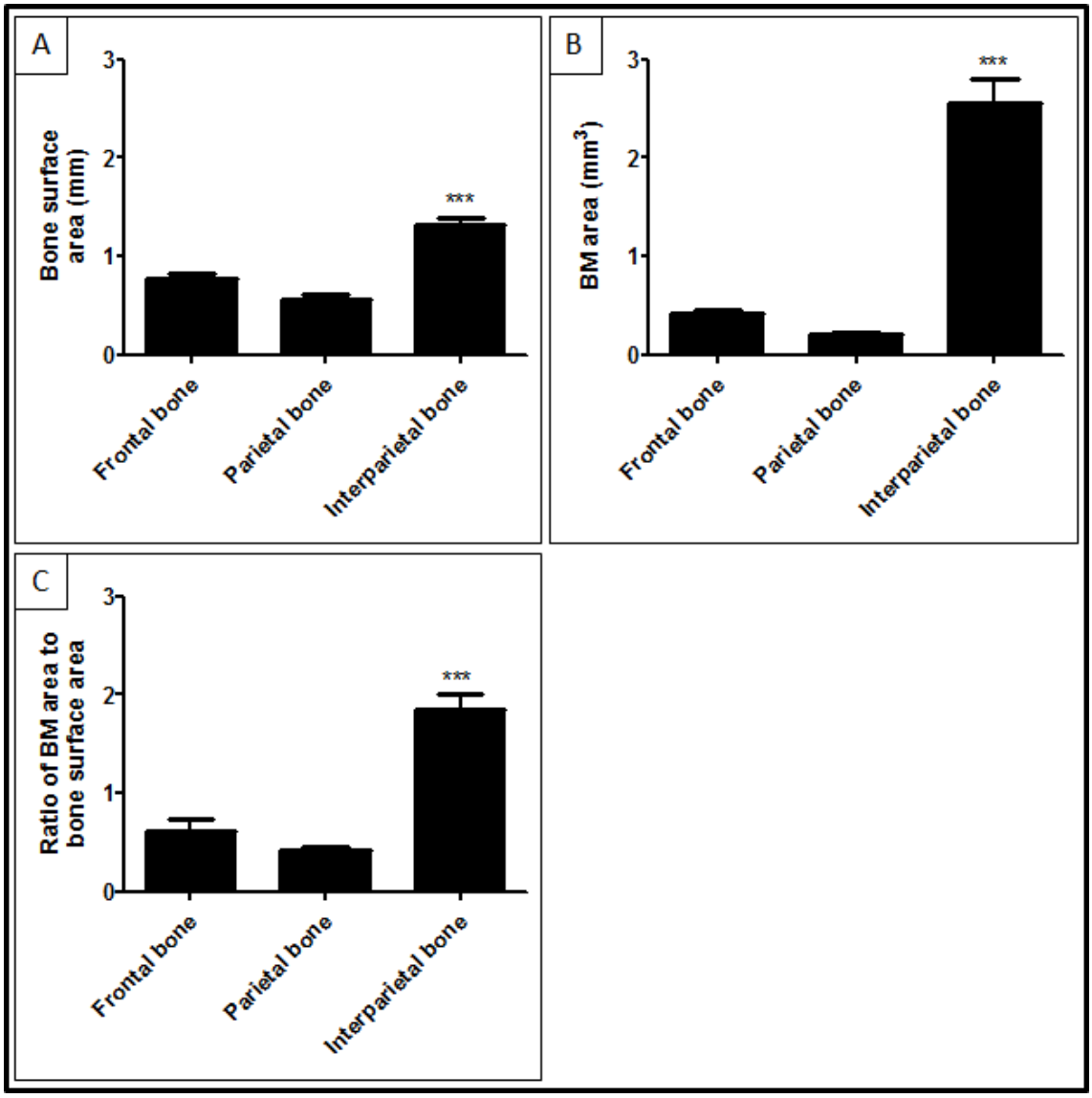


**Figure 5.3: There was an increase in the bone surface area and BM areas in the interparietal bones compared to frontal and parietal bones in male C57BL/KalwRiJHsD mice.** There was a significant increase in the bone surface in interparietal bones compared to frontal and parietal bones (A), in the volume of BM in interparietal bones compared to frontal and parietal bones (B) and in ration of the volume of BM to the bone surface (C). *** = $p<0.001$. ANOVA test was used. (n=5).

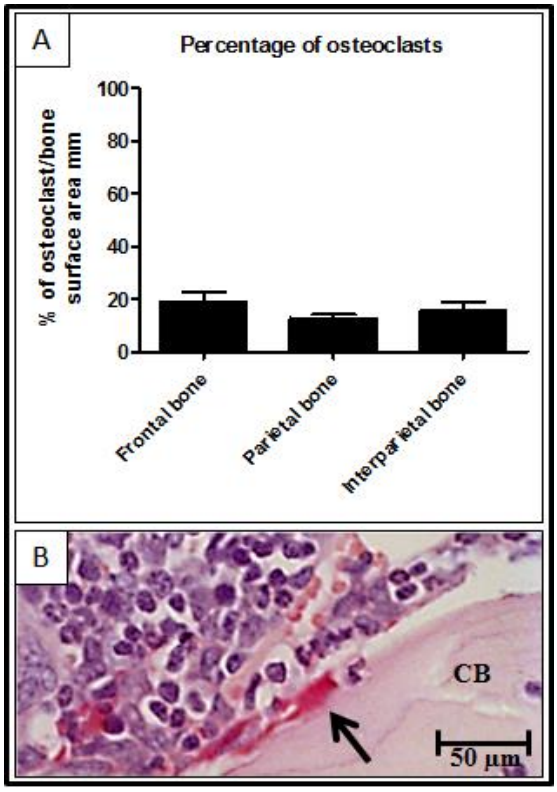


**Figure 5.4: There was no difference the percentage of osteoclast surfaces between the different parts of calvariae in male C57BL/KalwRiJHsD mice.** Frontal, parietal and interparietal sections of calvariae were stained with TRAP. Panel A shows there was no statistically significant difference in the distribution of osteoclasts in the different part of calvariae. Panels B shows a representative photomicrographic image of osteoclasts (black arrow). ANOVA test was used. (n=5).

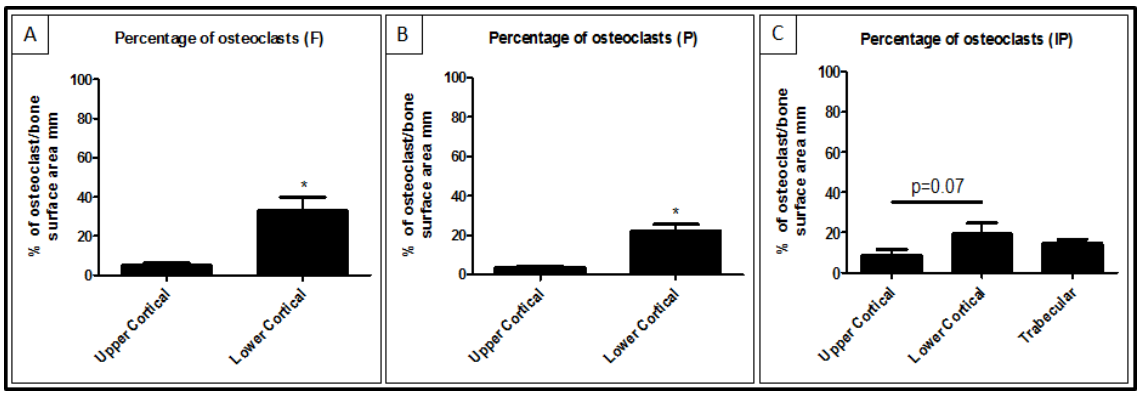


**Figure 5.5: There was an increase in the percentage of osteoclast covered surfaces in the lower endo-cortical surfaces compared to the upper endo-cortical surfaces in male C57BL/KalwRiJHsD mice.** There was a significant increase in the distribution of osteoclasts in the lower endo-cortical surfaces compared to the upper endo-cortical surfaces in frontal bones (A) and parietal (B), but not in interparietal (C). In the interparietal bones (C) there was no significant difference in the distribution of osteoblasts between trabecular surfaces and endo-cortical surfaces. * = $p<0.05$. ANOVA and Mann Whitney tests were used. (n=5).

### 5.4.3 Determination of the percentage of osteoblast surfaces in C57BL/KaLwRijHsd calvariae

The distribution of osteoblasts was determined on endo-cortical and trabecular surfaces in interparietal bones and on endo-cortical surfaces in frontal and parietal bones. Histological analysis demonstrated statistically significant increases in the distribution of osteoblasts in interparietal bones compared to frontal bones (55.05±5.47 versus 32.20±6.84, $P<0.01$) and parietal bones (55.05±5.47 versus 33.85±7.22, $P<0.01$) (Figure 5.6 A). Data showed there is no statistically significant difference in the distribution of osteoblasts between frontal and parietal bones (32.20±6.84 versus 33.85±7.22). Furthermore, data showed there was significant increase in the distribution of osteoblasts in the upper endo-cortical surfaces compared to the lower endo-cortical surfaces in parietal bones (40.29±6.45 versus 27.41±8.15, $p<0.05$) (Figure 5.7 A) but not in frontal bones (Figure 5.7 B) and interparietal bones (Figure 5.7 C).

### 5.4.4 Determination of the percentage of bone lining cell surfaces in C57BL/KaLwRijHsd calvariae

The distribution of bone lining cells was determined on endo-cortical and trabecular surfaces in interparietal bones and on endo-cortical surfaces in frontal and parietal bones. Histological analysis demonstrated statistically significant decreases in the distribution of bone lining cells in interparietal bones compared to frontal bones (30.65±10.72 versus 49.17±5.74, $P<0.05$) and parietal bones (30.65±10.72 versus 51.51±8.98, $P<0.05$) (Figure 5.14 A). Data showed there is no statistically significant deference in distribution of bone lining cells between frontal and parietal bones (Figure 5.8 A). Furthermore, data showed there was no statistically significant difference in the distribution of bone lining cells in the lower endo-cortical surfaces compared to the upper endo-cortical surfaces in frontals bones (Figure 5.9 A), in parietal bones (Figure 5.9 B) and interparietal bones (Figure 5.9 C).

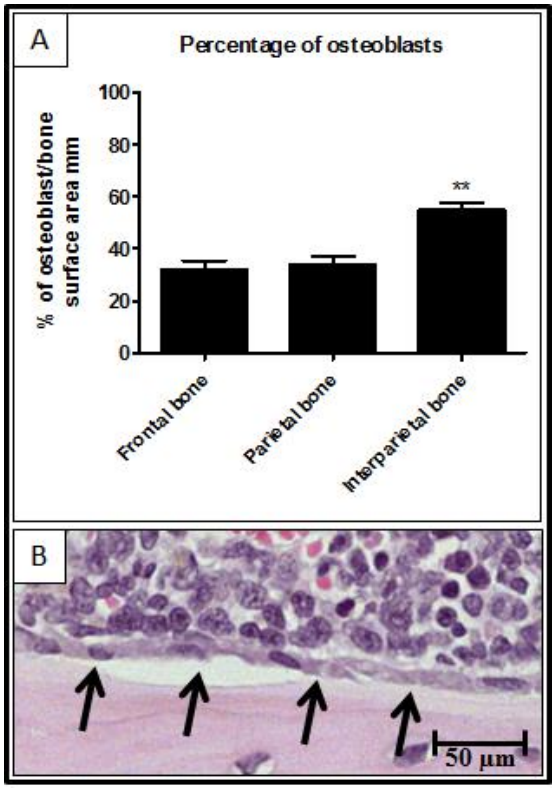


**Figure 5.6: There was an increase in the percentage of osteoblast surfaces in the interparietal bones compared to the frontal and parietal bones in male C57BL/KalwRiJHsD mice.** Frontal, parietal and interparietal sections of calvariae were stained with haematoxylin and eosin. Panel A shows there was a statistically significant increase in the distribution of osteoblasts in the interparietal bone of calvariae. Panels B shows a representative photomicrographic image of osteoblasts (black arrow). ** = $p<0.01$. ANOVA test was used. (n=5).

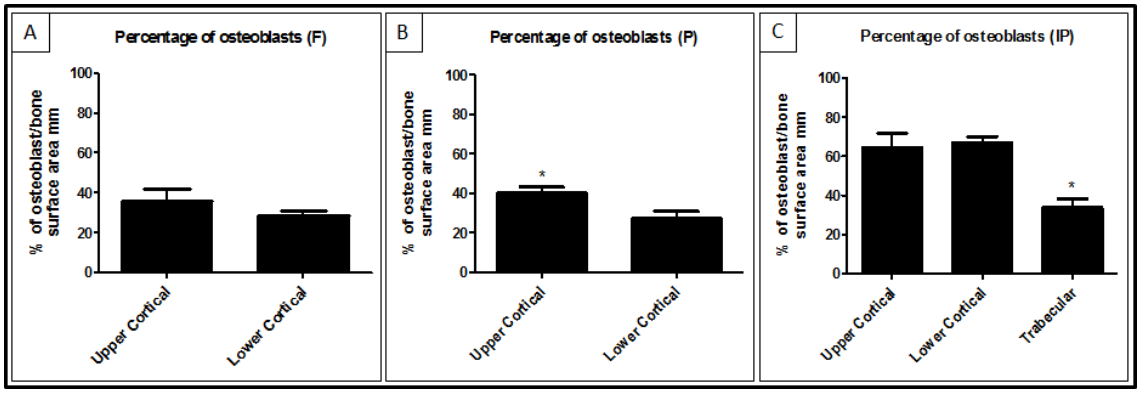


**Figure 5.7: The percentage of osteoblast surfaces in the lower endo-cortical surfaces compared to the upper endo-cortical surfaces in male C57BL/KalwRiJHsD mice.** There was a significant increase in the distribution of osteoblasts in the upper endo-cortical surfaces compared to the lower endo-cortical surfaces in parietal bones (B), but not in frontal (A) and interparietal (C). In the interparietal bones (C) there was a significant decrease in the distribution of osteoblasts in trabecular surfaces compared to endo-cortical surfaces. * = $p<0.05$. ANOVA and Mann Whitney tests were used. (n=5).

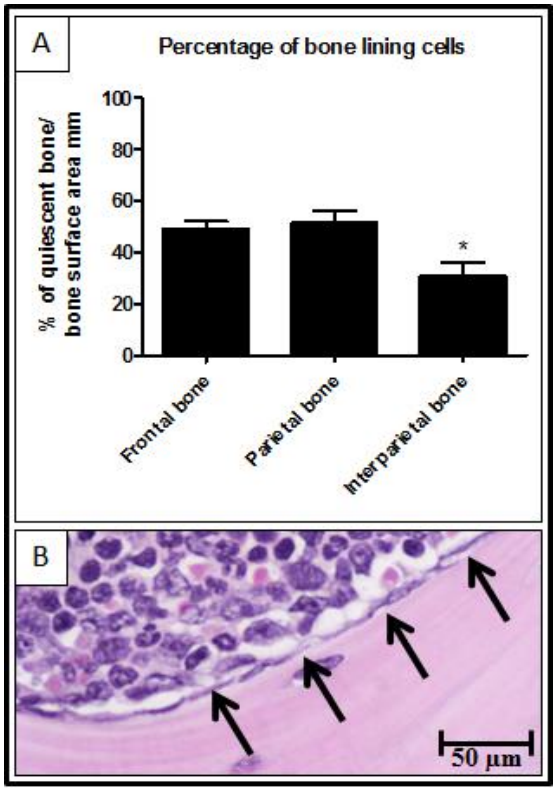


**Figure 5.8: There was a decrease in the percentage of bone lining cell surfaces in the interparietal bones compared to the frontal and parietal bones in male C57BL/KalwRiJHsD mice.** Frontal, parietal and interparietal sections of calvariae were stained with haematoxylin and eosin. Panel A shows there was a statistically significant decrease in the distribution of bone lining cells in the interparietal bone of calvariae. Panel B shows a representative photomicrographic image of bone lining cells (black arrow). * = $p<0.05$. ANOVA test was used. (n=5).

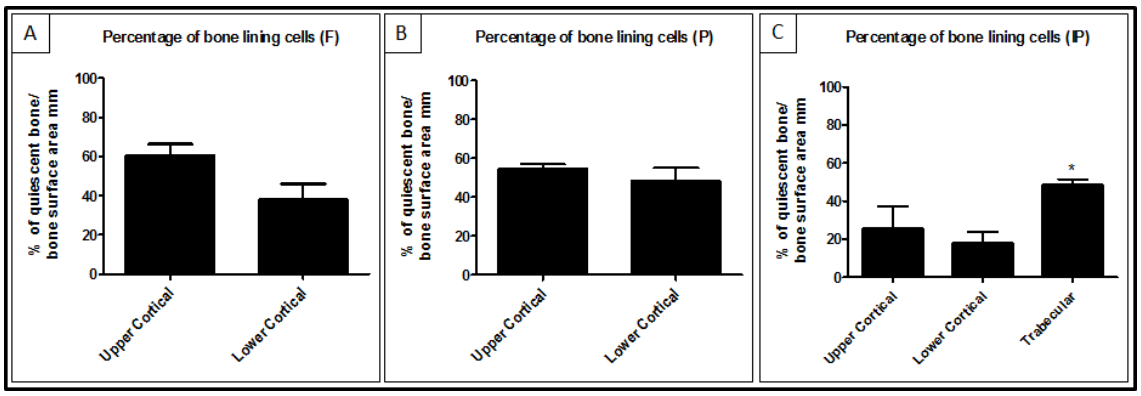


**Figure 5.9: The percentage of bone lining cells surfaces in the lower endo-cortical surfaces compared to the upper endo-cortical surfaces in male C57BL/KalwRiJHsD mice.** There was a significant decrease in the distribution of bone lining cells in the lower endo-cortical surfaces compared to the upper endo-cortical surfaces in frontal bones (A), but not in parietal (B) and interparietal (C). In the interparietal bones (C) there was a significant increase in the distribution of bone lining cells in trabecular surfaces compared to endo-cortical surfaces. * = $p<0.05$. ANOVA and Mann Whitney tests were used. (n=5).

### 5.4.5 Determination of the sites of new bone formation in C57BL/KaLwRijHsd calvariae

New bone formation was determined on endo-cortical and trabecular surfaces in interparietal bones and on endo-cortical surfaces in frontal and parietal bones. Mice were injected with 200µl of 3 mg/ml calcein-GFP each and after 3 days mice were sacrificed and calvariae were excised carefully. The results illustrated that there was an increase in the new bone formation (in green) in the interparietal bones compared to frontal bones (22.90±13.28 versus 10.83±4.11, p=0.09) and parietal bones (22.90±13.28 versus 9.26±1.00, p=0.07) after 3 days, but this is not significant (Figure 5.10 E). Figure 5.10 B, C & D show representative photomicrographic images of interparietal, parietal and frontal bones respectively 3 days post calcein-GFP injection.

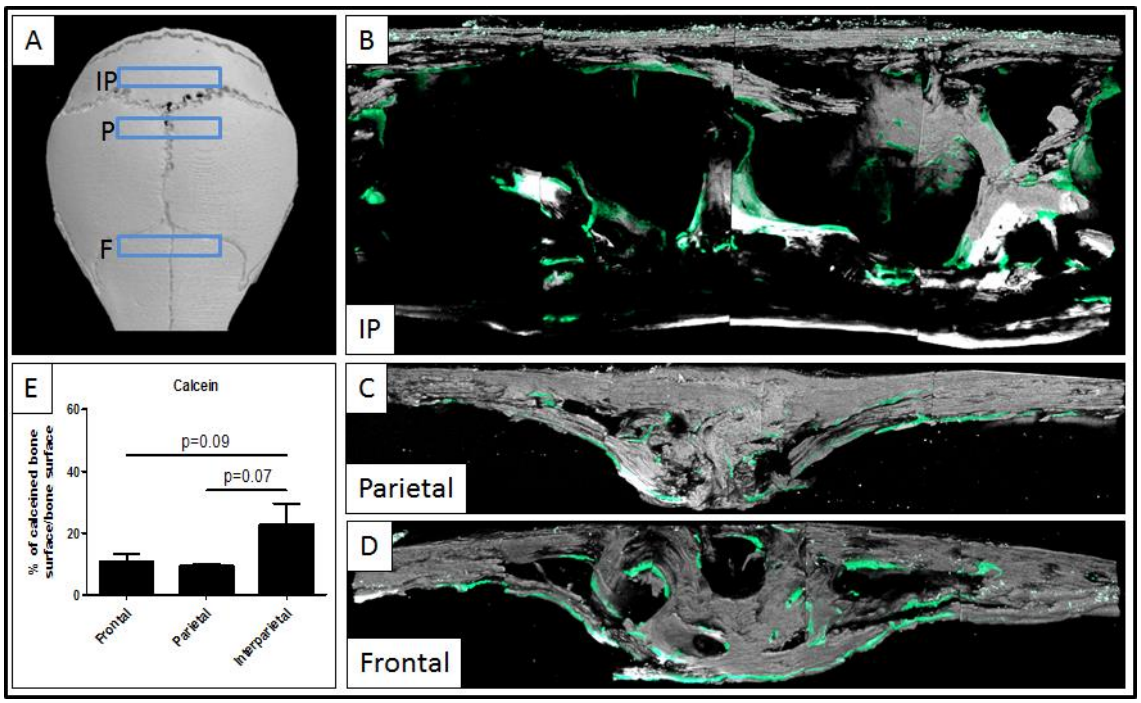


**Figure 5.10: There was an increase in new bone formation in the interparietal bones in male C57BL/KalwRiJHsD mice.** Mice were sacrificed and calvariae were excised carefully 3 days post calcein-GFP injection. The results illustrated an increase in the new bone formation (in green) in interparietal compared to frontal and parietal (E), but this is not significant. Panels B, C & D show representative photomicrographic images of interparietal, parietal and frontal bones. (n=4).

### 5.4.6 Determination the growth of tumour in C57BL/KaLwRijHsd calvarial BM using 5T33MM and 5TGM1 models

C57BL/KaLwRijHsd mice were inoculated with PBS, $2x10^6$ 5T33MM-GFP cells and 5TGM1-GFP cells via their tail vein. 21 days post inoculation calvariae were analysed using Fluorescence Lightools Illumatools System (LT-9900 Bright Light System). Figure 5.11 B shows GFP-expressing of 5T33MM tumour growth only in interparietal bones, but not in frontal or parietal bones. Figure 5.11 C shows GFP-expressing of 5TGM1 tumour growth in frontal and interparietal bones, but not in parietal bones. Figure 5.11 A shows a PBS injected control after 21 days. Figure 5.11 D shows the semi-quantitative analysis of myeloma tumour growth using 5T33MM model and 5TGM1 model. Data showed that there was a significant increase in the GFP signal in mice infected with tumour cells compared to the naive mice (5T33MM: 14.32±4.04 versus 0.00±0.00, P<0.001) (5TGM1: 26.39±2.00 versus 0.00±0.00, P<0.001).

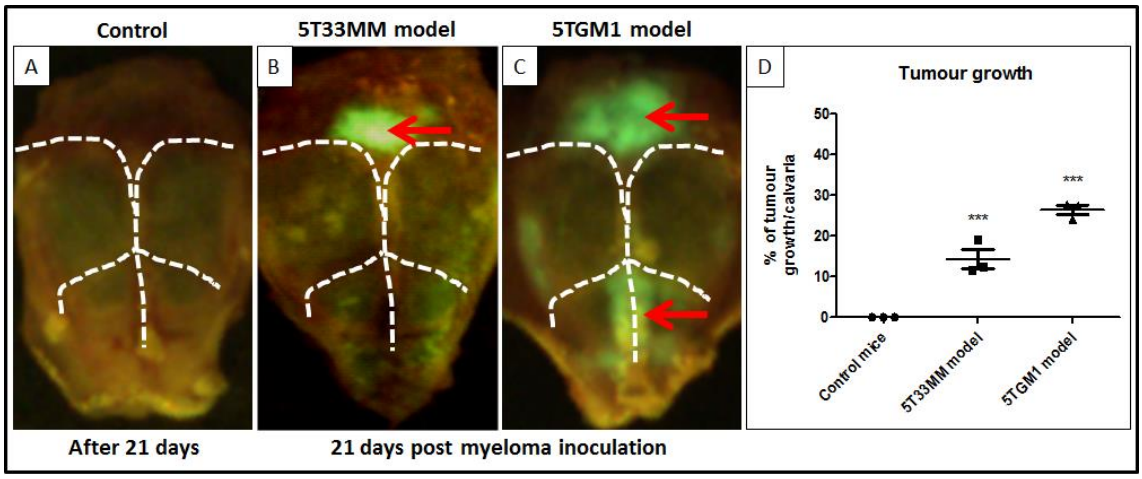


**Figure 5.11: Myeloma tumour growth was detected in calvarial BM male C57BL/KalwRiJHsD mice.** Mice were inoculated with 5T33MM-GFP and 5TGM1-GFP cells. 21 days post inoculation mice were sacrificed and calvariae were excised. The results illustrated that murine myeloma 5T33MM-GFP (B) and 5TGM1-GFP (C) tumour were detectable in calvarial BM. Panel A shows the PBS injected control mouse after 21 days. Panel D shows the percentage of myeloma tumour growth. ANOVA test was used. (n=3/group).

### 5.4.7 Determination of single cell numbers in C57BL/KaLwRijHsd calvarial BM using 5T33MM and 5TGM1 models

#### *5.4.7.1 Determination of single cell numbers in calvarial bone marrow using 5T33MM model in the early stage of disease*

C57BL/KaLwRijHsd mice were inoculated with $2x10^6$ 5T33MM-DiD cells via their tail vein. 3 days post inoculation, mice were harvested and calvariae were analysed using a Zeiss 510 laser scanning microscope. Figure 5.12 A shows that there was a statistically significant increase in the number of 5T33MM-DiD cells present in the interparietal bones compared to frontal bones (98.71±42.48 versus 20.71±15.98, P<0.001) and parietal bones (98.71±42.48 versus 5.57±3.45, P<0.001). Figure 5.12 B, C & D show representative photomicrographic images of frontal, parietal and interparietal bones respectively 3 days post 5T33MM-DiD cells inoculation.

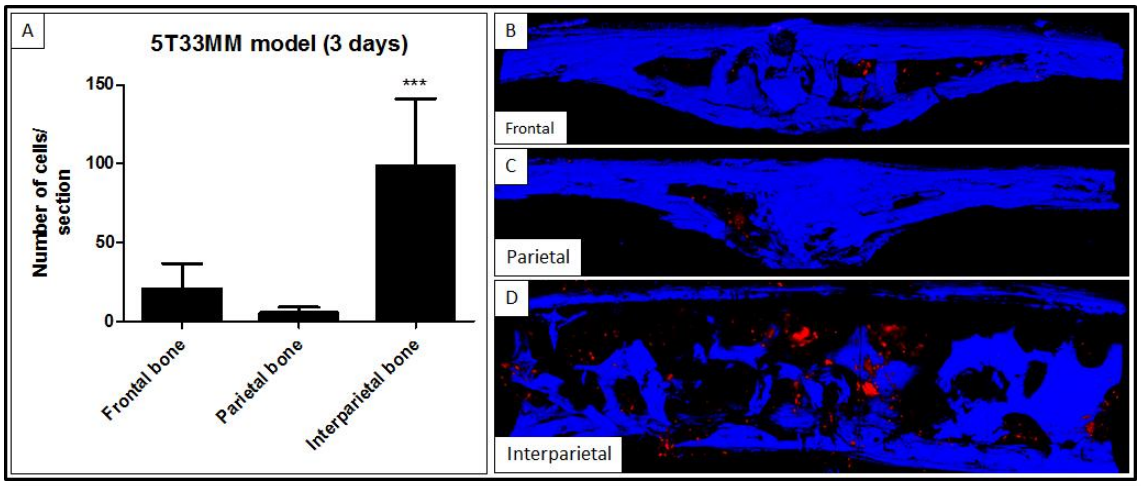


**Figure 5.12: 5T33MM cells are detectable in calvarial BM male C57BL/KalwRiJHsD mice.** Mice were inoculated with 5T33MM-DiD cells. 3 days post inoculation mice were sacrificed and calvariae were excised. Panel A shows a significant increase in the number of 5T33MM cells in interparietal bones compared to frontal and parietal bones. Panels B, C & D show representative photomicrographic images of interparietal, parietal and frontal bones. *** = p<0.001. ANOVA test was used. Blue fluorescence is the bone and red fluorescence is 5T33MM-DiD cells. Size between 500 – 20,000 $\mu m^3$ was considered as individual DiD labelled cell. (n=3).

### *5.4.7.2 Determination of single cell numbers in calvarial bone marrow using 5TGM1 model in the early stage of disease*

C57BL/KaLwRijHsd mice were inoculated with $2x10^6$ 5TGM1-DiD cells via their tail vein. 3 days post inoculation, mice were harvested and calvariae were analysed using a Zeiss 510 laser scanning microscope. Figure 5.13 A shows that there was a statistically significant increase in the number of 5TGM1-DiD cells present in the interparietal bones compared to frontal bones (81.67±40.50 versus 9.33±11.02, $P<0.05$) and parietal bones (81.67±40.50 versus 6.33±8.38, $P<0.05$). Figure 5.13 B, C & D show representative photomicrographic images of frontal, parietal and interparietal bones respectively 3 days post 5TGM1-DiD cells inoculation.

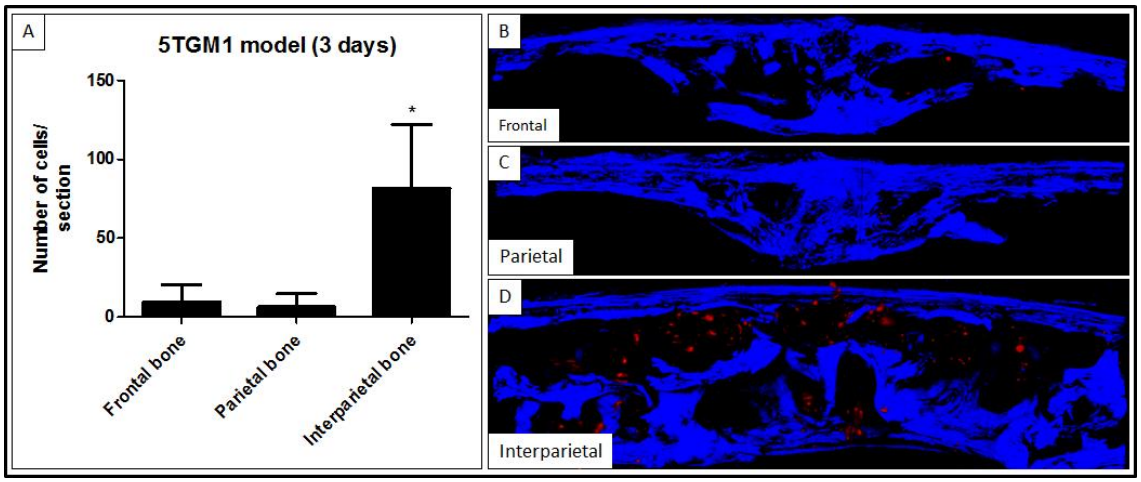


**Figure 5.13: 5TGM1 cells are detectable in calvarial BM male C57BL/KalwRiJHsD mice.** Mice were inoculated with 5TGM1-DiD cells. 3 days post inoculation mice were sacrificed and calvariae were excised. Panel A shows a significant increase in the number of 5TGM1 cells in interparietal bones compared to frontal and parietal bones. Panels B, C & D show representative photomicrographic images of interparietal, parietal and frontal bones. * = $p<0.05$. ANOVA test was used. Blue fluorescence is the bone and red fluorescence is 5TGM1-DiD cells. Size between 500 – 20,000 $\mu m^3$ was considered as individual DiD labelled cell. (n=3).

### *5.4.7.3 Determination of quiescent cell numbers in calvarial bone marrow using 5T33MM model in the late stage of disease*

C57BL/KaLwRijHsd mice were inoculated with $2x10^6$ 5T33MM-DiD cells via their tail vein. 21 days post inoculation, mice were harvested and calvariae were analysed using a Zeiss 510 laser scanning microscope. Figure 5.14 A shows that there was a statistically significant increase in the number of quiescent 5T33MM cells, cells did not losing DiD dye, present in the interparietal bones compared to frontal bones (562.00±178.90 versus 117.00±7.55, P<0.01) and parietal bones (562.00±178.90 versus 67.00±13.75, P<0.01). Figure 5.14 B, C & D show representative photomicrographic images of frontal, parietal and interparietal bones respectively 21 days post 5T33MM-DiD cells inoculation.

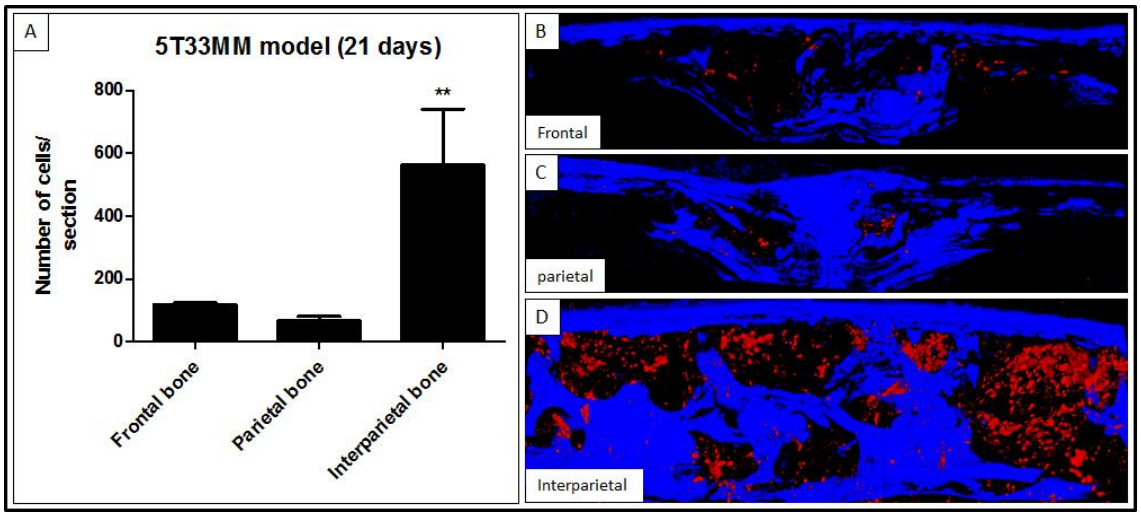


**Figure 5.14: 5T33MM cells are detectable in calvarial BM male C57BL/KalwRiJHsD mice.** Mice were inoculated with 5T33MM-DiD cells. 21 days post inoculation mice were sacrificed and calvariae were excised. Panel A shows a significant increase in the number of quiescent 5T33MM cells in interparietal bones compared to frontal and parietal bones. Panels B, C & D show representative photomicrographic images of interparietal, parietal and frontal bones. ** = p<0.01. ANOVA test was used. Blue fluorescence is the bone and red fluorescence is 5T33MM-DiD cells. Size between 500 – 20,000 $\mu m^3$ was considered as individual DiD labelled cell. (n=3).

### *5.4.7.4 Determination of quiescent cell numbers in calvarial bone marrow using 5TGM1 model in the late stage of disease*

C57BL/KaLwRijHsd mice were inoculated with $2x10^6$ 5TGM1-DiD cells via their tail vein. 21 days post inoculation, mice were harvested and calvariae were analysed using a Zeiss 510 laser scanning microscope. Figure 5.15 A shows that there was a statistically significant increase in the number of quiescent 5TGM1 cells, cells did not losing DiD dye, present in the interparietal bones compared to frontal bones (233.00±53.84 versus 79.67±18.77, P<0.05) and parietal bones (233.00±53.84 versus 27.33±10.41, P<0.05). Figure 5.15 B, C & D show representative photomicrographic images of frontal, parietal and interparietal bones respectively 21 days post 5TGM1-DiD cells inoculation.

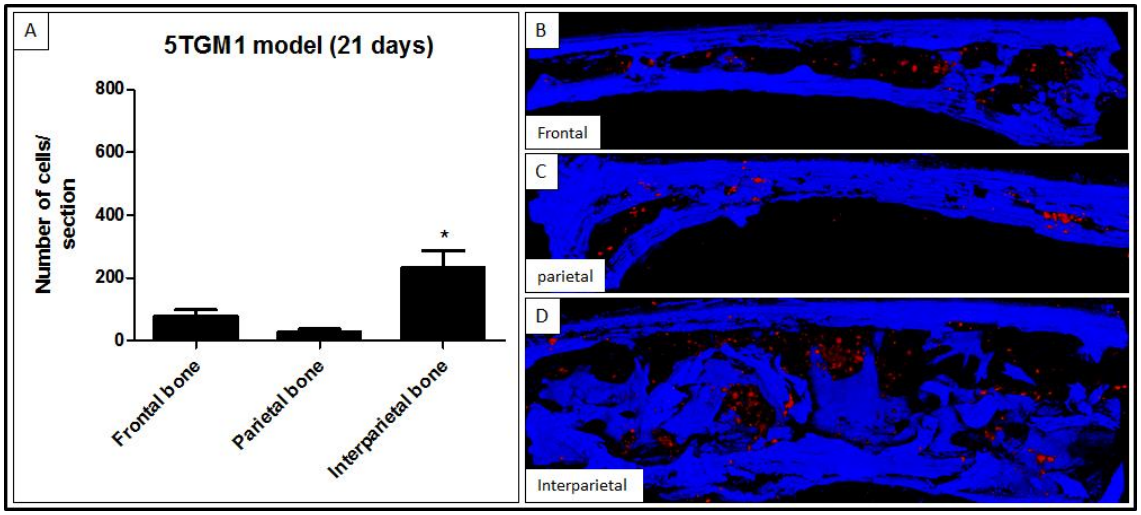


**Figure 5.15: 5TGM1 cells are detectable in calvarial BM male C57BL/KalwRiJHsD mice.** Mice were inoculated with 5TGM1-DiD cells. 21 days post inoculation mice were sacrificed and calvariae were excised. Panel A shows a significant increase in the number of quiescent 5TGM1 cells in interparietal bones compared to frontal and parietal bones. Panels B, C & D show representative photomicrographic images of interparietal, parietal and frontal bones. ** = p<0.05. ANOVA test was used. Blue fluorescence is the bone and red fluorescence is 5TGM1-DiD cells. Size between 500 – 20,000 $\mu m^3$ was considered as individual DiD labelled cell. (n=3).

## 5.5 Discussion

In this chapter the bone surfaces of calvariae: frontal, parietal and interparietal were analyzed. The primary aim was to test the hypothesis that calvarial bones contained different bone microenvironments. This was done by determining the frequency of osteoclasts, osteoblasts and bone lining cells, and new bone formation in C57BL/KaLwRijHsd calvariae to establish the potential myeloma niche, and then by inoculating mice with myeloma cells to determine the single cell/quiescent cell numbers and tumour growth in C57BL/KaLwRijHsd calvarial bones.

Previous studies demonstrated two HSC niches: osteoblastic niche on endosteal surfaces and the vascular niche (sinusoidal vessels). HSCs home to, and reside, in the HSC niche 'osteoblast niche' via attachment to spindle shaped N-cadherin$^{+}$ osteoblast cells on the endosteal bone surface (Zhang et al., 2003, Xie et al., 2009). This may represents a quiescent soil to maintain HSC survival and maintenance. Lo Celso et al (2009) analysed the frontal bones of calvariae to study individual HSC in their niche; the osteoblastic niche (Lo Celso et al., 2009). The authors offered no biological explanation why the frontal region of bone was analysed. The authors also did not report if there were discrete micro-anatomical sites within the region of bone analysed. However, it is unknown which part of the calvariae is a niche or containing a higher number of osteoblast responsible for quiescent HSCs. Micro-anatomical sites with different osteoblast numbers may exert different effect upon adjacent cells; for example, higher osteoblast numbers in one specific site may provide increase interaction between osteoblasts and myeloma cells compared to other sites. In my study bone surfaces area and BM area were analysed in frontal, parietal and interparietal regions of calvariae. In addition, the percentage of osteoclasts, osteoblasts and bone lining cells was determined on endo-cortical surfaces in frontal, parietal and interparietal bones to determine if different part of calvarial bone contains different bone microenvironments.

Parfitt et al (1987) summarised a unified system of terminology for bone histomorphometry. The bone histomorphometry community decided to measure BM volume as marrow area (Ma.Ar). In addition, they decided to measure bone surface as perimeter (B.Pm) (Parfitt et al., 1987). According to this terminology, in this study the bone surface areas and the BM areas of the frontal, parietal and interparietal regions of calvariae were analyzed. There were increases in the bone surface area and BM area in interparietal bones compared to frontal and parietal bones. The percentage of osteoclasts, osteoblasts and bone lining cells was also determined on endo-cortical surfaces in frontal, parietal and interparietal bones. The bone histomorphometry community (Parfitt et al., 1987) decided to measure osteoclast surface and osteoblast surface as a percentage of osteoclast surface or osteoblast surface to bone surface (Oc.S/BS or Ob.S/BS). Furthermore, they defined the osteoclasts as cells containing lysosomes and acid phosphate that are resorbing bone. The term of osteoblasts is defined as cells that are currently making bone and does not refer to all cells with osteogenic potential. The term, bone lining cells, is defined as inactive osteoblasts that may have osteogenic potential (Parfitt et al., 1987).

My study showed that there were increases in the percentage of osteoblasts observed in the interparietal bones compared to the frontal and parietal bones. In contrast, the percentage of bone lining cells was decreased in interparietal bones compared to frontal and parietal bones. Furthermore, we have shown that the percentage of osteoclasts did not change between the different parts of calvariae. These data suggest there are unique micro-anatomical sites in the interparietal bone compared to the frontal and parietal bones. Higher osteoblast numbers in interparietal bones may provide increased interactions between myeloma cells and osteoblasts compared to frontal and parietal bones. These data suggest that the interparietal bone is a novel model to study myeloma colonisation and growth *in vivo*.

In previous studies, Zhang et al (2003) showed that an increase in trabecular bone and/or trabecular N-cadherin$^{+}$ osteoblasts correlated with an increase in HSCs in long bone (Zhang et al., 2003). In addition, Xie et al (2009) demonstrated that 83.8% of HSCs homed to trabecular surfaces compared to 16.2% of HSCs homing to cortical surfaces in long bone (Xie et al., 2009). These studies suggested that the endosteal surfaces of trabecular bone are important to maintain HSCs in the long bone. In this study the percentages of osteoclasts, osteoblasts and bone lining cells were analysed on both cortical and trabeculae surfaces. No trabeculae were observed in frontal and parietal bones. This work demonstrated an increase in the surface area of osteoblasts on the endo-cortical surface of interparietal bones compared to the trabecular surfaces of interparietal bones. In contrast, there was a decrease in the surface area of bone lining cells on the endo-cortical surface of interparietal bones compared to the trabecular surfaces of interparietal bones. Moreover, there was no difference in the surface area of osteoclasts on the endo-cortical and trabecular surfaces of interparietal bones. These studies suggested that the endo-cortical bone surfaces may provide higher bone turnover and interaction between osteoblasts and myeloma cells compared with trabecular bone surfaces in the interparietal bones.

For further testing, the percentages of osteoclasts, osteoblasts and bone lining cells were analysed on the upper and lower endo-cortical surfaces to determine if there is a difference in cellular distribution frequency. This work demonstrated that the percentage of osteoblasts on the lower endo-cortical surface and upper endo-cortical surface did not change in frontal, parietal and interparietal bones. In addition, I found that the percentage of bone lining cells on the lower endo-cortical surface and upper endo-cortical surface did not change in frontal, parietal and interparietal bones. However, the study did show an increase in the percentage of osteoclasts on the lower endo-cortical surface of frontal, parietal and interparietal bones compared to the upper endo-cortical surface. This may provide the capacity for higher bone disease and osteolytic bone lesions in the lower cortical bones compared to the upper cortical bones in calvariae when myeloma cells colonize in the bone.

Further studies are required to establish if there is an increase in bone turnover in interparietal bones compared to frontal and parietal bones. Calcein ($C_{30}H_{26}N_2O_{13}$) is a fluorescent chromophore that binds to calcium and was used to determine the bone formation or bone turnover rate (Ducy et al., 2000, Du et al., 2001). In this study mice were injected with 200µl of 3 mg/ml calcein-GFP each and after 3 days mice were sacrificed and the calvariae excised and analysed to determine the differences in the new bone formation in different parts of the calvariae. This work suggested an increase in the new bone formation on the endo-cortical surface of interparietal bones compared to frontal and parietal bones, although this was not significant. Increases in the new bone formation together with an increase in the percentage of osteoblasts in the interparietal bones compared with frontal and parietal bones suggested that interparietal bones may have higher bone turnover compared with frontal and parietal bones. Previous studies demonstrated that tumour cells metastasise to skeletal sites with active bone turnover (Schneider et al., 2005, van der Pluijm et al., 2005). My data suggested that the higher bone turnover in interparietal bones may provide increased interactions between myeloma cells and osteoblasts compared to frontal and parietal bones.

The growth of myeloma tumour in C57BL/KaLwRijHsd calvarial BM was assessed using 5T33MM model and 5TGM1 model. These tumour cells may home to many tissues but there may be specific characteristics of particular bone marrows, or regions within bone marrow, that permit colonisation, survival and growth of these myeloma cells. This study demonstrated that 5T33MM-GFP tumours developed in the interparietal bones and not in the frontal and parietal bones after 3 weeks. In addition, I found that 5TGM1-GFP tumours developed in the interparietal bones and in the frontal bones, not in the parietal bones after 3 weeks. This observation is supported by Oyajobi et al (2007), in which 5TGM1-GFP cells were shown to grow in interparietal and frontal bones but not in parietal bones (Oyajobi et al., 2007). This study showed an increase in the bone surface area and BM area of the interparietal bones compared to frontal and parietal bones. There were also increases in the percentage of osteoblast surfaces in the interparietal bones compared to the frontal and parietal bones. The findings presented

here offer a potential explanation for why the myeloma cells, 5T33MM and 5TGM1, form large tumours in interparietal bones and not in frontal or parietal: more tumour cells arrive and are retained in theses bones and the environment is more conducive to growth. Together these studies demonstrated that the micro-anatomical site in the interparietal bone may have unique characteristics in which to study myeloma colonisation and growth in bone.

In this experiment, I found differences between the 5T33MM and 5TGM1 models. It was found that the 5T33MM and 5TGM1 models share some common features including the selective localization of MM cells in the BM, presence of serum M-component, and expression of LFA-1, CD44, VLA-4 and VLA-5 adhesion molecules. Both models represent a model of human MM disease and can grow *in vitro* and *in vivo*. However, mouse models do not essentially accurately reproduce human disease. Some differences were found between both models. The 5T33MM model does not induce osteolytic bone lesions however this could be due to the aggressive tumour causing rapid morbidity whereas the 5TGM1 model does induce osteolytic bone lesions similar to MM in humans (Radl et al., 1978, Radl et al., 1979, Vanderkerken et al., 1997). This study showed another difference between 5T33MM and 5TGM1 models, in which 5TGM1 grew in interparietal and frontal bones while 5T33MM only grew in interparietal bone and not in frontal bones. This is may be due to the 5TGM1 model being associated with an extensive osteolysis and would be worth exploring in future. Limitations of the 5T33MM and 5TGM1 models include the dependency on a particular mouse strain, C57BL/KaLwRijHsd, of limited availability. Another limitation for this experiment could be the number of animal used. I used 3 animals per group to determine the growth of tumours in calvariae due to the cost of animals. However, many published studies used 3 mice per group. Lo Celso et al (2009) used 3 mice per group to visualize individual HSCs in their niche (Lo Celso et al., 2009). Xie et al (2009) used 3 mice per group to monitoring individual HSC behaviour using real-time imaging (Xie et al., 2009). Hosokawa et al (2010) also used 3 mice per group to address the long-term engraftment of N-cadherin knockdown HSCs (Hosokawa et al., 2010).

Multiphoton microscopy was used to determine the location of myeloma cells with respect to proximity to bone in calvariae. Xie et al (2009) have recently used a confocal laser scanning microscope LSM 510, multiphoton microscopy, to trace the homing of $GFP^+$ HSCs and determine the distribution of these cells in the BM (Xie et al., 2009). In my study, 5T33MM cells and 5TGM1 cells were labelled with DiD (Invitrogen, UK), a dye bound to phospholipid bilayer membranes of the cells (http://products.invitrogen.com/ivgn/product/V22887). Previous work in our lab demonstrated that myeloma cells lose their DiD labelling during cell proliferation *in vitro*. However, some cells retained staining suggesting that these cells are mitotically quiescent. In the present study there was a significant increase in the numbers of DiD positive, 5T33MM and 5TGM1 myeloma cells observed in the interparietal BM compared to the frontal and parietal BM after 3 days. In addition, there was a significant increase in the numbers of DiD positive, 5T33MM and 5TGM1, myeloma cells observed in the interparietal BM compared to the frontal and parietal BM after 21 days. This suggests that the interparietal bone is a more favorable environment for attachment of MM cells. This may be because this bone offers greats access and volume for colonizing tumour cells but it may also be environmentally different from the other calvarial bones and this remains to be evaluated. The increased tumour growth in the interparietal bones may affect the increased frequency of potential colony forming cell or again may be a result of potential environmental differences stimulates growth.

As discussed before, the limitations of the 5T33MM and 5TGM1 models include the dependency on a particular mouse strain, C57BL/KaLwRijHsd, of limited availability. Another limitation for this experiment could be the number of animals used. I used 3 animals per group to determine the growth of tumours in calvariae and this was due to the cost of animals, although as stated previously, some published studies used 3 mice per group (Xie et al., 2009, Lo Celso et al., 2009, Hosokawa et al., 2010). Another limitation in this experiment could be the quantification of the single cells in calvarial BM. Volocity® 3D Image Analysis Software was used to quantify the single cells in calvarial BM in images captured by confocal laser scanning microscope LSM 510. The

size of red fluorescence, DiD dye, labelled objects between 500 – 20,000 $\mu m^3$ was considered as individual DiD labelled cells and others were excluded in this study. Differential counting of different size ranges may yield more information, but this was difficult to give the reliability in images produced by microscopy.

In my experiments, I found that different calvarial bones; frontal, parietal and interparietal contain different bone microenvironments. Using modern microscopy, multiphoton microscopy, permitted us to visualized single myeloma cells in the calvarial BM. Using Lightools analysis showed that myeloma cells homed and grew in areas of the skeletal with active bone turnover. These findings indicate that the 5T33MM and 5TGM1 models can be used and injected to C57BL/KaLwRijHsd mice to determine the effect of blocking N-cadherin in myeloma cells on myeloma colonization in bone, on myeloma tumour growth and on myeloma bone disease *in vivo*, and these will be investigated in the next chapter.

# 6 Chapter 6: N-cadherin in the interactions of myeloma cells with osteoblasts *in vivo*

## 6.1 Introduction

Recently, Xie et al (2009) demonstrated that HSCs home to, and reside in a state of quiescence in, the 'osteoblast niche' via attachment to N-cadherin$^{+}$ osteoblasts on endosteal bone surfaces using a new technology, *ex vivo* real-time imaging. In contrast, HSCs underwent active division and expansion in central BM area (Xie et al., 2009). On the other hand, increasing evidence indicates that expression of N-cadherin in solid tumour cells including melanoma, breast cancer, prostatic cancer, gastric carcinoma, bladder carcinoma, overian carcinoma and pancreatic cancer mediates the invasion, metastasis and interaction of cancer cells from their primary site to establish new interactions with the surrounding microenvironment (Li et al., 2001, Augustine et al., 2008, Hazan et al., 2004, Tanaka et al., 2010, Yanagimoto et al., 2001, Lascombe et al., 2006, Sarrio et al., 2006, Shintani et al., 2008).

In Chapter 4, I observed significant increases in the adhesion of myeloma cells to recombinant N-cadherin coated plates compared with PBS coated plates. In addition, N-cadherin expression was observed at the junction of myeloma cells and osteoblasts. Pre-treatment of myeloma cells with anti-N-cadherin antibody significantly reduced the adhesion of myeloma cells to recombinant N-cadherin coated plates and to osteoblasts *in vitro*. TaqMan analysis of mouse primary osteoblast cDNA demonstrated that the expression of N-cadherin was increased during osteoblastogenesis: by 3 fold in immature osteoblasts, 12 fold in mature osteoblasts and 24 fold in mature mineralised osteoblasts compared to pre-osteoblasts (1 fold), suggesting myeloma cells may have an increased capacity to interact with mature osteoblasts. These results were supported by recently published data by Groen et al (2011) who showed that N-cadherin was expressed by myeloma cells and that this facilitated the interaction of myeloma cells with N-cadherin$^{+}$ osteoblasts (Groen et al., 2011).

Pre-clinically the novel pentapeptide (ADH-1), an N-cadherin antagonist, significantly reduced the pancreatic tumour growth and the metastasis of these tumours to the lung in a mouse model (Shintani et al., 2008). In addition, ADH-1 pentapeptide in combination with chemotherapy (Melphalan) was used as novel therapeutic approach that significantly reduced tumour growth and enhanced the antitumor activity in the treatment of melanoma (Augustine et al., 2008). Clinically, ADH-1 in combination with melphalan was well-tolerated in a phase 1 study as a novel targeted therapeutics approach (Beasley et al., 2009). Critically, no study has addressed blocking N-cadherin in myeloma in preclinical mouse models.

Several murine models of MM exist, but the 5T2, 5T33 and 5TGM1 are the best well characterized and used in most recent studies (Vanderkerken et al., 2000, Croucher et al., 2003, Alici et al., 2004, Van Valckenborgh et al., 2012, Olson et al., 2005, Edwards et al., 2009, Fowler et al., 2012). In this study, the 5T33MM model and 5TGM1 model have been used to determine the effect of blocking N-cadherin in myeloma cells *in vivo*. The 5T2MM model was not used in this study because I did not have an access to use this model. As N-cadherin is expressed by osteoblasts and not by osteoclasts or osteocytes (Mbalaviele et al., 1995, Ferrari et al., 2000, Kawaguchi et al., 2001), and there being more osteoblasts compared to other cells in the calvariae compared the long bones (Nakashima and de Crombrugghe, 2003), calvarial bones were analysed in this study.

The present study uses a new technology, multiphoton microscopy, to study the early colonization of myeloma cells in bone. This chapter will describe studies that suggest N-cadherin expression is important in the interaction of myeloma cells with osteoblasts *in vivo*. Other studies will describe the effect of blocking N-cadherin on myeloma colonization in bone and myeloma bone disease *in vivo*.

## 6.2 Hypothesis and objectives of this chapter

### 6.2.1 Hypothesis:

Expression of N-cadherin is important in the interaction of myeloma cells with osteoblasts *in vivo*.

### 6.2.2 Objectives:

To test this hypothesis, I have used the 5T33MM and 5TGM1 mouse models of myeloma and:

1. Determined if myeloma cells reside near to N-cadherin$^{+}$ osteoblasts in IP bones of calvariae.
2. Determined the effect of blocking N-cadherin on myeloma colonization in bone *in vivo*.
3. Determined the effect of blocking N-cadherin on colonization of quiescent myeloma in bone *in vivo*.
4. Determined the effect of blocking N-cadherin on tumour burden *in vivo*.
5. Determined the effect of blocking N-cadherin on myeloma bone disease in *vivo*.

## 6.3 Materials and Methods

### 6.3.1 Assessment of the cellular distribution of N-cadherin *in vivo*

9 male C57BL/KaLwRijHsd mice, 6 weeks of age, were used in this experiment and separated to 3 groups to determine the distribution of N-cadherin in vivo as described in section 2.2.21. Rabbit monoclonal anti-N-cadherin antibody (Millipore, UK) and donkey anti-rabbit IgG antibodies (R&D systems, UK), isotype negative control were used as described in section 2.2.13.4.

### 6.3.2 Study to determine the effect of blocking N-cadherin on myeloma colonization in bone *in vivo*

18 male C57BL/KaLwRijHsd mice, 6 weeks of age, were used in this experiment and separated to 3 groups to determine the effect of blocking N-cadherin in the colonization of myeloma cells into the bone after 3 days as described in section 2.2.22. Section were analysed under Zeiss 510 multiphoton laser scanning microscope to determine the myeloma cell numbers and the distance of myeloma cells to bone between different groups in C57BL/KalwRij calvarial BM: frontal, parietal and interparietal.

### 6.3.3 Study to determine the effect of blocking N-cadherin on myeloma bone disease *in vivo*

9 male C57BL/KaLwRijHsd mice, 6 weeks of age, were used in this experiment and separated into 3 groups to determine the effect of blocking N-cadherin on myeloma bone disease after 21 days as described in section 2.2.23. Section (left side) were analysed under Zeiss 510 multiphoton laser scanning microscope to determine the quiescent myeloma cell numbers and the distance of quiescent myeloma cells to bone between different groups in C57BL/KalwRij calvarial BM. Section (right side) were analysed using the μCT to determine the bone disease.

### 6.3.4 Cell labelling with DiD and blocking N-cadherin using anti-N-cadherin antibody

5T33MM cells and 5TGM1 cells were labelled with DiD (Invitrogen, UK). Myeloma cells were re-suspended in RPMI1640 medium (Invitrogen, UK) in T75 flasks containing DiD (5 µl of 1 µg/ml DiD to each $1x10^6$ cells/ml) for 20 minutes at 37°C as described in section 2.2.11. Anti-N-cadherin GC-4 antibody (Sigma, UK) was used to block surface N-cadherin. Myeloma cells ($1x10^6$ cells/ml) were incubated with anti-N-cadherin GC-4 antibody (Sigma, UK) (40 µg/ml) or Mouse IgG1 antibody (Dako, Denmark) as a negative control for 30 minutes at 37 °C as described in section 2.2.11 .

### 6.3.5 Inoculation of MM cells into C57BL/KaLwRijHsd mice

Myeloma cells were re-suspended in PBS ($2x10^6$ cells/200 µl) for injection. C57BL/KaLwRijHsd mice were inoculated with 200 µl of those above suspension of each MM cell line: 5T33MM and 5TGM1 ($2x10^6$ cells/200 µl), via their tail veins as described in section 2.2.12.

### 6.3.6 Microscopic examination

Osteomeasure software version 4.10 (Osteomerics Incorporated, Atlanta, USA) was used with a Leitz DMRB microscope and a drawing tablet, (CalComp Drawing Broad III) to determine the myeloma growth between different groups in C57BL/KaLwRijHsd calvarial BM as described in section 2.2.14.2. A Zeiss 510 Multiphoton Laser Scanning Microscopy was used to visualise fluorescence as described in section 2.2.214.1.

### 6.3.7 High-resolution micro–computed tomography (µCT)

A high resolution µCT scanner (model 1172; Skyscan, Belgium) was used to scan calvarial bones to determine the extent of bone disease in different treatment groups of C57BL/KalwRij calvarial BM as described in section 2.2.16. This is a non-destructive technique that provides three-dimensional micro-structure of bone.

### 6.3.8 Statistical analysis

The data were analysed using an ANOVA test (one-way analysis of variance) for more than two group comparisons or with *t* test for two group comparisons if the data was normally distributed. Tukey's test was used as post-hoc analysis when ANOVA test was used in normal distribution data. When data not normally distributed, ANOVA test (non-parametric Kruskal-Wallis test) was used for more than two group comparisons or non-parametric Mann–Whitney test was used for two group comparisons. Dunns test was used as post-hoc analysis when ANOVA test was used in not normally distributed data. Data were considered statistically significant when a p-value was equal to or less than 0.05. Results are expressed as mean ± values of standard deviation (SD).

## 6.4 Results

### 6.4.1 N-cadherin was expressed at the junction of myeloma cells and osteoblasts *in vivo* in C57BL/KaLwRijHsd mice

C57BL/KaLwRijHsd mice were inoculated with either PBS, $2x10^6$ 5T33MM-DiD cells or $2x10^6$ 5T33MM-DiD cells separately via their tail veins. 7 days post inoculation mice were harvested as colonies of myeloma cells can be seen. Calvariae were excised and sections of interparietal bones of calvariae were dissected for immunohistochemistry. Figure 6.1 A shows strong N-cadherin staining in osteoblasts in interparietal bone of control mice. Figure 6.1 B shows immunohistochemistry analysis using isotype control in interparietal bone of naïve mice.

Figure 6.1 C and E show strong N-cadherin staining in osteoblasts and myeloma cells after 7 days of injection in interparietal bone of 5T33MM-bearing and 5TGM1-bearing mice, respectively. Myeloma cells were identified by their structure, in which they include large nuclei and atypical cytoplasmic features. N-cadherin expression was observed when myeloma cells were in contact with osteoblasts. In addition, some myeloma cells not in contact with osteoblast also expressed N-cadherin. Figure 6.1 D and F show immunohistochemistry analysis using isotype control in interparietal bone of tumour-bearing mice.

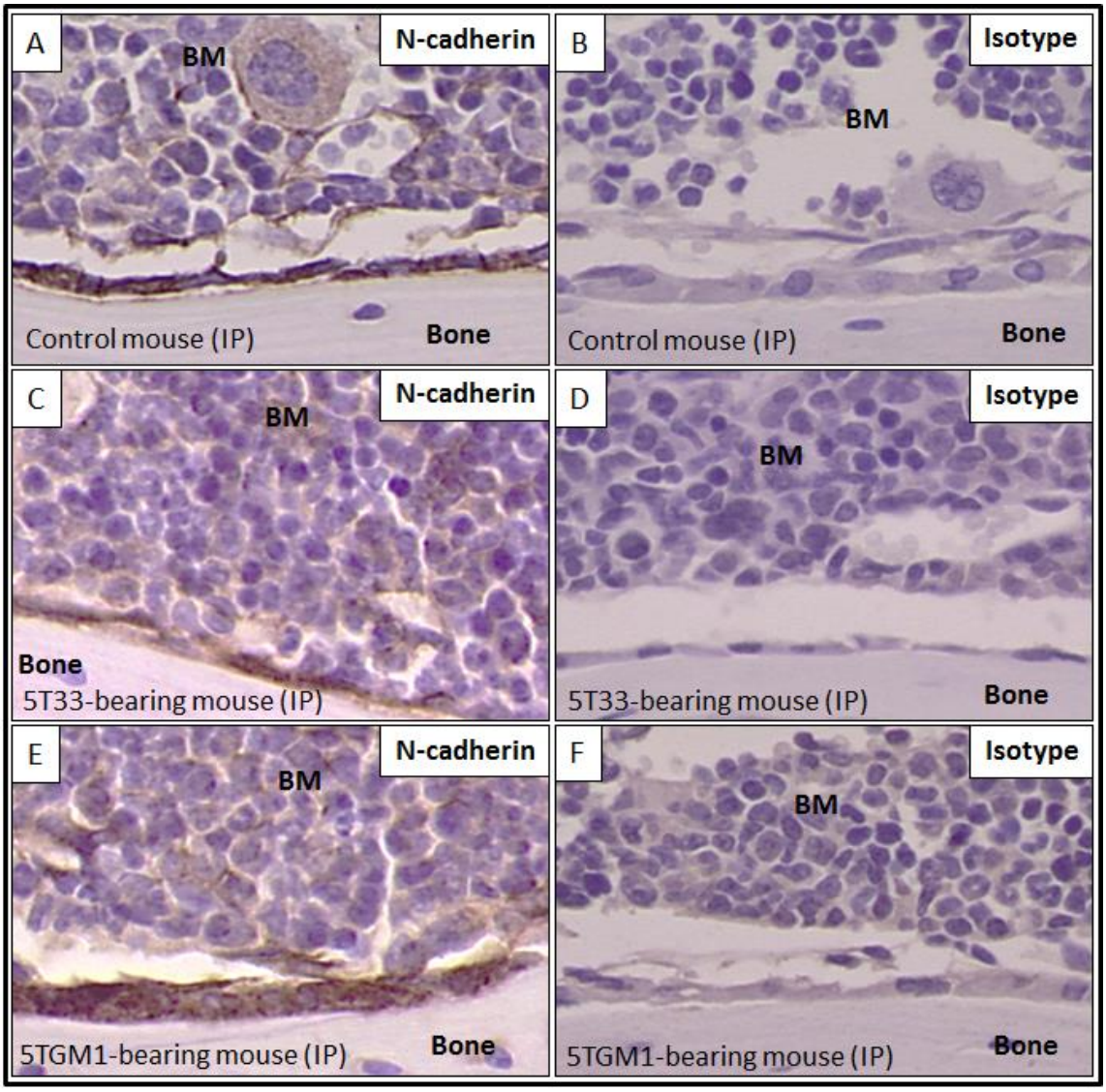


**Figure 6.1: N-cadherin was expressed at the junction of myeloma cells and osteoblasts *in vivo*.** Mice were inoculated with either PBS or myeloma cells. 7 days post inoculation mice were sacrificed and calvariae were excised. Panel A shows strong N-cadherin staining (brown) in osteoblasts of control mice in IP bones of calvariae. Panels C & E show N-cadherin expression (brown) was observed when myeloma cells were in contact with osteoblasts. Myeloma cells were identified by their structure, in which they include large nuclei and atypical cytoplasmic features. Panels B, D & F show isotype control in naïve mice, 5T33MM-bearing mice and 5TGM1-bearing mice. (n=3/group).

### 6.4.2 Effect of blocking N-cadherin on myeloma colonization in bone *in vivo* in C57BL/KaLwRijHsd mice

#### *6.4.2.1 Effect of blocking N-cadherin on 5T33MM colonization in frontal bones*

C57BL/KaLwRijHsd mice were inoculated with either $2x10^6$ 5T33MM-DiD cells, $2x10^6$ 5T33MM-DiD cells pre-treated with isotype or $2x10^6$ 5T33MM-DiD cells pre-treated with anti-N-cadherin antibody separately via their tail veins. 3 days post inoculation mice were harvested and calvariae were dissected. Frontal, parietal, and interparietal bones were analysed using a Zeiss 510 laser scanning microscope to determine the effect of blocking N-cadherin on myeloma colonization in bone. 5T33MM-DiD cells and 5T33MM-DiD cells pre-treated with isotype were used as a control groups. Figure 6.2 A shows that there was no difference in the total number of 5T33MM-DiD cells that arrived in the frontal BM 3 days after inoculation between cells treated with anti-N-cadherin antibody and the control, 5T33MM-DiD cells or 5T33MM-DiD cells pre-treated with isotype negative control.

However, the localization pattern of 5T33MM-DiD cells that arrived in the frontal BM after 3 days did show some differences. Figure 6.2 B shows that 5T33MM-DiD cells pre-treated with anti-N-cadherin antibody home significantly further from bone compared with 5T33MM-DiD cells control (19.21 µm ± 2.93 µm versus 8.77 µm ± 1.10 µm, $P<0.001$), but there was no difference compared with 5T33MM-DiD cells pre-treated with isotype control (19.21 µm ± 2.93 µm versus 15.98 µm ± 1.50 µm, $P=0.13$). Figure 6.2 C, D & E show representative photomicrographic images of frontal bones after 3 days post inoculation with 5T33MM-DiD cells, 5T33MM-DiD cells pre-treated with isotype and 5T33MM-DiD cells pre-treated with anti-N-cadherin antibody, respectively.

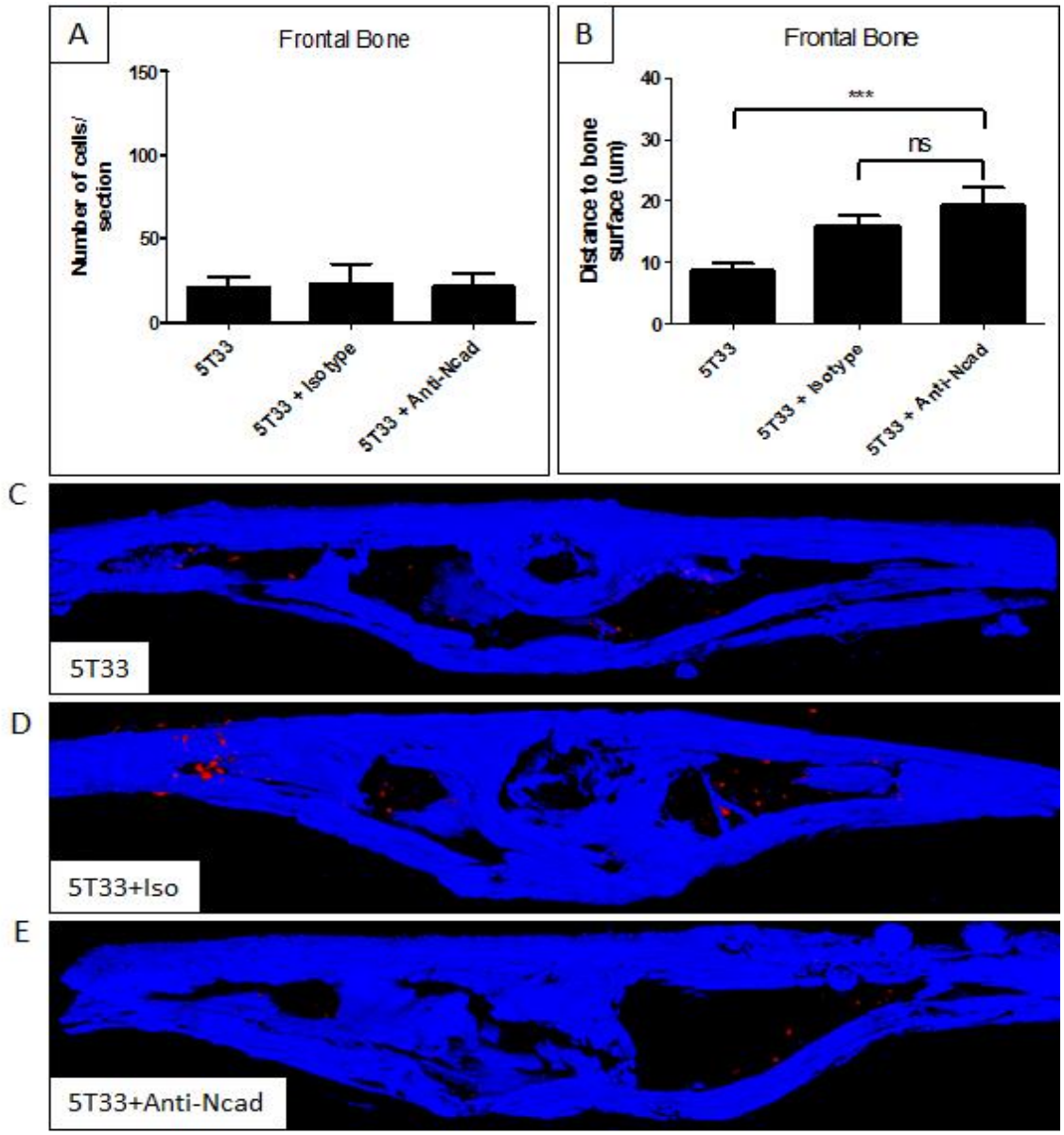


**Figure 6.2: Effect of blocking N-cadherin on myeloma colonization in frontal bones using male C57BL/KalwRiJHsD mice.** Mice were inoculated with 5T33MM-DiD cells. 3 days post inoculation, mice were sacrificed and calvariae were excised. Panel A shows there was no difference in the number of 5T33MM-DiD cells in frontal BM between groups. Panel B shows a significant increase in the distance of 5T33MM-DiD cells from bone when pre-treated with anti-N-cadherin antibody. Panels C, D & E show representative photomicrographic images inoculation of 5T33MM-DiD cells, 5T33MM-DiD cells pre-treated with isotype or anti-N-cadherin antibody, respectively, in frontal bones after 3 days. *** = $p<0.001$. ANOVA test was used. Blue fluorescent is the bone and red fluorescent is 5T33MM-DiD cells. Size between 500 – 20,000 $\mu m^3$ was considered as individual DiD labelled cell. (n=6/group).

#### *6.4.2.2 Effect of blocking N-cadherin on 5T33MM colonization in parietal bones*

C57BL/KaLwRijHsd mice were inoculated with 5T33MM-DiD cells +/- pre-treatment with isotype or anti-N-cadherin antibodies, as described above and animals killed 3 days later. Figure 6.3 A shows that there was no difference in the number of 5T33MM-DiD cells that arrived in the parietal BM 3 days post inoculation between cells treated with anti-N-cadherin antibody and the control, 5T33MM-DiD cells or 5T33MM-DiD cells pre-treated with isotype negative control. In contrast to the frontal bones, figure 6.3 B shows that there was no differences in the localization when 5T33MM-DiD cells pre-treated with anti-N-cadherin antibody compared with 5T33MM-DiD cells control or with 5T33MM-DiD cells pre-treated with isotype control. Figure 6.3 C, D & E show representative photomicrographic images of parietal bones after 3 days post inoculation with 5T33MM-DiD cells, 5T33MM-DiD cells pre-treated with isotype and 5T33MM-DiD cells pre-treated with anti-N-cadherin antibody, respectively.

#### *6.4.2.3 Effect of blocking N-cadherin on 5T33MM colonization in IP bones*

C57BL/KaLwRijHsd mice were inoculated with 5T33MM-DiD cells +/- pre-treatment with isotype or anti-N-cadherin antibodies, as described above and animals killed 3 days later. Figure 6.4 A shows that there was no difference in the number of 5T33MM-DiD cells arrived in the interparietal BM at 3 days post inoculation between cells treated with anti-N-cadherin antibody and the control, 5T33MM-DiD cells or 5T33MM-DiD cells pre-treated with isotype negative control. In contrast, there were differences in the localization of 5T33MM-DiD cells that arrived in the interparietal BM after 3 days. Figure 6.4 B shows that when 5T33MM-DiD cells pre-treated with anti-N-cadherin antibody homed significantly further from bone compared with 5T33MM-DiD cells control (29.28 μm ± 1.86 μm versus 20.00 μm ± 0.77 μm, $P<0.001$), and compared with 5T33MM-DiD cells pre-treated with isotype control (29.28 μm ± 1.86 μm versus 23.80 μm ± 1.23 μm, $P<0.05$). Figure 6.4 C, D & E show representative photomicrographic images of interparietal bones after 3 days post inoculation with 5T33MM-DiD cells,

5T33MM-DiD cells pre-treated with isotype and 5T33MM-DiD cells pre-treated with anti-N-cadherin antibody, respectively.

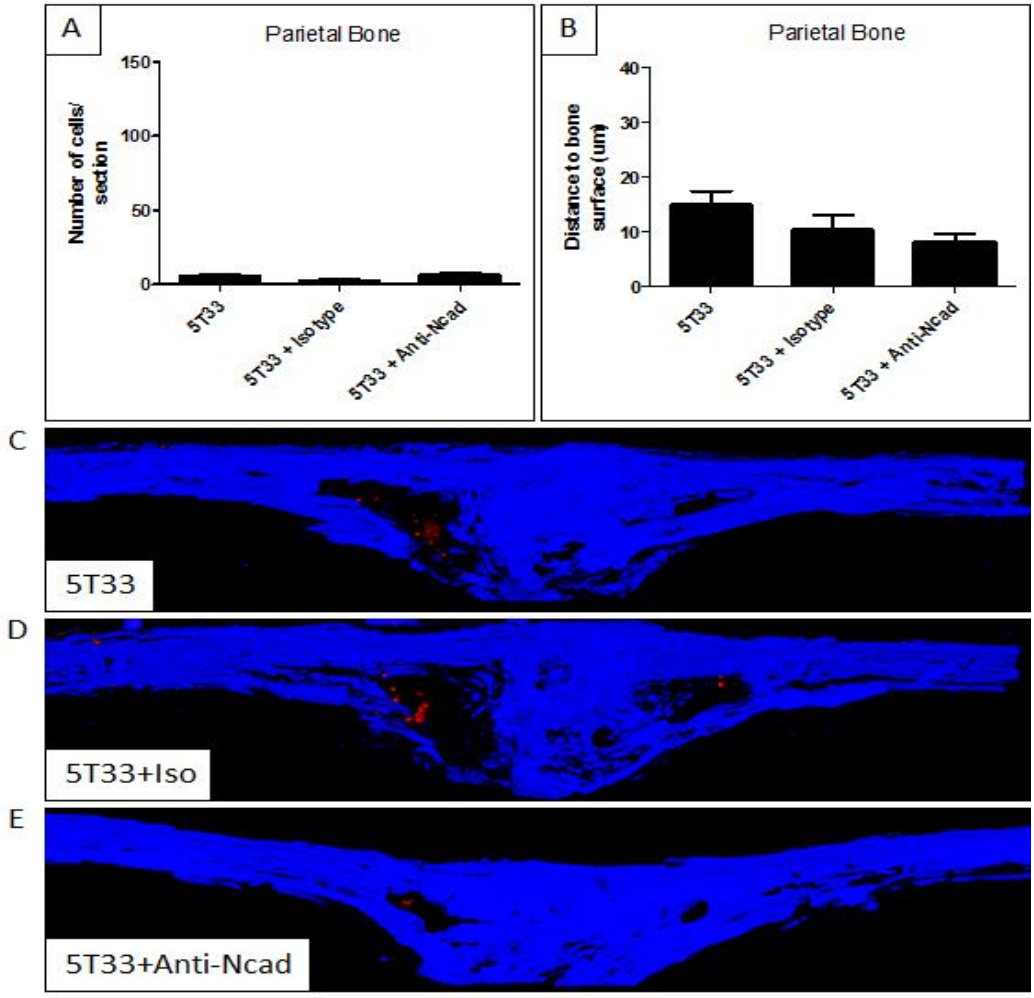


**Figure 6.3: Effect of blocking N-cadherin on myeloma colonization in parietal bones using male C57BL/KalwRiJHsD mice.** Mice were inoculated with 5T33MM-DiD cells. 3 days post inoculation, mice were sacrificed and calvariae were excised. Panel A shows there was no difference in the number of 5T33MM-DiD cells in parietal BM between groups. Panel B shows there was no difference in the distance of 5T33MM-DiD cells to the bone when cells pre-treated with anti-N-cadherin antibody. Panels C, D & E show representative photomicrographic images inoculation of 5T33MM-DiD cells, 5T33MM-DiD cells pre-treated with isotype or anti-N-cadherin antibody, respectively, in parietal bone after 3 days. *** = $p<0.001$. ANOVA test was used. Blue fluorescent is the bone and red fluorescent is 5T33MM-DiD cells. Size between 500 – 20,000 $\mu m^3$ was considered as individual DiD labelled cell. (n=6/group).

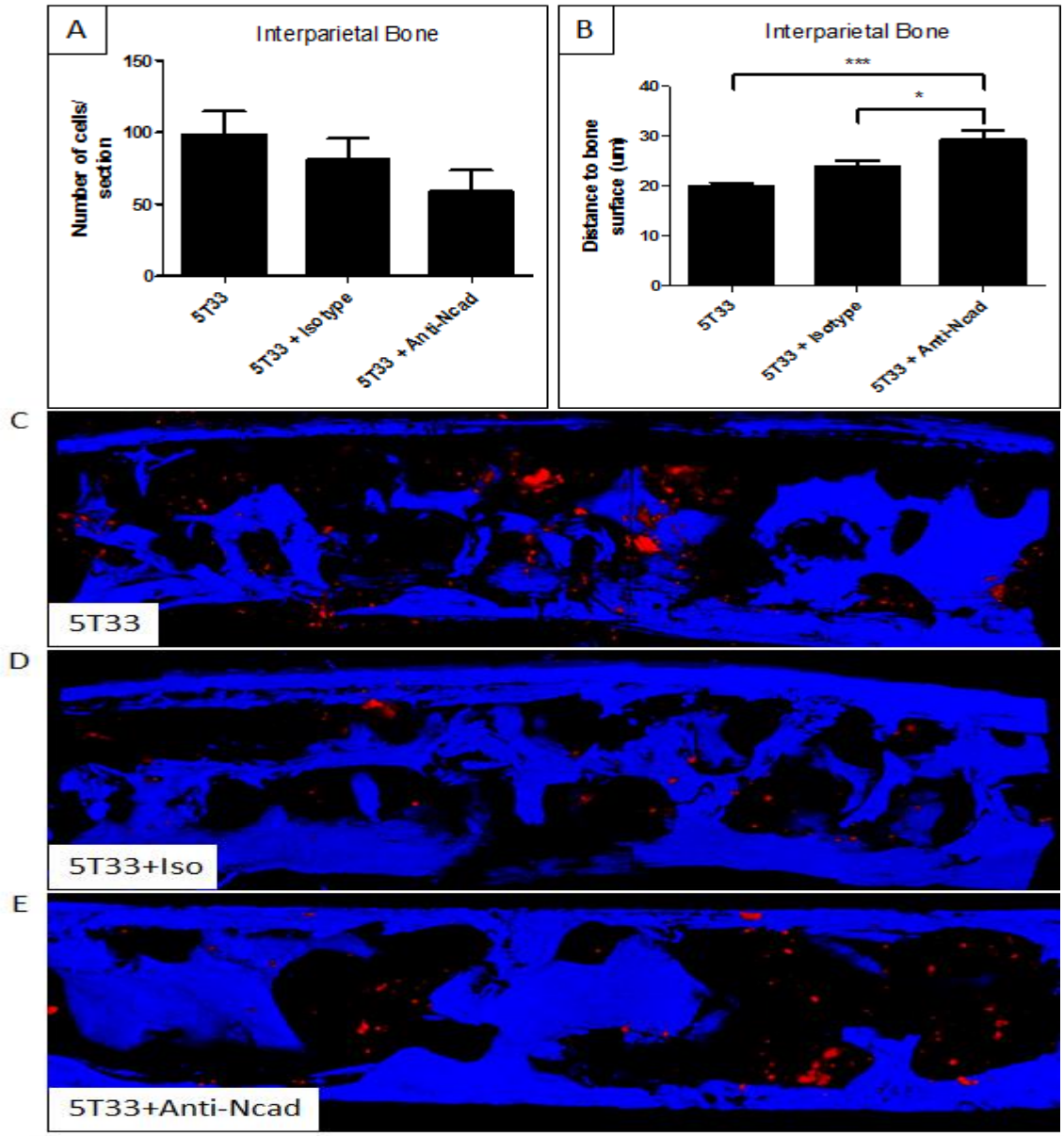


**Figure 6.4: Effect of blocking N-cadherin on myeloma colonization in interparietal bones using male C57BL/KalwRiJHsD mice.** Mice were inoculated with 5T33MM-DiD cells. 3 days post inoculation, mice were sacrificed and calvariae were excised. Panel A shows there was no difference in the number of 5T33MM-DiD cells in interparietal BM between groups. Panel B shows a significant increase in the distance of 5T33MM-DiD cells from bone when pre-treated with anti-N-cadherin antibody. Panels C, D & E show representative photomicrographic images inoculation of 5T33MM-DiD cells, 5T33MM-DiD cells pre-treated with isotype or anti-N-cadherin antibody, respectively, in interparietal bone after 3 days. *** = $p<0.001$. ANOVA test was used. Blue fluorescent is the bone and red fluorescent is 5T33MM-DiD cells. Size between 500 – 20,000 $\mu m^3$ was considered as individual DiD labelled cell. (n=6/group).

### 6.4.3 Effect of blocking N-cadherin on the colonization of quiescent myeloma cells *in vivo* in C57BL/KaLwRijHsd mice

#### *6.4.3.1 Effect of blocking N-cadherin on the colonization of 5TGM1 cells in frontal bones*

C57BL/KaLwRijHsd mice were inoculated with either $2x10^6$ 5TGM1-DiD cells, $2x10^6$ 5TGM1-DiD cells pre-treated with isotype or $2x10^6$ 5TGM1-DiD cells pre-treated with anti-N-cadherin antibody via their tail veins. 21 days post inoculation, mice were harvested and calvariae were carefully dissected. Frontal, parietal, and interparietal bones were analysed using a Zeiss 510 laser scanning microscope to determine the effect of blocking N-cadherin on colonization of mitotically quiescent myeloma cells in bone. 5TGM1-DiD cells and 5TGM1-DiD cells pre-treated with isotype were used as a control groups. Figure 6.5 A shows that there was no difference in the number of quiescent 5TGM1-DiD cells in the frontal BM at 21 days post inoculation between cells treated with anti-N-cadherin antibody and the control, 5TGM1-DiD cells or 5TGM1-DiD cells pre-treated with isotype negative control.

As in the previous experiment, when 5T33MM cells were injected and animals evaluated after 3 days, there were differences in the localization of quiescent 5TGM1 cells apparent in the frontal bones after 21 days. Figure 6.5 B shows that 5TGM1-DiD cells pre-treated with anti-N-cadherin antibody homed significantly further from bone compared with 5TGM1-DiD cells control (15.90 µm ± 1.77 µm versus 12.43 µm ± 1.14 µm, $P<0.05$), and compared with 5TGM1-DiD cells pre-treated with isotype control (15.90 µm ± 1.77 µm versus 11.49 µm ± 1.01 µm, $P<0.05$). Figure 6.5 C, D & E show representative photomicrographic images of frontal bones after 21 days post inoculation with 5TGM1-DiD cells, 5TGM1-DiD cells pre-treated with isotype and 5TGM1-DiD cells pre-treated with anti-N-cadherin antibody, respectively.

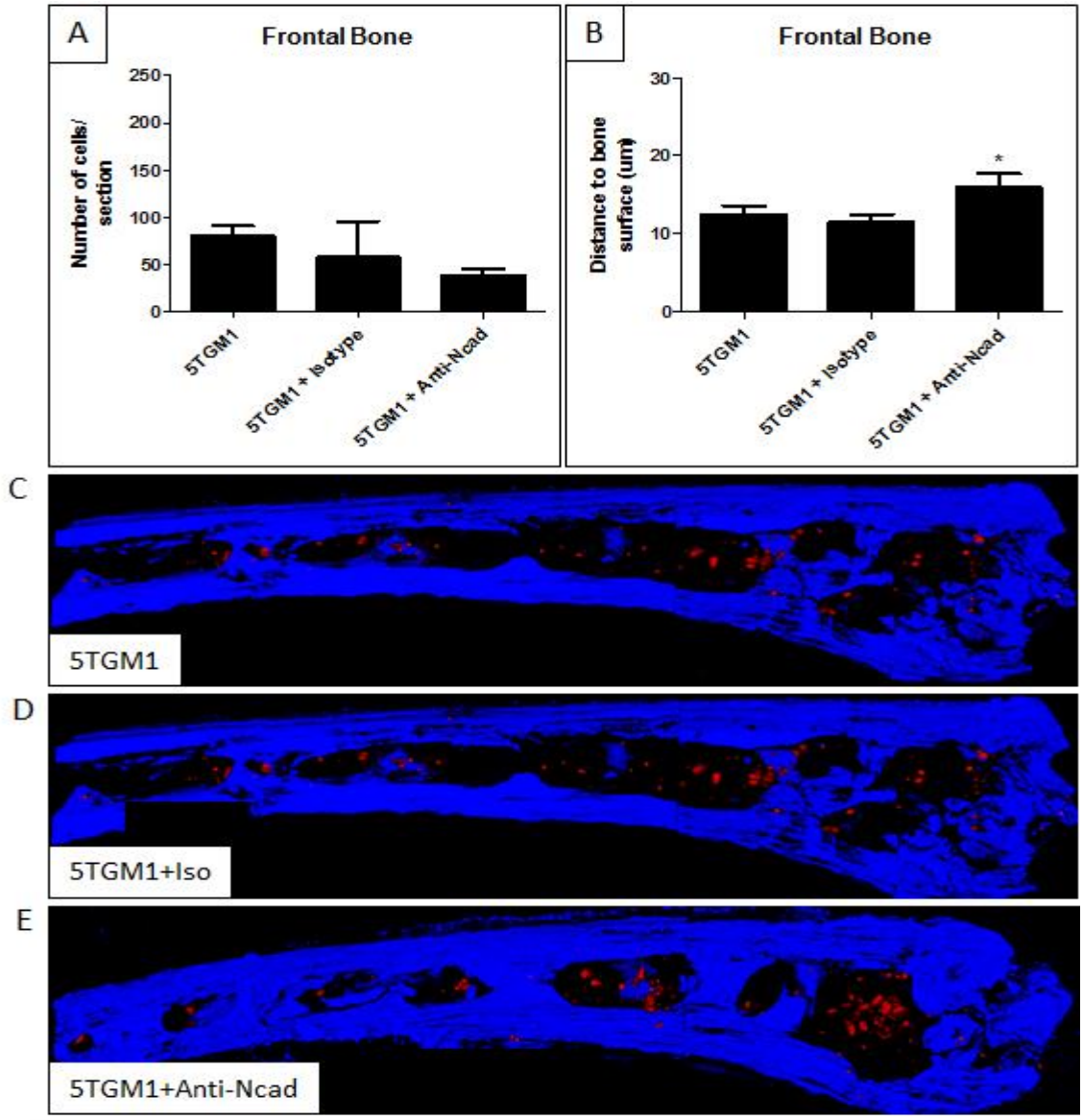


**Figure 6.5: Effect of blocking N-cadherin on colonization of quiescent myeloma cells in bone in frontal bones using male C57BL/KalwRiJHsD mice.** Mice were inoculated with 5TGM1-DiD cells. 21 days post inoculation, mice were sacrificed and calvariae were excised. Panel A shows there was no difference in the number of quiescent 5TGM1-DiD cells in frontal BM between groups. Panel B shows a significant increase in the distance of 5TGM1-DiD cells from bone when pre-treated with anti-N-cadherin antibody. Panels C, D & E show representative photomicrographic images inoculation of 5TGM1-DiD cells, 5TGM1-DiD cells pre-treated with isotype or anti-N-cadherin antibody, respectively, in frontal bones after 21 days. *** = $p<0.001$. ANOVA test was used. Blue fluorescence is the bone and red fluorescence is 5TGM1-DiD cells. Size between 500 – 20,000 $\mu m^3$ was considered as individual DiD labelled cell. (n=3/group).

#### *6.4.3.2 Effect of blocking N-cadherin on the colonization of 5TGM1 cells in parietal bones*

C57BL/KaLwRijHsd mice were inoculated with 5TGM1-DiD cells +/- pre-treatment with isotype or anti-N-cadherin antibodies, as described above and animals killed 21 days later. Figure 6.6 A shows that there was no difference in the number of quiescent 5TGM1-DiD cells in the parietal BM at 21 days post inoculation between cells treated with anti-N-cadherin antibody and the control, 5TGM1-DiD cells or 5TGM1-DiD cells pre-treated with isotype negative control. Experiments of localization of MM cells in the parietal bones also showed there was no difference in distances from bone between groups (Figure 6.6 B). Figure 6.6 C, D & E show images of parietal bones at 21 days post inoculation with 5TGM1-DiD cells, 5TGM1-DiD cells pre-treated with isotype and 5TGM1-DiD cells pre-treated with anti-N-cadherin antibody, respectively.

#### *6.4.3.3 Effect of blocking N-cadherin on the colonization of 5TGM1 cells in interparietal bones*

C57BL/KaLwRijHsd mice were inoculated with 5TGM1-DiD cells +/- pre-treatment with isotype or anti-N-cadherin antibodies, as described above and animals killed 21 days later. Figure 6.7 A shows that there was no difference in the number of quiescent 5TGM1-DiD cells in the parietal BM at 21 days post inoculation between cells treated with anti-N-cadherin antibody and the control, 5TGM1-DiD cells or 5TGM1-DiD cells pre-treated with isotype negative control. As in the frontal bones, there were differences in the localization of myeloma cells between groups. Figure 6.7 B shows that when 5TGM1-DiD cells pre-treated with anti-N-cadherin antibody, myeloma cells homed significantly further from bone compared with 5TGM1-DiD cells control (24.64 μm ± 1.28 μm versus 17.72 μm ± 0.86 μm, $P<0.001$), and compared with 5TGM1-DiD cells pre-treated with isotype control (24.64 μm ± 1.28 μm versus 18.56 μm ± 1.00 μm, $P<0.001$). Figure 6.7 C, D & E show representative photomicrographic images of parietal bones at 21 days post inoculation with 5TGM1-DiD cells, 5TGM1-DiD cells

pre-treated with isotype and 5TGM1-DiD cells pre-treated with anti-N-cadherin antibody, respectively.

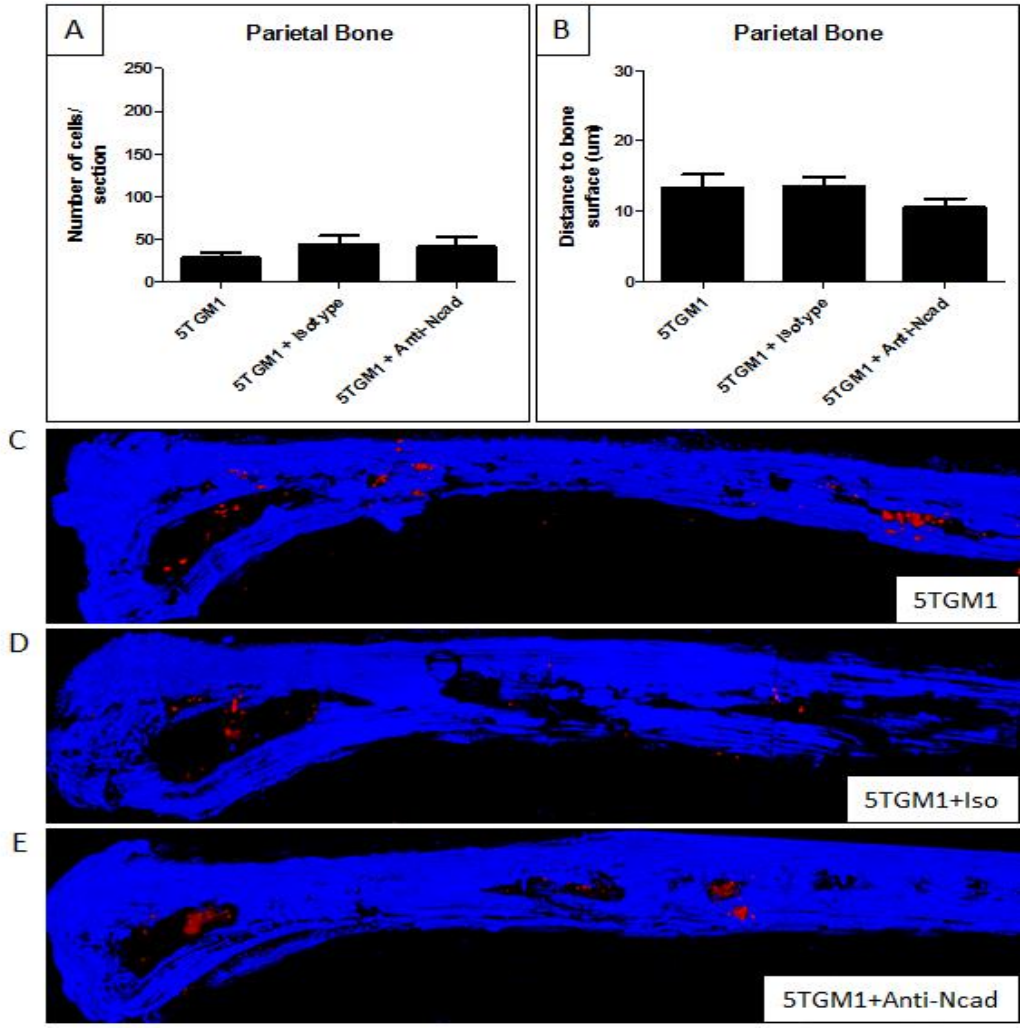


**Figure 6.6: Effect of blocking N-cadherin on colonization of quiescent myeloma cells in bone in parietal bones using male C57BL/KalwRiJHsD mice.** Mice were inoculated with 5TGM1-DiD cells. 21 days post inoculation, mice were sacrificed and calvariae were excised. Panel A shows there was no difference in the number of quiescent 5TGM1-DiD cells in parietal BM between groups. Panel B shows there was no difference in the distance of quiescent 5TGM1-DiD cells to the bone when cells pre-treated with anti-N-cadherin antibody. Panels C, D & E show representative photomicrographic images inoculation of 5TGM1-DiD cells, 5TGM1-DiD cells pre-treated with isotype or anti-N-cadherin antibody, respectively, in parietal bone after 21 days. *** = $p<0.001$. ANOVA test was used. Blue fluorescent is the bone and red fluorescent is 5TGM1-DiD cells. Size between 500 – 20,000 $\mu m^3$ was considered as individual DiD labelled cell. (n=3/group).

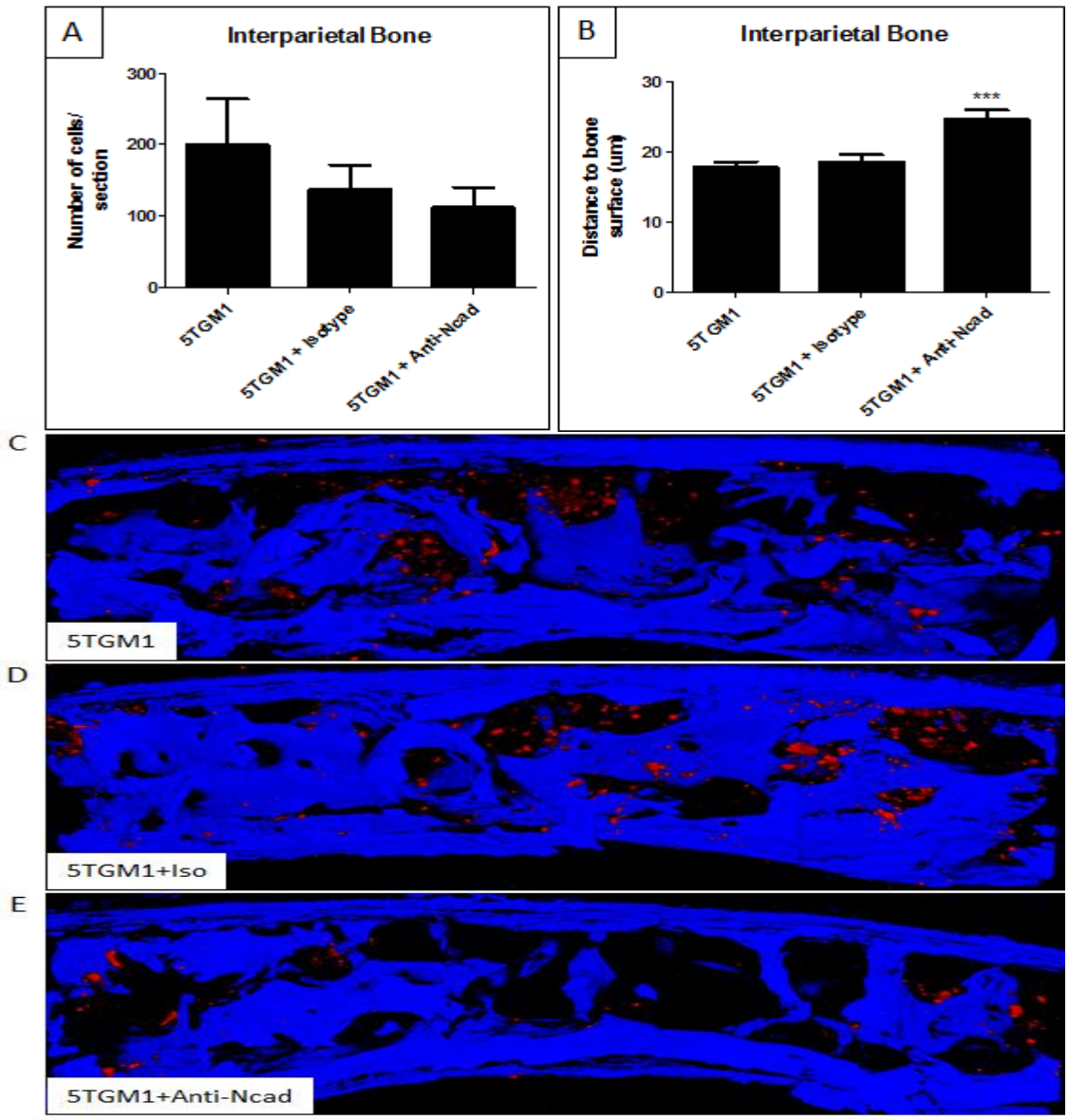


**Figure 6.7: Effect of blocking N-cadherin on colonization of quiescent myeloma cells in bone in interparietal bones using male C57BL/KalwRiJHsD mice.** Mice were inoculated with 5TGM1-DiD cells. 21 days post inoculation, mice were sacrificed and calvariae were excised. Panel A shows there was no difference in the number of quiescent 5TGM1-DiD cells in interparietal BM between groups. Panel B shows a significant increase in the distance of 5TGM1-DiD cells from bone when pre-treated with anti-N-cadherin antibody. Panels C, D & E show representative photomicrographic images inoculation of 5TGM1-DiD cells, 5TGM1-DiD cells pre-treated with isotype or anti-N-cadherin antibody, respectively, in interparietal bone after 21 days. *** = $p<0.001$. ANOVA test was used. Blue fluorescent is the bone and red fluorescent is 5TGM1-DiD cells. Size between 500 – 20,000 $\mu m^3$ was considered as individual DiD labelled cell. (n=3/group).

### 6.4.4 Effect of blocking N-cadherin on tumour burden *in vivo*

#### *6.4.4.1 Effect of blocking N-cadherin on overall tumour burden in frontal BM*

C57BL/KaLwRijHsd mice were inoculated with either $2x10^6$ 5TGM1 cells, $2x10^6$ 5TGM1 cells pre-treated with isotype or $2x10^6$ 5TGM1 cells pre-treated with anti-N-cadherin antibody via their tail veins and sacrificed after 21 days. Figure 6.8 A shows that there was a significant reduction in tumour growth in frontal BM when 5TGM1 cells were pre-treated with anti-N-cadherin antibody compared with untreated 5TGM1 control cells (59.92±5.96 versus 77.90±8.21, P<0.001), and compared with 5TGM1 cells pre-treated with isotype control antibody (59.92±5.96 versus 81.66±6.48, P<0.001). Figure 6.8 B, C & D show representative photomicrographic images of frontal BM at 21 days post inoculation with 5TGM1 cells, 5TGM1 cells pre-treated with isotype and 5TGM1 cells pre-treated with anti-N-cadherin antibody, respectively.

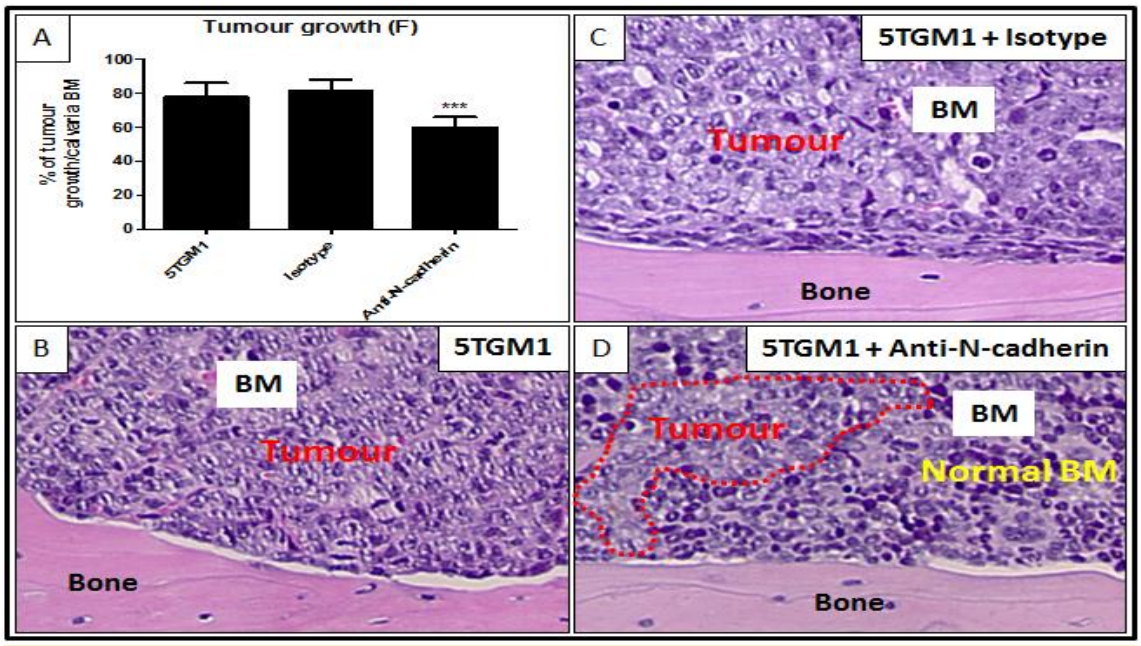


**Figure 6.8: Effect of blocking N-cadherin on tumour burden in frontal BM using male C57BL/KalwRiJHsD mice.** Mice were inoculated with 5TGM1 cells and sacrificed 21 days later. Panel A shows that there was a significant reduction in tumour growth in frontal BM when 5TGM1 cells pre-treated with anti-N-cadherin antibody. Panels B, C & D show representative photomicrographic images of frontal bones after 21 days of inoculation. *** = p<0.001. ANOVA test was used. (n=3/group).

### *6.4.4.2 Effect of blocking N-cadherin on tumour burden in interparietal BM*

C57BL/KaLwRijHsd mice were inoculated with either $2x10^6$ 5TGM1 cells, $2x10^6$ 5TGM1 cells pre-treated with isotype or $2x10^6$ 5TGM1 cells pre-treated with anti-N-cadherin antibody via their tail veins and sacrificed after 21 days. Figure 6.9 A shows that there was a significant reduction in tumour growth in interparietal BM when 5TGM1 cells were pre-treated with anti-N-cadherin antibody compared with untreated 5TGM1 control cells (60.93±5.63 versus 83.12±0.86, P<0.001), and compared with 5TGM1 cells pre-treated with isotype control antibody (60.93±5.63 versus 81.31±11.03, P<0.001). Figure 6.9 B, C & D show images of interparietal BM at 21 days post inoculation with 5TGM1 cells, 5TGM1 cells pre-treated with isotype and 5TGM1 cells pre-treated with anti-N-cadherin antibody, respectively.

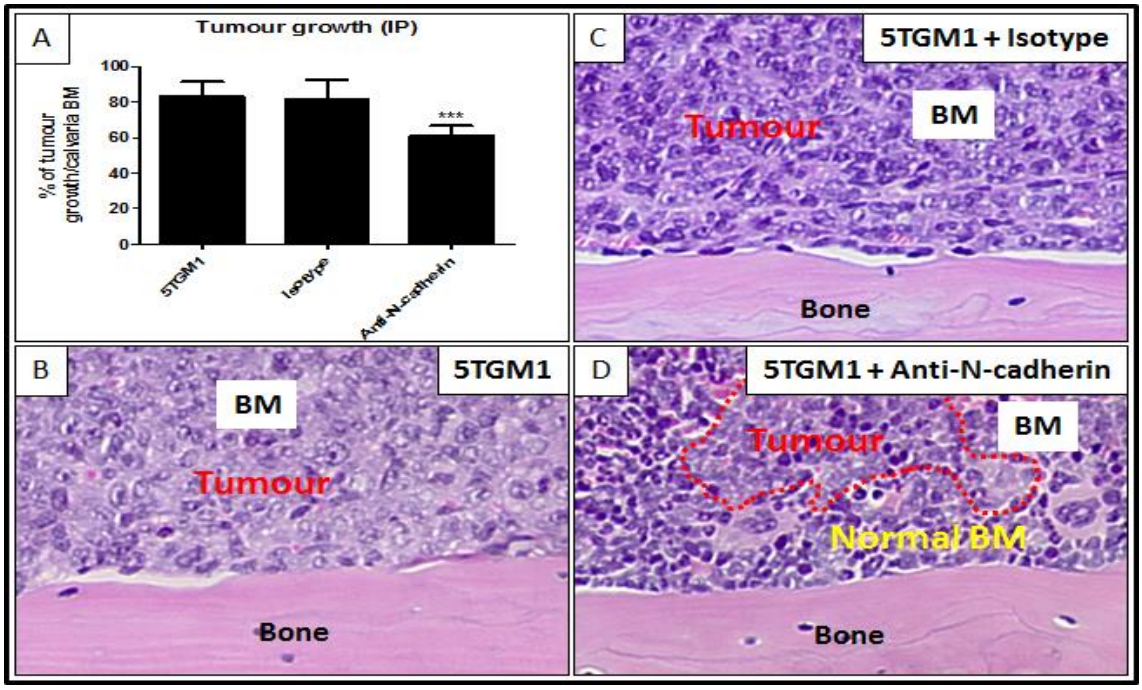


**Figure 6.9: Effect of blocking N-cadherin on tumour burden in IP BM using male C57BL/KalwRiJHsD mice.** Mice were inoculated with 5TGM1 cells and sacrificed in 21 days later. Panel A shows that there was a significant reduction in tumour growth in frontal BM when 5TGM1 cells pre-treated with anti-N-cadherin antibody. Panels B, C & D show representative photomicrographic images of interparietal bones after 21 days of inoculation. *** = p<0.001. ANOVA test was used. (n=3/group).

### 6.4.5 Effect of blocking N-cadherin on bone disease *in vivo* in C57BL/KaLwRijHsd mice

#### *6.4.5.1 Effect of blocking N-cadherin on the bone disease in the cortical interparietal bones*

C57BL/KaLwRijHsd mice were inoculated with either $2x10^6$ 5TGM1 cells, $2x10^6$ 5TGM1 cells pre-treated with isotype or $2x10^6$ 5TGM1 cells pre-treated with anti-N-cadherin antibody via their tail veins. 21 days post inoculation, mice were harvested and calvariae were carefully dissected. Interparietal bones were analysed using a high resolution µCT scanner (model 1172; Skyscan, Belgium) to determine the effect of blocking N-cadherin on bone disease. 5TGM1 cells and 5TGM1 cells pre-treated with isotype were used as a control groups. Figure 6.10 A shows there was no difference in the osteolytic lesion number in upper cortical of 5TGM1-bearing mice when cells were pre-treated with anti-N-cadherin antibody compared with 5TGM1-bearing mice or cells pre-treated with isotype control. Figure 6.10 B shows there was no difference in the osteolytic lesion number in lower cortical of 5TGM1-bearing mice when cells were pre-treated with anti-N-cadherin antibody compared with 5TGM1-bearing mice or cells pre-treated with isotype control. Figure 6.10 C, D, E and F show 3D µCT-reconstructed images of interparietal upper cortical bones showing there was no osteolytic lesions in the interparietal upper cortical bones in 5TGM1-bearing mice. Figure 6.10 G, H, I and J show 3D µCT-reconstructed images of interparietal lower cortical bones showing osteolytic lesions in the interparietal lower cortical bones in 5TGM1-bearing mice. Interestingly, the osteolytic bone lesions were only found in the lower cortical interparietal bones, but not in the upper cortical interparietal bones in 5TGM1 bearing-mice.

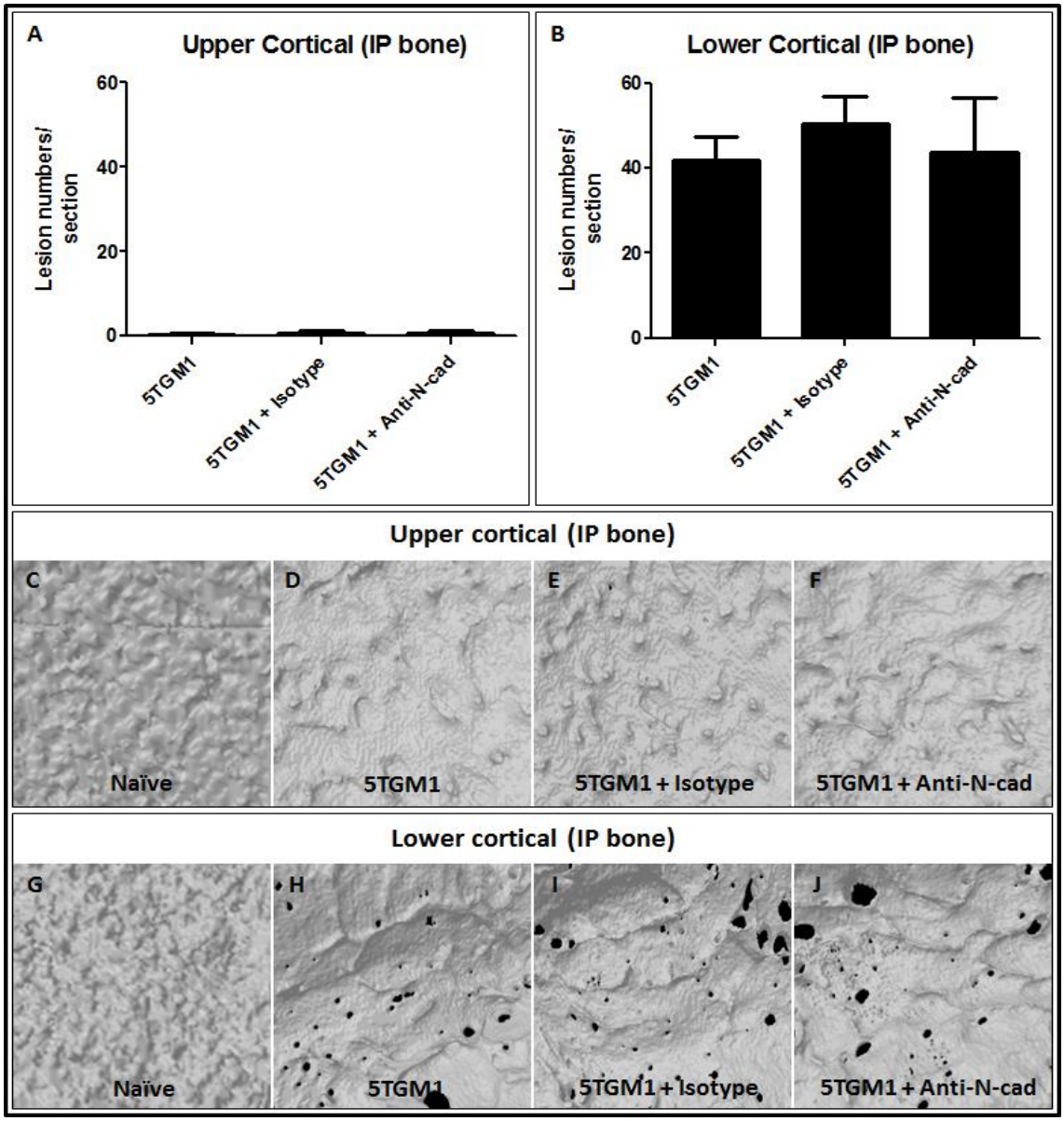


**Figure 6.10: Effect of blocking N-cadherin on bone disease in cortical interparietal bone using male C57BL/KalwRiJHsD mice.** Mice were inoculated with 5TGM1 cells and sacrificed after 21 days. Panel A & B show that there was no difference in the osteolytic lesion number in interparietal bones of 5TGM1-bearing mice when cells pre-treated with anti-N-cadherin antibody compared with 5TGM1-bearing mice or cells pre-treated with isotype control. Panels C, D, E & F show 3D µCT-reconstructed images of interparietal upper cortical bones after 21 days of inoculation. Panels G, H, I & J show 3D µCT-reconstructed images of interparietal lower cortical bones after 21 days of inoculation. White colour shows the bone surface. Black colour shows the osteolytic lesions in bone. ANOVA test was used. (n=3/group).

#### *6.4.5.2 Effect of blocking N-cadherin on the bone disease in the trabecular interparietal bones*

C57BL/KaLwRijHsd mice were inoculated with either $2x10^6$ 5TGM1 cells, $2x10^6$ 5TGM1 cells pre-treated with isotype or $2x10^6$ 5TGM1 cells pre-treated with anti-N-cadherin antibody via their tail veins. 21 days post inoculation, mice were harvested and calvariae were carefully dissected. Interparietal bones were analysed using a high resolution µCT scanner (model 1172; Skyscan, Belgium) to determine the effect of blocking N-cadherin on bone disease. 5TGM1 cells and 5TGM1 cells pre-treated with isotype were used as a control groups. Figure 6.16 A shows there was no difference in the trabecular bone volume of 5TGM1-bearing mice when cells were pre-treated with anti-N-cadherin antibody compared with 5TGM1-bearing mice or cells pre-treated with isotype control. Figure 6.16 B shows there was no difference in the trabecular number of 5TGM1-bearing mice when cells were pre-treated anti-N-cadherin antibody compared with 5TGM1-bearing mice or cells pre-treated with isotype control. Figure 6.16 C shows there was no difference in the trabecular thickness of 5TGM1-bearing mice when cells were pre-treated with anti-N-cadherin antibody compared with 5TGM1-bearing mice or cells pre-treated with isotype control. Figure 6.16 D, E and F show 3D µCT-reconstructed images of interparietal trabecular bones in 5TGM1-bearing mice, 5TGM1, 5TGM1 pre-treated with isotype control and 5TGM1 pre-treated with anti-N-cadherin antibody.

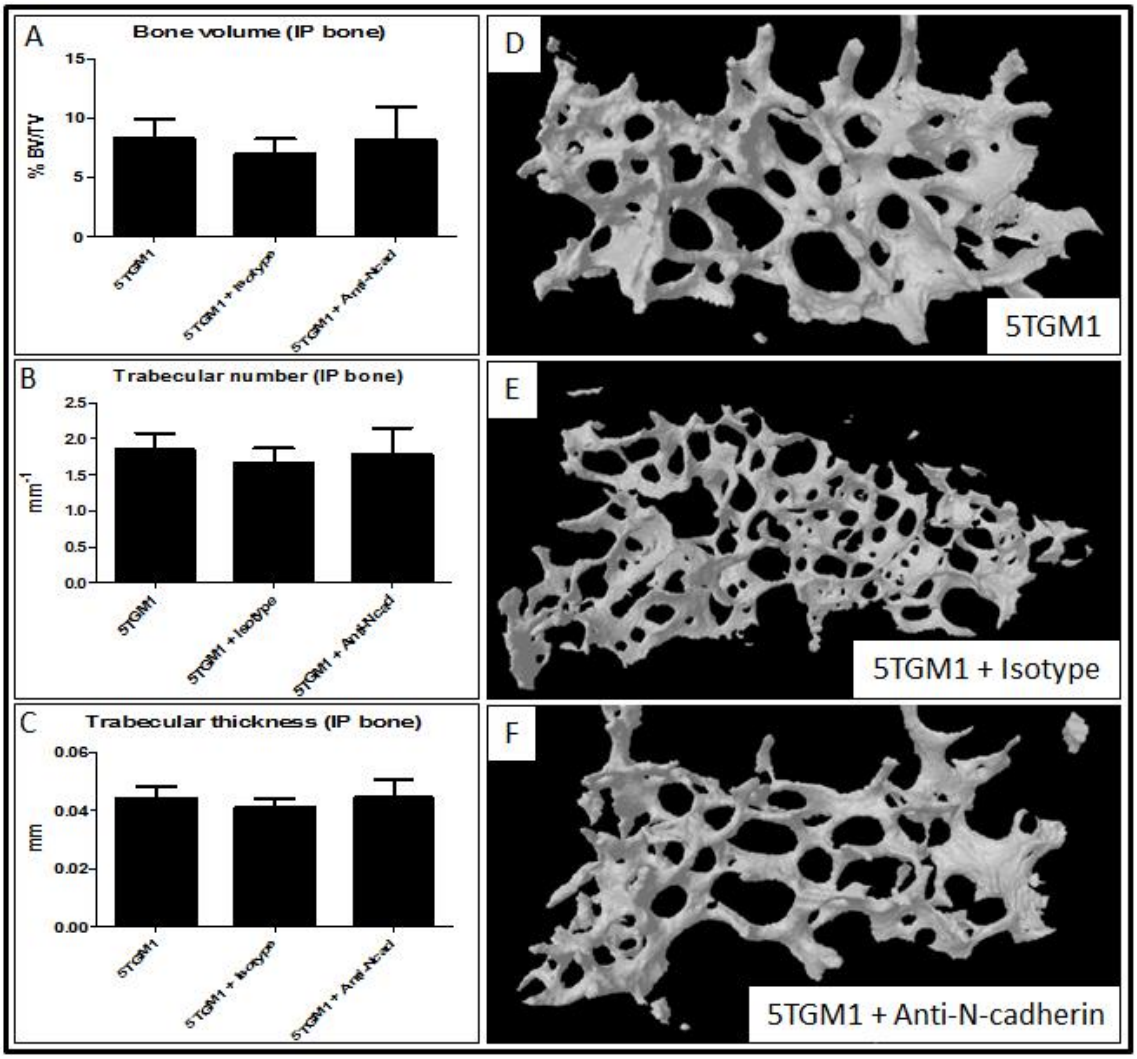


**Figure 6.16: Effect of blocking N-cadherin on bone disease in trabecular interparietal bone using male C57BL/KalwRiJHsD mice.** Mice were inoculated with 5TGM1 cells and sacrificed after 21 days. Panel A, B & C show that there was no difference in the trabecular bone volume, trabecular number and trabecular thickness of 5TGM1-bearing mice when cells pre-treated with anti-N-cadherin antibody compared with 5TGM1-bearing mice or cells pre-treated with isotype control. Panels D, E & F show 3D µCT-reconstructed images of interparietal trabecular bones after 21 days of inoculation. White colour shows the trabecular bone that found in the BM. ANOVA test was used. (n=3/group).

## 6.5 Discussion

In this chapter, I evaluated the interactions of MM cells with osteoblasts via the adhesion molecule, N-cadherin *in vivo*. In addition, I examined the effect of blocking N-cadherin on the colonization of myeloma cells, tumour burden and bone disease *in vivo*. Recently Groen et al (2011) demonstrated that N-cadherin mediated the adhesion of myeloma cells with osteoblasts and this adhesion of myeloma cells with osteoblasts is prevented by using an N-cadherin blocking antibody, GC-4 (10 μg/mL) *in vitro*. Immunohistochemistry in sections from a MM patients showed that N-cadherin is often localized between myeloma cells and bone-lining cells (Groen et al., 2011). Critically, no study has addressed blocking N-cadherin in myeloma *in vivo*. This is the first pilot study to determine the effect of blocking N-cadherin *in vivo* in C57BL/KaLwRijHsd mice using the 5T33MM and 5TGM1 models, the best characterized models that are used in most recent studies of MM applications (Vanderkerken et al., 2000, Croucher et al., 2003, Alici et al., 2004, Van Valckenborgh et al., 2012, Olson et al., 2005, Edwards et al., 2009, Fowler et al., 2012).

This study interestingly showed that all osteoblast lineage cells expressed N-cadherin. This observation supports work done by Ferrari et al (2000) who demonstrated that N-cadherin was expressed in rat and human bone *in vivo* (Ferrari et al., 2000). In addition, I observed N-cadherin expression at the junction of myeloma cells and osteoblasts *in vivo* using immunohistochemistry in mouse sections. This observation is supported by work done by Groen et al (2011) who demonstrated that the expression of N-cadherin is often localized between MM cells and the bone-lining cells in human sections from MM patients using immunohistochemistry (Groen et al., 2011). N-cadherin was not confined to the interaction between myeloma cells and osteoblasts however, and N-cadherin staining could clearly be seen in myeloma cells away from bone. This may suggests that N-cadherin is not only important for the adhesion of myeloma cells with osteoblasts, but also it could be important for the growth of myeloma tumours. In previous studies it was found that N-cadherin has a role in tumour

growth in solid tumours. Shintani et al (2008) demonstrated that using a cyclic pentapeptide, ADH-1, targeting N-cadherin, significantly reduced growth and metastasis of pancreatic cancer cells in transgenic mice (Shintani et al., 2008). In addition, Tanaka et al (2010) demonstrated that prostate cancer growth and metastasis can be affected by N-cadherin as targeting N-cadherin, using monoclonal antibodies against N-cadherin, resulted in a reduction in proliferation, adhesion and invasion of prostate cancer cells (Tanaka et al., 2010). I used 3 animals per group to determine if N-cadherin was expressed at the junction of myeloma cells and osteoblasts since these studies were essentially qualitative. One limitation in this experiment was that the identification of myeloma cells was only by their histological structure: large nuclei and atypical cytoplasmic features compared to BM cells. This did make identification of MM cells difficult when in low numbers. To resolve this issue, immunohistochemistry using an anti-CD138 antibody would be helpful in defining myeloma cells, however this was not possible in this study.

Using strategies to block N-cadherin may therefore be able to inhibit adhesion of myeloma cells to osteoblasts and act as a new therapeutic approach to inhibit disease spread in patients. To test the effects on adhesion in this study, 5T33MM cells were pre-treated with anti-N-cadherin antibody or mouse IgG1 antibody. After 3 days mice were harvested and the calvariae were dissected and analysed to determine the effect of blocking N-cadherin on myeloma colonization to bone. DiD labelling was used in these studies because this dye was easily and reliably identified in multiphoton imaging. Work in the Sheffield laboratories has also shows that this dye is lost as cells divide. This allows the identification of myeloma cells that arrive and are mitotically quiescent rather than cells that have proliferated. I observed that when 5T33MM-DiD cells were pre-treated with anti-N-cadherin antibody, cells homed significantly further away from bone compared with controls in both frontal and interparietal bones. However, in parietal bone there was no difference between groups. In contrast, I observed that there was no difference in the total number of 5T33MM-DiD cells that arrived in the frontal, parietal and interparietal BM after 3 days when 5T33MM-DiD cells were pre-treated

with anti-N-cadherin antibody. These results suggested that blocking N-cadherin in myeloma cells may have an important role in altering the location of myeloma cells in the bone, but not in the overall homing of myeloma cells into the BM. This finding was also observed previously in HSCs. Hosokawa et al (2010) showed that knockdown of N-cadherin in HSCs did not inhibit the homing of HSCs into the BM and spleen. However, knockdown of N-cadherin in HSCs significantly reduced the adhesion of HSCs onto the bone surface (Hosokawa et al., 2010). Interpretation of my experiment could be limited by the quantification of the single cells in calvarial BM. Volocity® 3D Image Analysis Software was used to quantify the single cells in calvarial BM in images captured by confocal laser scanning microscope LSM 510. The size of red fluorescence signals (DiD dye) between 500 – 20,000 $\mu m^3$ was considered as individual DiD labelled cells and others were excluded in this study. The consideration that this range specially identified single cells is utilized by other users, but it may be useful to revisit these in future studies to collect signal ranges of objectives.

In a separate study, 5TGM1-DiD cells were pre-treated with anti-N-cadherin antibody or mouse IgG1 antibody. After 21 days mice were harvested and the calvariae were dissected and analysed to determine the effect of blocking N-cadherin on the colonization of quiescent myeloma cells in bone. I observed that when 5TGM1-DiD cells were pre-treated with anti-N-cadherin antibody, cells homed significantly further away from bone compared with control in both frontal bones and interparietal bones. However, in parietal bone there was no difference between groups. In contrast, I observed that there was no difference in the total number of 5TGM1-DiD cells that arrived in the frontal, parietal and interparietal BM after 21 days when 5TGM1-DiD cells were pre-treated with anti-N-cadherin antibody. These results also suggested that blocking N-cadherin in myeloma cells may have an important role in targeting the colonization of quiescent myeloma cells into the bone, but not in the overall homing of myeloma cells into the BM. This finding also observed previously in HSCs (Hosokawa et al., 2010). Limitation for this experiment could be the number of animal used. I used 3 animals per group to determine the growth of tumours in calvariae and this was due to

the cost of animals. In addition, some published studies used 3 mice per group (Xie et al., 2009, Lo Celso et al., 2009, Hosokawa et al., 2010). As stated before interpretation of my experiment could be limited by the quantification of the single cells in calvarial BM, in which red fluorescence signal (DiD dye) between 500 – 20,000 $\mu m^3$ was considered as individual DiD labelled cells.

In this study both MM models showed similar responses when N-cadherin was blocked by anti-N-cadherin antibody on the homing of quiescent, non-proliferating, myeloma cells and on the colonization into the bone. However, the 5T33MM-bearing mice were analysed after 3 days whereas the 5TGM1-bearing mice were analysed after 21 days. This was due to the limited availability of mice. We decided to use the 5T33MM model for the early stages of MM disease and the 5TGM1 model for the late stage of MM disease where we know this model caused osteolysis. In future work, N-cadherin will be blocked in 5TGM1 cells and 5TGM1-bearing mice will be analysed after 3 days to study the effect of N-cadherin blocking in early stage of MM disease. Given more time and resources we would have studied both models at early (3 days post-injection) and late (21 days post-injection) time points.

The growth of myeloma tumour in C57BL/KaLwRijHsd calvarial BM was also assessed when N-cadherin was blocked with anti-N-cadherin antibody using the 5TGM1 model. 5TGM1 cells were pre-treated with anti-N-cadherin antibody or with mouse IgG1 antibody. 5TGM1 cells and 5TGM1 cells pre-treated with isotype were used as a control groups. After 21 days, I observed a small but significant reduction in overall myeloma tumour size when 5TGM1 cells were pre-treated with anti-N-cadherin antibody compared with control in both frontal BM and interparietal BM. However, immunohistochemistry using anti-CD138 antibody would have been helpful in defining tumours in these studies but this was not applicable to my samples. This study suggested that blocking N-cadherin may have a role to target the growth of myeloma tumours. This finding was also observed previously in solid tumours. Shintani et al

(2008) demonstrated that using a cyclic pentapeptide, ADH-1, targeting N-cadherin, significantly reduced growth and metastasis of pancreatic cancer cells in transgenic mice (Shintani et al., 2008). The limitation of this experiment could be the number of animal used. I used 3 animals per group to determine the growth of tumours in calvariae and this was due to the cost of animals. In addition, some published studies used 3 mice per group (Xie et al., 2009, Lo Celso et al., 2009, Hosokawa et al., 2010).

In addition, in this study I also addressed the effect of blocking N-cadherin on osteolysis in C57BL/KaLwRijHsd *in vivo* using the 5TGM1 model. After 21 days I observed that there was no difference in the osteolytic lesion number in the cortical bones when 5TGM1 cells were pre-treated with an anti-N-cadherin antibody compared with control. In addition, I observed there was no difference in the trabecular bone volume, trabecular number and trabecular thickness of 5TGM1-bearing mice when cells were pre-treated with anti-N-cadherin antibody compared with control. These results suggested that blocking N-cadherin in myeloma cells with anti-N-cadherin antibody did not affect myeloma bone disease and this could be due to N-cadherin turn over and doubling time of myeloma cells. Wein et al (2010) showed that N-cadherin was efficiently knocked down by siRNA in human mesenchymal stromal cells after 14 hours of the transfection and lasted for about 7 days suggesting a high protein turn over. After 7 days the N-cadherin expression levels slowly normalized again. Limitation for these experiments is that N-cadherin was only blocked in myeloma cells before they were injected into mice. Normalization of N-cadherin expression could be the reason why blocking N-cadherin in myeloma cells with anti-N-cadherin antibody did not affect myeloma bone disease. To resolve this issue, in future studies an alternative approach would be to use stable knock down of N-cadherin in myeloma cells or treat myeloma-bearing mice with anti-N-cadherin antibody instead of pre-treating the myeloma cells. Another limitation in this experiment could be the number of animals used. I used 3 animals per group to determine the growth of tumours in calvariae and this was due to the cost and availability of animals. In addition, some published studies used 3 mice per group (Xie et al., 2009, Lo Celso et al., 2009, Hosokawa et al., 2010).

This study interestingly showed that 5TGM1-bearing mice after 21 days induced osteolytic bone lesions in the lower cortical bones and not in the upper cortical bones. This is could be due to an increase in the percentage of osteoclasts on the lower endo-cortical surface of frontal, parietal and interparietal bones compared to the upper endo-cortical surface as discussed in **chapter 5**. In addition, the brain could be contributing to this osteolysis in the lower cortical bones. This implication would be investigated in future studies.

A number of conclusions can be drawn from these studies. Firstly, it is clear that N-cadherin is stably expressed by osteoblasts and is variably expressed by colonising myeloma cells. N-cadherin appears to be present at the interface between myeloma cells and osteoblasts but this is not exclusive. Myeloma cells away from bone also express N-cadherin. Attempts to block N-cadherin in these models by pre-incubation of cells with anti-N-cadherin antibody appeared to increase the distance of DiD labelled myeloma cells from bone and to produce a modest decrease in tumour volume in the interparietal and frontal bones, but this effect while significant was small and was not accompanied by decrease either cell numbers arriving or by alteration in lytic disease as might be expected in this model. Since this is the case, this data a preliminary and would gain more extensive validation with continuous blocking of N-cadherin using antibody systemically and with larger animal cohorts.

# 7 Chapter 7: General discussion and future work

## 7.1 General discussion

Present treatments for MM target end stage disease but understanding how bone lesions are initiated may offer new approaches to prevent/suppress colonization. It is clear that myeloma cells form specific interactions with the bone microenvironment, where they can remain dormant and protected from current therapy to eventually proliferate and cause disease progression. The aim of this study was to test the hypothesis that **myeloma cells utilise N-cadherin to adhere to osteoblasts *in vitro* and *in vivo* during colonization of myeloma cells into the bone**. In general terms, the data generated tends to support this hypothesis.

In this study, two myeloma models were used 5T33MM and 5TGM1. I have shown that these cells expressed N-cadherin. I used recombinant N-cadherin and calvarial mouse osteoblasts to study the adherence of myeloma cells *in vitro*. These observations supported the above hypothesis, as I showed that N-cadherin on myeloma cells has a role in the adhesion of myeloma cells to osteoblasts. My study demonstrated that there was a significant increase in the adhesion of myeloma cells to mature osteoblasts compared with immature osteoblasts as the expression of N-cadherin significantly increased in mature osteoblasts compared to immature osteoblasts. Blocking of N-cadherin by an N-cadherin specific antibody significantly decreased the adhesion of myeloma cells to pre-osteoblasts and mature osteoblasts *in vitro*.

In addition, in this study I addressed the effect of blocking N-cadherin on the homing of myeloma cells to the bone in C57BL/KaLwRijHsd mice. This study demonstrated that the blocking of N-cadherin by an N-cadherin specific antibody did not affect the homing of myeloma cells into the BM. In contrast, quiescent myeloma cells significantly homed farther from the bone when N-cadherin blocked with anti-N-cadherin antibody after 3 and 21 days in both frontal bones and interparietal bones. It also showed a small but significant reduction in overall myeloma tumour growth in

these bones at a later time point. However, this study demonstrated that there was no effect on the bone disease when N-cadherin was blocked by N-cadherin specific antibody and this could be due to N-cadherin turn over and doubling time of myeloma cells. As discussed in previous chapters, these finding are interesting but preliminary and need validation with alternative approaches to N-cadherin suppression *in vivo* and larger cohorts of animals. One approach would be to stably knock-down N-cadherin expression in myeloma cells and study their colonization compared to the present population. An alternative would be to use the N-cadherin blocking antibody or N-cadherin antagonist to treat myeloma-bearing mice during colonization with a continues dose of antibody to completely block N-cadherin and prevent N-cadherin turn over.

Blaschuk et al (1990) reported that extracellular-1 of the N-cadherin extracellular domain contains a His-Ala-Val (HAV) motif sequence, which plays an important role in N-cadherin functions (Blaschuk et al., 1990). ADH-1, N-Ac-CHAVC-NH2, is an agent targeting the HAV motif on extracellular-1 of N-cadherin and was recently used as N-cadherin antagonist agent. Shintani et al (2008) demonstrated that using a cyclic pentapeptide, ADH-1, targeting N-cadherin, significantly reduced the growth and metastasis of pancreatic cancer cells in transgenic mice (Shintani et al., 2008). In addition, Augustine et al (2008) showed that targeting N-cadherin with ADH-1 pentapeptide, in combination with a chemotherapy drug (Melphalan), was used as a novel therapeutic approach and significantly reduced tumour growth and enhanced the antitumor activity to treat melanoma (Augustine et al., 2008). Clinically, Beasley et al (2009) demonstrated that ADH-1 at a dose of 4000 mg in combination with melphalan on days 1 and 8 was used in phase I studies in melanoma patients and was a potential novel targeted therapy approach in melanoma (Beasley et al., 2009). In addition, monoclonal antibodies against the ectodomain of N-cadherin were recently used to target N-cadherin (Tanaka et al., 2010). Critically, no study has addressed blocking N-cadherin in myeloma in preclinical mouse models or in patients.

In HSCs, Zhang et al (2003) demonstrated that there is a correlation between an increase in the number of spindle-shaped N-cadherin$^{+}$CD45$^{-}$ osteoblastic cells and an increase in the number of HSCs. In addition, it was found that persistent HSCs attached to SNO cells via N-cadherin and β-catenin (Zhang et al., 2003). *In vitro,* Aria and Suda showed enhancements of both HSCs and stromal cell adhesion and inhibition of cell division of HSCs by enforced N-cadherin expression suggesting a key role of N-cadherin-mediated adhesion and maintaining HSCs quiescence in the osteoblastic niche (Arai and Suda, 2007). Using a new technology, *ex vivo* real-time imaging, and immunoassaying found that HSCs home to the 'osteoblast niche' via attachment to N-cadherin$^{+}$ osteoblasts on endosteal bone surfaces (Xie et al., 2009). In addition, Hosokawa et al (2010) showed that N-cadherin is expressed in long-term HSCs and in the osteoblasts mediating cell adhesion in the HSC niche. Knockdown of N-cadherin in HSCs reduced long-term engraftment activity of HSCs in the BM *in vivo* (Hosokawa et al., 2010). More recently, Arai et al (2012) showed that N-cadherin is in HSCs that promote the HSCs to be quiescence. Knockdown of N-cadherin showed a reduction in the long-term HSCs to the endosteal surfaces (Arai et al., 2012).

In contrast, Kiel et al (2009) showed that deleted N-cadherin from HSCs in adult Mx-1-Cre$^{+}$N-cadherin$^{fl/-}$ mice has no effect on hematopoiesis in the bone marrow. Deleted N-cadherin from HSCs did not affect HSC frequency, HSC maintenance, or function over time suggesting that N-cadherin expression by HSCs is not necessary for niche function (Kiel et al., 2009). Greenbaum et al (2012) ablated N-cadherin (*Cdh2*) in osteoblasts using Cdh2$^{flox/flox}$ Osx-Cre mice. Ablated N-cadherin did not affect HSC number, cell cycle status, long-term repopulating activity, and self-renewal capacity suggesting that N-cadherin expression in osteoblast lineage cells is dispensable for HSC maintenance in mice (Greenbaum et al., 2012). In my study myeloma cells could still colonize after treatment with N-cadherin antibody and form bone lesions. This may be because the efficacy of blocking was less than 100% with the approach used or could indicate that N-cadherin is just one of a member of molecules, such as Notch/Jag, Tie2/Ang-1 or CXCR4/CXCL12, required for myeloma colonization in bone.

Increasing evidence indicates that expression of N-cadherin in solid tumour cells including melanoma, breast cancer, prostatic cancer, gastric carcinoma, bladder carcinoma, overian carcinoma and pancreatic cancer mediates the invasion, metastasis and interaction of cancer cells from their primary site to establish new interactions with the surrounding microenvironment (Li et al., 2001, Augustine et al., 2008, Hazan et al., 2004, Tanaka et al., 2010, Yanagimoto et al., 2001, Lascombe et al., 2006, Sarrio et al., 2006, Shintani et al., 2008). N-cadherin has an important role in tumour development by forming cell-cell junctions mediating tumour cell invasion and promoting cancer cell survival. A cyclic pentapeptide (ADH-1, N-Ac-CHAVC-NH2, agent targeting the HAV motif on EC1 of N-cadherin) was recently used as an anticancer agent. Shintani et al (2008) showed ADH-1 (50 mg/kg, 1 per day, 5 per week for 4 weeks) significantly reduced growth and metastasis of pancreatic cancer cells in transgenic mice (Shintani et al., 2008). In addition, a monoclonal anti-N-cadherin antibody was recently used as an anticancer agent. Tanaka et al (2010) demonstrated that prostate cancer metastasis and castration resistance are mainly caused by N-cadherin. Targeting N-cadherin using monoclonal antibody (500 μl at 10 or 20 mg per kg twice weekly) against N-cadherin showed a reduction in proliferation, adhesion, invasion of prostate cancer cells and delays the castration resistance progression (Tanaka et al., 2010).

In myeloma, Groen et al (2011) showed that myeloma cells express N-cadherin and this expression mediates the interaction of myeloma cells with the BM microenvironment, in particular the osteoblasts (Groen et al., 2011). From the above it would seem that targeting N-cadherin could have complex effects. On one hand, blocking tumour N-cadherin would be likely to reduce the numbers of cells arriving in niches but on the other, the lack of the growth inhibition provided by the niche, could allow those tumours that did arrive to proliferate. This suggests that targeting N-cadherin would have to be considered carefully. One approach could be to target N-cadherin to prevent myeloma cells residing in niche in a quiescent state and simultaneously to use cytotoxic drugs to target proliferating cells. This may be an approach to combat tumour dormancy in patients, a major problem in myeloma and other tumour types.

In this study, we showed that there was a positive correlation between increased N-cadherin mRNA expression and differentiation during osteoblastogenesis suggesting low levels of N-cadherin expression in pre-osteoblasts and relatively high levels of N-cadherin expression in mature osteoblasts. These observations are supported with previous work done by Ferrari et al (2000) and by Kawaguchi et al (2001) that demonstrated an increase in the relative expression of N-cadherin mRNA during osteoblastogenesis (Ferrari et al., 2000, Kawaguchi et al., 2001). In contrast, Greenbaum et al (2012) demonstrated a decrease in the relative expression of N-cadherin during osteoblastogenesis using western blot and this may be due to differences in culture conditions and N-cadherin analysis methods. They reported that osteoblasts were originated from $Cdh2^{flox/flox}$ mice, backcrossed to more than 99% congenic with the C57BL/6 background. In addition, for differentiation they used 20% FCS, 50 μM ascorbic acid and 10 μM β-glycerophosphate (Greenbaum et al., 2012). However, my data clearly showed an increase in the relative levels of N-cadherin mRNA and protein during osteoblastogenesis in culture using TaqMan analysis, immunofluorescence and western blot. This may be important: in interactions with mature osteoblasts the attachment of myeloma cells would be likely to be less directed due to the ubiquitous distribution of N-cadherin.

My study showed by immunohistochemistry that myeloma favoured attachment to N-cadherin at junctions. The functional significance of junction versus random N-cadherin in relation to myeloma attachment needs to be investigated. Moreover, this study showed that N-cadherin is expressed in murine myeloma cell lines; 5T33MM and 5TGM1. A novel finding was that expression of N-cadherin in both 5T33MM cells and 5TGM1 cells was focal when evaluated using immunofluorescence and immunocytochemistry similar to N-cadherin expression in mouse HSCs (Xie et al., 2009) and human HSCs (Wein et al., 2010). In addition, we found that N-cadherin expression and surface levels of N-cadherin are higher in 5TGM1 cells than in 5T33MM cells.

Groen et al (2011) showed that myeloma cells adhere to osteoblasts, and this adhesion could be prevented by using an N-cadherin blocking antibody (Groen et al., 2011). However, they did not show the differences between the adhesions of myeloma cells with immature or mature osteoblasts. In this study, we showed that *in vitro* there was a higher frequency of myeloma cells adherence to mature osteoblasts compared with immature osteoblasts. This may reflect the expression of N-cadherin which this study showed significantly higher in mature osteoblasts compared to pre-osteoblast. However as discussed above, I observed that N-cadherin was expressed at the junction between myeloma cells and osteoblasts, and this long term significance of attachment to cell surfaces or junctions is unknown in respect of control of myeloma growth or quiescence. Furthermore, we showed that N-cadherin blocking antibody (10 μg/mL) reduced the adhesion of myeloma cells to osteoblasts *in vitro*. Together these data strongly suggest that N-cadherin is an important mediator in the interaction between myeloma cells and osteoblasts at least in the early stages of attachment.

C57BL/KaLwRijHsd mice develop high frequency of monoclonal proliferative B-cell disorders. Cells within BM provide a microenvironment for myeloma cells where these tumours can survive and drug resistance can be acquired. To study these processes, murine models of multiple myeloma have been developed over the last four decades. 5TMM series a myeloma models originate from spontaneously developed MM in C57BL/KaLwRijHsd mice and have many of the features of the disease in humans (Radl et al., 1978, Radl et al., 1979, Vanderkerken et al., 1997). In this study, I analysed the discrete micro-anatomical sites within calvarial bones and showed that the interparietal bones of calvariae in C57BL/KaLwRijHsd mice have distinct micro-anatomical features compared to frontal and parietal bones. I found that interparietal bones contained higher BM area compared to frontal and parietal bones. In addition, I found that interparietal bones contained a higher percentage of osteoblast surfaces and bone turnover compared with frontal and parietal bones. In contrast, interparietal bones contained a lower percentage of bone lining cell surfaces compared with frontal and parietal bones. However, there was no difference in the percentage of osteoclast

surfaces between frontal, parietal and interparietal bones. These defined differences between the calvarial bones offer an opportunity to study the different requirements for myeloma growth offered by these microenvironments.

Oyajobi et al (2007) demonstrated the murine myeloma 5TGM1-GFP cells tumour were detectable in calvarial BM between 10-14 days post-inoculation suggesting that these myeloma cells home to calvarial BM (Oyajobi et al., 2007). However, this study lacked the imaging capability to study single cell arrival in calvarial BM. To date, there is no publication demonstrating that the murine myeloma 5T33MM cells can home to calvarial BM in C57BL/KaLwRijHsd mice. Previous studies demonstrated that tumour cells metastasize to skeletal sites with active bone turnover (Schneider et al., 2005, van der Pluijm et al., 2005). In this study, myeloma cells were inoculated into C57BL/KaLwRijHsd mice for 3 weeks. Interestingly, we showed that both 5T33MM and 5TGM1 form large tumours in interparietal bones and not in frontal or parietal bones. One potential explanation for this is that the interparietal bones contain higher BM area, higher bone surface area and higher bone turnover compared to frontal and parietal bones, but there is also another explanation: that there is a difference in the cellular composition, particularly in osteoblasts, between these bones.

Xie et al (2009) have recently used a confocal laser scanning microscope LSM 510, multiphoton microscopy, to trace the homing of $GFP^+$ HSCs and determining the distribution of these cells in the BM (Xie et al., 2009). In this study, myeloma cells were labelled with DiD (Invitrogen, UK), a dye bound to phospholipid bilayer membranes of the cells. Previous work in the Sheffield labs demonstrated that myeloma cells lose their DiD labelling during cell proliferation *in vitro*. However, some cells retained staining suggesting that these cells are mitotically quiescent. I found that there was an increase in the numbers of DiD positive, 5T33MM and 5TGM1, myeloma cells observed in the interparietal BM compared to the frontal and parietal BM after 3 days. In addition, I found that there was an increase in the numbers of DiD positive, 5T33MM and 5TGM1,

myeloma cells observed in the interparietal BM compared to the frontal and parietal BM after 3 weeks. These observations indicate that although there is an increased frequency of myeloma cell arrival in the interparietal bone compared to other calvarial bones, tumour cells nevertheless do arrive in the frontal BM and parietal BM. The frequency of growing tumours in these bones suggests that there are differences in activation of proliferation in colonizing tumour cells provided by these bone microenvironments. The presence of apparently quiescent cells as long as 21 days after injection is also interesting since it suggests that these cells are growth suppressed, possibly within niches, as they are present alongside rapidly growing myeloma populations.

In this study, myeloma cells were inoculated into C57BL/KaLwRijHsd mice and after 7 days mice were harvested and calvariae were dissected. Rabbit monoclonal anti-N-cadherin antibody (Millipore, UK) (1:200 dilution) or donkey anti-rabbit IgG antibodies (R&D systems, UK) (1:200 dilution), isotype negative control were used to determine if N-cadherin was present in the points of adhesion of myeloma cells, 5T33MM and 5TGM1 to osteoblasts *in vivo*. Interestingly, we found that the majority of osteoblast lineage cells expressed N-cadherin. This observation supported work done by Ferrari et al (2000) who demonstrated that N-cadherin was expressed in rat and human bone *in vivo* (Ferrari et al., 2000). In addition, we observed that N-cadherin was localized at the junction between myeloma cells and osteoblasts *in vivo* using immunohistochemistry in mouse sections. This observation supports work done by Groen et al (2011) who demonstrated that expression of N-cadherin is often localized between MM cells and the bone-lining cells using immunohistochemistry (Groen et al., 2011).

Using ADH-1 or monoclonal antibody against N-cadherin to inhibit adhesion of myeloma cells to osteoblasts will produce functional information for the role of N-cadherin in myeloma-osteoblast interaction. In this study, 5T33MM cells were pre-treated with 10 μg/ml of anti-N-cadherin antibody or 10 μg/ml of mouse IgG1 antibody. I observed that when 5T33MM cells pre-treated with anti-N-cadherin antibody,

myeloma cells have homed significantly further from bone compared with 5T33MM cells control and with 5T33MM cells pre-treated with isotype control antibody in frontal and interparietal bones after 3 days. These results suggested that blocking N-cadherin in myeloma cells may have a role in targeting the colonization of myeloma cells into the bone. In a separate study, 5TGM1 cells were pre-treated with 10 μg/ml of anti-N-cadherin antibody or 10 μg/ml of mouse IgG1 antibody. Again I observed that when these cells were pre-treated with anti-N-cadherin antibody, they homed further from bone with a modest reduction in myeloma tumour size at day 21 in frontal and interparietal bones compared with 5TGM1 cells control and with 5TGM1 cells pre-treated with isotype control antibody. However, immunohistochemistry using anti-CD138 antibody would have been helpful in defining tumours in these studies but this was not applicable to my samples. These were preliminary studies as has been discussed elsewhere in this thesis. Taken together, these results while interesting need to be repeated and alternative approaches for myeloma N-cadherin blocking considered.

In addition, I analysed the effect of blocking N-cadherin on myeloma bone disease in interparietal bones. I observed that there were no differences in the osteolytic lesion number in the cortical bones and there were no differences in the trabecular bone volume, trabecular number and trabecular thickness when 5TGM1 cells were pre-treated with anti-N-cadherin antibody compared with 5TGM1-bearing mice or compared with 5TGM1 pre-treated with isotype control antibody in interparietal bones of myeloma-bearing mice after 21 days. These results suggested that blocking N-cadherin in myeloma cells with anti-N-cadherin antibody did not affect myeloma bone disease and this may be due to the efficacy of blocking with the approach used. Alternatively, this could be due to the N-cadherin turn over and doubling time of myeloma cells. This was observed previously by Wein et al (2010) who showed that N-cadherin was knocked down in human mesenchymal stromal cells but this was lasted for about a week, then the levels of N-cadherin expression slowly normalized again (Wein et al., 2010).

Recent studies have shown the early stages of myeloma development are dependent on the surrounding BM microenvironment. However, in late stage disease the myeloma cells are not BM microenvironment depended. As mentioned before, the BM microenvironment promotes the survival and growth of myeloma cells. Several molecules and cytokines have been identified that mediate MM pathogenesis by stimulating the expansion of myeloma cells that ultimately affects bone. Most MM treatment strategies focus on stopping MM activity: melphalan or zoledronic acid, or to stop the interaction of MM cells to BM stromal cells: Denosumab, Lenalidomide, Thalidomide or Bortezomib (Andrews et al., 2013). This study focused to disrupt the colonizing of myeloma cells by one of the molecular machinery of HSCs, N-cadherin, and hijack the HSC niche. I think stopping colonization of myeloma cells into the niche in combination with anti-tumour agent could be completely cure MM patients.

In conclusion, figure 7.1 shows a model of a possible interaction between N-cadherin positive myeloma cells and N-cadherin positive osteoblasts in the HSC niche or bone microenvironment. TaqMan analysis of calvarial mouse primary osteoblast cDNA obtained from cultures over time courses during differentiation demonstrated that N-cadherin expression is increased in mature osteoblasts compared with immature osteoblasts. N-cadherin positive myeloma cells home to the endosteal surfaces and bind to an as yet undefined population of osteoblasts expressing N-cadherin. Here they survive in a quiescent state for extended periods. In response to an initiating event, myeloma cells are released from their quiescent state and start growing. My studies support the concept of myeloma cells interacting with osteoblasts through N-cadherin but the nature of the trigger for releasing attachment remains to be determined. The concept of myeloma quiescence and its maintenance also requires further studies. Targeting N-cadherin using monoclonal antibody against N-cadherin showed a reduction in the adhesion of myeloma cells to osteoblasts *in vitro* and showed some effects on adhesion of myeloma cells to bone and on tumour size *in vivo*. However, these finding are interesting but preliminary and need validation with alternative approaches to N-cadherin suppression *in vivo* and larger cohorts of animals.

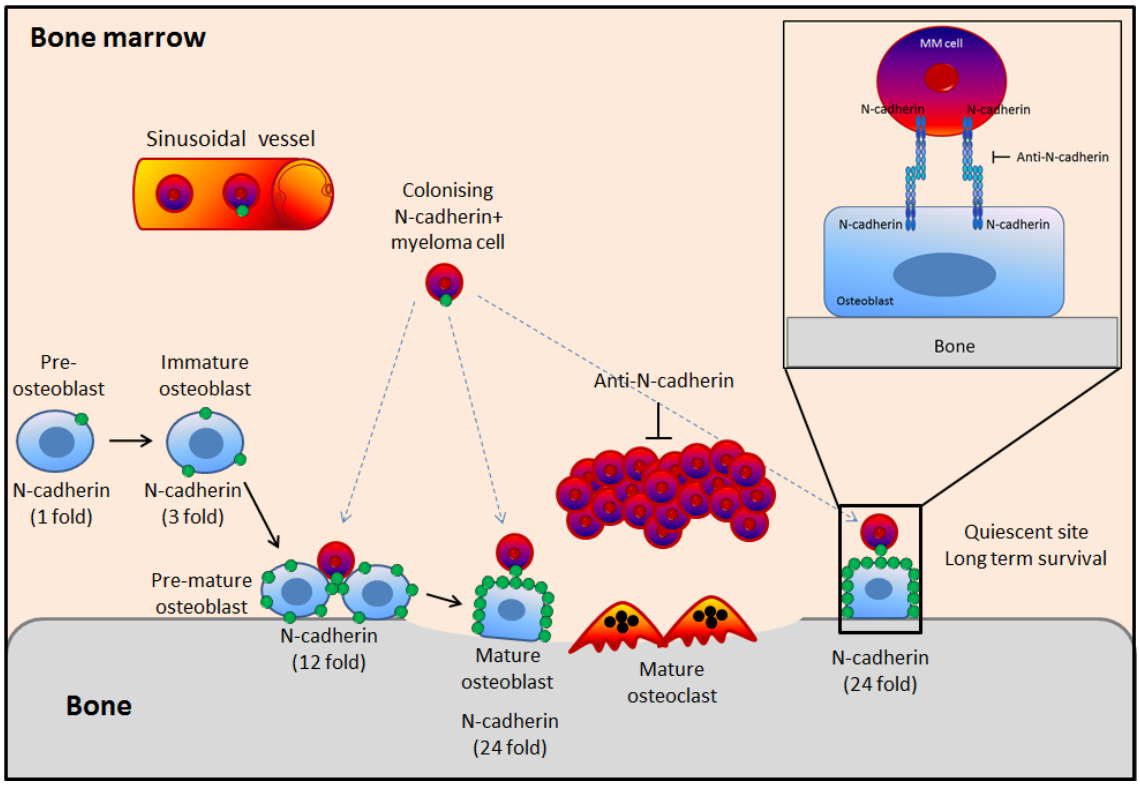


**Figure 7.1: Model of the possible interaction between N-cadherin$^+$ myeloma and N-cadherin$^+$ osteoblast in the HSC niche.** TaqMan analysis of calvarial mouse primary osteoblast cDNA obtained from cultures over time course during differentiation demonstrated expression of N-cadherin is increased during osteoblastogenesis. N-cadherin$^+$ myeloma cells more probably bind to a population of osteoblasts expressing high level of N-cadherin. Targeting N-cadherin using monoclonal antibody against N-cadherin showed a reduction in the tumour growth and adhesion of myeloma cells to osteoblasts.

## 7.2 Future work

Future studies need to be done to more effectively block N-cadherin function in myeloma cells. Hosokawa et al (2010) showed that N-cadherin is expressed in long-term HSCs and in the osteoblasts mediating cells adhesion in the HSC niche. Knockdown of N-cadherin showed a reduction in the long-term engraftment activity of HSCs in the BM *in vivo* (Hosokawa et al., 2010). In addition, Arai et al (2012) showed that Knockdown of N-cadherin reduced the long-term HSCs to the endosteal surfaces (Arai et al., 2012). In future work, N-cadherin should be knocked-down in myeloma cells and these myeloma cells inoculated into mice to determine the effect of depleting N-cadherin levels on myeloma colonization in bone, on tumour growth and on myeloma bone disease.

Tanaka et al (2010) demonstrated that prostate cancer metastasis and castration resistance was induced by N-cadherin. Targeting N-cadherin using monoclonal antibody against N-cadherin showed a reduction in proliferation, adhesion and invasion of prostate cancer cells *in vitro* and delayed the castration resistance progression *in vivo* (Tanaka et al., 2010). In future work, monoclonal antibodies against the ectodomain of N-cadherin could be generated to treat myeloma-bearing mice instead of pre-treating the myeloma cells then injecting them into mice as I did, to determine the effect of N-cadherin on myeloma colonization in bone, on tumour growth and on bone disease. Alternatively, ADH-1 pentapeptide, an agent targeting ectodomain of N-cadherin, could be used to determine the effect of N-cadherin on myeloma colonization in bone, on tumour growth and on myeloma bone disease. Earlier studies by Shintani et al (2008) demonstrated that using the cyclic ADH-1 pentapeptide significantly reduced growth and metastasis of pancreatic cancer cells in transgenic mice (Shintani et al., 2008).

Augustine et al (2001) showed that N-cadherin was expressed in human melanoma-derived cell lines. Targeting N-cadherin with ADH-1 pentapeptide in combination with chemotherapy drug (Melphalan) was used as a novel therapeutic approach significantly reduced tumour growth and enhanced the antitumor activity of Melphalan (Augustine et al., 2008). Clinically, Beasley et al (2009) demonstrated that ADH-1 at a dose of 4000 mg in combination with melphalan on days 1 and 8 was safe and well tolerated by patient in phase I studies and provided novel targeted therapy approach in melanoma (Beasley et al., 2009). In addition, Vitovski et al (2012) demonstrated that targeting tumour-initiating cells with TRAIL, tumour necrosis factor-related apoptosis-inducing ligand, in combination with doxorubicin completely eradicated of MM cells *in vivo* (Vitovski et al., 2012). Future studies could be performed with combination treatments such as ADH-1 or a monoclonal antibody against N-cadherin in combination with chemotherapic agents such as TRAIL or doxorubicin or in combination with bone anabolic agents such as anti-Dkk1 or anti-Activin-A.

## References


AARDEN, E. M., BURGER, E. H. & NIJWEIDE, P. J. 1994. Function of osteocytes in bone. *J Cell Biochem,* 55**,** 287-99.

AKASHI, K., TRAVER, D., MIYAMOTO, T. & WEISSMAN, I. L. 2000. A clonogenic common myeloid progenitor that gives rise to all myeloid lineages. *Nature,* 404**,** 193-7.

ALICI, E., KONSTANTINIDIS, K. V., AINTS, A., DILBER, M. S. & ABEDI-VALUGERDI, M. 2004. Visualization of 5T33 myeloma cells in the C57BL/KaLwRij mouse: establishment of a new syngeneic murine model of multiple myeloma. *Exp Hematol,* 32**,** 1064-72.

ALSAYED, Y., NGO, H., RUNNELS, J., LELEU, X., SINGHA, U. K., PITSILLIDES, C. M., SPENCER, J. A., KIMLINGER, T., GHOBRIAL, J. M., JIA, X., LU, G., TIMM, M., KUMAR, A., COTE, D., VEILLEUX, I., HEDIN, K. E., ROODMAN, G. D., WITZIG, T. E., KUNG, A. L., HIDESHIMA, T., ANDERSON, K. C., LIN, C. P. & GHOBRIAL, I. M. 2007. Mechanisms of regulation of CXCR4/SDF-1 (CXCL12)-dependent migration and homing in multiple myeloma. *Blood,* 109**,** 2708-17.

ANDREWS, S. W., KABRAH, S., MAY, J. E., DONALDSON, C. & MORSE, H. R. 2013. Multiple myeloma: the bone marrow microenvironment and its relation to treatment. *Br J Biomed Sci,* 70**,** 110-20.

ARAI, F., HIRAO, A., OHMURA, M., SATO, H., MATSUOKA, S., TAKUBO, K., ITO, K., KOH, G. Y. & SUDA, T. 2004. Tie2/angiopoietin-1 signaling regulates hematopoietic stem cell quiescence in the bone marrow niche. *Cell,* 118**,** 149-61.

ARAI, F., HOSOKAWA, K., TOYAMA, H., MATSUMOTO, Y. & SUDA, T. 2012. Role of N-cadherin in the regulation of hematopoietic stem cells in the bone marrow niche. *Ann N Y Acad Sci,* 1266**,** 72-7.

ARAI, F. & SUDA, T. 2007. Maintenance of quiescent hematopoietic stem cells in the osteoblastic niche. *Ann N Y Acad Sci,* 1106**,** 41-53.

ASKMYR, M., SIMS, N. A., MARTIN, T. J. & PURTON, L. E. 2009. What is the true nature of the osteoblastic hematopoietic stem cell niche? *Trends Endocrinol Metab,* 20**,** 303-9.

ASOSINGH, K., GUNTHERT, U., BAKKUS, M. H., DE RAEVE, H., GOES, E., VAN RIET, I., VAN CAMP, B. & VANDERKERKEN, K. 2000a. In vivo induction of insulin-like growth factor-I receptor and CD44v6 confers homing and adhesion to murine multiple myeloma cells. *Cancer Res,* 60**,** 3096-104.

ASOSINGH, K., RADL, J., VAN RIET, I., VAN CAMP, B. & VANDERKERKEN, K. 2000b. The 5TMM series: a useful in vivo mouse model of human multiple myeloma. *Hematol J,* 1**,** 351-6.

AUGUSTINE, C. K., YOSHIMOTO, Y., GUPTA, M., ZIPFEL, P. A., SELIM, M. A., FEBBO, P., PENDERGAST, A. M., PETERS, W. P. & TYLER, D. S. 2008. Targeting N-cadherin enhances antitumor activity of cytotoxic therapies in melanoma treatment. *Cancer Res,* 68**,** 3777-84.

AZAB, A. K., HU, J., QUANG, P., AZAB, F., PITSILLIDES, C., AWWAD, R., THOMPSON, B., MAISO, P., SUN, J. D., HART, C. P., ROCCARO, A. M., SACCO, A., NGO, H. T., LIN, C. P., KUNG, A. L., CARRASCO, R. D., VANDERKERKEN, K. & GHOBRIAL, I. M. 2012. Hypoxia promotes dissemination of multiple myeloma through acquisition of epithelial to mesenchymal transition-like features. *Blood,* 119**,** 5782-94.

AZAB, A. K., RUNNELS, J. M., PITSILLIDES, C., MOREAU, A. S., AZAB, F., LELEU, X., JIA, X., WRIGHT, R., OSPINA, B., CARLSON, A. L., ALT, C., BURWICK, N., ROCCARO, A. M., NGO, H. T., FARAG, M., MELHEM, M. R., SACCO, A., MUNSHI, N. C., HIDESHIMA, T., ROLLINS, B. J., ANDERSON, K. C., KUNG, A. L., LIN, C. P. & GHOBRIAL, I. M. 2009. CXCR4 inhibitor AMD3100 disrupts the interaction of multiple

myeloma cells with the bone marrow microenvironment and enhances their sensitivity to therapy. *Blood,* 113**,** 4341-51.

BANCROFT, G. N., SIKAVITSAS, V. I., VAN DEN DOLDER, J., SHEFFIELD, T. L., AMBROSE, C. G., JANSEN, J. A. & MIKOS, A. G. 2002. Fluid flow increases mineralized matrix deposition in 3D perfusion culture of marrow stromal osteoblasts in a dose-dependent manner. *Proc Natl Acad Sci U S A,* 99**,** 12600-5.

BARLOGIE, B., RABER, M. N., SCHUMANN, J., JOHNSON, T. S., DREWINKO, B., SWARTZENDRUBER, D. E., GOHDE, W., ANDREEFF, M. & FREIREICH, E. J. 1983. Flow cytometry in clinical cancer research. *Cancer Res,* 43**,** 3982-97.

BEASLEY, G. M., MCMAHON, N., SANDERS, G., AUGUSTINE, C. K., SELIM, M. A., PETERSON, B., NORRIS, R., PETERS, W. P., ROSS, M. I. & TYLER, D. S. 2009. A phase 1 study of systemic ADH-1 in combination with melphalan via isolated limb infusion in patients with locally advanced in-transit malignant melanoma. *Cancer,* 115**,** 4766-74.

BLASCHUK, O. W., SULLIVAN, R., DAVID, S. & POULIOT, Y. 1990. Identification of a cadherin cell adhesion recognition sequence. *Dev Biol,* 139**,** 227-9.

BONEWALD, L. F. 2011. The amazing osteocyte. *J Bone Miner Res,* 26**,** 229-38.

BOYLE, W. J., SIMONET, W. S. & LACEY, D. L. 2003. Osteoclast differentiation and activation. *Nature,* 423**,** 337-42.

BRITISH COMMITTEE FOR STANDARDS IN HAEMATOLOGY, U. M. F. 2001. Diagnosis and management of multiple myeloma. *Br J Haematol,* 115**,** 522-40.

BROXMEYER, H. E., ORSCHELL, C. M., CLAPP, D. W., HANGOC, G., COOPER, S., PLETT, P. A., LILES, W. C., LI, X., GRAHAM-EVANS, B., CAMPBELL, T. B., CALANDRA, G., BRIDGER, G., DALE, D. C. & SROUR, E. F. 2005. Rapid mobilization of murine and human hematopoietic stem and progenitor cells with AMD3100, a CXCR4 antagonist. *The Journal of experimental medicine,* 201**,** 1307-18.

BUCAY, N., SAROSI, I., DUNSTAN, C. R., MORONY, S., TARPLEY, J., CAPPARELLI, C., SCULLY, S., TAN, H. L., XU, W., LACEY, D. L., BOYLE, W. J. & SIMONET, W. S. 1998. osteoprotegerin-deficient mice develop early onset osteoporosis and arterial calcification. *Genes Dev,* 12**,** 1260-8.

BURGER, J. A. & KIPPS, T. J. 2006. CXCR4: a key receptor in the crosstalk between tumor cells and their microenvironment. *Blood,* 107**,** 1761-7.

CALVI, L. M., ADAMS, G. B., WEIBRECHT, K. W., WEBER, J. M., OLSON, D. P., KNIGHT, M. C., MARTIN, R. P., SCHIPANI, E., DIVIETI, P., BRINGHURST, F. R., MILNER, L. A., KRONENBERG, H. M. & SCADDEN, D. T. 2003. Osteoblastic cells regulate the haematopoietic stem cell niche. *Nature,* 425**,** 841-6.

CHANTRY, A. D., HEATH, D., MULIVOR, A. W., PEARSALL, S., BAUD'HUIN, M., COULTON, L., EVANS, H., ABDUL, N., WERNER, E. D., BOUXSEIN, M. L., KEY, M. L., SEEHRA, J., ARNETT, T. R., VANDERKERKEN, K. & CROUCHER, P. 2010. Inhibiting activin-A signaling stimulates bone formation and prevents cancer induced bone destruction in vivo. *J Bone Miner Res*.

CHEN, D., ZHAO, M. & MUNDY, G. R. 2004. Bone morphogenetic proteins. *Growth Factors,* 22**,** 233-41.

CHOI, S. J., CRUZ, J. C., CRAIG, F., CHUNG, H., DEVLIN, R. D., ROODMAN, G. D. & ALSINA, M. 2000. Macrophage inflammatory protein 1-alpha is a potential osteoclast stimulatory factor in multiple myeloma. *Blood,* 96**,** 671-5.

CHRISTOFORI, G. 2006. New signals from the invasive front. *Nature,* 441**,** 444-50.

CIOLCZYK-WIERZBICKA, D., AMORESANO, A., CASBARRA, A., HOJA-LUKOWICZ, D., LITYNSKA, A. & LAIDLER, P. 2004. The structure of the oligosaccharides of N-cadherin from human melanoma cell lines. *Glycoconj J,* 20**,** 483-92.

COHEN, M. M., JR. 2006. The new bone biology: pathologic, molecular, and clinical correlates. *Am J Med Genet A,* 140**,** 2646-706.

COLLIN-OSDOBY, P., ROTHE, L., BEKKER, S., ANDERSON, F., HUANG, Y. & OSDOBY, P. 2002. Basic fibroblast growth factor stimulates osteoclast recruitment, development, and

bone pit resorption in association with angiogenesis in vivo on the chick chorioallantoic membrane and activates isolated avian osteoclast resorption in vitro. *J Bone Miner Res,* 17**,** 1859-71.

COLLINS, C. D. 2005. Problems monitoring response in multiple myeloma. *Cancer Imaging,* 5 Spec No A**,** S119-26.

CROUCHER, P. I., DE HENDRIK, R., PERRY, M. J., HIJZEN, A., SHIPMAN, C. M., LIPPITT, J., GREEN, J., VAN MARCK, E., VAN CAMP, B. & VANDERKERKEN, K. 2003. Zoledronic acid treatment of 5T2MM-bearing mice inhibits the development of myeloma bone disease: evidence for decreased osteolysis, tumor burden and angiogenesis, and increased survival. *J Bone Miner Res,* 18**,** 482-92.

CROUCHER, P. I., SHIPMAN, C. M., LIPPITT, J., PERRY, M., ASOSINGH, K., HIJZEN, A., BRABBS, A. C., VAN BEEK, E. J., HOLEN, I., SKERRY, T. M., DUNSTAN, C. R., RUSSELL, G. R., VAN CAMP, B. & VANDERKERKEN, K. 2001. Osteoprotegerin inhibits the development of osteolytic bone disease in multiple myeloma. *Blood,* 98**,** 3534-40.

DALLAS, S. L., GARRETT, I. R., OYAJOBI, B. O., DALLAS, M. R., BOYCE, B. F., BAUSS, F., RADL, J. & MUNDY, G. R. 1999. Ibandronate reduces osteolytic lesions but not tumor burden in a murine model of myeloma bone disease. *Blood,* 93**,** 1697-706.

DAMIANO, J. S., CRESS, A. E., HAZLEHURST, L. A., SHTIL, A. A. & DALTON, W. S. 1999. Cell adhesion mediated drug resistance (CAM-DR): role of integrins and resistance to apoptosis in human myeloma cell lines. *Blood,* 93**,** 1658-67.

DAMIANO, J. S. & DALTON, W. S. 2000. Integrin-mediated drug resistance in multiple myeloma. *Leuk Lymphoma,* 38**,** 71-81.

DATTA, H. K., NG, W. F., WALKER, J. A., TUCK, S. P. & VARANASI, S. S. 2008. The cell biology of bone metabolism. *J Clin Pathol,* 61**,** 577-87.

DAY, T. F., GUO, X., GARRETT-BEAL, L. & YANG, Y. 2005. Wnt/beta-catenin signaling in mesenchymal progenitors controls osteoblast and chondrocyte differentiation during vertebrate skeletogenesis. *Dev Cell,* 8**,** 739-50.

DI LULLO, G. A., SWEENEY, S. M., KORKKO, J., ALA-KOKKO, L. & SAN ANTONIO, J. D. 2002. Mapping the ligand-binding sites and disease-associated mutations on the most abundant protein in the human, type I collagen. *J Biol Chem,* 277**,** 4223-31.

DING, L. & MORRISON, S. J. 2013. Haematopoietic stem cells and early lymphoid progenitors occupy distinct bone marrow niches. *Nature,* 495**,** 231-5.

DING, L., SAUNDERS, T. L., ENIKOLOPOV, G. & MORRISON, S. J. 2012. Endothelial and perivascular cells maintain haematopoietic stem cells. *Nature,* 481**,** 457-62.

DOWNEY, P. A. & SIEGEL, M. I. 2006. Bone biology and the clinical implications for osteoporosis. *Phys Ther,* 86**,** 77-91.

DRING, A. M., DAVIES, F. E., FENTON, J. A., RODDAM, P. L., SCOTT, K., GONZALEZ, D., ROLLINSON, S., RAWSTRON, A. C., REES-UNWIN, K. S., LI, C., MUNSHI, N. C., ANDERSON, K. C. & MORGAN, G. J. 2004. A global expression-based analysis of the consequences of the t(4;14) translocation in myeloma. *Clin Cancer Res,* 10**,** 5692-701.

DU, S. J., FRENKEL, V., KINDSCHI, G. & ZOHAR, Y. 2001. Visualizing normal and defective bone development in zebrafish embryos using the fluorescent chromophore calcein. *Dev Biol,* 238**,** 239-46.

DUCY, P., DESBOIS, C., BOYCE, B., PINERO, G., STORY, B., DUNSTAN, C., SMITH, E., BONADIO, J., GOLDSTEIN, S., GUNDBERG, C., BRADLEY, A. & KARSENTY, G. 1996. Increased bone formation in osteocalcin-deficient mice. *Nature,* 382**,** 448-52.

DUCY, P., SCHINKE, T. & KARSENTY, G. 2000. The osteoblast: a sophisticated fibroblast under central surveillance. *Science,* 289**,** 1501-4.

DUCY, P., ZHANG, R., GEOFFROY, V., RIDALL, A. L. & KARSENTY, G. 1997. Osf2/Cbfa1: a transcriptional activator of osteoblast differentiation. *Cell,* 89**,** 747-54.

EDWARDS, C. M., LWIN, S. T., FOWLER, J. A., OYAJOBI, B. O., ZHUANG, J., BATES, A. L. & MUNDY, G. R. 2009. Myeloma cells exhibit an increase in proteasome activity and an

enhanced response to proteasome inhibition in the bone marrow microenvironment in vivo. *Am J Hematol,* 84**,** 268-72.

EDWARDS, C. M., ZHUANG, J. & MUNDY, G. R. 2008. The pathogenesis of the bone disease of multiple myeloma. *Bone,* 42**,** 1007-13.

EHRLICH, L. A., CHUNG, H. Y., GHOBRIAL, I., CHOI, S. J., MORANDI, F., COLLA, S., RIZZOLI, V., ROODMAN, G. D. & GIULIANI, N. 2005. IL-3 is a potential inhibitor of osteoblast differentiation in multiple myeloma. *Blood,* 106**,** 1407-14.

ENGIN, F. & LEE, B. 2010. NOTCHing the bone: insights into multi-functionality. *Bone,* 46**,** 274-80.

ESTEVE, F. R. & ROODMAN, G. D. 2007. Pathophysiology of myeloma bone disease. *Best Pract Res Clin Haematol,* 20**,** 613-24.

EVERTS, V., DELAISSE, J. M., KORPER, W., JANSEN, D. C., TIGCHELAAR-GUTTER, W., SAFTIG, P. & BEERTSEN, W. 2002. The bone lining cell: its role in cleaning Howship's lacunae and initiating bone formation. *J Bone Miner Res,* 17**,** 77-90.

FERRARI, S. L., TRAIANEDES, K., THORNE, M., LAFAGE-PROUST, M. H., GENEVER, P., CECCHINI, M. G., BEHAR, V., BISELLO, A., CHOREV, M., ROSENBLATT, M. & SUVA, L. J. 2000. A role for N-cadherin in the development of the differentiated osteoblastic phenotype. *J Bone Miner Res,* 15**,** 198-208.

FERRETTI, M., PALUMBO, C., CONTRI, M. & MAROTTI, G. 2002. Static and dynamic osteogenesis: two different types of bone formation. *Anat Embryol (Berl),* 206**,** 21-9.

FILGUEIRA, L. 2004. Fluorescence-based staining for tartrate-resistant acidic phosphatase (TRAP) in osteoclasts combined with other fluorescent dyes and protocols. *J Histochem Cytochem,* 52**,** 411-4.

FISCHER, A. H., JACOBSON, K. A., ROSE, J. & ZELLER, R. 2008. Hematoxylin and eosin staining of tissue and cell sections. *CSH Protoc,* 2008**,** pdb prot4986.

FLIEDNER, T. M. 1998. The role of blood stem cells in hematopoietic cell renewal. *Stem Cells,* 16**,** 361-74.

FOWLER, J. A., MUNDY, G. R., LWIN, S. T. & EDWARDS, C. M. 2012. Bone marrow stromal cells create a permissive microenvironment for myeloma development: a new stromal role for Wnt inhibitor Dkk1. *Cancer Res,* 72**,** 2183-9.

GARCIA, T., ROMAN-ROMAN, S., JACKSON, A., THEILHABER, J., CONNOLLY, T., SPINELLA-JAEGLE, S., KAWAI, S., COURTOIS, B., BUSHNELL, S., AUBERVAL, M., CALL, K. & BARON, R. 2002. Behavior of osteoblast, adipocyte, and myoblast markers in genome-wide expression analysis of mouse calvaria primary osteoblasts in vitro. *Bone,* 31**,** 205-11.

GARRETT, I. R., DALLAS, S., RADL, J. & MUNDY, G. R. 1997. A murine model of human myeloma bone disease. *Bone,* 20**,** 515-20.

GILBERT, L., HE, X., FARMER, P., RUBIN, J., DRISSI, H., VAN WIJNEN, A. J., LIAN, J. B., STEIN, G. S. & NANES, M. S. 2002. Expression of the osteoblast differentiation factor RUNX2 (Cbfa1/AML3/Pebp2alpha A) is inhibited by tumor necrosis factor-alpha. *J Biol Chem,* 277**,** 2695-701.

GIULIANI, N., COLLA, S., LAZZARETTI, M., SALA, R., ROTI, G., MANCINI, C., BONOMINI, S., LUNGHI, P., HOJDEN, M., GENESTRETI, G., SVALDI, M., COSER, P., FATTORI, P. P., SAMMARELLI, G., GAZZOLA, G. C., BATAILLE, R., ALMICI, C., CARAMATTI, C., MANGONI, L. & RIZZOLI, V. 2003. Proangiogenic properties of human myeloma cells: production of angiopoietin-1 and its potential relationship to myeloma-induced angiogenesis. *Blood,* 102**,** 638-45.

GONG, Y., SLEE, R. B., FUKAI, N., RAWADI, G., ROMAN-ROMAN, S., REGINATO, A. M., WANG, H., CUNDY, T., GLORIEUX, F. H., LEV, D., ZACHARIN, M., OEXLE, K., MARCELINO, J., SUWAIRI, W., HEEGER, S., SABATAKOS, G., APTE, S., ADKINS, W. N., ALLGROVE, J., ARSLAN-KIRCHNER, M., BATCH, J. A., BEIGHTON, P., BLACK, G. C., BOLES, R. G., BOON, L. M., BORRONE, C., BRUNNER, H. G., CARLE, G. F., DALLAPICCOLA, B., DE PAEPE, A., FLOEGE, B., HALFHIDE, M. L.,

HALL, B., HENNEKAM, R. C., HIROSE, T., JANS, A., JUPPNER, H., KIM, C. A., KEPPLER-NOREUIL, K., KOHLSCHUETTER, A., LACOMBE, D., LAMBERT, M., LEMYRE, E., LETTEBOER, T., PELTONEN, L., RAMESAR, R. S., ROMANENGO, M., SOMER, H., STEICHEN-GERSDORF, E., STEINMANN, B., SULLIVAN, B., SUPERTI-FURGA, A., SWOBODA, W., VAN DEN BOOGAARD, M. J., VAN HUL, W., VIKKULA, M., VOTRUBA, M., ZABEL, B., GARCIA, T., BARON, R., OLSEN, B. R. & WARMAN, M. L. 2001. LDL receptor-related protein 5 (LRP5) affects bone accrual and eye development. *Cell,* 107**,** 513-23.

GRAVDAL, K., HALVORSEN, O. J., HAUKAAS, S. A. & AKSLEN, L. A. 2007. A switch from E-cadherin to N-cadherin expression indicates epithelial to mesenchymal transition and is of strong and independent importance for the progress of prostate cancer. *Clin Cancer Res,* 13**,** 7003-11.

GREENBAUM, A. M., REVOLLO, L. D., WOLOSZYNEK, J. R., CIVITELLI, R. & LINK, D. C. 2012. N-cadherin in osteolineage cells is not required for maintenance of hematopoietic stem cells. *Blood*.

GROEN, R. W., DE ROOIJ, M. F., KOCEMBA, K. A., REIJMERS, R. M., DE HAAN-KRAMER, A., OVERDIJK, M. B., AALDERS, L., ROZEMULLER, H., MARTENS, A. C., BERGSAGEL, P. L., KERSTEN, M. J., PALS, S. T. & SPAARGAREN, M. 2011. N-cadherin-mediated interaction with multiple myeloma cells inhibits osteoblast differentiation. *Haematologica,* 96**,** 1653-61.

GUMBINER, B. M. 2005. Regulation of cadherin-mediated adhesion in morphogenesis. *Nat Rev Mol Cell Biol,* 6**,** 622-34.

HADJIDAKIS, D. J. & ANDROULAKIS, II 2006. Bone remodeling. *Ann N Y Acad Sci,* 1092**,** 385-96.

HARRISON, D. E. & ZHONG, R. K. 1992. The same exhaustible multilineage precursor produces both myeloid and lymphoid cells as early as 3-4 weeks after marrow transplantation. *Proc Natl Acad Sci U S A,* 89**,** 10134-8.

HAY, E., LAPLANTINE, E., GEOFFROY, V., FRAIN, M., KOHLER, T., MULLER, R. & MARIE, P. J. 2009a. N-cadherin interacts with axin and LRP5 to negatively regulate Wnt/beta-catenin signaling, osteoblast function, and bone formation. *Mol Cell Biol,* 29**,** 953-64.

HAY, E., NOURAUD, A. & MARIE, P. J. 2009b. N-cadherin negatively regulates osteoblast proliferation and survival by antagonizing Wnt, ERK and PI3K/Akt signalling. *PLoS One,* 4**,** e8284.

HAZAN, R. B., QIAO, R., KEREN, R., BADANO, I. & SUYAMA, K. 2004. Cadherin switch in tumor progression. *Ann N Y Acad Sci,* 1014**,** 155-63.

HEATH, D. J., CHANTRY, A. D., BUCKLE, C. H., COULTON, L., SHAUGHNESSY, J. D., JR., EVANS, H. R., SNOWDEN, J. A., STOVER, D. R., VANDERKERKEN, K. & CROUCHER, P. I. 2009. Inhibiting Dickkopf-1 (Dkk1) removes suppression of bone formation and prevents the development of osteolytic bone disease in multiple myeloma. *J Bone Miner Res,* 24**,** 425-36.

HEIDER, U., FLEISSNER, C., ZAVRSKI, I., KAISER, M., HECHT, M., JAKOB, C. & SEZER, O. 2006. Bone markers in multiple myeloma. *Eur J Cancer,* 42**,** 1544-53.

HIDESHIMA, T., CHAUHAN, D., HAYASHI, T., PODAR, K., AKIYAMA, M., GUPTA, D., RICHARDSON, P., MUNSHI, N. & ANDERSON, K. C. 2002. The biological sequelae of stromal cell-derived factor-1alpha in multiple myeloma. *Mol Cancer Ther,* 1**,** 539-44.

HOCK, J. M., KRISHNAN, V., ONYIA, J. E., BIDWELL, J. P., MILAS, J. & STANISLAUS, D. 2001. Osteoblast apoptosis and bone turnover. *J Bone Miner Res,* 16**,** 975-84.

HOLLAND, P. M., ABRAMSON, R. D., WATSON, R. & GELFAND, D. H. 1991. Detection of specific polymerase chain reaction product by utilizing the 5'----3' exonuclease activity of Thermus aquaticus DNA polymerase. *Proc Natl Acad Sci U S A,* 88**,** 7276-80.

HOSOKAWA, K., ARAI, F., YOSHIHARA, H., IWASAKI, H., NAKAMURA, Y., GOMEI, Y. & SUDA, T. 2010. Knockdown of N-cadherin suppresses the long-term engraftment of hematopoietic stem cells. *Blood,* 116**,** 554-63.

HUNTLY, B. J. & GILLILAND, D. G. 2005. Leukaemia stem cells and the evolution of cancer-stem-cell research. *Nat Rev Cancer,* 5**,** 311-21.

HURLEY, M. M., LEE, S. K., RAISZ, L. G., BERNECKER, P. & LORENZO, J. 1998. Basic fibroblast growth factor induces osteoclast formation in murine bone marrow cultures. *Bone,* 22**,** 309-16.

JUNDT, F., PROBSTING, K. S., ANAGNOSTOPOULOS, I., MUEHLINGHAUS, G., CHATTERJEE, M., MATHAS, S., BARGOU, R. C., MANZ, R., STEIN, H. & DORKEN, B. 2004. Jagged1-induced Notch signaling drives proliferation of multiple myeloma cells. *Blood,* 103**,** 3511-5.

KARSENTY, G. 1999. The genetic transformation of bone biology. *Genes Dev,* 13**,** 3037-51.

KAWABATA, M., IMAMURA, T. & MIYAZONO, K. 1998. Signal transduction by bone morphogenetic proteins. *Cytokine Growth Factor Rev,* 9**,** 49-61.

KAWAGUCHI, J., KII, I., SUGIYAMA, Y., TAKESHITA, S. & KUDO, A. 2001. The transition of cadherin expression in osteoblast differentiation from mesenchymal cells: consistent expression of cadherin-11 in osteoblast lineage. *J Bone Miner Res,* 16**,** 260-9.

KAWANO, Y. & KYPTA, R. 2003. Secreted antagonists of the Wnt signalling pathway. *J Cell Sci,* 116**,** 2627-34.

KIEL, M. J., ACAR, M., RADICE, G. L. & MORRISON, S. J. 2009. Hematopoietic stem cells do not depend on N-cadherin to regulate their maintenance. *Cell Stem Cell,* 4**,** 170-9.

KING, J. A., MARKER, P. C., SEUNG, K. J. & KINGSLEY, D. M. 1994. BMP5 and the molecular, skeletal, and soft-tissue alterations in short ear mice. *Dev Biol,* 166**,** 112-22.

KLEIN-NULEND, J., NIJWEIDE, P. J. & BURGER, E. H. 2003. Osteocyte and bone structure. *Current osteoporosis reports,* 1**,** 5-10.

KOMORI, T., YAGI, H., NOMURA, S., YAMAGUCHI, A., SASAKI, K., DEGUCHI, K., SHIMIZU, Y., BRONSON, R. T., GAO, Y. H., INADA, M., SATO, M., OKAMOTO, R., KITAMURA, Y., YOSHIKI, S. & KISHIMOTO, T. 1997. Targeted disruption of Cbfa1 results in a complete lack of bone formation owing to maturational arrest of osteoblasts. *Cell,* 89**,** 755-64.

KONDO, M., WEISSMAN, I. L. & AKASHI, K. 1997. Identification of clonogenic common lymphoid progenitors in mouse bone marrow. *Cell,* 91**,** 661-72.

KRUM, S. A., MIRANDA-CARBONI, G. A., HAUSCHKA, P. V., CARROLL, J. S., LANE, T. F., FREEDMAN, L. P. & BROWN, M. 2008. Estrogen protects bone by inducing Fas ligand in osteoblasts to regulate osteoclast survival. *EMBO J,* 27**,** 535-45.

KUEHL, W. M. & BERGSAGEL, P. L. 2002. Multiple myeloma: evolving genetic events and host interactions. *Nat Rev Cancer,* 2**,** 175-87.

KURIHARA, N., BERTOLINI, D., SUDA, T., AKIYAMA, Y. & ROODMAN, G. D. 1990. IL-6 stimulates osteoclast-like multinucleated cell formation in long term human marrow cultures by inducing IL-1 release. *J Immunol,* 144**,** 4226-30.

KYLE, R. A. & RAJKUMAR, S. V. 2004. Multiple myeloma. *N Engl J Med,* 351**,** 1860-73.

LAIB, A., BAROU, O., VICO, L., LAFAGE-PROUST, M. H., ALEXANDRE, C. & RUGSEGGER, P. 2000. 3D micro-computed tomography of trabecular and cortical bone architecture with application to a rat model of immobilisation osteoporosis. *Med Biol Eng Comput,* 38**,** 326-32.

LASCOMBE, I., CLAIROTTE, A., FAUCONNET, S., BERNARDINI, S., WALLERAND, H., KANTELIP, B. & BITTARD, H. 2006. N-cadherin as a novel prognostic marker of progression in superficial urothelial tumors. *Clin Cancer Res,* 12**,** 2780-7.

LEE, J. W., CHUNG, H. Y., EHRLICH, L. A., JELINEK, D. F., CALLANDER, N. S., ROODMAN, G. D. & CHOI, S. J. 2004. IL-3 expression by myeloma cells increases both osteoclast formation and growth of myeloma cells. *Blood,* 103**,** 2308-15.

LI, G., SATYAMOORTHY, K. & HERLYN, M. 2001. N-cadherin-mediated intercellular interactions promote survival and migration of melanoma cells. *Cancer Res,* 61**,** 3819-25.

LIAN, J. B. & STEIN, G. S. 2003. Runx2/Cbfa1: a multifunctional regulator of bone formation. *Curr Pharm Des,* 9**,** 2677-85.

LLEWELLYN, B. D. 2009. Nuclear staining with alum hematoxylin. *Biotech Histochem,* 84**,** 159-77.

LO CELSO, C., FLEMING, H. E., WU, J. W., ZHAO, C. X., MIAKE-LYE, S., FUJISAKI, J., COTE, D., ROWE, D. W., LIN, C. P. & SCADDEN, D. T. 2009. Live-animal tracking of individual haematopoietic stem/progenitor cells in their niche. *Nature,* 457**,** 92-6.

LYONS, K. M., HOGAN, B. L. & ROBERTSON, E. J. 1995. Colocalization of BMP 7 and BMP 2 RNAs suggests that these factors cooperatively mediate tissue interactions during murine development. *Mech Dev,* 50**,** 71-83.

MANNING, L. S., BERGER, J. D., O'DONOGHUE, H. L., SHERIDAN, G. N., CLARINGBOLD, P. G. & TURNER, J. H. 1992. A model of multiple myeloma: culture of 5T33 murine myeloma cells and evaluation of tumorigenicity in the C57BL/KaLwRij mouse. *Br J Cancer,* 66**,** 1088-93.

MANOLAGAS, S. C. 2000. Birth and death of bone cells: basic regulatory mechanisms and implications for the pathogenesis and treatment of osteoporosis. *Endocr Rev,* 21**,** 115-37.

MAO, B., WU, W., DAVIDSON, G., MARHOLD, J., LI, M., MECHLER, B. M., DELIUS, H., HOPPE, D., STANNEK, P., WALTER, C., GLINKA, A. & NIEHRS, C. 2002. Kremen proteins are Dickkopf receptors that regulate Wnt/beta-catenin signalling. *Nature,* 417**,** 664-7.

MAO, B., WU, W., LI, Y., HOPPE, D., STANNEK, P., GLINKA, A. & NIEHRS, C. 2001. LDL-receptor-related protein 6 is a receptor for Dickkopf proteins. *Nature,* 411**,** 321-5.

MARIE, P. J. 2002. Role of N-cadherin in bone formation. *J Cell Physiol,* 190**,** 297-305.

MBALAVIELE, G., CHEN, H., BOYCE, B. F., MUNDY, G. R. & YONEDA, T. 1995. The role of cadherin in the generation of multinucleated osteoclasts from mononuclear precursors in murine marrow. *J Clin Invest,* 95**,** 2757-65.

MCSHEEHY, P. M. & CHAMBERS, T. J. 1986a. Osteoblast-like cells in the presence of parathyroid hormone release soluble factor that stimulates osteoclastic bone resorption. *Endocrinology,* 119**,** 1654-9.

MCSHEEHY, P. M. & CHAMBERS, T. J. 1986b. Osteoblastic cells mediate osteoclastic responsiveness to parathyroid hormone. *Endocrinology,* 118**,** 824-8.

MCSHEEHY, P. M. & CHAMBERS, T. J. 1987. 1,25-Dihydroxyvitamin D3 stimulates rat osteoblastic cells to release a soluble factor that increases osteoclastic bone resorption. *J Clin Invest,* 80**,** 425-9.

MIKUNI-TAKAGAKI, Y., KAKAI, Y., SATOYOSHI, M., KAWANO, E., SUZUKI, Y., KAWASE, T. & SAITO, S. 1995. Matrix mineralization and the differentiation of osteocyte-like cells in culture. *J Bone Miner Res,* 10**,** 231-42.

MILAT, F. & NG, K. W. 2009. Is Wnt signalling the final common pathway leading to bone formation? *Mol Cell Endocrinol,* 310**,** 52-62.

MINKIN, C. 1982. Bone acid phosphatase: tartrate-resistant acid phosphatase as a marker of osteoclast function. *Calcif Tissue Int,* 34**,** 285-90.

MIYATANI, S., COPELAND, N. G., GILBERT, D. J., JENKINS, N. A. & TAKEICHI, M. 1992. Genomic structure and chromosomal mapping of the mouse N-cadherin gene. *Proc Natl Acad Sci U S A,* 89**,** 8443-7.

MUGURUMA, Y., YAHATA, T., MIYATAKE, H., SATO, T., UNO, T., ITOH, J., KATO, S., ITO, M., HOTTA, T. & ANDO, K. 2006. Reconstitution of the functional human hematopoietic microenvironment derived from human mesenchymal stem cells in the murine bone marrow compartment. *Blood,* 107**,** 1878-87.

MUKHERJEE, P. M., WANG, C. J., CHEN, I. P., JAFAROV, T., OLSEN, B. R., UEKI, Y. & REICHENBERGER, E. J. 2010. Cherubism gene Sh3bp2 is important for optimal bone

formation, osteoblast differentiation, and function. *Am J Orthod Dentofacial Orthop,* 138**,** 140 e1-140 e11; discussion 140-1.

NAKAMURA, I., DUONG LE, T., RODAN, S. B. & RODAN, G. A. 2007a. Involvement of alpha(v)beta3 integrins in osteoclast function. *J Bone Miner Metab,* 25**,** 337-44.

NAKAMURA, I., GAILIT, J. & SASAKI, T. 1996. Osteoclast integrin alphaVbeta3 is present in the clear zone and contributes to cellular polarization. *Cell Tissue Res,* 286**,** 507-15.

NAKAMURA, T., IMAI, Y., MATSUMOTO, T., SATO, S., TAKEUCHI, K., IGARASHI, K., HARADA, Y., AZUMA, Y., KRUST, A., YAMAMOTO, Y., NISHINA, H., TAKEDA, S., TAKAYANAGI, H., METZGER, D., KANNO, J., TAKAOKA, K., MARTIN, T. J., CHAMBON, P. & KATO, S. 2007b. Estrogen prevents bone loss via estrogen receptor alpha and induction of Fas ligand in osteoclasts. *Cell,* 130**,** 811-23.

NAKASHIMA, K. & DE CROMBRUGGHE, B. 2003. Transcriptional mechanisms in osteoblast differentiation and bone formation. *Trends Genet,* 19**,** 458-66.

NAKASHIMA, K., ZHOU, X., KUNKEL, G., ZHANG, Z., DENG, J. M., BEHRINGER, R. R. & DE CROMBRUGGHE, B. 2002. The novel zinc finger-containing transcription factor osterix is required for osteoblast differentiation and bone formation. *Cell,* 108**,** 17-29.

NIEHRS, C. 2006. Function and biological roles of the Dickkopf family of Wnt modulators. *Oncogene,* 25**,** 7469-81.

NIJWEIDE, P. J., BURGER, E. H. & FEYEN, J. H. 1986. Cells of bone: proliferation, differentiation, and hormonal regulation. *Physiol Rev,* 66**,** 855-86.

NILSSON, S. K., JOHNSTON, H. M., WHITTY, G. A., WILLIAMS, B., WEBB, R. J., DENHARDT, D. T., BERTONCELLO, I., BENDALL, L. J., SIMMONS, P. J. & HAYLOCK, D. N. 2005. Osteopontin, a key component of the hematopoietic stem cell niche and regulator of primitive hematopoietic progenitor cells. *Blood,* 106**,** 1232-9.

OKAMOTO, M., MURAI, J., YOSHIKAWA, H. & TSUMAKI, N. 2006. Bone morphogenetic proteins in bone stimulate osteoclasts and osteoblasts during bone development. *J Bone Miner Res,* 21**,** 1022-33.

OLSON, D. L., BURKLY, L. C., LEONE, D. R., DOLINSKI, B. M. & LOBB, R. R. 2005. Anti-alpha4 integrin monoclonal antibody inhibits multiple myeloma growth in a murine model. *Mol Cancer Ther,* 4**,** 91-9.

OSHIMA, T., ABE, M., ASANO, J., HARA, T., KITAZOE, K., SEKIMOTO, E., TANAKA, Y., SHIBATA, H., HASHIMOTO, T., OZAKI, S., KIDO, S., INOUE, D. & MATSUMOTO, T. 2005. Myeloma cells suppress bone formation by secreting a soluble Wnt inhibitor, sFRP-2. *Blood,* 106**,** 3160-5.

OYAJOBI, B. O., MUNOZ, S., KAKONEN, R., WILLIAMS, P. J., GUPTA, A., WIDEMAN, C. L., STORY, B., GRUBBS, B., ARMSTRONG, A., DOUGALL, W. C., GARRETT, I. R. & MUNDY, G. R. 2007. Detection of myeloma in skeleton of mice by whole-body optical fluorescence imaging. *Mol Cancer Ther,* 6**,** 1701-8.

PAGNUCCO, G., CARDINALE, G. & GERVASI, F. 2004. Targeting multiple myeloma cells and their bone marrow microenvironment. *Ann N Y Acad Sci,* 1028**,** 390-9.

PARFITT, A. M., DREZNER, M. K., GLORIEUX, F. H., KANIS, J. A., MALLUCHE, H., MEUNIER, P. J., OTT, S. M. & RECKER, R. R. 1987. Bone histomorphometry: standardization of nomenclature, symbols, and units. Report of the ASBMR Histomorphometry Nomenclature Committee. *J Bone Miner Res,* 2**,** 595-610.

PASSEGUE, E., WAGERS, A. J., GIURIATO, S., ANDERSON, W. C. & WEISSMAN, I. L. 2005. Global analysis of proliferation and cell cycle gene expression in the regulation of hematopoietic stem and progenitor cell fates. *J Exp Med,* 202**,** 1599-611.

PROFF, P. & ROMER, P. 2009. The molecular mechanism behind bone remodelling: a review. *Clin Oral Investig,* 13**,** 355-62.

PUCH, S., ARMEANU, S., KIBLER, C., JOHNSON, K. R., MULLER, C. A., WHEELOCK, M. J. & KLEIN, G. 2001. N-cadherin is developmentally regulated and functionally involved in early hematopoietic cell differentiation. *J Cell Sci,* 114**,** 1567-77.

QIANG, Y. W., BARLOGIE, B., RUDIKOFF, S. & SHAUGHNESSY, J. D., JR. 2008. Dkk1-induced inhibition of Wnt signaling in osteoblast differentiation is an underlying mechanism of bone loss in multiple myeloma. *Bone,* 42**,** 669-80.

QUINN, J. M., ITOH, K., UDAGAWA, N., HAUSLER, K., YASUDA, H., SHIMA, N., MIZUNO, A., HIGASHIO, K., TAKAHASHI, N., SUDA, T., MARTIN, T. J. & GILLESPIE, M. T. 2001. Transforming growth factor beta affects osteoclast differentiation via direct and indirect actions. *J Bone Miner Res,* 16**,** 1787-94.

RAAB, M. S., PODAR, K., BREITKREUTZ, I., RICHARDSON, P. G. & ANDERSON, K. C. 2009. Multiple myeloma. *Lancet,* 374**,** 324-39.

RADL, J., CROESE, J. W., ZURCHER, C., VAN DEN ENDEN-VIEVEEN, M. H., BRONDIJK, R. J., KAZIL, M., HAAIJMAN, J. J., REITSMA, P. H. & BIJVOET, O. L. 1985. Influence of treatment with APD-bisphosphonate on the bone lesions in the mouse 5T2 multiple myeloma. *Cancer,* 55**,** 1030-40.

RADL, J., DE GLOPPER, E. D., SCHUIT, H. R. & ZURCHER, C. 1979. Idiopathic paraproteinemia. II. Transplantation of the paraprotein-producing clone from old to young C57BL/KaLwRij mice. *J Immunol,* 122**,** 609-13.

RADL, J., HOLLANDER, C. F., VAN DEN BERG, P. & DE GLOPPER, E. 1978. Idiopathic paraproteinaemia. I. Studies in an animal model--the ageing C57BL/KaLwRij mouse. *Clin Exp Immunol,* 33**,** 395-402.

RAGGATT, L. J. & PARTRIDGE, N. C. 2010. Cellular and molecular mechanisms of bone remodeling. *J Biol Chem,* 285**,** 25103-8.

RAWADI, G. & ROMAN-ROMAN, S. 2005. Wnt signalling pathway: a new target for the treatment of osteoporosis. *Expert Opin Ther Targets,* 9**,** 1063-77.

ROBLING, A. G., CASTILLO, A. B. & TURNER, C. H. 2006. Biomechanical and molecular regulation of bone remodeling. *Annu Rev Biomed Eng,* 8**,** 455-98.

ROODMAN, G. D. 2007. Treatment strategies for bone disease. *Bone Marrow Transplant,* 40**,** 1139-46.

SANCHEZ-HERAS, E., HOWELL, F. V., WILLIAMS, G. & DOHERTY, P. 2006. The fibroblast growth factor receptor acid box is essential for interactions with N-cadherin and all of the major isoforms of neural cell adhesion molecule. *J Biol Chem,* 281**,** 35208-16.

SARRIO, D., MORENO-BUENO, G., SANCHEZ-ESTEVEZ, C., BANON-RODRIGUEZ, I., HERNANDEZ-CORTES, G., HARDISSON, D. & PALACIOS, J. 2006. Expression of cadherins and catenins correlates with distinct histologic types of ovarian carcinomas. *Hum Pathol,* 37**,** 1042-9.

SCHNEIDER, A., KALIKIN, L. M., MATTOS, A. C., KELLER, E. T., ALLEN, M. J., PIENTA, K. J. & MCCAULEY, L. K. 2005. Bone turnover mediates preferential localization of prostate cancer in the skeleton. *Endocrinology,* 146**,** 1727-36.

SCHOFIELD, R. 1978. The relationship between the spleen colony-forming cell and the haemopoietic stem cell. *Blood Cells,* 4**,** 7-25.

SEIDL, S., KAUFMANN, H. & DRACH, J. 2003. New insights into the pathophysiology of multiple myeloma. *Lancet Oncol,* 4**,** 557-64.

SHINTANI, Y., FUKUMOTO, Y., CHAIKA, N., GRANDGENETT, P. M., HOLLINGSWORTH, M. A., WHEELOCK, M. J. & JOHNSON, K. R. 2008. ADH-1 suppresses N-cadherin-dependent pancreatic cancer progression. *Int J Cancer,* 122**,** 71-7.

SILA-ASNA, M., BUNYARATVEJ, A., MAEDA, S., KITAGUCHI, H. & BUNYARATAVEJ, N. 2007. Osteoblast differentiation and bone formation gene expression in strontium-inducing bone marrow mesenchymal stem cell. *Kobe J Med Sci,* 53**,** 25-35.

SIMONET, W. S., LACEY, D. L., DUNSTAN, C. R., KELLEY, M., CHANG, M. S., LUTHY, R., NGUYEN, H. Q., WOODEN, S., BENNETT, L., BOONE, T., SHIMAMOTO, G., DEROSE, M., ELLIOTT, R., COLOMBERO, A., TAN, H. L., TRAIL, G., SULLIVAN, J., DAVY, E., BUCAY, N., RENSHAW-GEGG, L., HUGHES, T. M., HILL, D., PATTISON, W., CAMPBELL, P., SANDER, S., VAN, G., TARPLEY, J., DERBY, P., LEE, R. &

BOYLE, W. J. 1997. Osteoprotegerin: a novel secreted protein involved in the regulation of bone density. *Cell,* 89**,** 309-19.

SMITH, P. K., KROHN, R. I., HERMANSON, G. T., MALLIA, A. K., GARTNER, F. H., PROVENZANO, M. D., FUJIMOTO, E. K., GOEKE, N. M., OLSON, B. J. & KLENK, D. C. 1985. Measurement of protein using bicinchoninic acid. *Anal Biochem,* 150**,** 76-85.

STIER, S., KO, Y., FORKERT, R., LUTZ, C., NEUHAUS, T., GRUNEWALD, E., CHENG, T., DOMBKOWSKI, D., CALVI, L. M., RITTLING, S. R. & SCADDEN, D. T. 2005. Osteopontin is a hematopoietic stem cell niche component that negatively regulates stem cell pool size. *J Exp Med,* 201**,** 1781-91.

SUBRAMANIAM, M., GORNY, G., JOHNSEN, S. A., MONROE, D. G., EVANS, G. L., FRASER, D. G., RICKARD, D. J., RASMUSSEN, K., VAN DEURSEN, J. M., TURNER, R. T., OURSLER, M. J. & SPELSBERG, T. C. 2005. TIEG1 null mouse-derived osteoblasts are defective in mineralization and in support of osteoclast differentiation in vitro. *Mol Cell Biol,* 25**,** 1191-9.

SUGIMOTO, T., KANATANI, M., KAJI, H., YAMAGUCHI, T., FUKASE, M. & CHIHARA, K. 1993. Second messenger signaling of PTH- and PTHRP-stimulated osteoclast-like cell formation from hemopoietic blast cells. *Am J Physiol,* 265**,** E367-73.

SUGIYAMA, T., KOHARA, H., NODA, M. & NAGASAWA, T. 2006. Maintenance of the hematopoietic stem cell pool by CXCL12-CXCR4 chemokine signaling in bone marrow stromal cell niches. *Immunity,* 25**,** 977-88.

SUYAMA, K., SHAPIRO, I., GUTTMAN, M. & HAZAN, R. B. 2002. A signaling pathway leading to metastasis is controlled by N-cadherin and the FGF receptor. *Cancer Cell,* 2**,** 301-14.

TAMAI, K., SEMENOV, M., KATO, Y., SPOKONY, R., LIU, C., KATSUYAMA, Y., HESS, F., SAINT-JEANNET, J. P. & HE, X. 2000. LDL-receptor-related proteins in Wnt signal transduction. *Nature,* 407**,** 530-5.

TANAKA, H., KONO, E., TRAN, C. P., MIYAZAKI, H., YAMASHIRO, J., SHIMOMURA, T., FAZLI, L., WADA, R., HUANG, J., VESSELLA, R. L., AN, J., HORVATH, S., GLEAVE, M., RETTIG, M. B., WAINBERG, Z. A. & REITER, R. E. 2010. Monoclonal antibody targeting of N-cadherin inhibits prostate cancer growth, metastasis and castration resistance. *Nat Med*.

TEITELBAUM, S. L. 2000. Bone resorption by osteoclasts. *Science,* 289**,** 1504-8.

THOMSON, B. M., SAKLATVALA, J. & CHAMBERS, T. J. 1986. Osteoblasts mediate interleukin 1 stimulation of bone resorption by rat osteoclasts. *J Exp Med,* 164**,** 104-12.

TIAN, E., ZHAN, F., WALKER, R., RASMUSSEN, E., MA, Y., BARLOGIE, B. & SHAUGHNESSY, J. D., JR. 2003. The role of the Wnt-signaling antagonist DKK1 in the development of osteolytic lesions in multiple myeloma. *N Engl J Med,* 349**,** 2483-94.

UNEDA, S., HATA, H., MATSUNO, F., HARADA, N., MITSUYA, Y., KAWANO, F. & MITSUYA, H. 2003. Macrophage inflammatory protein-1 alpha is produced by human multiple myeloma (MM) cells and its expression correlates with bone lesions in patients with MM. *Br J Haematol,* 120**,** 53-5.

VALLET, S., MUKHERJEE, S., VAGHELA, N., HIDESHIMA, T., FULCINITI, M., POZZI, S., SANTO, L., CIRSTEA, D., PATEL, K., SOHANI, A. R., GUIMARAES, A., XIE, W., CHAUHAN, D., SCHOONMAKER, J. A., ATTAR, E., CHURCHILL, M., WELLER, E., MUNSHI, N., SEEHRA, J. S., WEISSLEDER, R., ANDERSON, K. C., SCADDEN, D. T. & RAJE, N. 2010. Activin A promotes multiple myeloma-induced osteolysis and is a promising target for myeloma bone disease. *Proc Natl Acad Sci U S A,* 107**,** 5124-9.

VAN DER PLUIJM, G., QUE, I., SIJMONS, B., BUIJS, J. T., LOWIK, C. W., WETTERWALD, A., THALMANN, G. N., PAPAPOULOS, S. E. & CECCHINI, M. G. 2005. Interference with the microenvironmental support impairs the de novo formation of bone metastases in vivo. *Cancer Res,* 65**,** 7682-90.

VAN LENTHE, G. H., HAGENMULLER, H., BOHNER, M., HOLLISTER, S. J., MEINEL, L. & MULLER, R. 2007. Nondestructive micro-computed tomography for biological imaging and quantification of scaffold-bone interaction in vivo. *Biomaterials,* 28**,** 2479-90.

VAN VALCKENBORGH, E., MATSUI, W., AGARWAL, P., LUB, S., DEHUI, X., DE BRUYNE, E., MENU, E., EMPSEN, C., VAN GRUNSVEN, L., AGARWAL, J., WANG, Q., JERNBERG-WIKLUND, H. & VANDERKERKEN, K. 2012. Tumor-initiating capacity of CD138- and CD138+ tumor cells in the 5T33 multiple myeloma model. *Leukemia,* 26**,** 1436-9.

VANDERKERKEN, K., DE GREEF, C., ASOSINGH, K., ARTETA, B., DE VEERMAN, M., VANDE BROEK, I., VAN RIET, I., KOBAYASHI, M., SMEDSROD, B. & VAN CAMP, B. 2000. Selective initial in vivo homing pattern of 5T2 multiple myeloma cells in the C57BL/KalwRij mouse. *Br J Cancer,* 82**,** 953-9.

VANDERKERKEN, K., DE RAEVE, H., GOES, E., VAN MEIRVENNE, S., RADL, J., VAN RIET, I., THIELEMANS, K. & VAN CAMP, B. 1997. Organ involvement and phenotypic adhesion profile of 5T2 and 5T33 myeloma cells in the C57BL/KaLwRij mouse. *Br J Cancer,* 76**,** 451-60.

VINCENT, T. & MECHTI, N. 2004. IL-6 regulates CD44 cell surface expression on human myeloma cells. *Leukemia,* 18**,** 967-75.

VISNJIC, D., KALAJZIC, Z., ROWE, D. W., KATAVIC, V., LORENZO, J. & AGUILA, H. L. 2004. Hematopoiesis is severely altered in mice with an induced osteoblast deficiency. *Blood,* 103**,** 3258-64.

VITOVSKI, S., CHANTRY, A. D., LAWSON, M. A. & CROUCHER, P. I. 2012. Targeting tumour-initiating cells with TRAIL based combination therapy ensures complete and lasting eradication of multiple myeloma tumours in vivo. *PLoS One,* 7**,** e35830.

WANG, X., HISHA, H., TAKETANI, S., ADACHI, Y., LI, Q., CUI, W., CUI, Y., WANG, J., SONG, C., MIZOKAMI, T., OKAZAKI, S., FAN, T., FAN, H., LIAN, Z., GERSHWIN, M. E. & IKEHARA, S. 2006. Characterization of mesenchymal stem cells isolated from mouse fetal bone marrow. *Stem Cells,* 24**,** 482-93.

WATKINS, B. A., LIPPMAN, H. E., LE BOUTEILLER, L., LI, Y. & SEIFERT, M. F. 2001. Bioactive fatty acids: role in bone biology and bone cell function. *Prog Lipid Res,* 40**,** 125-48.

WEI, S., KITAURA, H., ZHOU, P., ROSS, F. P. & TEITELBAUM, S. L. 2005. IL-1 mediates TNF-induced osteoclastogenesis. *J Clin Invest,* 115**,** 282-90.

WEIN, F., PIETSCH, L., SAFFRICH, R., WUCHTER, P., WALENDA, T., BORK, S., HORN, P., DIEHLMANN, A., ECKSTEIN, V., HO, A. D. & WAGNER, W. 2010. N-cadherin is expressed on human hematopoietic progenitor cells and mediates interaction with human mesenchymal stromal cells. *Stem Cell Res,* 4**,** 129-39.

WENNBERG, C., HESSLE, L., LUNDBERG, P., MAURO, S., NARISAWA, S., LERNER, U. H. & MILLAN, J. L. 2000. Functional characterization of osteoblasts and osteoclasts from alkaline phosphatase knockout mice. *J Bone Miner Res,* 15**,** 1879-88.

WENSTRUP, R. J., COHN, D. H., COHEN, T. & BYERS, P. H. 1988. Arginine for glycine substitution in the triple-helical domain of the products of one alpha 2(I) collagen allele (COL1A2) produces the osteogenesis imperfecta type IV phenotype. *J Biol Chem,* 263**,** 7734-40.

WESTENDORF, J. J., KAHLER, R. A. & SCHROEDER, T. M. 2004. Wnt signaling in osteoblasts and bone diseases. *Gene,* 341**,** 19-39.

WILLIAMS, E. J., WILLIAMS, G., HOWELL, F. V., SKAPER, S. D., WALSH, F. S. & DOHERTY, P. 2001. Identification of an N-cadherin motif that can interact with the fibroblast growth factor receptor and is required for axonal growth. *J Biol Chem,* 276**,** 43879-86.

WILSON, A. & TRUMPP, A. 2006. Bone-marrow haematopoietic-stem-cell niches. *Nat Rev Immunol,* 6**,** 93-106.

WINKLER, D. G., SUTHERLAND, M. K., GEOGHEGAN, J. C., YU, C., HAYES, T., SKONIER, J. E., SHPEKTOR, D., JONAS, M., KOVACEVICH, B. R., STAEHLING-HAMPTON, K., APPLEBY, M., BRUNKOW, M. E. & LATHAM, J. A. 2003. Osteocyte control of bone formation via sclerostin, a novel BMP antagonist. *EMBO J,* 22**,** 6267-76.

WU, J. Y., SCADDEN, D. T. & KRONENBERG, H. M. 2009. Role of the osteoblast lineage in the bone marrow hematopoietic niches. *J Bone Miner Res,* 24**,** 759-64.

XIAO, Z., ZHANG, S., MAHLIOS, J., ZHOU, G., MAGENHEIMER, B. S., GUO, D., DALLAS, S. L., MASER, R., CALVET, J. P., BONEWALD, L. & QUARLES, L. D. 2006. Cilia-like structures and polycystin-1 in osteoblasts/osteocytes and associated abnormalities in skeletogenesis and Runx2 expression. *J Biol Chem,* 281**,** 30884-95.

XIE, Y., YIN, T., WIEGRAEBE, W., HE, X. C., MILLER, D., STARK, D., PERKO, K., ALEXANDER, R., SCHWARTZ, J., GRINDLEY, J. C., PARK, J., HAUG, J. S., WUNDERLICH, J. P., LI, H., ZHANG, S., JOHNSON, T., FELDMAN, R. A. & LI, L. 2009. Detection of functional haematopoietic stem cell niche using real-time imaging. *Nature,* 457**,** 97-101.

YAMAGUCHI, A., ISHIZUYA, T., KINTOU, N., WADA, Y., KATAGIRI, T., WOZNEY, J. M., ROSEN, V. & YOSHIKI, S. 1996. Effects of BMP-2, BMP-4, and BMP-6 on osteoblastic differentiation of bone marrow-derived stromal cell lines, ST2 and MC3T3-G2/PA6. *Biochem Biophys Res Commun,* 220**,** 366-71.

YAMAGUCHI, A., KOMORI, T. & SUDA, T. 2000. Regulation of osteoblast differentiation mediated by bone morphogenetic proteins, hedgehogs, and Cbfa1. *Endocr Rev,* 21**,** 393-411.

YANAGIMOTO, K., SATO, Y., SHIMOYAMA, Y., TSUCHIYA, B., KUWAO, S. & KAMEYA, T. 2001. Co-expression of N-cadherin and alpha-fetoprotein in stomach cancer. *Pathol Int,* 51**,** 612-8.

YIN, T. & LI, L. 2006. The stem cell niches in bone. *J Clin Invest,* 116**,** 1195-201.

ZAIDI, M., INZERILLO, A. M., MOONGA, B. S., BEVIS, P. J. & HUANG, C. L. 2002. Forty years of calcitonin--where are we now? A tribute to the work of Iain Macintyre, FRS. *Bone,* 30**,** 655-63.

ZHANG, J., NIU, C., YE, L., HUANG, H., HE, X., TONG, W. G., ROSS, J., HAUG, J., JOHNSON, T., FENG, J. Q., HARRIS, S., WIEDEMANN, L. M., MISHINA, Y. & LI, L. 2003. Identification of the haematopoietic stem cell niche and control of the niche size. *Nature,* 425**,** 836-41.

ZHANG, M., XUAN, S., BOUXSEIN, M. L., VON STECHOW, D., AKENO, N., FAUGERE, M. C., MALLUCHE, H., ZHAO, G., ROSEN, C. J., EFSTRATIADIS, A. & CLEMENS, T. L. 2002. Osteoblast-specific knockout of the insulin-like growth factor (IGF) receptor gene reveals an essential role of IGF signaling in bone matrix mineralization. *J Biol Chem,* 277**,** 44005-12.

ZHAO, G., MONIER-FAUGERE, M. C., LANGUB, M. C., GENG, Z., NAKAYAMA, T., PIKE, J. W., CHERNAUSEK, S. D., ROSEN, C. J., DONAHUE, L. R., MALLUCHE, H. H., FAGIN, J. A. & CLEMENS, T. L. 2000a. Targeted overexpression of insulin-like growth factor I to osteoblasts of transgenic mice: increased trabecular bone volume without increased osteoblast proliferation. *Endocrinology,* 141**,** 2674-82.

ZHAO, S., ZHANG, Y. K., HARRIS, S., AHUJA, S. S. & BONEWALD, L. F. 2002. MLO-Y4 osteocyte-like cells support osteoclast formation and activation. *Journal of bone and mineral research : the official journal of the American Society for Bone and Mineral Research,* 17**,** 2068-79.

ZHAO, Y., LIN, Y., ZHAN, Y., YANG, G., LOUIE, J., HARRISON, D. E. & ANDERSON, W. F. 2000b. Murine hematopoietic stem cell characterization and its regulation in BM transplantation. *Blood,* 96**,** 3016-22.

ZHONG, R. K., ASTLE, C. M. & HARRISON, D. E. 1996. Distinct developmental patterns of short-term and long-term functioning lymphoid and myeloid precursors defined by competitive limiting dilution analysis in vivo. *J Immunol,* 157**,** 138-45.